GALVANIC AND PITTING CORROSION —

Field and Laboratory Studies

Baboian/France/Rowe/Rynewicz

STP 576

AMERICAN SOCIETY FOR TESTING AND MATERIALS

GALVANIC AND PITTING CORROSION—FIELD AND LABORATORY STUDIES

Two symposia
presented at the
1974 Materials Engineering Congress
AMERICAN SOCIETY FOR
TESTING AND MATERIALS
Detroit, Mich., 22-23 Oct. 1974

ASTM SPECIAL TECHNICAL PUBLICATION 576
Robert Baboian, W. D. France, Jr.,
L. C. Rowe, and J. F. Rynewicz, editors

List price $29.75
04-576000-27

American Society for Testing and Materials
1916 Race Street, Philadelphia, Pa. 19103

Library of Congress Catalog Card Number: 75-2510

Printed in Cockeysville, Md.
February 1976

Foreword

The two symposia, Galvanic Corrosion and Pitting Corrosion, were presented at the 1974 Materials Engineering Congress held in Detroit, Mich., 22-23 Oct. 1974, respectively. The symposia were sponsored by the American Society for Testing and Materials Subcommittees G01.05 on Laboratory Corrosion Tests and G01.07 on Galvanic Corrosion of Committee G-1 on Corrosion of Metals. L. C. Rowe, General Motors Corporation, presided as symposium chairman and W. D. France, Jr., General Motors Corporation, served as symposium cochairman of the Symposium on Pitting Corrosion. For the Symposium on Galvanic Corrosion, J. F. Rynewicz, Lockheed Missiles and Space Company, presided as symposium chairman and Robert Baboian, Texas Instruments, served as symposium cochairman.

Related
ASTM Publications

Stress Corrosion Cracking of Metals—A State of the Art, STP 518 (1972), $11.75, 04-518000-27

Manual of Industrial Corrosion Standards and Control, STP 534 (1974), $16.75, 04-534000-27

Corrosion in Natural Environments, STP 558 (1974), $29.75, 04-558000-27

A Note of Appreciation to Reviewers

This publication is made possible by the authors and, also, the unheralded efforts of the reviewers. This body of technical experts whose dedication, sacrifice of time and effort, and collective wisdom in reviewing the papers must be acknowledged. The quality level of ASTM publications is a direct function of their respected opinions. On behalf of ASTM we acknowledge their contribution with appreciation.

ASTM Committee on Publications

Editorial Staff

Contents

GALVANIC CORROSION

PITTING CORROSION

Introduction

Galvanic and pitting corrosion are widely different forms of degradation; however, both lead to the same result, premature failure. Galvanic corrosion is the accelerated corrosion of a metal due to an electrical contact with a more noble metal or nonmetallic conductor in a corrosive electrolyte. Pitting corrosion is attack of a metal surface at a point or small area resulting in the formation of cavities (or pits).

The problems associated with galvanic and pitting corrosion have been extensively investigated but are far from being solved. Therefore, ASTM Committee G-1 on Corrosion of Metals sponsored a symposium from which the papers form the basis of this STP. These papers, which cover practical aspects, mechanisms, and testing techniques, will be useful to those who need to prevent, understand, or test for galvanic and pitting corrosion.

The galvanic corrosion papers include laboratory investigations and field testing results. In addition to a review of electrochemical techniques for predicting galvanic corrosion, laboratory studies include the behavior of aluminum alloys coupled to iron, nickel, and titanium, welded materials exposed to seawater, and cathodic protection of dissimilar metal assemblies. Reports on field tests include such subjects as galvanic corrosion of underground power cables, galvanic corrosion of stressed stainless steels exposed in various soils, and the coupled behavior of structural materials ranging from magnesium to titanium in atmospheric, seawater, and soil environments.

The pitting corrosion papers include descriptions of new test techniques such as rapid scan potentiodynamic measurements and a multiple crevice test assembly for statistical analysis. A review of the measurement and evaluation of pitting corrosion provides a standardized approach to the examination of this type of corrosion. Practical applications information on pitting corrosion of copper tubing in cold water service and evaluation of galvanized steel in corrosive atmospheres are included.

The information in the book should be useful to those involved with materials research and development, material selection, materials processing, and corrosion evaluation and test techniques. In addition to the wide range of materials investigated, the broad range of conditions covered include atmospheric, oil, and aqueous environments. In addition to being a valuable guide for testing and evaluation of galvanic and pitting corrosion, this STP provides practical information on these two forms of corrosion and a direction for future investigation.

J. F. Rynewicz
Lockheed Missiles and Space Company,
Sunnyvale, Calif. 94088; chairman of
Galvanic Corrosion symposium.

Galvanic Corrosion

Robert Baboian[1]

Electrochemical Techniques for Predicting Galvanic Corrosion

REFERENCE: Baboian, Robert, "**Electrochemical Techniques for Predicting Galvanic Corrosion,**" *Galvanic and Pitting Corrosion—Field and Laboratory Studies, ASTM STP 576*, American Society for Testing and Materials, 1976, pp. 5-19.

ABSTRACT: The various electrochemical techniques for predicting galvanic corrosion behavior of metals are described. Each method is evaluated on the basis of practicality using specific galvanic couples as examples. The paper describes some serious shortcomings of the existing techniques and warns of the dangers of their improper use.

KEY WORDS: corrosion, galvanic corrosion tests, metals, alloys, galvanic series, zero resistance ammeter, localized corrosion, polarization measurements, galvanic current, mixed potential

Corrosion of metals can be treated by application of the mixed potential theory first described by Wagner and Traud [*1*].[2] The theory is based on two simple hypotheses. First, any electrochemical reaction can be divided into two or more oxidation or reduction reactions, and second, there can be no net accumulation of electrical charge during an electrochemical reaction. That the various partial reactions can be treated separately, as stated in the first hypothesis, can be demonstrated experimentally.

The oxidation (corrosion) and reduction reactions at a reversible electrode are illustrated graphically in Fig. 1. The equation relating reaction rate and overvoltage is

$$\eta_{\text{act}} = \pm\beta \log \frac{i}{i_0} \qquad (1)$$

Equation 1 is called the Tafel equation and β is termed the Tafel constant or slope. Notice that for high overvoltage values, the relationship is a linear function on a logarithmic scale (Fig. 1). The value for β is usually between

---

[1] Manager, Electrochemical and Corrosion Laboratory, Texas Instruments Incorporated, Attleboro, Mass. 02703.

[2] The italic numbers in brackets refer to the list of references appended to this paper.

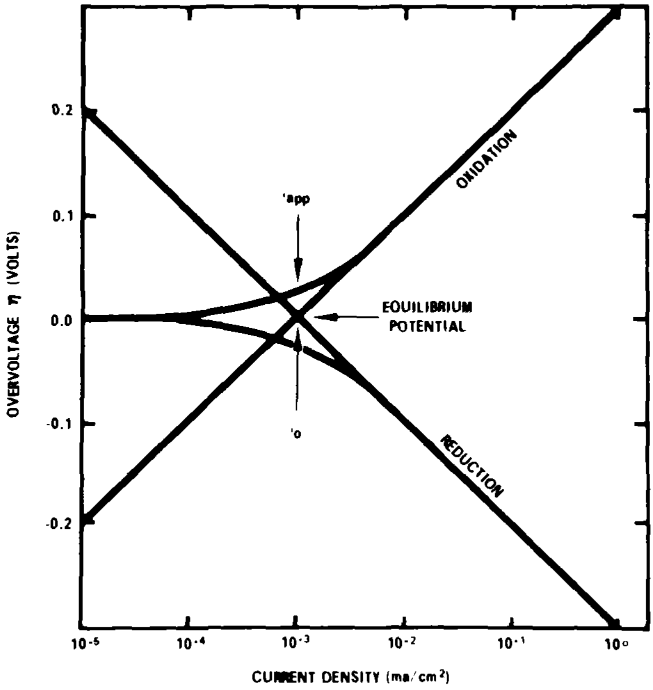

FIG. 1—*Activation polarization curves for a reversible electrode system.*

0.05 and 0.15 V. In Fig. 1, β is 0.1 V, so that for a 0.1 V change in overvoltage, the reaction rate changes by one order of magnitude. At the equilibrium potential, the net rate of oxidation, i_0, equals the net rate of reduction.

Under the simplest circumstances, metallic corrosion would involve only two reactions, oxidation and reduction. The corrosion of iron in sulfuric acid involves the anodic dissolution of iron and the evolution of hydrogen. This is demonstrated by the polarization curves for iron in 1.0 *N* sodium sulfate in Fig. 2. The first hypothesis of the mixed potential theory is satisfied if one considers that each reaction has its own reversible potential and polarization parameters. The second hypothesis, that the total rate of oxidation equals the total rate of reduction, is only satisfied at the intersection E_{corr} the corrosion or "mixed" potential. At this point, the rate of iron dissolution is equal to the rate of hydrogen evolution. The potential is so displaced from the equilibrium potential that the reverse reactions occur at a negligible rate and do not influence the corrosion rate.

In Fig. 2, the data indicate that iron will corrode at a rate of about 5.0 mA/cm^2 and will exhibit a potential of about -0.814 V versus the saturated calomel electrode (SCE).

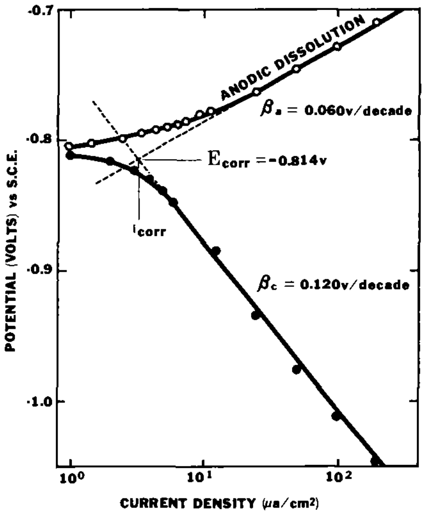

FIG. 2—*Polarization behavior of iron in 1.0 N sodium sulfate.*

One of the most important applications of the mixed potential theory to corroding systems is the treatment of galvanically coupled metals [*2*]. When two different corroding metals are coupled electrically in the same electrolyte, both metals are polarized so that each corrodes at a new rate. In Fig. 3 the corrosion potentials and polarization parameters for uncoupled Metals A and B are shown. Metal A is more noble than Metal B in that the equilibrium potential is less negative. When the mixed potential theory is applied to the individual reactions (A/A^+, H_2/H^+, B/B^+, H_2/H^+) the uncoupled corrosion rates are $i_{corr,A}$ for Metal A and $i_{corr,B}$ for Metal B. When equal areas of Metals A and B are coupled, the resultant mixed potential of the system $E_{corr,AB}$ is at the intersection where the total oxidation rate equals the total reduction rate. The rate of oxidation of the individual coupled metals is such that Metal A corrodes at a reduced rate $i'_{corr,A}$ and Metal B corrodes at in increased rate $i'_{corr,B}$.

Electrochemical techniques for predicting galvanic corrosion are based on mixed potential theory. These include potential measurements, current measurements, and polarization measurements.

These techniques have been used successfully in various applications; however, caution must be taken not to depend exclusively on one technique for all circumstances. Frequently, the use of electrochemical techniques leads to erroneous results. This is usually due to improper experimentation or interpretation of the system. In some cases, more time consuming, conventional investigations are required.

In general, it should be emphasized that in making the electrochemical measurement, one does not disturb the system so that results are meaning-

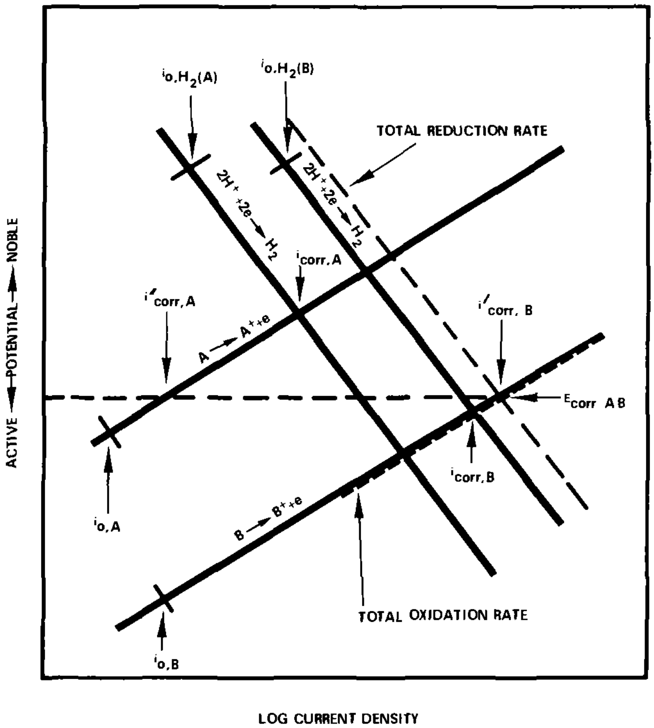

FIG. 3—*Mixed potential behavior of galvanically coupled Metals A and B.*

less. Also, it is important that the measurements be conducted in the actual corrosive environment or in one which closely simulates that environment.

Potential Measurements

The use of potential measurements for predicting galvanic corrosion is based on the measurement of E_{corr}, the corrosion potential of metals. When the metals are arranged according to their potential measured in a particular environment (Table 1) the result is termed the galvanic series [3].

In general, the corrosion rate of the more noble metal in a galvanic couple will be reduced and that for the more active metal will be increased. In some cases, the separation between the two metals in the galvanic series gives an indication of the magnitude of these effects.

When the polarization characteristics for metals are straightforward such as demonstrated in Fig. 4 for lead, iron, and zinc, the galvanic series is quite useful in predicting not only the relative galvanic behavior of the metals but also the magnitude of the effects of coupling the metals. The order and relative positions of these three metals in the galvanic series

TABLE 1—*Arrangement of metals and alloys in a galvanic series based on potential measurements in seawater velocity of flow, 13 ft/s, seawater temperature, 25°C (77°F) (from LaQue).*

Zinc
Aluminum (Alclad 3S)
Aluminum 3S-H
Aluminum 61S-T
Aluminum 52S-H
Cast iron
Carbon steel
Stainless steel Type 430 (17C)
Nickel-resistant cast iron (20N)
Stainless steel Type 304 (18C, 8N)
Stainless steel Type 410 (13C)
Nickel-resistant cast iron (30N)
Nickel-resistant cast iron (20N + Cu)
Naval-rolled brass
Yellow brass
Copper
Red brass
Composition G bronze
Admiralty brass
90-10 cupro nickel (0.8 Fe)
70-30 cupro nickel (0.06 Fe)
70-30 cupro nickel (0.47 Fe)
Stainless steel Type 430 (17C)
Nickel
Stainless steel Type 316 (18 C, 12N, 3M)
Inconel
Stainless steel Type 410 (13C)
Titanium (commercial)
Silver
Titanium (high purity from iodide)
Stainless steel Type 304 (18 C, 8N)
Hastelloy C
Monel
Stainless steel Type 316 (18C, 12N, 3M)

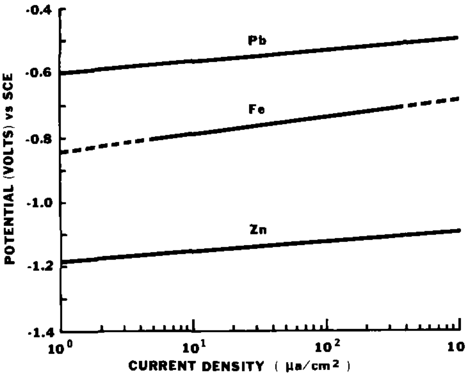

FIG. 4—*Potentiodynamic polarization curves for lead, iron, and zinc in 5 percent sodium chloride solution (30°C).*

(Table 1) is correct for the 5 percent sodium chloride environment. Measurement of the corrosion potential for these metals is sufficient.

There are several factors which lead to drawbacks in the use of potential measurements and the galvanic series. First, the formation of films on the metal surface will influence the corrosion rate so that over a wide range of potentials the surface remains passive [*4*]. This is illustrated (Fig. 5) by the polarization curves for Types 310 and 434 stainless steel in 5 percent sodium chloride solution. Their positions in the galvanic series (according to E_{corr}) may indicate what effects they may have on other metals in a galvanic couple, but the reverse is not necessarily true due to their wide passive potential ranges [*5*].

The potential variation with time in a particular environment is another concern when constructing the galvanic series [*4*]. The relative position of metals in the series may change, depending on the time of immersion. For example, in Fig. 6 the measured corrosion potentials for Types 304 and 316 stainless steel vary considerably even after 10 or 15 months immersion in seawater. The relative position of nickel, Type 304 stainless steel, and copper-nickel alloy clearly depends on the time of potential measurement.

The polarizability of metals varies according to the environment in which they are subjected. Metals which are easily polarized have a lesser affect than ones which are not readily polarized. Simple measurement of the corrosion potential does not provide information on the polarizability of the metal so that in many cases their relative positions and their separation in the galvanic series are not a valid basis for predicting galvanic corrosion behavior.

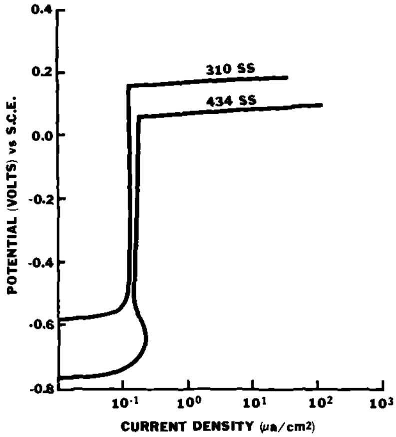

FIG. 5—*Potentiodynamic polarization curves for Types 434 and 310 stainless steel in 5 percent sodium chloride solution (30°C).*

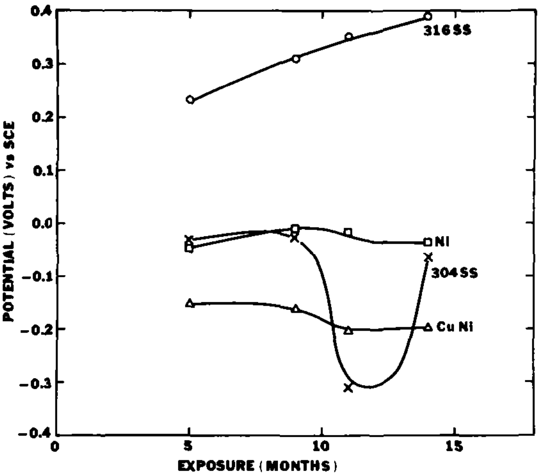

FIG. 6—*Variation of corrosion potential with time for nickel 90 to 10 copper-nickel, Types 304 and 316 stainless steel in seawater.*

Current Measurements

Measurement of galvanic currents between galvanically coupled metals is based on zero resistance ammeter techniques [*6*]. The basic zero resistance ammeter circuit, which has been used extensively, is shown in Fig. 7. The galvanic current is measured by an ammeter, *A*, by adjusting the voltage, *E*, or resistance, *R*, so that the potential difference between the two elements is zero as indicated by the electrometer, *V*. Since short circuiting in a galvanic couple is indicated by zero potential drop, this current is the true short circuit current. For continuous recording of galvanic currents, the basic circuit is simplified to include a decade resistance box adjusted so that a recorder, set to 1 mV full scale, indicates the potential between the two elements [*7*]. The galvanic current is calculated knowing the resistance and the potential.

The data in Fig. 8 for galvanic couples of copper with 1006 carbon steel, and Types 409 and 430 stainless steel were obtained using the basic zero

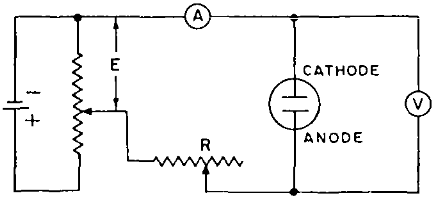

FIG. 7—*Schematic circuit of elementary zero resistance ammeter.*

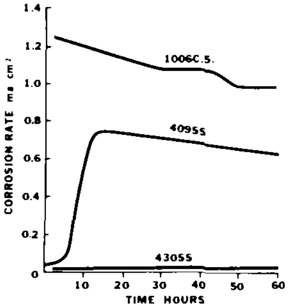

FIG. 8—*Galvanic current versus time for 1006 carbon steel and 409 and 430 stainless steel coupled to copper in 5 percent sodium chloride solution (30°C).*

resistance ammeter circuit. The magnitude of the galvanic current provides an indication of the severity of galvanic corrosion which occurs in the specific 5 percent sodium chloride environment. Notice the slow drift to lower galvanic currents for 1006 carbon steel with time. The sharp increase in galvanic current for Type 409 stainless steel is due to the initiation of localized corrosion. Initiation of localized corrosion is not indicated by the galvanic current for Type 430 stainless steel. This effect is observed, however, beyond the 60-h test time shown in Fig. 8.

The drawbacks of the basic zero resistance ammeter circuit shown in Fig. 7 are (*a*) during time periods in which the circuit is not balanced, polarization of the members in the galvanic couple occurs leading to incorrect values or long recovery times or both and (*b*) the continuous monitoring of the galvanic current requires constant attention. These disadvantages have been the focal point of new developments and improvements in the zero resistance ammeter techniques.

The development of self balancing, zero resistance ammeters allows continuous monitoring of galvanic currents. This was accomplished by electronic automatic adjustment of either R [*8*] or E [*9*] in the basic circuit. High-input resistance voltage sensing systems placed across the galvanic cell allow more accurate measurements in high-resistance electrolytes.

More recent developments include the use of a potentiostat incorporating the operational amplifier circuitry [*10*]. In the arrangement in Fig. 9 [*11*], the control potential of the potentiostat is set to zero volt. One member of the galvanic couple is connected to the working electrode terminal while the other is connected to the reference electrode terminal. The auxiliary electrode terminal is connected directly to the reference electrode terminal whereby the galvanic current is indicated directly by the potentiostat current meter, or, it is connected through an external feedback resistor (R_f in Fig. 9) and the galvanic current is measured by a voltmeter between the

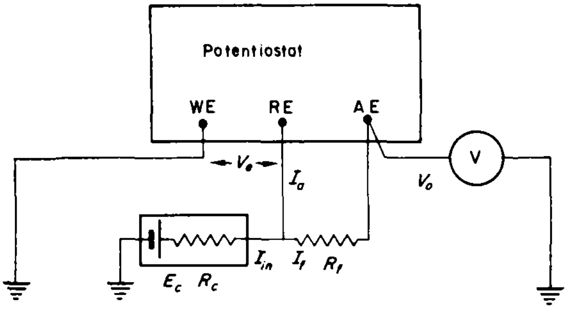

FIG. 9—*Schematic circuit for use of a potentiostat as a zero resistance ammeter* (*Ref* 11).

auxiliary and working electrode terminals. A null balance is thus maintained by means of the potentiostat solid state operational amplifier circuit.

A commercial operational amplifier can be used as the voltage control and will give the same results as a potentiostat. The use of a simple operational amplifier as an alternate to the potentiostat was described by Lauer and Mansfeld [*12*] and later by Henry and Wilde [*13*]. The advantages here include lower cost and smaller size. In Fig. 10 [*12*], one member of the galvanic couple is connected, through ground, to the positive input of the amplifier. The other is connected to the negative of the high-gain operational amplifier. The members of the galvanic couple are maintained at zero potential difference and the galvanic current is derived from V_0, the voltage output of the amplifier, and R_m, the feedback resistance (standard resistor). This arrangement allows measurements to be made in high resistivity electrolytes and continuous monitoring of the galvanic current

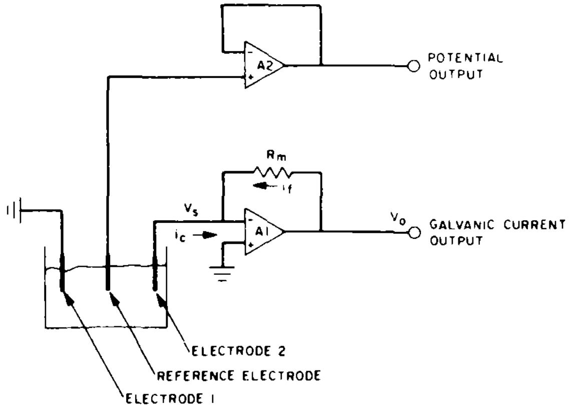

FIG. 10—*Schematic circuit of a zero resistance ammeter using an operational amplifier* (*Ref* 12).

using strip chart recorders. The reference electrode in Fig. 10 is only used to measure the mixed potential of the galvanic couple.

Typical galvanic current data obtained by Mansfeld [*13*] with the operational amplifier circuitry are shown in Fig. 11. The zero resistance current is plotted versus time for five aluminum alloys coupled to Type 4130 steel in 3.5 percent sodium chloride solution. The data show that all of the aluminum alloys are anodic to the steel in this environment. However, the relative position of the five alloys shifts with time as indicated by the crossing of the galvanic current curves during the 24-h time period. Longer test times are, therefore, required in many instances. This is especially true when localized corrosion such as pitting is possible in the galvanic couple. Frequently, several weeks induction period is observed before galvanic pitting is initiated [*4*].

The measured galvanic current is not always a measure of the true corrosion current because it is the algebraic sum of the currents due to anodic and cathodic reactions. When cathodic currents are appreciable at the mixed potential of the galvanic couple, the measured galvanic current will be significantly lower than the true corrosion current. Thus, large differences between the true corrosion rate calculated by weight loss and the rate obtained by galvanic current measurements have been observed. Calculation of the true corrosion current by correcting the measured galvanic current in some cases involves more work than actually measuring the corrosion rate by conventional weight loss techniques.

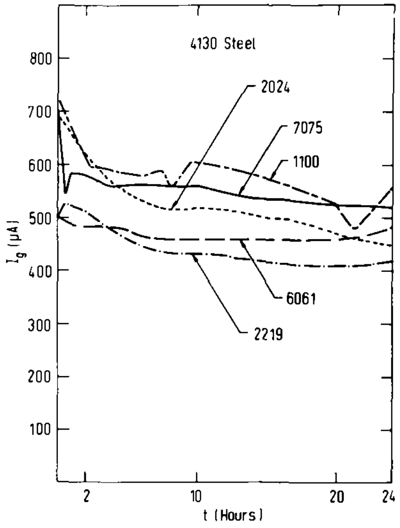

FIG. 11—*Galvanic current versus time for aluminum alloys coupled to 4130 steel in 3.5 percent sodium chloride solution* (*Ref* 13).

Polarization Measurements

Corrosion behavior of galvanically coupled metals was described previously (Fig. 3) using mixed potential theory. The information required are anodic polarization curves for the individual metals in the galvanic couple and the mixed potential E_{corr} in the actual electrolyte environment. Since the cathodic reactions also influence the mixed potential, measurements must be made duplicating the environment (such as geometry and area ratio) of the couple. It is important to note that this treatment can be applied to two [*4,5,14*] or more [*15*] metals in a galvanic couple.

In this treatment, the corrosion potential of the galvanic couple is measured, and the nature of corrosion in this potential region is determined for each metal from the individual polarization curves. For example, anodic polarization curves for DHP copper and 1006 carbon steel in 5 percent sodium chloride solution are shown in Fig. 12. The corrosion potentials of the isolated metals, obtained under actual corroding conditions in aerated 5 percent sodium chloride solution, are used to determine the rates of corrosion $i_{\mathrm{corr,Cu}}$ and $i_{\mathrm{corr,Fe}}$ from the polarization curves in Fig. 12.

When copper and iron are coupled galvanically under these conditions, the mixed potential is E'_{corr}; and, from the polarization curves in Fig. 12, the rate of corrosion of copper, $i'_{\mathrm{corr,Cu}}$, is decreased and the rate of corrosion of iron, $i'_{\mathrm{corr,Fe}}$, is increased.

Increasing the copper/iron area ratio in the galvanic couple shifts the mixed potential (E'_{corr}) to less negative values so that galvanic corrosion of iron is accelerated.

An important application of the use of polarization measurements in galvanic corrosion is in the prediction of localized corrosion. Polarization techniques and critical potentials have been used widely as a measure of pitting and crevice corrosion susceptibility of alloys in chloride solution [*16-19*]. For example, a schematic potentiodynamic polarization curve for a stainless steel in sodium chloride solution is shown in Fig. 13. The solid line represents anodic polarization from active to noble potentials.

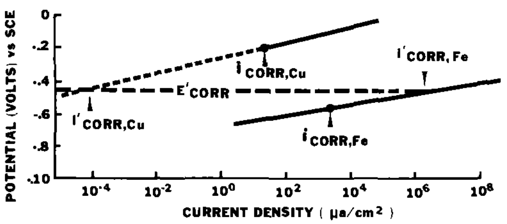

FIG. 12—*Galvanic corrosion behavior of copper and iron in 5 percent sodium chloride solution (30°C) using polarization measurements.*

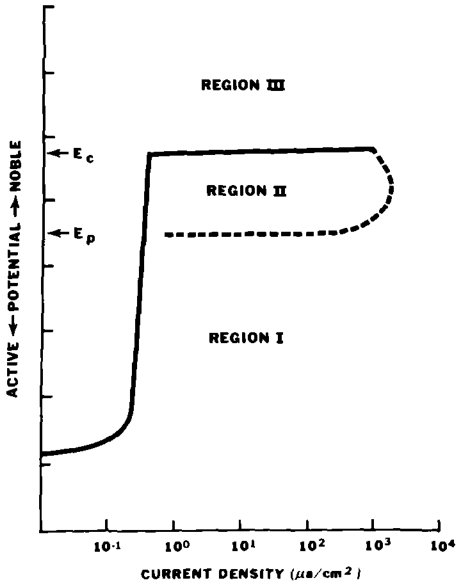

FIG. 13—*Schematic potentiodynamic polarization curve for stainless steel in 5 percent solution chloride solution showing three corrosion potential regions.*

The dashed line represents reverse polarization back to more active potentials.

Polarization above the critical breakdown potential, E_c, results in a marked increase in current density due to initiation of pitting. Reverse polarization below E_c does not reduce the current density appreciably, indicating that propagation of existing pits and crevice corrosion occurs. At the critical potential, E_p, the current density approaches zero. Below E_p, propagation of existing pits and crevice corrosion does not occur.

The corrosion behavior of stainless steel can be thus separated into three potential regions: Region I, where protection from pitting and crevice corrosion are observed; Region II, where propagation of existing pits and crevice corrosion occurs; and Region III, where initiation of pitting and crevice corrosion occurs.

Thus, galvanic couples of stainless steel can lead to three performance categories in chloride containing environments.

In Fig. 14*a*, the mixed potential for the galvanic couple between stainless steel A and Metal B lies in Region III where initiation of pitting and crevice corrosion on the stainless steel occurs. This behavior is observed in the presence of stray currents or sometimes in galvanic couples with platinum group metals.

In Fig. 14*b*, the mixed potential lies in Region II, the crevice corrosion and pit propagation region for stainless steel. Types 430 and 304 stainless steel undergo this type of corrosion when coupled to copper.

In Fig. 14*c*, stainless steel A and Metal B mixed potential lies in Region I where protection from pitting and crevice corrosion occurs. Stainless steels, such as Type 304, are protected from this type of localized corrosion in galvanic couples with carbon steel because their mixed potentials are in this region.

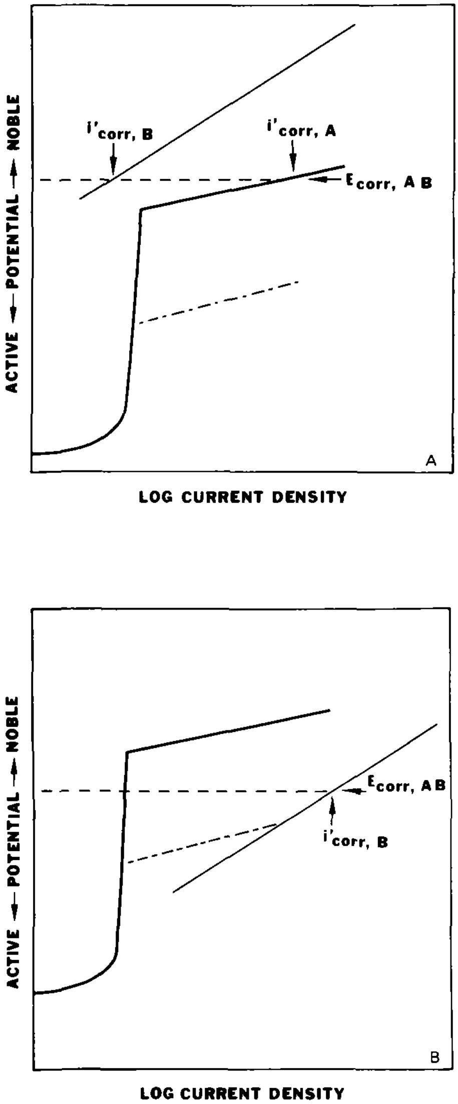

FIG. 14—*Schematic polarization curves showing corrosion behavior of stainless steel A and Metal B in galvanic couple:* (a) *mixed potential is within Region III* (b) *mixed potential is within Region II; and* (c) *mixed potential is within Region I.*

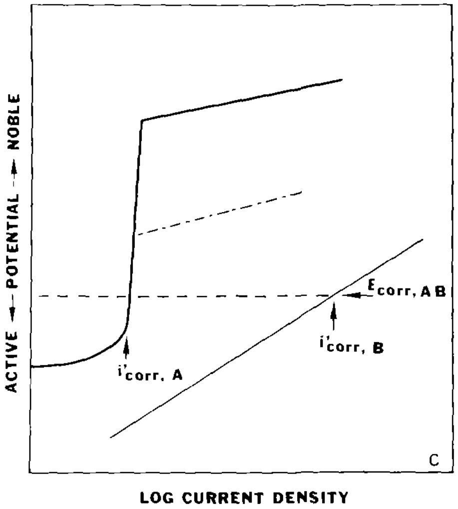

FIG. 14—(*continued*).

Summary

The following electrochemical techniques are used in predicting the galvanic corrosion behavior of metals: potential measurements, current measurements, and polarization measurements.

The success of these techniques is based on making appropriate measurements in the actual environment to which the galvanic couple is exposed. In many cases, simple measurement of the potential of each member in a galvanic couple is sufficient to predict the galvanic corrosion behavior. The resulting galvanic series of metals for a particular environment can be quite useful. However, frequently, more precise information is required. Measurement of galvanic currents can furnish more useful information regarding galvanic corrosion. Recent developments with zero resistance ammeters allow continuous measurement of the galvanic current during true short-circuiting conditions. This current, however, is not always equivalent to the corrosion current because it is the algebraic sum of the currents due to anodic and cathodic reactions. Thus, where cathodic currents are significant, the measured galvanic current may be appreciably smaller than the true corrosion current.

The use of polarization measurements in conjunction with the mixed potential of a galvanic couple can provide precise information regarding the behavior of galvanically coupled metals. This treatment has been used successfully for three member couples as well as for predicting galvanic localized corrosion.

References

[*1*] Wagner, C. and Traud, W., *Zeitschrift für Electrochemie*, Vol. 44, 1938, p. 391.
[*2*] Fontana, M. and Greene, N. in *Corrosion Engineering*, McGraw-Hill, New York.
[*3*] LaQue, F. L. in *Corrosion Handbook*, Wiley, New York.
[*4*] Baboian, R. in *Localized Corrosion—Cause of Metal Failure, ASTM STP 516*, American Society for Testing and Materials, 1972, pp. 145–163.
[*5*] Baboian, R. and Haynes, G. S. in *Corrosion in Natural Environments, ASTM STP 558*, American Society for Testing and Materials, 1974, pp. 171–184.
[*6*] Brown, R. H. and Mears, R. B., *Transactions*, Electrochemical Society, Vol. 74, 1938, p. 510.
[*7*] Greene, N. D., "Experimental Electrode Kinetics," Rensselaer Polytechnic Institute, Troy, N.Y., 1965.
[*8*] Godard, H. P., *Corrosion*, Vol. 7, 1951, p. 93.
[*9*] Maker, D. R. and Francis, H. T., *Journal of the Electrochemical Society*, Vol. 102, 1955, p. 669.
[*10*] Devay, J., Lenyal, B., and Meszaros, L., *Acta Chimica Academiae Scientiarum Hungaricae*, Vol. 62, 1969, p. 157.
[*11*] von Fraunhofer, J. A. and Staheli, P. J., *Corrosion Science*, Vol. 12, 1972, p. 767.
[*12*] Lauer, G. and Mansfeld, F., *Corrosion*, Vol. 26, 1970, p. 504.
[*13*] Mansfeld, F., *Werkstoffe und Korrosion*, Vol. 25, 1974, p. 578.
[*14*] Baboian, R., *Transactions*, Society of Automotive Engineers, Vol. 81, 1972, p. 1117.
[*15*] Baboian, R., "Clad Metals in Automotive Trim Applications," Paper 710276, Society of Automotive Engineers, Detroit, 1971.
[*16*] Horvath, J. and Uhlig, H. H., *Journal of the Electrochemical Society*, Vol. 115, 1968, p. 791.
[*17*] Pourbaix, M., Klimzack-Mathieiu, L., Mertens, C., Meunier, J., Vanleugenhaghe, C., DeNuncky, L., Laverys, J., Neelemens, L., and Warzee, M., *Corrosion Science*, Vol. 3, 1963, p. 239.
[*18*] Defranoux, J. M., *Corrosion Science*, Vol. 3, 1963, p. 75.
[*19*] Pourbaix, M., *Corrosion*, Vol. 26, 1970, p. 431.

Florian Mansfeld[1] *and J. V. Kenkel*[1]

Laboratory Studies of Galvanic Corrosion of Aluminum Alloys

REFERENCE: Mansfeld, Florian and Kenkel, J. V., "**Laboratory Studies of Galvanic Corrosion of Aluminum Alloys,**" *Galvanic and Pitting Corrosion—Field and Laboratory Studies, ASTM STP 576,* American Society for Testing and Materials, 1976, pp. 20–47.

ABSTRACT: In a systematic study of galvanic corrosion of aluminum alloys the effects of the dissimilar metal, the solution composition, and area ratio have been evaluated using galvanic current and weight loss measurements. In 3.5 percent sodium chloride, galvanic corrosion rates of the aluminum alloys 1100, 2024, 2219, 6061, and 7075 decrease with the nature of the dissimilar metal in the order: silver > copper > 4130 steel ≫ stainless steel ≈ nickel > Inconel 718 ≫ Ti-6Al-4V ≈ Haynes 188 > tin > cadmium. Coupling to zinc did not lead to cathodic protection of the aluminum alloys as shown by weight loss data, although the aluminum alloys were the cathode in the aluminum-zinc couple. The potential difference of uncoupled dissimilar metals has been found to be a poor indicator of galvanic corrosion rates. Dissolution rates of aluminum alloys coupled to a given dissimilar material are higher in 3.5 percent sodium chloride than in tap water and distilled water where they are found to be comparable. The effect of area ratio A^C/A^A has been studied in 3.5 percent sodium chloride for area ratios of 0.1, 1.0, or 10. The galvanic curent was found to be independent of the area of the anode, but directly proportional to the area of the cathode. The galvanic current density i_g^A with respect to the anode has been found to be directly proportional to the area ratio ($i_g^A = k_1 A^C/A^A$), while the dissolution rate r_A of the anode was related to area area ratio by $r_A = k_2 (1 + A^C/A^A)$. The results obtained have been explained based on mixed potential theory. Electrochemical methods for measurements of galvanic currents are described in the Appendix.

KEY WORDS: corrosion, aluminum alloys, galvanic corrosion

Accelerated corrosion of dissimilar metals which are electrically coupled and exposed to a corrosive environment is one of the most common and most severe forms of corrosion. Although the danger of galvanic corrosion has been recognized generally, very little work has been done to quantitatively measure the extent of corrosion of various galvanic couples and

---

[1] Member of technical staff and staff associate, respectively, Science Center, Rockwell International, Thousand Oaks, Calif. 91360.

use such measurements as a basis for a ranking of galvanic couples. Usually uncoupled metals and alloys instead of actual galvanic couples are ranked in a galvanic series according to their corrosion potentials in a given environment, for example, seawater [*1*].[2] While this type of classification of metals and alloys might be quite useful as an indication of general trends in galvanic corrosion, it cannot give an indication of the actual extent of galvanic corrosion when dissimilar materials are coupled. As pointed out recently [*2,3*], the magnitude of galvanic corrosion depends not only on the potential difference of dissimilar metals, but also on kinetic parameters such as corrosion rates or exchange current densities of the uncoupled materials and Tafel slopes, and on area ratios.

In light of the rather complicated interaction of reduction and oxidation reactions on coupled metals, it is important to measure directly the extent of galvanic corrosion of those materials which may come in electrical contact in various structures rather than rely on measurements of only one of the parameters involved, for example, potential differences. Various methods for measurements of galvanic current have been summarized in the Appendix. The authors have been using the zero impedance ammeter described by Lauer and Mansfeld [*4*] and applied in this laboratory to evaluation of inorganic conversion coatings on aluminum alloys [*5*] and to studies of the effect of metallic coatings on PH13-8Mo on galvanic corrosion of aluminum alloys in sodium chloride [*6*].

This paper summarizes results of a systematic investigation of galvanic corrosion in which the galvanic interaction of 20 metals and alloys have been measured in order to establish a galvanic series based on quantitative measurements of dissolution rates of the metals in a galvanic couple. Results for the 95 galvanic couples in which an aluminum alloy is one of the two dissimilar metals are summarized here for immersion in air-saturated 3.5 percent sodium chloride [*7*]. Also included are results of galvanic corrosion tests in tap and distilled water for some selected couples [*8*] and studies of the effect of area ratio [*9*].

Experimental

Materials and Test Method

Table 1 lists the materials studied. The specimens were flat coupons (1 by 3 in. by variable thickness). They were degreased for 5 min in boiling benzene, cleaned by conventional chemical methods, if necessary, and weighed to 0.1 mg. The specimens to be coupled were then placed into a lucite holder with a ½ by ½ by ⅛ in. lucite spacer between the specimens as described elsewhere [*5,6*]. About 20 cm^2 of each specimen were exposed to the electrolyte.[3] After assembly, the holder containing the specimens

---

[2] The italic numbers in brackets refer to the list of references appended to this paper.

[3] In studies of the effect of area ratio, this holder was not used.

TABLE 1—*List of materials studied.*

Ag (99.9%)
Cu (OFHC)
Ni 270
Sn (99.9999%)
Cd (99.98%)
Zn (99.9%)
Type 301 SS
Type 304L SS
Type 347 SS
PH13-8Mo
A286
4130 steel
Haynes 188
Inconel 718
Ti-6Al-4V
Al 1100-0
Al 2024-T851
Al 2219-T87
Al 6061-T651
Al 7075-T76

was placed in a solution of air-saturated 3.5 percent sodium chloride and the corrosion potential of the two uncoupled materials followed for 15 min immediately after immersion (all potentials refer to the saturated calomel electrode (SCE)). The specimens were then connected to the zero impedance ammeter [*4*] (see Fig. 15 in the Appendix). The output of this instrument, which is proportional to the galvanic current I_g, was connected to a two-pen strip-chart recorder. The potential ϕ_g of the couple was also recorded continuously for 24 h. From plots of galvanic current I_g versus time t, the average galvanic current density $\bar{i}_g = I_g/A$, where A is the area of the aluminum alloy tested, was calculated by graphical integration.

After the 24-h test, the aluminum alloys were deoxidized using a commercial cleaner, washed, dried, and weighed again. The weight loss caused by the deoxidizing treatment was also measured using separate uncorroded aluminum specimens, and this correction was applied to the weight loss of the corroded specimen. If necessary, the other materials were freed of corrosion products using standard techniques (National Association of Corrosion Engineers Laboratory Corrosion Testing of Metals for the Process Industries (TM-01-69)). The corrected weight loss, the duration of the test, and the specimen area were used to calculate the dissolution rate r of the specimen in milligrams per square decimeters per day (mdd).

Results

Effect of the Dissimilar Metal [7]

Corrosion Parameters of Uncoupled Aluminum Alloys—All galvanic couples studied include one aluminum alloy. In order to relate galvanic couple data to corrosion parameters of aluminum alloys, the corrosion rates of uncoupled aluminum alloys were determined in 24-h immersion tests. Table 2 shows corrosion potentials Φ_{corr} (average of 19 tests, 15-min exposure) and corrosion rates r_0 (average of 3 tests, 24 h).

Galvanic Current Data—Typical galvanic current data are shown in Figs. 1 and 2. Figure 1 shows that the galvanic current I_g is appreciably higher when 7075 aluminum is coupled to copper than when it is coupled to Type 304 stainless steel (SS) or Ti-6Al-4V. When coupled to zinc, the

TABLE 2—*Corrosion potentials and corrosion rates of uncoupled aluminum alloys, 3.5 percent sodium chloride, 21 ± 1°C.*

Al Alloy	Φ_{corr} millivolt versus SCE	r_0, mdd
1100	− 756 ± 39	0.24
2024-T851	− 733 ± 4	5.25
2219-T87	− 724 ± 6	4.62
6061-T651	− 756 ± 28	0.56
7075-T76	− 814 ± 18	0.95

galvanic current is negative with respect to aluminum, because zinc was the anode in the galvanic couple. After an initial period of 2 h, the galvanic current remained more or less constant except for the couple involving cadmium, where the current increased constantly.

Despite the appreciable initial potential differences between 7075 aluminum and copper, Type 304 SS or Ti-6-4, respectively, the galvanic potentials of the corresponding couples with 7075 aluminum have similar values which are only slightly more noble than the corrosion potential of the uncoupled aluminum alloy (Fig. 1*b*) [7]. This is probably due to the fact that the pitting potential is also only slightly more noble than the corrosion potential of the aluminum alloys and the fact that the aluminum alloys cannot be polarized more noble than to the pitting potential.

Figure 2 shows that similar results are obtained when the five aluminum alloys are coupled to the same, more noble material, 4130 steel. A comparison of the curves in Fig. 2 with those in Fig. 1 shows that coupling of aluminum alloys to copper leads to higher galvanic currents than coupling to 4130 steel which in turn produces higher galvanic currents than the stainless steel and the titanium alloy.

Based on the galvanic current I_g versus time t traces the galvanic current density $\bar{i}_g$ with respect to the aluminum alloy in a galvanic couple has been calculated. Tables have been prepared [7] for each of the aluminum alloys studied in which the galvanic couples have been ranked according to the value of $\bar{i}_g$. Table 3 is an example for such a galvanic series; in this case, 6061 aluminum has been coupled to 19 dissimilar metals and alloys. Also listed in Table 3 are the corrosion potential differences $\Delta\phi^s$ of the two uncoupled metals before the start of the galvanic current test and the dissolution rates r_A based on weight loss data (see following section). The overall ranking in the last column of Table 3 is obtained by a ranking of all 95 couples studied (for details, see Ref 7).

Weight Loss Data—The dissolution rate r_A of the aluminum alloy in the galvanic couples as calculated from weight loss data has also been listed in Table 3.

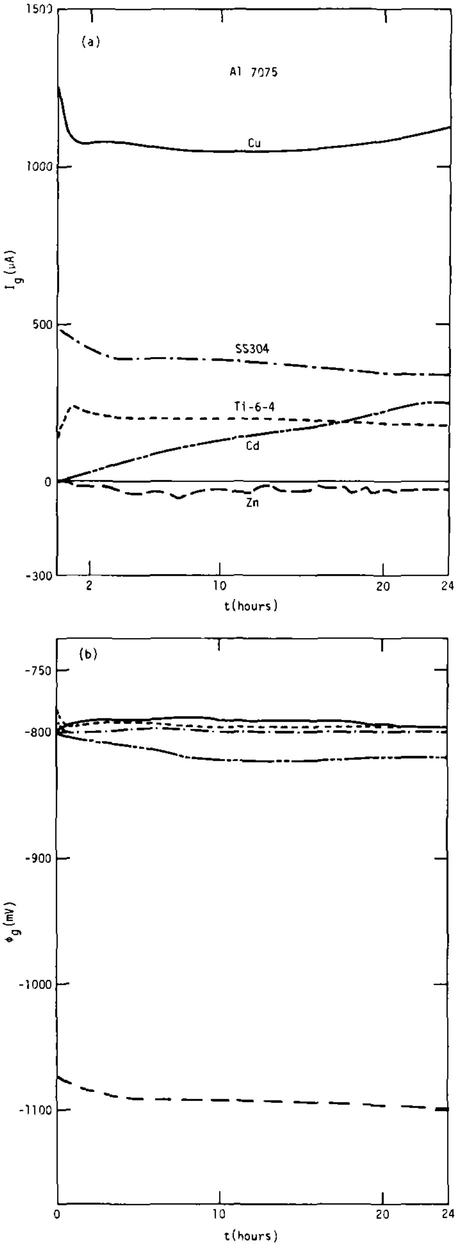

FIG. 1—*Time behavior of the galvanic current* I_g *for aluminum 7075 coupled to copper, Type 304L SS, Ti-6Al-4V, cadmium, or zinc in 3.5 percent sodium chloride.*

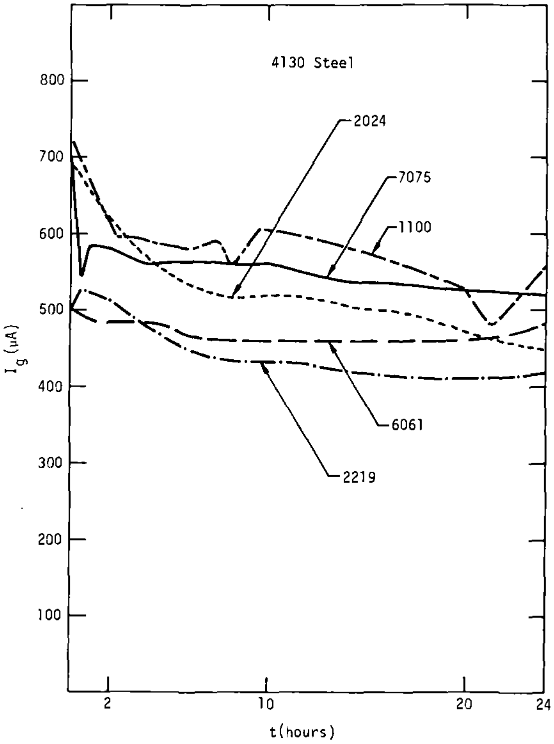

FIG. 2—*Time behavior of the galvanic current* I_g *for aluminum alloys coupled to 4130 steel in 3.5 percent sodium chloride.*

Only very small weight changes were recorded for silver, copper, nickel, the stainless steels, Ti-6Al-4V, Haynes 188, and Inconel 718. The 4130 steel was covered with rust after galvanic tests; after removal of corrosion products, weight gains or weight losses were found (−7 to +8 mdd). The dissolution rates for tin ranged between 0 and 5 mdd, those for cadmium between 5 and 22 mdd, and those for zinc between 90 and 175 mdd depending on the type of aluminum alloy to which these materials had been coupled.

In all cases, silver, copper, and 4130 steel have the greatest accelerating effect on corrosion of the aluminum alloys, followed by the stainless steels, nickel, and Inconel 718. The group which has least effect includes the titanium alloy, Haynes 188, tin, cadmium, and zinc. A ranking of metals and alloys with respect to the corrosive damage aluminum alloys suffer when coupled to these materials would be for all aluminum alloys studied: silver > copper > 4130 $\gg$ stainless steels $\approx$ nickel, Inconel 718 $\gg$ Ti-6-4 $\approx$ Haynes 188 > tin > cadmium. It will be noted that for all aluminum alloys, dissolution rates are increased when the aluminum

TABLE 3—*Galvanic series for aluminum 6061-T651 in 3.5 percent sodium chloride*, r_0 = *0.56 mdd.*

	Coupled to	$\bar{i}_g$, µA/cm²	r_A, mdd	$\Delta\phi^s$ mV	Overall Number
1	Ag	54.5	65.6	−721	2
2	Cu	43.6	47.7	−507	7
3	4130	24.3	27.0	−205	14
4	Ni	21.9	29.7	−481	16
5	PH13-8Mo	16.0	19.8	−664	25
6	A286	14.7	18.7	−704	27
7	Type 347 SS	14.1	21.2	−653	28
8	Type 301 SS	12.4	17.3	−672	36
9	Type 304L SS	11.3	16.1	−679	42
10	Inco 718	8.1	7.0	−556	53
11	Ti-6-4	5.2	8.3	−510	59
12	Haynes 188	5.0	7.7	−543	60
13	Al 2219	3.1	−0.5[a]	−99	66
14	Al 2024	1.95	10.0	−6	71
15	Sn	1.59	5.9	−183	72
16	Al 1100	0.66	3.7	−68	75
17	Cd	0.28	4.0	−95	77
18	Al 7075	−0.66	−1.4[a]	+36	81
19	Zn	−1.51	6.6	+298	85

[a] Negative values of r_A correspond to weight gain.

alloys are coupled to zinc, although galvanic currents are negative. A ranking according to corrosion potentials of uncoupled alloys would have led to: stainless steels > silver > Inconel 718 > nickel > copper > Haynes 188 > Ti-6-4 > tin > 4130 > cadmium > zinc.

Effect of Corrosive Environment

Having studied the effect of the dissimilar metal, it seemed also of interest to investigate the effect of the corrosive environment [*8*]. From the many possible electrolytes tap and distilled water were chosen due to the obvious practical applications involving galvanic couples. Distilled water was of additional interest since only dissolved oxygen and the water molecule can, at least initially, react on the surface of the dissimilar metals. The very low conductivity of distilled water did not represent an experimental problem; due to the characteristics of the zero impedance ammeter, the potential difference of coupled dissimilar metals was less than 0.1 mV, even in distilled water.

Galvanic Corrosion Data—Typical galvanic current data obtained in tap water are shown in Fig. 3*a* for 2024 aluminum coupled to copper, Type 304L SS, Ti-6Al-4V, or zinc. Similar to the results in 3.5 percent sodium chloride, higher galvanic currents were observed for all aluminum alloys tested when the aluminum alloy was coupled to copper than when it was coupled to Type 304L SS or Ti-6Al-4V. For the aluminum-zinc couples a

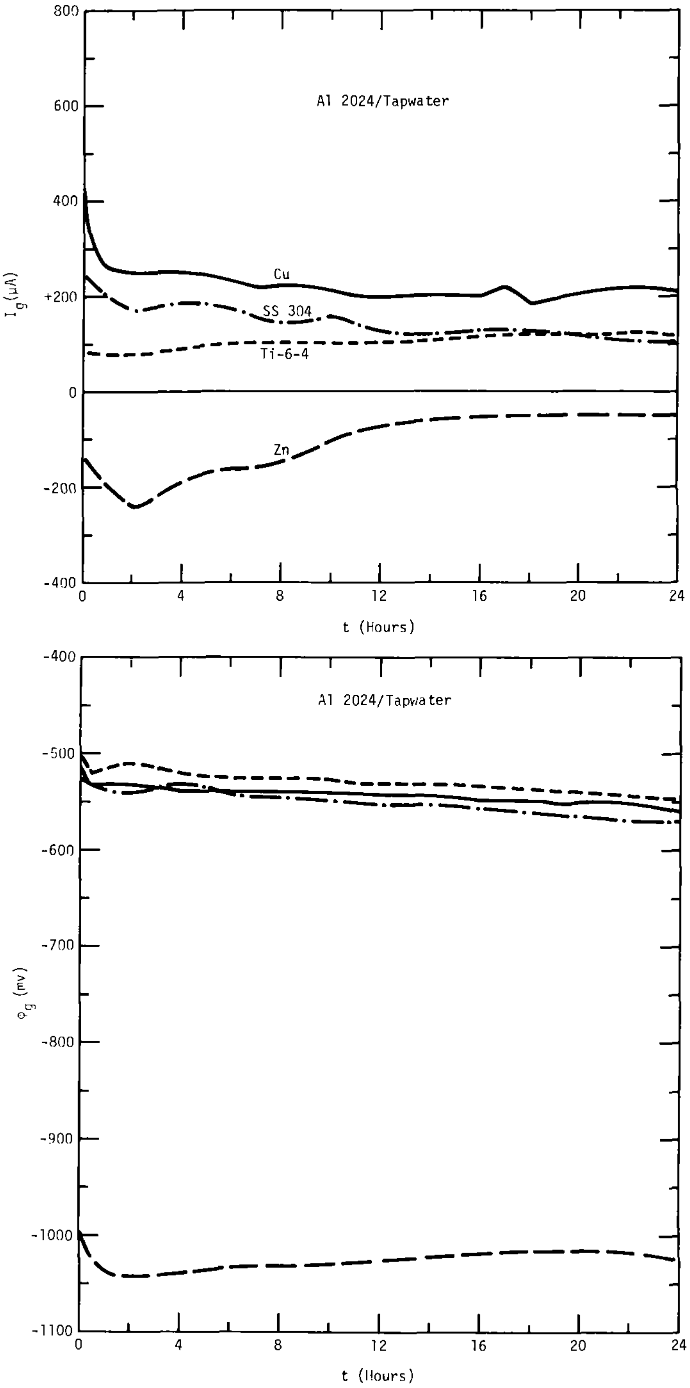

FIG. 3—*Time behavior of galvanic current* I_g *for* (a) *Aluminum 2024 coupled to copper, Type 304L SS, Ti-6Al-4V, or zinc in tap water, and* (b) *for galvanic potential* Φ_g.

negative galvanic current I_g was observed due to the fact that zinc was the anode in the galvanic couple.

Despite the appreciable potential differences between uncoupled aluminum alloys and copper, Type 304L SS or Ti-6Al-4V, the galvanic potentials Φ_g of the corresponding couples were always very close to the corrosion potential of an uncoupled aluminum alloy, Fig. 3*a*. The difference between the corrosion potential of an uncoupled aluminum alloy and the initial galvanic potential was found to be larger in tap water than in 3.5 percent sodium chloride. For couples involving zinc, the galvanic potential was found to be slightly more noble than the corrosion potential of the uncoupled zinc. The changes of the galvanic potential ϕ_g in tap water with time were small in all cases.

In experiments in distilled water, much larger changes of galvanic current I_g and galvanic potential ϕ_g as a function of time were observed than in 3.5 percent sodium chloride or tap water. Figure 4*a* shows the time dependence of the galvanic current I_g for galvanic couples involving aluminum 2024 in distilled water. Similar to results in tap water (Fig. 3*a*), the galvanic current decreases in the order copper > Type 304 SS > Ti-6Al-4V, while for the aluminum-zinc couples the galvanic current was negative. The time-dependence of the galvanic potential ϕ_g is very different in distilled water compared to tap water, values of ϕ_g becoming more active (negative) during the test and showing larger differences for different cathode materials. The reason for the large shift of Φ_g (Fig. 4*b*) was found to be due to large shifts of the corrosion potential of the aluminum alloys in the negative direction during the galvanic current test. Similar behavior was observed for 4130 steel and zinc, while the corrosion potentials of copper, Type 304L SS, and Ti-6Al-4V did not change much.

Figure 5 shows a comparison of galvanic current data in tap water (Fig. 5*a*) and distilled water (Fig. 5*b*) for aluminum alloys coupled to 4130 steel. In tap water the steel is the anode when coupled to aluminum 7075, while in distilled water it is the anode when coupled to aluminum 1100; in all other cases, it is the cathode material.

Figure 6 shows a comparison of galvanic current measurements for aluminum 7075/copper in 3.5 percent sodium chloride, tap water, and distilled water. The average galvanic current density $\bar{i}_g$ is much higher in 3.5 percent sodium chloride than in tap water and distilled water. In the latter two solutions, the average galvanic current density values of $\bar{i}_g$ are comparable. Note the different time behavior of the galvanic current in tap water and distilled water.

The average galvanic current density $\bar{i}_g$ with respect to the aluminum alloy as determined from graphical integration of the $\bar{i}_g$ versus time curves and the initial potential difference $\Delta\Phi^s$ between the two dissimilar metals before coupling have been listed in tables for the five aluminum alloys tested in tap water and distilled water in Ref *8*.

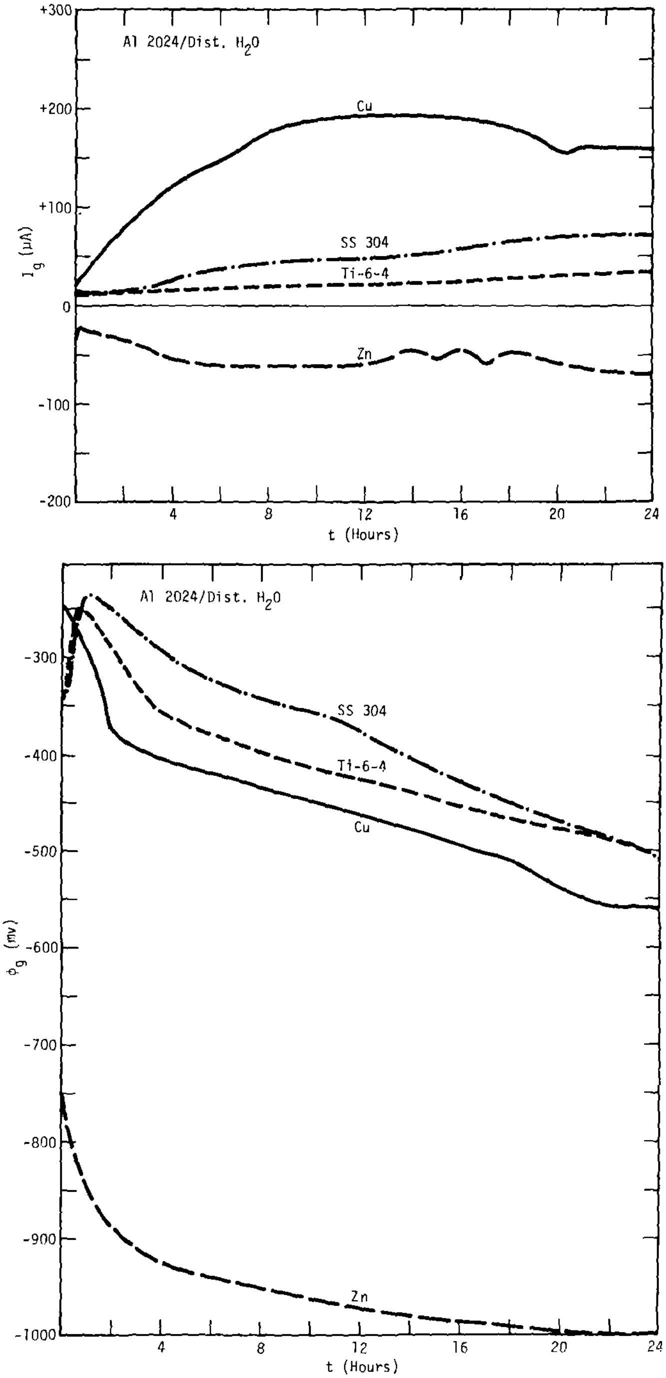

FIG. 4—*Time behavior of galvanic current for* (a) *aluminum 2024 coupled to copper, Type 304L SS, Ti-6Al-4V, or zinc in distilled water, and* (b) *galvanic potential* ϕ_g.

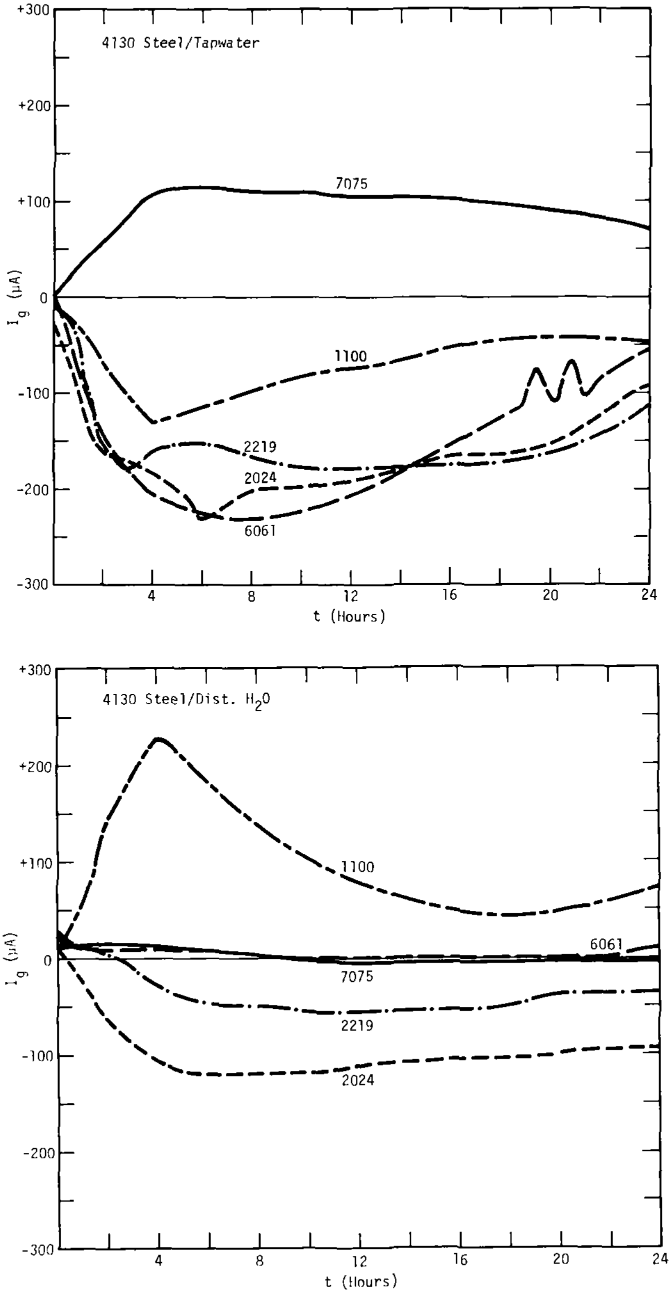

FIG. 5—*Galvanic current data for aluminum alloys coupled to 4130 steel:* (a) *tapwater and* (b) *distilled water.*

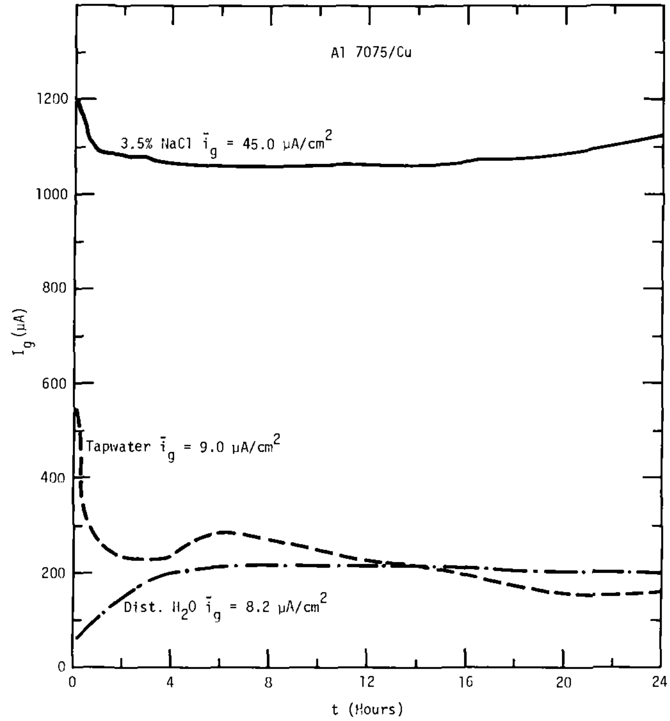

FIG. 6—*Comparison of galvanic currents in 3.5 percent sodium chloride, tap water and distilled water for aluminum 7075/copper.*

Weight Loss Data—Table 4 is a summary of weight loss data recorded for aluminum alloys coupled to 4130 steel in 3.5 percent sodium chloride, tap water, and distilled water. The increase of dissolution rates $r_A - r_0$ over the corrosion rate r_0 of uncoupled aluminum alloys is very pronounced in 3.5 percent sodium chloride due to pitting attack of the aluminum alloys caused by polarization in the noble direction. In tap water and distilled

TABLE 4—*Increase of dissolution rates* $r_A - r_0$ *(mdd) of aluminum alloys due to galvanic coupling to 4130 steel in 3.5 percent sodium chloride, tap water, and distilled water.*

	3.5% NaCl	Tap Water	Distilled Water
Al 1100	30.0	3.4	8.1
Al 2024	32.8	−2.4[a]	−4.7
Al 2219	34.1	0.5	4.7
Al 6061	26.4	−2.8	−1.4
Al 7075	25.0	−6.9	−3.7

[a] Negative values refer to weight gain.

water small weight losses or gains have been recorded, while galvanic current measurements have shown (Fig. 5) that depending on the couple and the environmental studied, the aluminum alloy can be either the anode or the cathode.

Only very small weight changes were recorded for Type 304L SS, copper, or Ti-6Al-4V. For 4130 steel the dissolution rates in tap water and distilled water were higher than in 3.5 percent sodium chloride due to the lack of cathodic protection by the aluminum alloys as discussed elsewhere [*10*]. The dissolution rates of zinc were high in all media studied since zinc was the anode in all cases.

Effect of Area Ratio [9]

Materials and Test Methods—In the study of the effect of the area ratio on galvanic corrosion of aluminum alloys, the aluminum alloys 2024-T841 and 7075-T76 were coupled to copper stainless steel Type 304L, 4130 steel, Ti-6Al-4V, cadmium, or zinc in air-saturated 3.5 percent sodium chloride at 21 ± 1°C. Flat specimens were prepared so that an area of about 2 or 20 cm^2 was exposed to the electrolyte. Area ratios used were approximately 0.1, 1.0, or 10. Weight loss data for the materials in a given couple were used to calculate dissolution rates of anode and cathode as a function of area ratio.

Galvanic Current Data—Figure 7*a* shows galvanic current I_g minus time traces recorded for the aluminum 2024-copper couple for area ratios $A^C/A^A = 0.1, 1, \text{or } 10$. For area ratios of $A^{\text{Cu}}/A^{\text{Al}} = 1$ or 10 the area of the copper electrode was kept constant at about 20 cm^2 while for $A^{\text{Cu}}/A^{\text{Al}} = 0.1$ the area of copper was about 2 cm^2. Figure 7*a* shows that under these conditions the galvanic current I_g is independent of area ratio for $A^{\text{Cu}}/A^{\text{Al}} = 1$ or 10, but decreases by about a factor of 10 for $A^{\text{Cu}}/A^{\text{Al}} = 0.1$.

When the galvanic current data are replotted as galvanic current density i_g versus time, different behavior is observed for the galvanic current density $i_g{}^{\text{Al}} = I_g/A^{\text{Al}}$ and $i_g{}^{\text{Cu}} = I_g/A^{\text{Cu}}$. Figure 7*b* shows that the galvanic current density $i_g{}^{\text{Al}}$ with respect to the aluminum alloy (the anode) increases by about a factor of 10 when the area ratio $A^{\text{Cu}}/A^{\text{Al}}$ is increased by a factor of 10. The galvanic current density $i_g{}^{\text{Cu}}$ with respect to copper (the cathode) seems to be independent of area ratio (Fig. 7*c*); $i_g{}^{\text{Cu}}$ is negative, since copper is the cathode in the aluminum 2024-copper couple. Similar results were obtained for the other galvanic couples studied.

Weight Loss Data—For all galvanic couples in which the aluminum alloys were the anodes, the dissolution rate r_A calculated from weight loss data increases with increasing area ratio A^C/A^A. For the couples aluminum 2024/cadmium, aluminum 2024/zinc, and aluminum 7075/zinc, in which the aluminum alloy was the cathode, no systematic changes with area ratio were observed for galvanic current or weight loss data. As observed earlier

(Table 3) coupling to zinc did not result in cathodic protection of aluminum 2024 or 7075, but accelerated corrosion.

Discussion

Theoretical Considerations

A general discussion of the factors determining the rate of galvanic corrosion has been given earlier [*2,3*] for the cases of charge transfer and diffusion control. A more detailed analysis will be given here for the case of diffusion control in order to be able to discuss the experimental data.

For the discussion of galvanic corrosion under diffusion control of the cathodic reaction it is assumed that the only reaction occurring on the cathode at the galvanic potential ϕ_g is reduction of oxygen. The galvanic current I_g is then equal to the difference between the anodic and cathodic currents for the anode and equal to the cathodic current for the cathode at the potential of the couple ϕ_g

$$I_g = I_a^A(\phi_g) - I_c^A(\phi_g) = I_c^C(\Phi_g) \tag{1}$$

where I_a^A and I_c^A are the anodic and cathodic current for the anode and I_c^C is the cathodic current for the cathode. Equation 1 can be written in terms of current densities and area A^A and A^C of anode and cathode, respectively

$$i_g^A A^A = i_a^A A^A - i_c^A A^A = i_c^C A^C \tag{2}$$

Due to diffusion control

$$i_c^A = i_c^C = i_{O_2}^L \tag{3}$$

where $i_{O_2}^L$ is the limiting current density for oxygen reduction. Combined with Eq 2, this leads to

$$i_g^A = i_a^A - i_{O_2}^L = i_{O_2}^L(A^C/A^A) \tag{4}$$

Since, for diffusion control

$$i_{O_2}^L = i_{\text{corr}}^A \tag{5}$$

Eq 4 can also be written as

$$i_g^A = i_a^A - i_{\text{corr}}^A \tag{6}$$

According to Eq 6, the galvanic current density i_g^A is a measure of the galvanic effect, which is the increase of the anodic dissolution current density i_a^A of the anode due to galvanic coupling over its corrosion current density i_{corr}^A. Equation 6 can be used to compare galvanic current data with dissolution rates in the form

$$i_g^A = k(r_A - r_0) \tag{7}$$

using Faraday's law.

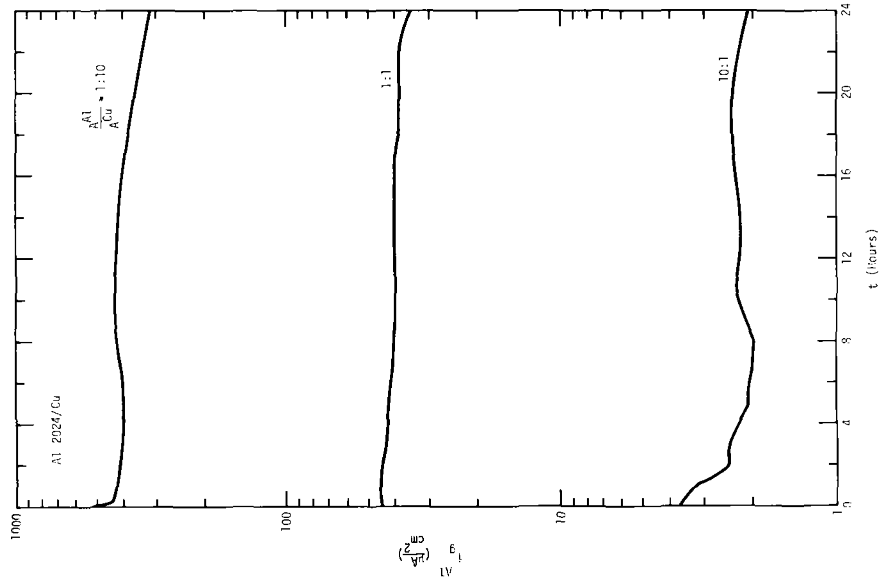
Al 2024/Cu
A^{Al}/A^{Cu} = 1:10
1:1
10:1
i_g^{Al} ($\mu A/cm^2$)
1000
100
10
1
t (Hours)
0
4
8
12
16
20
24

(a)

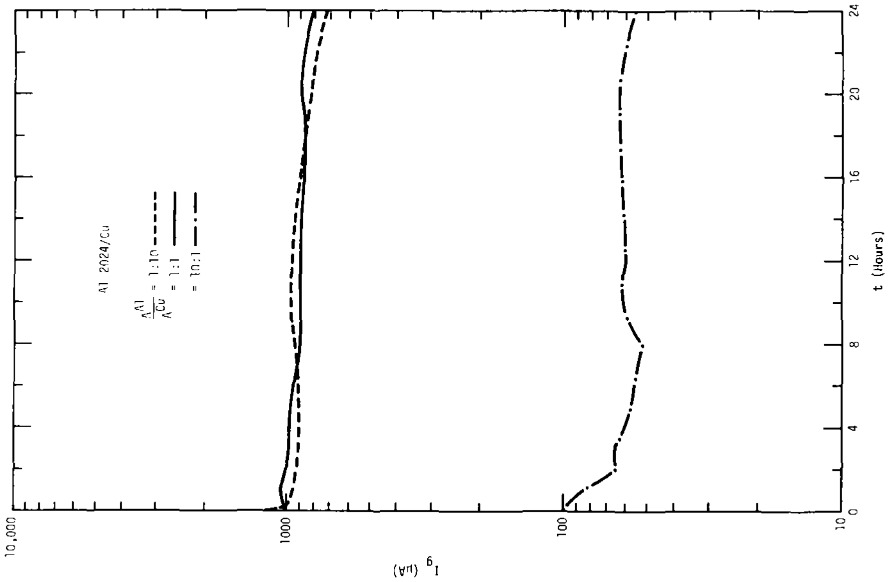
Al 2024/Cu
A^{Al}/A^{Cu} = 1:10
= 1:1
= 10:1
I_g (μA)
10,000
1000
100
10
t (Hours)
0
4
8
12
16
20
24

(b)

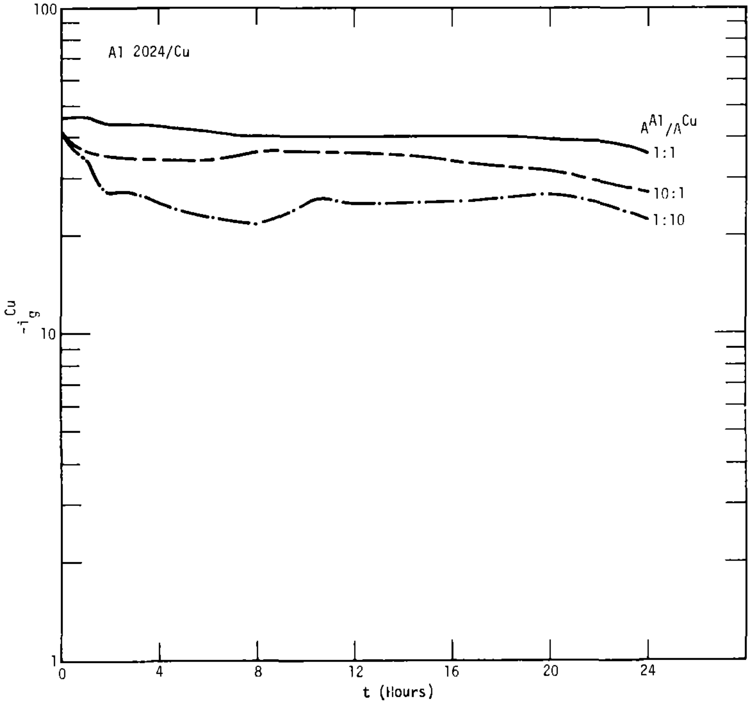

(c)

FIG. 7—*Galvanic current data for aluminum 2024/copper in 3.5 percent sodium chloride;* (a) *galvanic current* I_g, (b) *galvanic current density* i_g^{Al} *with respect to aluminum 2024, and* (c) *galvanic current density* i_g^{Cu} *with respect to copper.*

Figure 8 shows a plot of the average galvanic current density $\bar{i}_g$ with respect to the aluminum alloy against the difference of dissolution rates $r_A - r_0$ for coupled (r_A) and uncoupled (r_0) aluminum alloys determined from weight loss data for the 95 galvanic couples studied in 3.5 percent sodium chloride [7]. Each data point represents a different galvanic couple. Most points fall close to a straight line with a slope of 0.8 $\mu A/cm^2 \times$ mdd. The theoretical slope for pure aluminum would be 1.24 $\mu A/cm^2 \times$ mdd. The observed deviation is most likely due to the fact that aluminum alloys containing copper (1 $\mu A/cm^2$ = 2.85 mdd) and zinc (1 $\mu A/cm^2$ = 2.93 mdd) were studied rather than pure aluminum. A correction for aluminum-copper or aluminum-zinc would move the theoretical slope closer to the one observed experimentally. Similar correlations have been obtained in tap water and distilled water [8].

Rearrangement of Eq 4 leads to

$$i_a^A = i_{O_2}^L + i_{O_2}^L A^C/A^A = i_{O_2}^L(1 + A^C/A^A) \qquad (8)$$

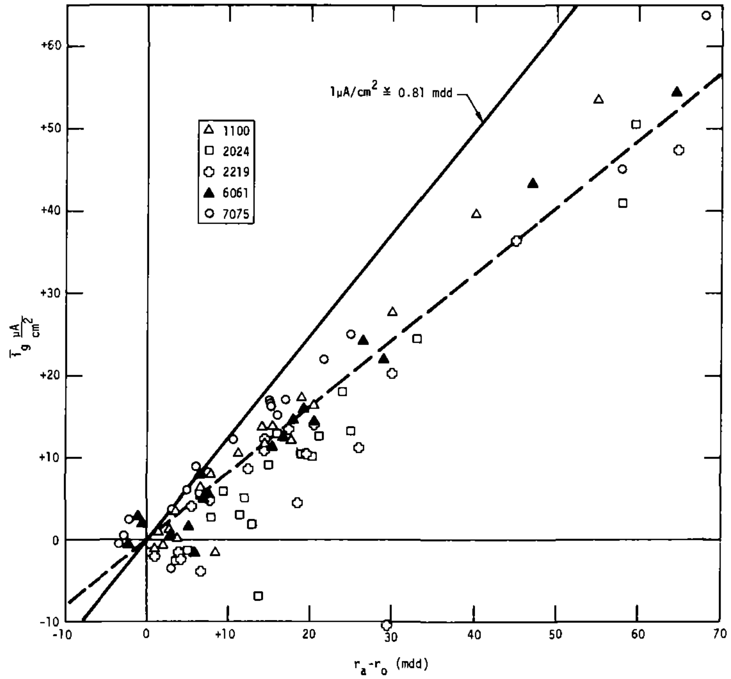

FIG. 8—*Correlation between the average galvanic current density* i_g *and increase of dissolution rates* $r_A - r_g$ *due to coupling.*

which is the so-called "catchment principle" according to which the dissolution rate of the anode in a galvanic couple is proportional to the area ratio A^C/A^A.

The relationship between the galvanic current density i_g^A and the area ratio is also given by Eq 4 as

$$i_g^A = i_{0_2}^L A^C/A^A \tag{9}$$

From Eq 8 it follows that the galvanic current I_g is proportional to the area A^C of the cathode and independent of the area of the anode

$$i_g^A A^A = I_g = i_{0_2}^L A^C \tag{10}$$

Equation 10 explains the results in Fig. 7*a*, where for $A^{Al}/A^{Cu} = 0.1$ and 1 the galvanic current I_g was independent of area ratio. For these two area ratios the area of copper (A^C) had been held constant. To obtain an area ratio $A^{Al}/A^{Cu} = 10$ the area of copper was reduced by a factor of 10, and consequently the galvanic current was lower by about a factor of 10.

According to Eq 9 the galvanic current density i_g^A with respect to the anode is directly proportional to the area ratio A^C/A^A. This is qualitatively confirmed by the data in Fig. 7*b* which show an increase of i_g^{Al} with A^{Cu}/A^{Al}.

A plot of log i_g^{Al} versus log A^C/A^A according to Eq 9 results in a straight line with a slope of one for both aluminum 2024 and aluminum 7075 (Fig. 9). The data for aluminum 2024/cadmium, aluminum 2024/zinc, and aluminum 7075/zinc have been omitted from Fig. 9 since in these couples the aluminum alloys were the cathodes. The different values of i_g^{Al} at a constant value of A^C/A^A are assumed to result from the fact that contrary to the normal assumption, that the limiting diffusion current density $i_{O_2}{}^L$ is independent of cathode material (Eq 3), experimental values of $i_{O_2}{}^L$ are found to be dependent on the nature of the cathode. Mansfeld and Parry [5] have shown, based on potentiostatic polarization curves, that in 3.5 percent sodium chloride $i_{O_2}{}^L$ is larger for Type 304 SS than for Ti-6Al-4V. The decrease of the galvanic current density i_g^A at a given area ratio in the order copper > 4130 > Type 304L stainless steel > Ti-6Al-4V > cadmium is then related to a corresponding decrease of $i_{O_2}{}^L$. Based on experimental evidence, Eq 3 is not exactly fulfilled and Eq 9 has to be rewritten as

$$i_g^A = i_{O_2}{}^{L,C} \frac{A^C}{A^A} \qquad (11)$$

where $i_{O_2}{}^{L,C}$ is the material-dependent limiting current density for oxygen diffusion.

The dissolution rates calculated from the weight loss data for the aluminum alloys in galvanic couples have been plotted versus $1 + A^C/A^A$ in

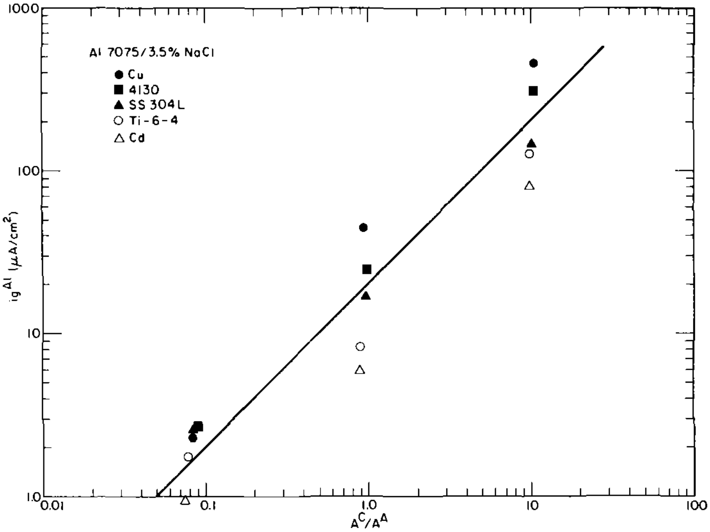

FIG. 9—*Dependence of galvanic current density* i_g *aluminum on area ratio* A^C/A^A *for aluminum 7075 in 3.5 percent sodium chloride.*

log-log plots in Fig. 10 for aluminum 7075. The approximately straight line relationship with a slope of one confirms Eq 8 since the dissolution current density i_a^A is related to the dissolution rate r_A by Faraday's law. The dependence of dissolution rates on cathode material at a constant area ratio has to be explained as was shown in Eq 11. For material-dependent cathodic current density $i_{O_2}^{L,C}$ the catchment principle has to be expressed as

$$i_a^A = i_{O_2}^{L,A} + i_{O_2}^{L,C} \frac{A^C}{A^A} \tag{12}$$

Based on these relationships which are confirmed by the experimental result presented here, the dissolution rate of an anode in a galvanic couple can be calculated for any area ratio if it has been measured for one area ratio, for example, of one.

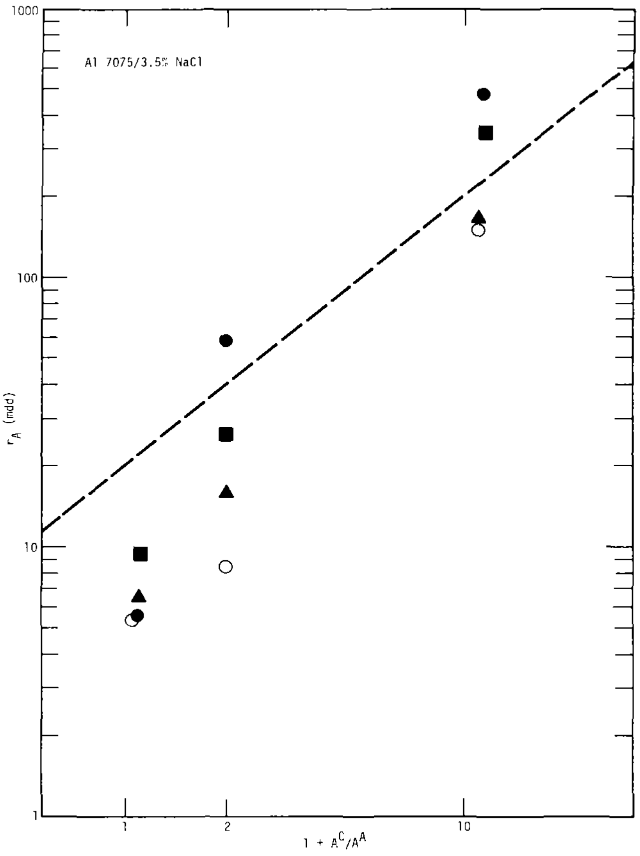

FIG. 10—*Dependence of dissolution rates* r_A *on area ratio* A^C/A^A *for aluminum 7075.*

Effect of Environment

The main difference between the effect of sodium chloride, tap water, and distilled water on galvanic corrosion of aluminum alloys seems to be the fact that due to the high chloride content in 3.5 percent sodium chloride the pitting potential of aluminum alloys is only slightly more noble than the corrosion potential. Potentiostatic polarization studies with ohmic-drop compensation in tap water [11] have shown that the pitting potential in tap water is much more noble than in 3.5 percent sodium chloride while in distilled water pitting does not occur. The aluminum alloys can, therefore, not be polarized more noble than their pitting potential and consequently dissolve with high rates due to pitting. In tap water and distilled water, polarization to more noble potentials is possible, and changes in polarity of the dissimilar metals in a galvanic couple are also possible as seen for aluminum alloy/4130 steel couples (Fig. 5) [8].

Undoubtedly, some of the many substances contained in Thousand Oaks, Calif., tap water can and will influence the rate of electrochemical reactions occurring on the metals studied. The details of such effects have not been studied, however.

Effect of Potential Difference Between Dissimilar Metals

It is often assumed that the rate of galvanic corrosion can be judged based on the difference of the corrosion potential of uncoupled dissimilar metals. For a diffusion controlled cathodic process the dissolution rate of the anode in a galvanic couple should, however, be independent of the nature of the cathode and therefore also independent of the potential difference between anode and cathode. As pointed out previously, the diffusion current density $i_{O_2}^L$ has been found to be material dependent to some extent, most likely due to the formation of surface films which change the ratio D/δ of diffusion coefficient D for oxygen and diffusion layer thickness δ. Due to this fact, a material dependence of the rate of galvanic corrosion could be experimentally observed, which in turn could be interpreted incorrectly as being due to the difference of corrosion potentials $\Delta\phi^s$ of the uncoupled dissimilar metals.

The experimental data of this study [7] have been plotted in Fig. 11 as i_g^A versus $\Delta\phi^s = \Phi_{\text{corr}}^C - \phi_{\text{corr}}^A$ for the 95 galvanic couples studied in 3.5 percent sodium chloride. In Fig. 12 the relative increase of dissolution rates $(r_A - r_0)/r_0$ due to coupling has been plotted versus $\Delta\phi^s$ using weight loss data.

Figure 11, which represents the absolute increase of dissolution rates due to coupling ($\bar{i}_g = k(r_A - r_0)$, Eq 7), and Fig. 12, which represents the relative increase of dissolution rates with respect to the corrosion rate of the uncoupled aluminum alloy, show that the initial potential difference $\Delta\phi^s$ of uncoupled metals cannot be used as a reliable indicator of the extent of galvanic corrosion. While one can distinguish two groups of data in

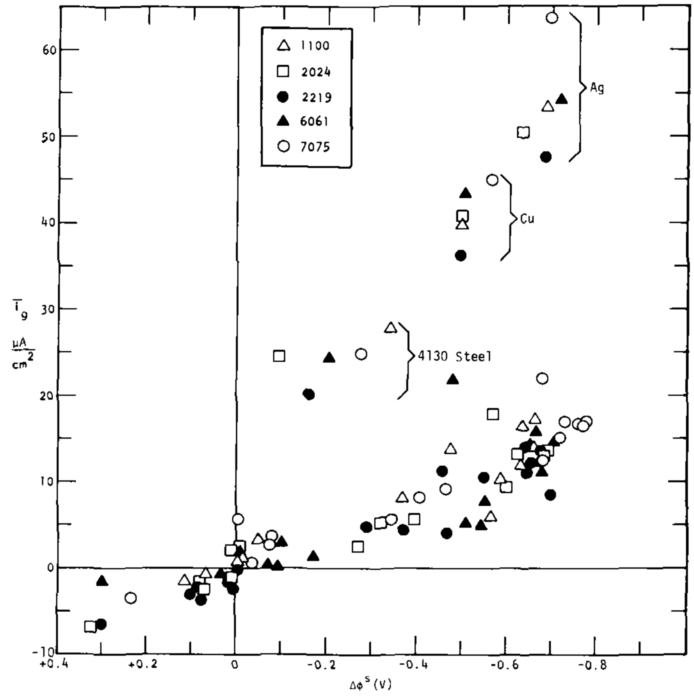

FIG. 11—*Average galvanic current density* $\bar{i}_g$ *as a function of difference* $\Delta\phi^s$ *of corrosion potentials of uncoupled materials.*

Fig. 11 which show a general increase of the galvanic current density with increasing potential difference $\Delta\phi^s$, a measurement of $\Delta\phi^s$ alone cannot give information about the rate of galvanic corrosion to be expected for a given galvanic couple. Figure 12 shows that for $\Delta\Phi^s$ values between -600 and -700 mV, the relative increase of dissolution rates can be between 3 and 5 for aluminum 2219 and 2024, but between 60 and 230 for aluminum 1100. One can also find a relative increase of about 46 at $\Delta^s\phi = -200$ mV and a relative increase of dissolution rates of only 10 at $\Delta\phi^s = -550$ mV for aluminum 6061. Galvanic series based on corrosion potentials of uncoupled materials have, therefore, to be considered as only very qualitative guidelines.

The effect of the dissimilar metals is shown clearly if galvanic current data, which represent the absolute increase of the dissolution rate of the aluminum alloy over the corrosion rate of the uncoupled alloy, are considered. The large effect of silver, copper, and 4130 steel can be recognized in Fig. 11 where the five aluminum alloys studied appear in clusters at $\Delta\phi^s = -630$ to -720 mV (silver), at $\Delta\phi^s = -500$ to -570 mV (copper) and $\Delta\phi^s = -90$ to -340 mV (steel 4130). A second group of galvanic couples

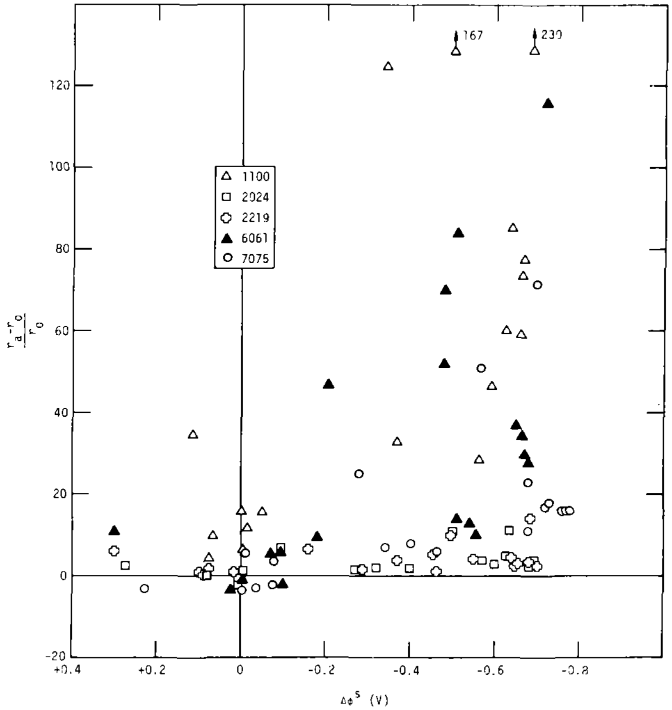

FIG. 12—*Relative increase* $r_A - r_0/r_0$ *of dissolution rates of aluminum alloys* (*weight loss data*) *as a function of* $\Delta\phi^s$.

ranges from couples involving zinc and aluminum alloys of different composition, where galvanic currents are negative with respect to the aluminum alloys, to couples involving the stainless steels and nickel ($\Delta\phi^s$ = −600 to −800 mV). Couples involving Ti-6Al-4V, Haynes 188, Inconel 718, tin, and cadmium fall between these two extremes.

Ranking of Galvanic Couples

The results obtained have shown that reliable classification of galvanic couples can only be achieved if kinetic data such as galvanic current data are collected for the couples of interest. The galvanic couples can then be ranked according to the absolute increase of dissolution rates ($\bar{i}_g$) (see Ref 7) or the relative increase of dissolution rates ($r_A - r_0/r_0 = \bar{i}_g/i_{\text{corr}}^A$). The continuous monitoring of galvanic currents has the advantage over weight loss data that dissolution rates can be followed as a function of time with great accuracy (fractions of microamperes to many milliamperes can be accurately measured). Problems of removal of corrosion products before reweighing after the test are avoided.

TABLE 5—*Compatibility of aluminum alloys and dissimilar materials.*

Class	Al 1100	Al 2024	Al 2219	Al 6061	Al 7075
I Compatible	Cd	Cd, 7075, 1100, Sn, Haynes. 2219, Ti-6-4, 6061, Zn, Inco 718, PH13-8Mo, Type 347 SS, A286, Type 304 SS, Ni, Type 301 SS	Cd, 2024, 6061, 1100, Haynes, 7075, Zn, PH13-8Mo, Type 301 SS, Type 304 SS, A286, Inco 718, Ti-6-4, Type 347 SS	7075, 2219, 2024	1100, 6061, 2024, Zn, 2219
II Borderline	2024, 6061, 2219	4130, Cu, Ag	Ni, Zn, 4130, Cu, Ag	1100, Cd, Sn, Inco 718, Zn, Haynes, Ti-6-4	Cd, Haynes, Sn, Ti-6-4, Inco 718
III Incompatible	Sn, 7075, Haynes, Ti-6-4, Zn, Inco 718, A286, Type 304 SS, PH13-8Mo, Type 301 SS, 4130, Cu, Ag			Type 304 SS, Type 301 SS, A286, PH13-8Mo Type 347 SS, 4130, Ni, Cu, Ag	Type 304 SS, Type 347 SS, PH13-8Mo, Type 301 SS, A286, Ni, 4130, Cu, Ag

General Classification

If the general compatibility of an aluminum alloy with other materials is of interest, then the relative increases of dissolution rates should be considered. In Table 4 compatibility of the five aluminum alloys with the 15 other materials is indicated by placing the dissimilar materials in three classes according to relative increases of dissolution rates $r_A - r_0/r_0 = \bar{i}_g/i_{\text{corr}}^A$ below 5 (Class I), between 5 and 15 (Class II), and above 15 (Class III).

Table 5 shows that under this classification aluminum 1100 is compatible only with cadmium, aluminum 6061 only with the aluminum alloys 7075, 2219, and 2024, while aluminum 7075 is compatible only with zinc and the other aluminum alloys tested. The aluminum alloys 2024 and 2219 are compatible with most materials tested, borderline cases involve 4130 steel, copper, and silver (and nickel and zinc for aluminum 2219), no combinations have been found to be incompatible based on the present criteria. These criteria have been arbitrarily selected and might have to be modified for special applications.

Acknowledgments

This work has been funded by the Rockwell International IR & D Interdivisional Technology Panel under sponsorship of the Corrosion Panel.

APPENDIX

Instrumentation for Measurements of Galvanic Currents

The following describes some of the methods which can be used to measure the galvanic current flowing between two dissimilar metals which are electrically coupled and immersed in an electrolyte.

Voltage Drop Across a Resistor

Galvanic currents have been measured in the past by placing a small resistor between the two dissimilar metals to be coupled and measuring the voltage drop ΔV across the resistor R_m (Fig. 13*a*). This simple technique is not satisfactory because the two dissimilar metals in the galvanic couple are not at the same potential, but are separated by the voltage $\Delta V = I_g' R_m$, where I_g' is the current flowing between the two metals and R_m is the measuring resistor. The current I_g' measured is, therefore, always smaller than the galvanic current I_g.

An improved approach would limit the voltage drop ΔV to a fixed maximum value; for example, 1 mV, by adjusting R_m as the galvanic current changes by orders of magnitude. A difficulty might arise, however, when voltages smaller than 1 mV have to be accurately measured and recorded.

Similar objections can be raised against the use of a galvanometer, which generally has high internal resistance. In addition, it is desirable to record continuously the galvanic current with greater sensitivity which requires the use of amplifiers.

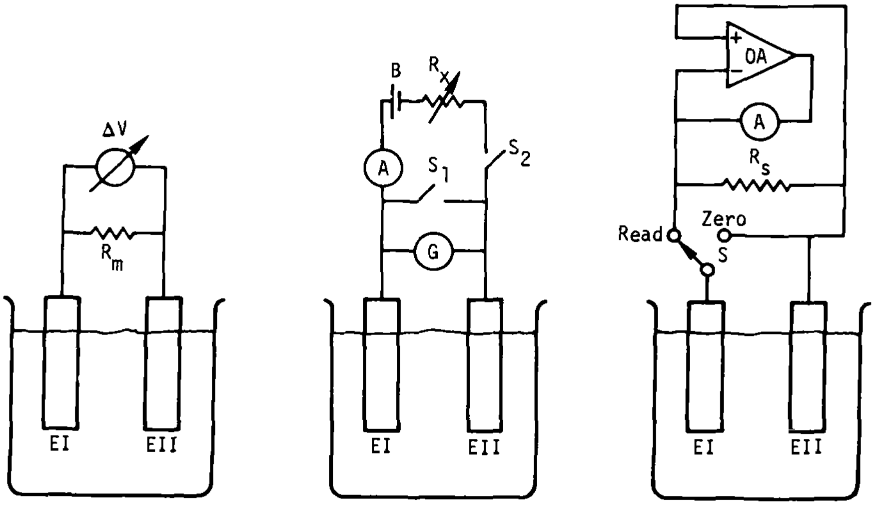

(a)
R_m = measuring resistor
ΔV = potential drop
EI, EII = dissimilar test materials

(b)
B = battery
R_x = variable resistance
S_1/S_2 = switches
A = ammeter
G = galvanometer

(c)
OA = operational amplifier
A = microammeter
R_s = standard resistor

FIG. 13—*Various techniques for galvanic current measurements:* (a) *voltage drop across resistor,* (b) *manual null balancing zero resistance ammeter* [13]; *and* (c) *electronic zero resistance ammeter with instantaneous null characteristics* [14].

In the past few years a number of new methods of electrochemical measurements of the galvanic current have been introduced which are summarized in the following.

Earlier Zero Resistance Ammeter Circuits (Manual Null Balancing)

Earlier attempts to eliminate the effect of a measuring resistor have been described by Brown and Mears [*12*] as shown in Fig. 13*b* [*13*]. If switch S_1 is closed, no potential difference exists between the electrodes and the galvanometer G reads zero deflection. The galvanic current I_g is measured by closing the switch S_2 and adjusting the variable resistor R_x in such a way that the galvanometer G reads zero millivolts potential difference. The current flowing through the ammeter A is the galvanic current I_g.

Automatic Zero Resistance Ammeters

The manual zero resistance ammeters (ZRA) circuit has the disadvantages that for the time at which the circuit is not balanced, the galvanic couple is polarized, which leads to errors and in many cases to long periods of recovery. It is also not possible to monitor continuously the galvanic current, a basic necessity in many applications. Godard [*13*] and Henry and Wilde [*14*] have made attempts to overcome these disadvantages. Godard [*13*] described an "automatic galvanic corrosion current apparatus," while Henry and Wilde [*14*] developed "an electronic zero resistance ammeter with instantaneous null characteristics." The circuit of Henry and Wilde [*14*] is shown in Fig. 13*c*.

The principle of operation is based on the use of an operational amplifier to replace the manual balancing of the ZRA described previously. With the switch S in the zero position, the operational amplifier OA is adjusted so that the voltage drop across R_s is zero millivolts between the positive input and the output. With the switch in the read position, the current flow through R_s is counteracted within the rise time of the amplifier (~1 μs) by a reverse current from the amplifier to maintain the voltage drop across R_s at zero millivolts. This current which represents the galvanic current I_g is measured on the microammeter A. Henry and Wilde developed a compact and portable unit which is fully described in their paper [*14*].

Use of Potentiostats

The method of using a potentiostat for the measurement of galvanic corrosion currents was first described by Dévay, Lengyel, and Mészáros [*15*] and applied to measurements of galvanic corrosion currents in dental amalgam by von Fraunhofer and Staheli [*16*]. Figure 14 [*17*] shows the experimental arrangement. One electrode is connected to the working electrode terminal (WE) the other one to the reference electrode terminal (REF) which is connected directly to the auxiliary electrode terminal (AUX). With the potentiostat set at exactly zero millivolts applied potential, the galvanic current is read directly on the current meter of the potentiostat. Note that von Fraunhofer [*16,17*] uses a feedback resistor R_f between REF and AUX, which can introduce an error depending on the gain of the potentiostat and the output potential. The use of R_f was not found necessary with Wenking or Princeton Applied Research potentiostats.

Use of an Operational Amplifier

By far simpler and more economic is the use of an operational amplifier as first described by Lauer and Mansfeld [*4*]. Figure 15 shows the experimental arrangement [*4*].

One of the electrodes of the couple is grounded. The other is connected to the negative input of a high-gain operational amplifier. The output of this amplifier is given by

$$V_0 = GV_s \tag{13}$$

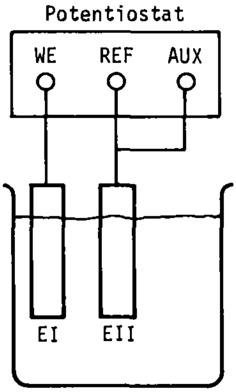

FIG. 14—*Potentiostat wired as zero impedance ammeter.*

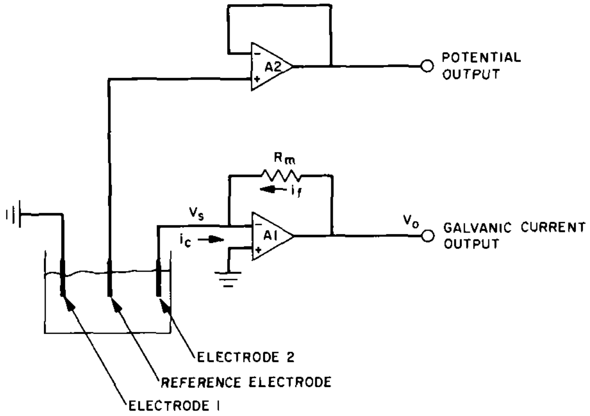

FIG. 15—*Instrument for monitoring galvanic current and potentials* [4].

where V_s is the voltage, referred to ground, of the electrode and G is the open loop gain, $>10^6$. Thus, values of V_0 up to the amplifier output limit ($\sim$12 V) correspond to negligible V_s values.

The impedance of the amplifier is much greater than feedback resistance R_m. At the amplifier input

$$i_c + i_f = 0 \tag{14}$$

where i_c is the cell current and i_f the feedback current. The value of the feedback current is given by

$$i_f = \frac{V_s - V_0}{R_m} \tag{15}$$

Since, from Eq 13 and the value of G, $V_s = V_0$, then

$$i_f = -i_c \cong \frac{-V_0}{R_m} \tag{16}$$

Since, for Electrode 2 in Fig. 13, $V_s \approx 0$, the potential difference between Electrode 1 and Electrode 2 is essentially zero. Thus, output voltage V_0 is directly proportional to the cell current, so that we have a "zero impedance" ammeter.

The time-dependent galvanic current is measured using an operational amplifier. The potential of the couple is measured with respect to a SCE connected to an electrometer amplifier wired as a high impedance (10^{14} Ω) unit gain follower. The galvanic current and the potential were simultaneously recorded as a function of time on strip chart recorders. This arrangement allows continuous monitoring of the galvanic current over many orders of magnitude with no internal resistive loss using strip chart recorders. It can be used even in distilled water, since irrespective of the conductivity of electrolyte the amplifier will always provide zero millivolts potential difference between the members of the couple. Mansfeld [5–8] has used this zero impedance ammeter for studies of galvanic couples in sodium chloride, tap water, and distilled water [*7,8*], of inorganic conversion coatings on aluminum alloys coupled to Type 304 SS or Ti-6Al-4V [*5*] and of metallic coatings on aluminum alloys [*6*].

References

[*1*] LaQue, F. L., *Proceedings*, American Society for Testing and Materials, Vol. 51, 1951, p. 495.
[*2*] Mansfeld, F., *Corrosion*, Vol. 27, 1971, p. 436.
[*3*] Mansfeld, F., *Corrosion*, Vol. 29, 1973, p. 403.
[*4*] Lauer, G. and Mansfeld, F., *Corrosion*, Vol. 26, 1970, p. 504.
[*5*] Mansfeld, F. and Parry, E. P., *Corrosion Science*, Vol. 13, 1973, p. 605.
[*6*] Mansfeld, F., *Corrosion*, Vol. 29, 1973, p. 276.
[*7*] Mansfeld, F., Hengstenberg, D. H., and Kenkel, J. V., *Corrosion*, Vol. 30, 1974, p. 343.
[*8*] Mansfeld, F. and Kenkel, J. V., *Corrosion Science*, Vol. 15, 1975, p. 183.
[*9*] Mansfeld, F. and Kenkel, J. V., *Corrosion Science*, Vol. 15, 1975, p. 239.
[*10*] Mansfeld, F. and Kenkel, J. V., *Corrosion*, Vol. 31, 1975, p. 298.
[*11*] Mansfeld, F., Myers, R. L., and Lauer, G., "Instrumentation for Corrosion Studies in Low Conductivity Media," Technical Report, Rockwell International, 1973.
[*12*] Brown, R. H. and Mears, R. B., *Transactions*, Electrochemical Society, Vol. 74, 1938, p. 495.
[*13*] Goddard, H. P., *Corrosion*, Vol. 7, 1951, p. 93.
[*14*] Henry, W. D. and Wilde, B. E., *Corrosion*, Vol. 27, 1971, p. 479.
[*15*] Dévay, J., Lengyel, B., Jr., and Mészáros, L., *Acta Chimica Academiae Scientiarum Hungaricae*, Vol. 62, 1962, p. 157.
[*16*] von Fraunhofer, J. A. and Staheli, P. J., *Corrosion Science*, Vol. 12, 1972, p. 767.
[*17*] von Fraunhofer, J. A. and Banks, C. H., *Potentiostat and its Applications*, Butterworths, London, 1972.

K. G. Compton[1]

Current Density Distribution on Composite Structures Under Cathodic Protection in Seawater

REFERENCE: Compton, K. G., "**Current Density Distribution on Composite Structures Under Cathodic Protection in Seawater,**" *Galvanic and Pitting Corrosion—Field and Laboratory Studies, ASTM STP 576,* American Society for Testing and Materials, 1976, pp. 48–55.

ABSTRACT: The distribution of cathodic protection current between members of copper-steel and stainless steel-aluminum galvanic couples was found to vary by ratio of 940 to 0.05 as the relative areas were varied from 100:1 to 1:100. Polarization curves and the distribution of current are given. Above a 1:1 ratio of cathode to anode, cathodic protection does not appear to be practical.

KEY WORDS: corrosion, bimetallic couples, cathodic protection, polarization, dissimilar metal corrosion, composite structures, current density

Very often dissimilar metals must be used in electrical contact for structural or functional purposes and are exposed to seawater. There is a considerable body of literature on the subject; however, very little definitive information is available on the cathodic protection of such a composite structure because the ratio of the areas of the two metal surfaces is varied. In the present work, the polarization behavior of each metal and of the couple was determined, and the division of the "protection" current between the two members was measured. Copper and carbon steel were selected for one couple and aluminum and stainless steel for the other. These combinations are of practical interest in the marine field.

The polarization curves were prepared by the usual standard galvanostatic technique using a time interval of 3 min. The measurement of current to the individual members was accomplished by use of the zero resistance ammeter technique while holding the polarized couple potential constant by means of a polaristat. In this case, the "protection voltage" was arbitrarily set at −0.80 V to the saturated calomel reference electrode for both

---

[1] Professor of Ocean Engineering, University of Miami, Miami, Fla. 33149.

couples. This value seems to satisfy a consensus of opinion and is given elsewhere [*1*].[2]

No attempt was made to determine rates of corrosion of either the individual members or of the anodic members of the couples since this was not within the scope of the program. The objective was to determine the feasibility of cathodically protecting systems where the cathode area might be large compared to that of the anode and to establish the relationship between area ratios and polarization behavior.

The carbon steel contained 0.16C, 0.63Mn, and 0.010Cu. The copper content was 99.976 with some silver. The aluminum was mill product 5052, and no analysis was made. The stainless steel was Type 316 with 0.06C, 1.8Mn, 2.15Mo, and 12.9Ni. Both the Type 316 and the carbon steel were supplied by Armco with their heat analysis. All materials were in sheet form, 0.040 to 0.050 in. thick, and in the as-rolled condition with no consideration given to temper or hardness.

The seawater was drawn from Bear Cut, a channel connecting lower Biscayne Bay with the Atlantic Ocean and was normal with respect to salinity and pH. As used, it was essentially saturated with air at the ambient temperature. The seawater was pumped into a large shallow tank for settling of any silt and piped to the various laboratories on a continuous flow basis.

Procedure

The specimens were cut to the desired size and abrasively cleaned with 600 grit waterproof silicon carbide paper. Leads were attached and the backs and edges, and part of the front surfaces were coated with wax. The size of the panels plus the wax masking permitted a ratio of areas from 100:1 to 0.01:1.

All specimens were allowed to stand in a tank of seawater for 24 h prior to testing. While this was a short exposure period, it was observed that the specimens tended to become relatively stabilized in this period of time as compared to erratic behavior for initial short periods. They were not connected as couples during this conditioning period.

The first polarization run was made on the composite structure (couple) starting about 5 min after they had been coupled together. After the composite run, the specimens were allowed to depolarize to their initial potentials, and then polarization runs were made on the uncoupled individual metals. They were again allowed to depolarize to their initial potentials, then recoupled and cathodically polarized to −0.80 V saturated calomel electrode (SCE). Initial current measurements (to each member) were made by the zero resistance ammeter method. The potential was held constant for 24 h and the currents measured again.

---

[2] The italic numbers in brackets refer to the list of references appended to this paper.

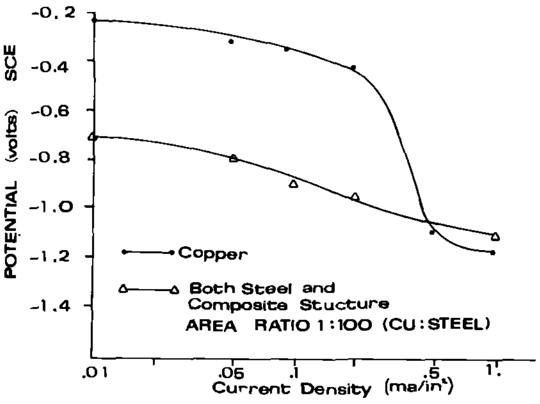

FIG. 1—*Polarization curves of copper and steel.*

Results

Where the area ratio of copper to steel is 1:100, the polarization curves are as shown in Fig. 1. Here the copper is so highly polarized that the polarization curve for the composite structure[3] is identical to that of carbon steel alone. Increasing the relative area of copper to 1:10 and 1:1 as shown in Figs. 2 and 3 produces a slight decrease in the polarization of the composite with a crossover below the protection potential in the case of the equal areas. However, an increase in the protection current has been required. As the relative copper area increases as shown in Figs. 4 and 5, the composite structure curve begins to resemble the copper curve, and the protective current is further increased. From Fig. 1 to Fig. 5, the protective current is increased about 5.5 fold.

The division of the protective current in terms of current density when the couple is held at a potential of 0.80 V (SCE) was measured with the "zero resistance ammeter" and is shown in Fig. 6. It is clear from this figure that at high ratios of copper to steel, the copper draws an excessive amount of current when the steel is polarized to protection, but at low ratios the "wasted" current is relatively insignificant. In the former case the current density ratio is about 56 and in the latter, about 0.05.

Where the ratio of aluminum to stainless steel is 1:100, the polarization of the couple is identical to that of stainless steel. Decreasing the ratio by a factor of 10 permits the couple to polarize more like aluminum at low current densities. This is shown in Figs. 7 and 8. The polarization of the couple is about midway between stainless steel and aluminum as shown in Fig. 9 and approaches that of the aluminum in Fig. 10. In Fig. 11, the

---

[3] The current density figure used is the current divided by the total area of the couple and is not strictly a true "current density" as this varies on the two parts of the couple. The true current densities are given in Figs. 6 and 12.

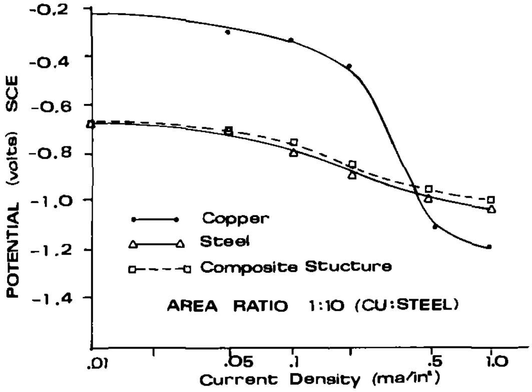

FIG. 2—*Polarization curves of copper and steel.*

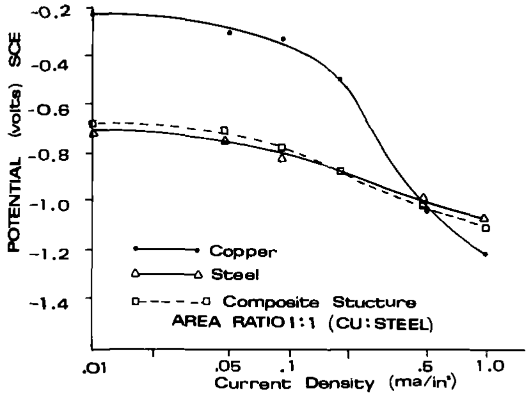

FIG. 3—*Polarization curves of copper and steel.*

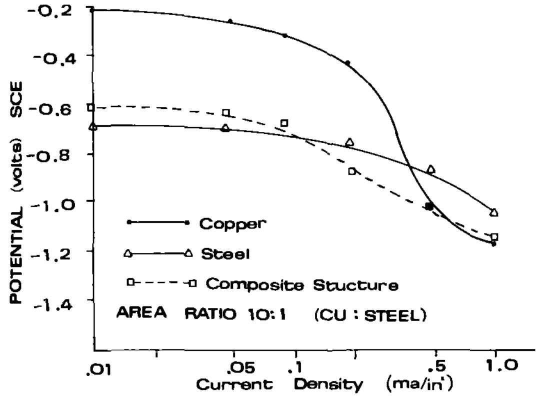

FIG. 4—*Polarization curves of copper and steel.*

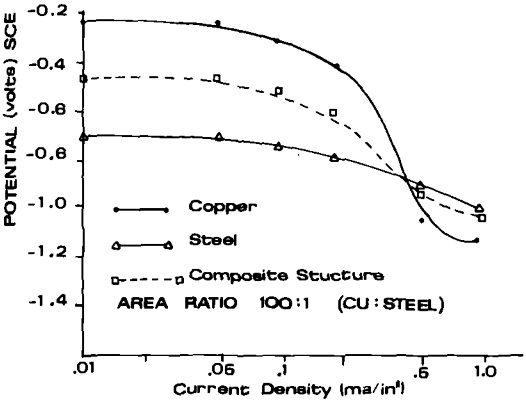

FIG. 5—*Polarization curves of copper and steel.*

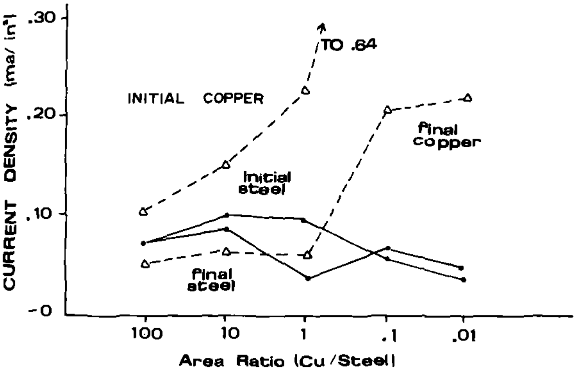

FIG. 6—*Current density distribution of exposed copper and steel couples.*

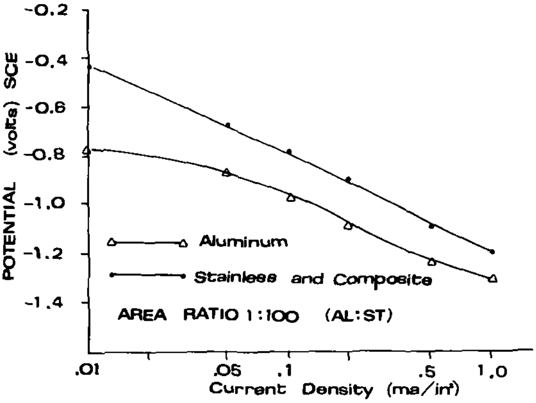

FIG. 7—*Polarization curves of aluminum and stainless steel.*

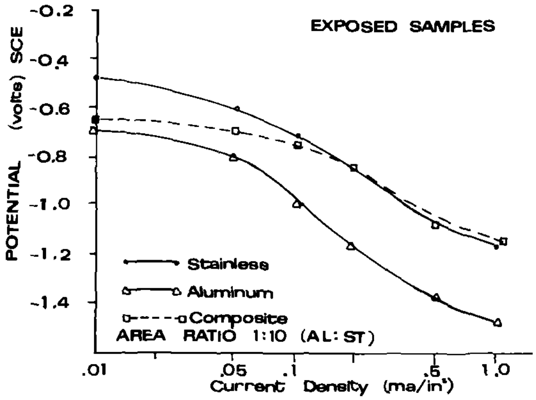

FIG. 8—*Polarization curves of aluminum and stainless steel.*

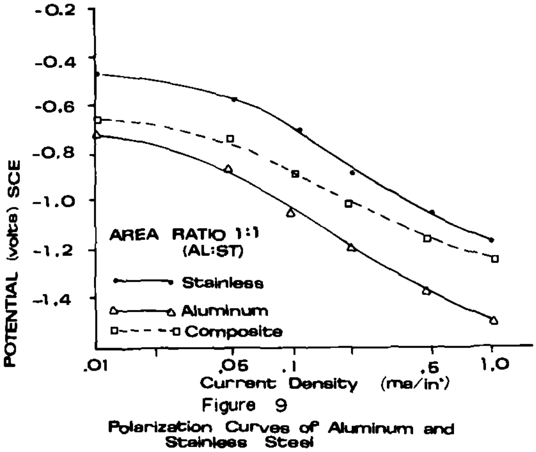

FIG. 9—*Polarization curves of aluminum and stainless steel.*

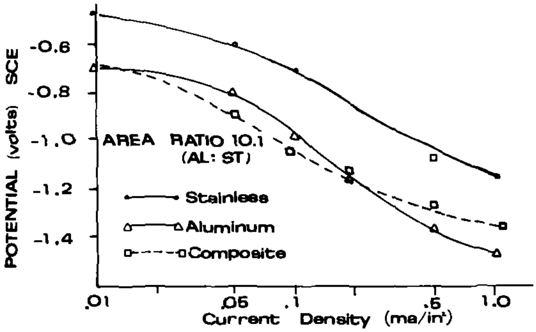

FIG. 10—*Polarization curves of aluminum and stainless steel.*

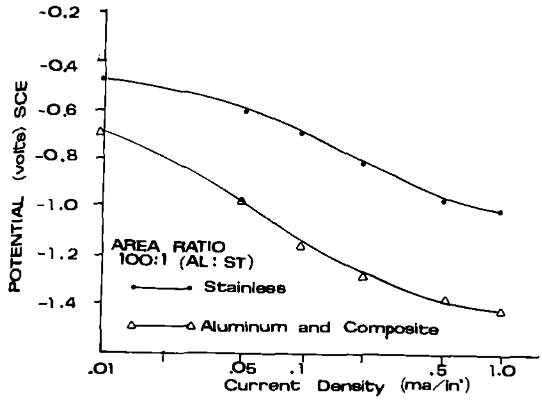

FIG. 11—*Polarization curves of aluminum and stainless steel.*

polarization of the couple is identical to that of the aluminum. It is apparent from the polarization curves that as the ratio of the area of stainless steel to aluminum decreases, the amount of protective current decreases.

Figure 12 gives the current densities of each member of the couple as measured with the zero resistance ammeter when held at a potential of −0.80 V (SCE). Here again the big difference in current required to polarize the couple when the stainless steel area is large compared to that of the aluminum is shown in contrast to that when the stainless steel area is small. The stainless steel takes about 940 times as much current as the aluminum in the former case and only 0.05 when the area is small.

The differences between the current densities when the couples are first immersed (5 min) and after 24 h, indicates that any adjustment of a cathodic

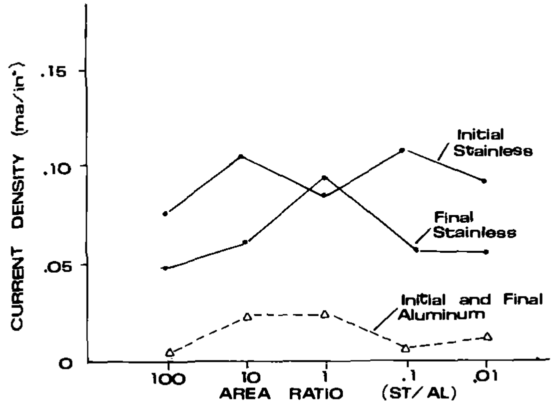

FIG. 12—*Current density distribution of aluminum and stainless steel.*

protection system should be accompanied by a suitable stabilization period. In these tests, the stainless steel and aluminum appeared to be more stable with time than the copper and carbon steel.

Conclusions

The widely held opinion that the cathodic member of the couple tends to control the polarization has been confirmed. This was discussed by Hill [*2*], Waber [*3*], Wagner [*4*], Miller [*5*], and by the principal authorities, Mears and Brown [*6*], but not in specific terms such as the data obtained in this study. From the curves presented here, one can estimate whether cathodic protection of the system is feasible when these couples are encountered or ones of similar characteristics. The ratio of the currents, cathode to anode, are given by the following.

Ratio of Areas	I_{Cu}/I_{Cs}	I_{SS}/I_{Al}
100:1	56.0	940
10:1	7.8	23.1
1:1	1.66	4.5
1:10	0.527	0.62
1:100	0.05	0.50

NOTE—I = current, C_s = carbon steel, and SS = stainless steel.

It is apparent from the preceding table that in any system where the ratio of areas is greater than 1 : 1 a very significant waste of protective current would occur, unless it was felt that the cathode needed protection.

Acknowledgments

The author wishes to express his appreciation to the Anaconda American Brass Company, the Armco Steel Company, and Reynolds Metals Company for supplying the materials used and their analyses. Many of the laboratory measurements were made by H. A. Murphy, while a graduate student at the University of Miami.

References

[*1*] Morgan, J. H., *Cathodic Protection*, Leonard Hill Limited, London, 1959, p. 172.
[*2*] Hill, G. R., "The Corrosion of Copper and of Metals in Bi-Metallic Systems," *Corrosion*, Vol. 8, 1952.
[*3*] Waber, J. T. and Rosenbluth, M., *Journal of the Electrochemical Society*, Vol. 102, 1955, p. 344, and Waber, J. T., *Corrosion*, Vol. 13, 1957, p. 25.
[*4*] Wagner, C., *Journal of the Electrochemical Society*, Vol. 98, 1951, pp. 116-128.
[*5*] Miller, "Galvanic Couples and Cathodic Protection," *Petroleum Engineer*, Vol. 19, 1946.
[*6*] Brown, R. H., and Mears, R. B., *Journal of the Electrochemical Society*, Vol. 81, 1942, pp. 455-483.

K. G. Compton[1] *and J. A. Turley*[2]

Electrochemical Examination of Fused Joints Between Metals

REFERENCE: Compton, K. G. and Turley, J. A., "**Electrochemical Examination of Fused Joints Between Metals,**" *Galvanic and Pitting Corrosion—Field and Laboratory Studies, ASTM STP 576*, American Society for Testing and Materials, 1976, pp. 56–68.

ABSTRACT: Nine combinations of butt welded plates were studied in seawater for galvanic couple, dissimilar metal type behavior. The potential differences and corrosion currents were determined for the filler material, heat affected zone, and parent metal. In seven of the nine cases, the heat affected zone was found to be anodic to the parent metal. In only one case was there a prospect of cathodic protection from the parent metal to the weld.

KEY WORDS: corrosion, welded joints, weld decay, galvanic couples, heat affected zone

Scattered through the literature one finds references to "knife-line" corrosion and intergranular corrosion. Nowhere does one find a careful and in-depth study of the corrosion associated with welds or the electrochemical behavior of welds. This paper records some preliminary results of investigations of the electrochemistry of welds in natural seawater by the senior author and his students.

Basically, a weld consists of a filler material (FM) in the "as-cast" condition; a zone containing diffusion products of the FM and the parent material (PM) and the PM that has been affected by the heat of welding, and the unaffected PM. The heat affected zone (HAZ) may suffer many metallurgical modifications of the PM, but the most common is segregation of certain components at the crystal boundaries. For instance, copper rich material segregates at the grain boundaries in the copper bearing aluminum alloys (2000 Series, Aluminum Association standards) and chromium carbides segregate at the grain boundaries in stainless steels. Various aspects of the problem have been considered by Ketcham [*1*],[3] Guy [*2*],

---

[1] Professor of Ocean Engineering, University of Miami, Miami, Fla. 33149.

[2] Petroleum engineer, Marathon Oil Company, Findlay, Ohio.

[3] The italic numbers in brackets refer to the list of references appended to this paper.

Henthorne [3], and Schumaker [4] but the basic electrochemical studies of segregation in welds have not progressed very much beyond the early work of Mears and Brown [5].

Procedure

Measurements were made of the open circuit potentials of the filler material, several parts of the HAZ, and the PM. The polarization characteristics of these same areas were determined, and then the current interchange between areas was measured. As a result, some concept of the corrosion forces at work in a welded structure has been obtained.

All of the studies were made in fresh seawater which was renewed in the test chamber at a rate of about 3 gal per day. This rate was estimated as an optimum in keeping down velocity, yet ensuring the removal of corrosion products. Earlier work by Snodgrass [6] and Smith [7] had indicated the sensitivity of electrochemical measurements to velocity in seawater. It was felt that the seawater was replenished but essentially quiescent.

Specimens supplied by various metal suppliers were prepared as butt welded plates (Fig. 1) which were cut into four units; three were intended for electrochemical studies and one for metallographic examination. The welding technique was supposed to represent the best practice of the supplier. No study of variation in welding technique was intended. The materials used are listed in Table 1. The actual analysis of most of the materials was obtained but is not given here in the interest of brevity. Insulating coatings were applied to all the surfaces of the specimen except the area being studied as shown in Figs. 2 and 3. Measurements of the

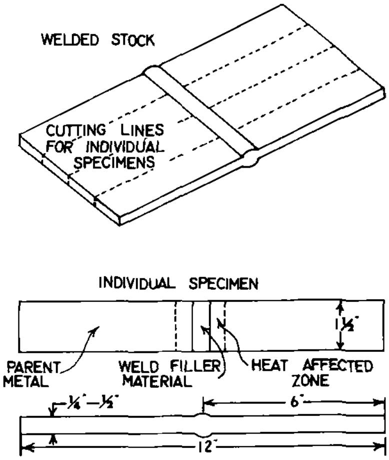

FIG. 1—*Welded specimens.*

TABLE 1—*List of specimens giving the PM and FM.*

Specimen	PM	FM
1	aluminum 6061 T6	4043 aluminum
2	aluminum 5083 H112	5356
3	aluminum 5086 H112	5356
4	aluminum 7002 T6	5356
5	aluminum 6061 (pipe)	
6	Monel K-500	Monel WE 134
7	INX-50[a]	Atomark 8018
8	T-1A[a]	Atomark 8018
9	HY 130/150	not specified

[a] Two plates of the indicated steel welded together with Atomark 8018.

potentials of the various areas were made to a saturated calomel reference electrode as shown schematically in Fig. 2 using a recording electrometer. The addition of an auxiliary electrode and a power supply permitted the determination of conventional polarization curves of potential plotted against the log of the current.

In measuring the galvanic couple corrosion current between the different zones, a "zero resistance ammeter" circuit was employed as shown in Fig. 3. Different combinations of areas having approximately the same surface area were exposed which provided a current measurement between the HAZ and the FM; the HAZ and the PM; and the FM and the PM.

During the study, the temperature, salinity, and pH were monitored. The pH remained relatively constant at 8.2, the temperature range was approximately 4°C with an average of 23°C, and the salinity was 33 ± 2 percent. None of these minor fluctuations would affect the reliability of the data, as

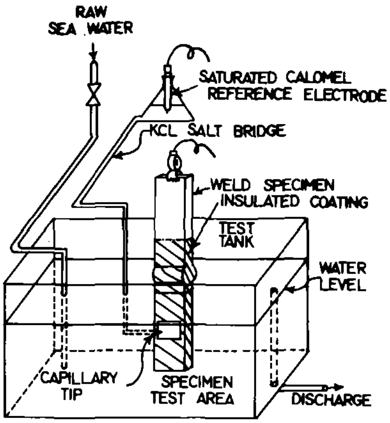

FIG. 2—*Arrangement of apparatus for measuring single potentials and polarization resistance.*

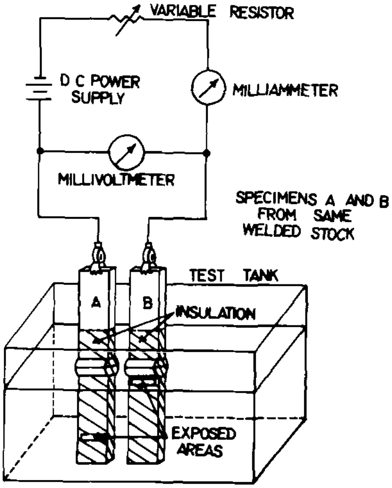

FIG. 3—*Arrangement of apparatus for measuring galvanic currents.*

the variability in the specimens would have a greater influence. The dissolved oxygen was not monitored, but was presumed to be near saturation under the conditions of the experiments.

Specimen Preparation

Cleaning and surface preparation of the specimens appeared to be important in obtaining reproducibility. In order to minimize the effect of mill scale, oxide coatings, and old corrosion products on the surface of the specimens, and in order to ensure duplication of test-surface cleanliness, the following cleaning procedure was employed on every test surface prior to measurement.

1. Lightly file the surface to a smooth finish and polish with 280- and 400-grit silicon carbide paper, respectively.
2. Wash the surface with Alconox to remove loose particles, dirt, and oil films.
3. Then thoroughly rinse with tap water to remove all traces of the cleaning compound.
4. Rinse with distilled water and with acetone.
5. Immediately submerge the cleaned surface in the test tank.

Potential Measurements

The potential data presented in Figs. 4 to 6 quite vividly illustrate the anode/cathode relationships between the different zones of each weldment

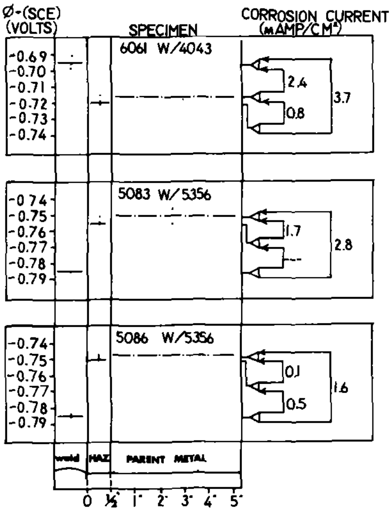

FIG. 4—*Potentials and galvanic currents of and between various segments of the welded specimens.*

studied. The potential differences shown between the HAZ and associated PM readily indicate the necessity for knowledge of the corrosion characteristics of HAZ.

In seven of the nine cases studied, the HAZ was found to be electronegative (anodic) to the parent metal. No attempt was made to precisely define the HAZ of any of the metals tested. In every case the one-half inch

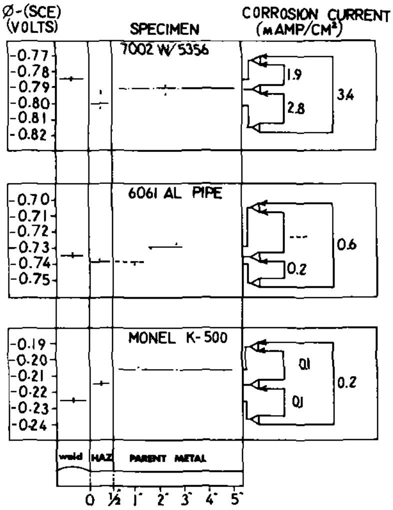

FIG. 5—*Potentials and galvanic currents of and between various segments of the welded specimens.*

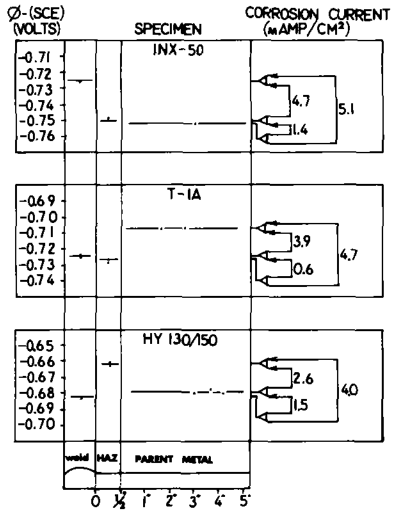

FIG. 6—*Potentials and galvanic currents of and between various segments of the welded specimens.*

immediately adjacent to the weld (on either or both sides) was designated and treated as the HAZ. The HAZ of any particular specimen might have been more or less than the arbitrary one-half inch, but the data revealed only one exception (Fig. 5, 6061 aluminum pipe). As can be seen from the potential measurements, the HAZ extends out over an inch and a half from the weld or filter material.

The potential data (Figs. 4 to 6) also show the relationship between the weld metal and the rest of the weldment. The data indicate that nearly half of the weldments studied are in the highly unfavorable condition of the weld or filter material being the most electronegative area. The importance of this relationship will be more apparent after consideration of the associated bimetallic galvanic corrosion currents.

The potential data reveal what was expected with respect to the existence of galvanic couples. The zone combination on a particular specimen with the greatest driving potential would seem likely to have the highest corrosion rate of the possible combinations, but the magnitude of any of the rates was impossible to predict based solely on the potential data. The interrelationship of the potential data and the measured galvanic corrosion currents also is presented in Figs. 4 to 6.

Polarization data for each zone of interest in a typical specimen is presented in Fig. 7. An estimation of the corrosion rate based on the intersection of the extension of the Tafel section of the cathodic protection curve with the corrosion potential gives an interesting indication of the local action corrosion current. The corrosion rates obtained by polarization techniques are helpful in describing the relative corrosion susceptibility of

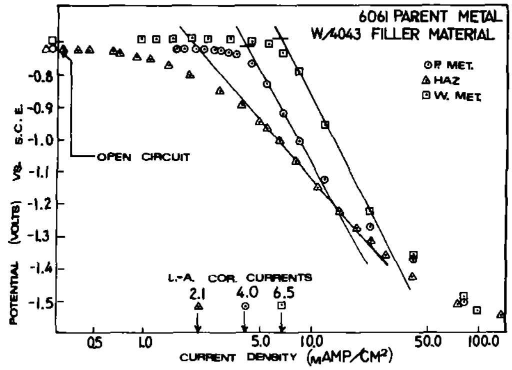

FIG. 7—*Cathodic polarization curves of different segments of the welded specimens from which corrosion rates can be estimated by the Tafel extrapolation method.*

the different zones comprising a weldment; but like the potential data, their use has limited application. For example, Fig. 7 presents the zonal corrosion currents for an aluminum alloy weldment (6061 PM and 4043 FM). The cathode polarization curve for the weld metal indicates a corrosion current of 6.5 μmA/cm^2. This is to say that if a portion of the weld material was exposed to quiescent seawater and if the zone were completely isolated from any galvanic couples the corrosion rate would be proportional to the noted corrosion current. Actually, the weld does have multiple galvanic couples, and its corrosion rate is greatly influenced by them.

The local-action corrosion rates of the PM and the HAZ for the same example indicate that both zones are less susceptible to local-action corrosion than the weld metal. The limitations of the data with respect to actual field conditions where all three zones are connected galvanically are obvious, and the individual local-action rates are practically meaningless when the overall galvanic action is considered. In this example, the weld is the inherent cathode and its corrosion rates, as influenced by cathodic protection (from the other zone corroding), would be significantly lower (or even nil) than its inherent local-action rate. Conversely, the other two zones, with the higher resistance to corrosion than the weld, would suffer accelerated corrosion because of the cathodic action at the weld.

Galvanic Corrosion Currents

A multiplicity of galvanic couples exists on a weldment, and one can only measure the corrosion currents of representative couples. Using the zero resistance ammeter technique and isolating various parts of the weldment some of these galvanic corrosion currents have veen measured. In every case studied, the galvanic corrosion currents correlated with the observed interrelationship of the zonal open-circuit potentials. Figures 4 to 6 present the observed galvanic corrosion currents and the respective zonal potentials.

All galvanic corrosion current data were taken using equal anode and cathode areas and presented on a microinch per ampere per centimeter squared basis. The areas of the weld metal and the HAZ are limited as compared to the area of the PM. If the same data were taken, but the exposed area of the PM was increased to a size more indicative of actual conditions, the results of the galvanic corrosion data would be affected as follows.

1. If the PM was the most electropositive area of the specimen, the corrosion rate of the inherent anode would be greatly increased. The maximum corrosion rate of the anodic zone would depend on its relative area ratio with respect to the PM and on the polarization characteristics of both zones.
2. If the PM was the most electronegative area of the weldment, its corrosion behavior would tend towards its local-action corrosion characteristics as its area ratio was increased. The larger the PM area, the more extensive would be the cathodic protection of the rest of the specimen.

In both these cases the magnitude of the corrosion current is limited by the area of the cathode. For the cathode-controlled specimens in this investigation, the maximum galvanic corrosion current possible (with increasing cathode/anode area ratio) is governed mainly by the concentration polarization characteristics of the environment; the effect of anode polarization towards limiting the maximum current density would be evident to a somewhat lesser extent.

An actual field specimen is shown in Fig. 8 for which data are given in Fig. 5. The same and other field specimens are shown in Figs. 9 and 10. In this case, the weldments (6061 with an unknown filler material said to be unsatisfactory) were removed from a pipeline that had been in service for several years. During this time, the bare external surface of sections of the pipe at the welds were exposed to seawater. It is obvious from the pictures, and supported by the experimental data, that the HAZ of this pipe are prone to selective corrosion while the weld metal and the parent metal remain relatively unharmed. Ultimate failure of the pipe system several miles in length occurred because of extensive destruction of HAZ material at various weld areas. This shows what can happen if the wrong combinations of PM and FM are used. Many examples of the proper selection of materials could be cited to show satisfactory performance.

Another example of the significance of data on open circuit potentials of the three areas of interest is shown in the weldment of 5086 aluminum alloy with 5356 FM as shown in Fig. 4. Here, the PM and the HAZ are considerably positive to the FM. This information indicates that the weld area would suffer accelerated corrosion as influenced by the large cathode

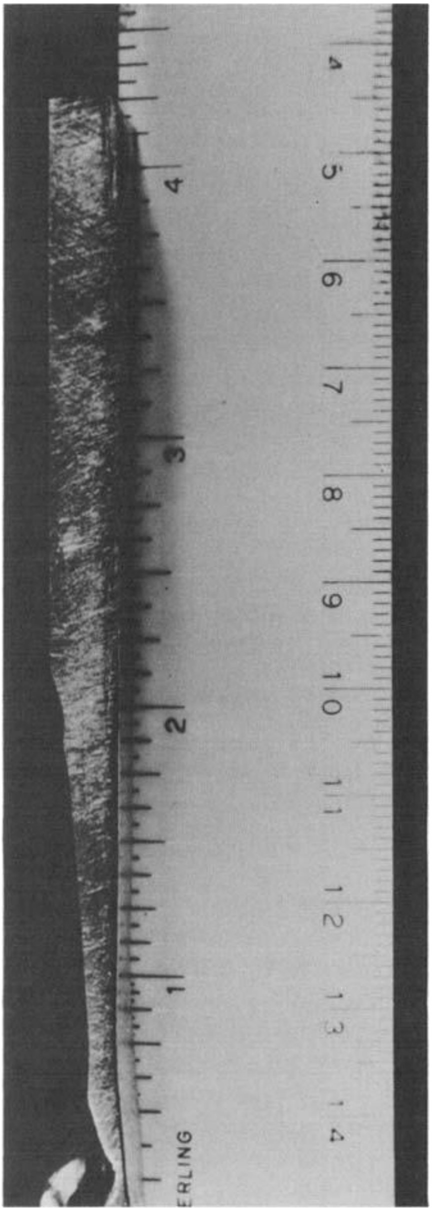

FIG. 8—*Specimen showing the FM, HAZ, and PM after several years of service in the field; electrochemical data in Fig. 5.*

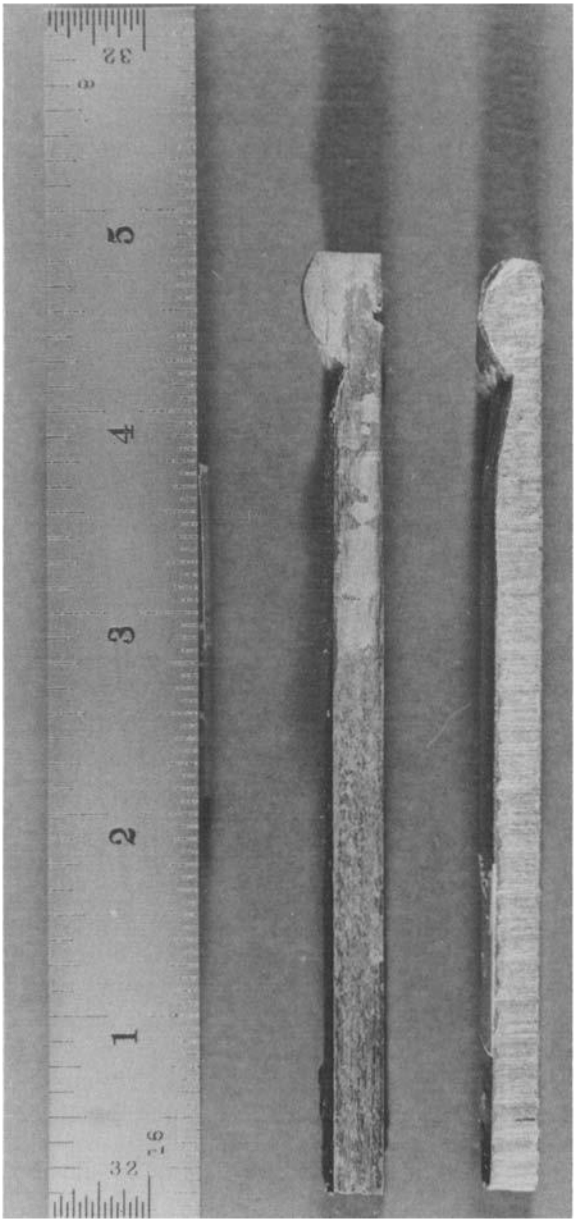

FIG. 9—*Specimens similar to those in Fig. 8 showing a difference in the corrosion of the HAZ.*

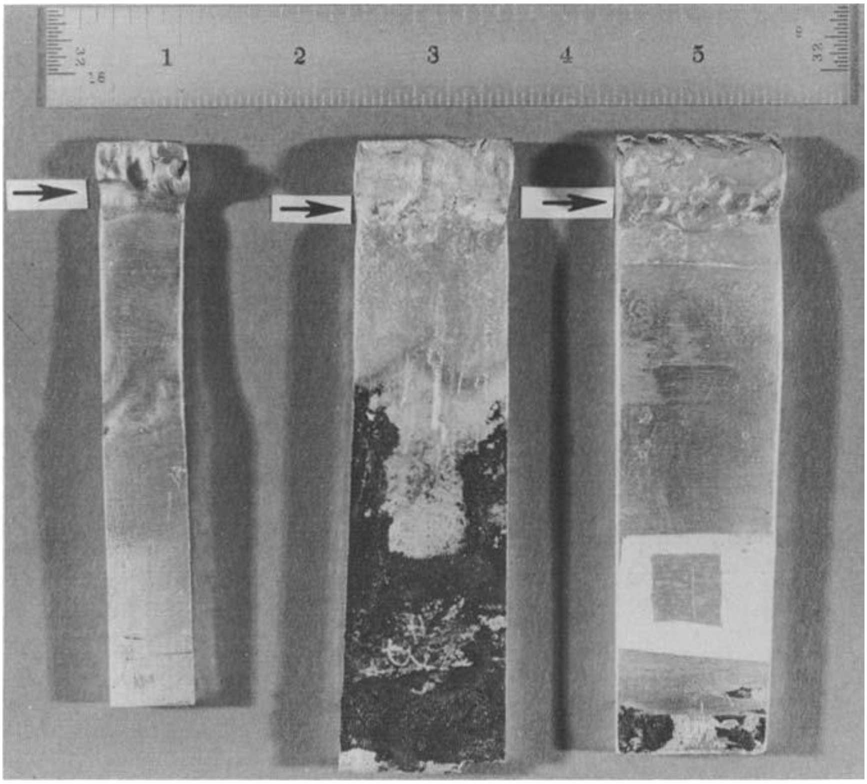

FIG. 10—*Three specimens from Figs. 8 and 9 showing the corrosion in the HAZ and the lesser attack on the FM.*

area, but no quantitative analysis can be made without additional information.

Galvanic corrosion of the weld material was influenced directly by the open-circuit potentials and the polarization characteristics of all three zones. Figure 4 illustrates the magnitude of the galvanic corrosion currents associated with corrosion of the weld area. The most prominent reaction was between the PM and the weld. According to the data, the weld would corrode at a rate proportional to the current density noted ($-1.6\ \mu A/\text{cm}^2$) and would be directly influenced by the ratio of the PM area to the weld area. This area-ratio influence could be as high as one order of magnitude before concentration-polarization effects began to predominate. This is to say that the corrosion of the weld associated with galvanic action could be as high as 16 μm A/cm^2, depending on the environment and the anode polarization characteristics of the weld metal.

Because the weld area was found to be the most electronegative area, none of the associated galvanic couples have the possibility of affording the weld cathodic protection, and the ultimate rate of the weld's destruction would be a direct sum of its local-action corrosion rate and the galvanically induced corrosion rate.

An attempt to summarize the results in terms of relative behavior is presented in Table 2. The maximum galvanic susceptibility is 2.5 mpy. The local-action corrosion rate of the same zone is 0.9 mpy. By summation, its total corrosion rate would be 3.4 mpy. This total rate is, obviously, a minimum corrosion rate. Many factors can act to accelerate the corrosion

TABLE 2—*Potentials and galvanic currents between various segments of the specimens.*

	6061	5083	5085	7002	6061
	4043	5356	5356	5356	Pipe
Potential (V-SCE)[a]					
PM	−0.715	−0.750	−0.745	−0.790	−0.730
HAZ	−0.720	−0.755	−0.750	−0.800	−0.740
weld metal	−0.695	−0.785	−0.785	−0.785	−0.735
Local-action corrosion rate (mpy)					
PM	1.7	0.9	1.1	0.5	6.8
HAZ	0.9	0.9	1.0	0.3	1.0
weld metal	2.8	1.6	2.8	2.7	1.6
Maximum galvanic susceptibility					
zone	HAZ	weld	weld	HAZ	HAZ
rate	2.5	2.8	3.5	1.8	1.2
Total corrosion rate, most susceptible zone					
zone	HAZ	weld	weld	HAZ	HAZ
rate (mpy)	3.4	4.4	6.3	2.1	2.2

	Monel K-500	INX 50	T-1A	HY 130/150
Potential (V-SCE)[a]				
PM	−0.205	−0.755	−0.705	−0.680
HAZ	−0.215	−0.750	−0.730	−0.660
weld metal	−0.225	−0.725	−0.725	−0.685
Local-action corrosion rate (mpy)				
PM	0.7	5.3	4.6	3.2
HAZ	0.3	5.6	6.8	5.5
Weld metal	1.5	4.8	4.5	6.4
Maximum galvanic susceptibility				
zone	weld	PM	HAZ	weld
rate	1.6	7.7	9.0	7.3
Total corporation rate, most susceptible zone				
zone	weld	PM	HAZ	weld
rate (mpy)	3.1	13.0	15.8	13.7

[a] V-SCE = voltage per saturated calomel electrode.

of the susceptible zone, the most important, in the case of immersion in quiescent seawater, being the area effect of the large PM.

Conclusions

The corrosion of welds in quiescent seawater has been investigated by electrochemical laboratory techniques and the investigative procedures described in this paper are adequate to allow characterization of the following: (*a*) relative anode/cathode behavior of each zone comprising the weldment, namely, the PM, the HAZ, and the weld metal; (*b*) inherent corrosion properties of each zone, including polarization characteristics and local-action corrosion rates; (*c*) magnitude of galvanic action between zones; and (*d*) corrosion rate of zone with greatest susceptibility to corrosion as influenced by its local-action corrosion rate and by its galvanic action with the rest of the weldment.

Acknowledgments

The welded specimens were provided by the Naval Applied Science Laboratories in Brooklyn, New York, the Huntington Alloys Division of the International Nickel Company, the Inland Steel Company, and the Reynolds Metals Company. Most of the laboratory work was performed by J. A. Turley in connection with his thesis research leading to the Masters Degree in Ocean Engineering.

References

[*1*] Ketcham, S. J. and Haynie, F. H., *Corrosion*, Vol. 19, 1963, pp. 242t–246t.
[*2*] Guy, A. G. in *Elements of Physical Metallurgy*, Addison-Wesley London, 1960, pp. 32–35.
[*3*] Henthorne, M., *Corrosion*, Vol. 30, 1974, p. 39.
[*4*] Schumaker, M. B., Kelsey, R. A., Sprowls, D. O., and Williamson, J. G., in *Stress Corrosion Testing, ASTM STP 425*, American Society for Testing Material, 1967, p. 317.
[*5*] Mears, R. B., and Brown R. H., *Industrial and Engineering Chemistry*, Vol. 33, 1941, p. 1003.
[*6*] Snodgrass, J. S., "The Effects of Velocity on the Polarization of Low Carbon Steel in Sea Water," thesis, University of Miami, 1969.
[*7*] Smith, C. A., "The Effect of Aerobic Marine Bacteria on the Corrosion of Steel in Sea Water: A Preliminary Study," thesis, University of Miami, 1968.

George Schick[1] *and D. A. Mitchell*[2]

Galvanic Corrosion of Underground Power Distribution Cable Materials

---

REFERENCE: Schick, George and Mitchell, D. A., "**Galvanic Corrosion of Underground Power Distribution Cable Materials,**" *Galvanic and Pitting Corrosion—Field and Laboratory Studies, ASTM STP 576*, American Society for Testing and Materials, 1976, pp. 69–80.

ABSTRACT: Bare concentric neutral conductors of buried power cables have failed due to corrosion in several areas of the United States. Galvanic corrosion, between the neutral conductor anode and a "semiconducting polyethylene" tape cathode, was investigated as one of the possible corrosion mechanisms. The results indicate that the rate of the galvanic corrosion is controlled by the cathode and in the present cable design contributes little to the neutral wire failure. If a semiconducting polyethylene jacket is extruded over the neutral conductors, the contribution of galvanic corrosion at jacket defects may become significant.

KEY WORDS: corrosion, galvanic corrosion, power lines, conductors

Power cables with bare concentric neutral wires are used extensively in buried power distribution networks throughout the United States. In the past two years there was an increasing awareness of the fact that the neutral wires are corroding to the point of complete failure (see Fig. 1). As a result of these failures, alternating currents of high intensity can leak into the earth or onto other buried structures, such as telephone cables, which are not designed to carry these currents. Since the earth is a relatively good conductor, the neutral wire failure often goes unnoticed by the power companies and power consumers. However, on at least two occasions in New Jersey, 20 to 37 A of alternating current caused service affecting failures of the buried telephone plant in joint use trenches as reported by McLellan and Schick [*1*].[3] As a result of an inquiry at 31 power companies, Huston[4] surmised that between 1965 and 1973, these companies found 155 corrosion areas on 59 216 miles of cables with tinned

[1] Member of the technical staff, Bell Laboratories, Whippany, N.J. 07981.
[2] Metallurgical engineer, General Public Utilities, Reading, Pa.
[3] The italic numbers in brackets refer to the list of references appended to this paper.
[4] Huston, G. H., General Public Utilities, Parsippany, N.J., private communication.

FIG. 1—Corrosion failure of netutral wires.

copper neutral wires and 18 corrosion areas on 1520 miles of cables with bare copper neutral wires. Zastrow [*2–4*] and Puschel [*5*] have studied this corrosion problem by conducting field measurements and attempting to correlate their findings with environmental factors. As of this date, a number of failure mechanisms have been proposed, that is, stray currents, long line corrosion cell current, galvanic corrosion, corrosion by sulfides in anaerobic soils, cathodic protection interference currents, alternating current corrosion, and differential aeration. The present study investigates galvanic corrosion in detail and its consequences on a factory applied protective system.

Materials in the Concentric Neutral Power Cable

Two different cables were examined in this study. The first one has 19 stranded AWG 4/0 EC aluminum center conductors insulated with 0.2-in. (0.51-cm) thick polyethylene. The outer surface of this insulation is covered by a 0.040-in. (0.1-cm) thick semiconducting polyethylene (SCPE) layer. The SCPE is not a semiconductor in the classical physical sense. It is polyethylene containing carbon particles which render it a modest conductor. The outside diameter of this cable is 1 in. (2.54 cm). There are 19 helically wound 14-gage tinned copper neutral wires in direct contact with the SCPE layer. The tinning on the neutral wires of this cable is actually 50 μin. (1.27×10^{-5} cm) thick alloy of the following composition: 84 percent lead, 13 percent tin, 2 percent antimony, and 1 percent bismuth [*6*].

The second type of cable construction is basically the same as the first one with some exceptions. It has seven stranded AWG 2 EC aluminum center conductors. The outside diameter of this cable is 0.75 in. (1.9 cm) and the neutral wires are ten helically wound 12-gage bare copper conductors.

Experimental Procedure

The present investigation used the galvanostatic polarization technique to establish the corrosion potential and corrosion current density of the galvanic cells operating between the SCPE cathode and copper or lead-tin alloy anode. This technique has been described by Fontana and Greene [*7*].

The neutral wire electrodes were prepared by enclosing 12-in. (30.48-cm) long wire sections in pyrex tubes with epoxy resin, leaving approximately 1-in. (2.54-cm) long wire to be exposed to the corrosive environment. The wire ends were also masked with epoxy resin filled glass cups (see Fig. 2). The SCPE was hot pressed on 0.003 in. (0.0076 cm) thick, 0.5 in. (1.27 cm) wide copper ribbons and the edges trimmed 0.125 in. (0.317 cm) beyond the edges of the copper. The copper ribbon and a small portion of the SCPE

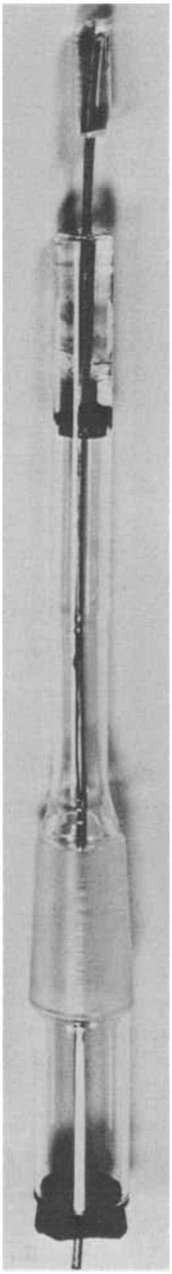

FIG. 2—*Neutral wire electrode.*

were tightly enclosed between two Lucite blocks in which a 0.5 in. (1.27 cm) wide, 0.004 in. (0.01 cm) deep channel was machined. This channel is 0.75 in. (1.9 cm) wide and 0.030 in. (0.076 cm) deep at one end to accommodate a small segment of the SCPE. In order to assure that the copper ribbon does not get in contact with the corrosive environment, the channel in the Lucite was precoated with silicon grease, and the two blocks were tightened together with nylon screws (Fig. 3).

The polarization experiments were conducted in 0.1 *M* sodium sulfate (Na_2SO_4) + 0.01 *M* sodium chloride (NaCl) solutions at three different pH (2.85, 6.4, and 10). The original pH of the solution was 6.4; the other two were prepared by an addition of sulfuric acid (H_2SO_4) or sodium hydroxide (NaOH). The experiments were carried out in both air containing and nitrogen (N_2) gas deaerated solutions. Polarization experiments were also carried out in a moist soil that was collected at one of the corrosion failure sites in Parsippany, N.J. The analysis of this soil is listed in Table 1.

TABLE 1—*Chemical analysis of soil from the Parsippany, N. J. failure site.*

Chemical Components in 100-g Soil	
Ca^{++}	1.0 mg
Mg^{++}	1.0 mg
Na^+ and K^+ as Na^+	4.0 mg
Cl^-	7.0 mg
SO_4^{--}	<5.0 mg
NH_4^+	ND
CO_3^{--}	ND

NOTE—ND = not detected, and
pH = 6.4 based on 100-ml water extract of 1-g soil.

The test electrodes were cleaned in acetone for 3 min at room temperature before placing them in the corrosive media. The neutral wire electrodes were exposed for 24 h and the SCPE electrodes for 48 h before the application of polarizing currents. The open circuit potentials were measured during the last 2 h of these time periods. The applied galvanostatic current step rate was 50 min/decade. All experiments were carried out at 22 ± 1°C.

Another series of experiments were carried out to measure the galvanic currents, resulting from the anodic and cathodic reactions, with a zero resistance milliammeter. The circuit of this instrument was previously described by Henry and Wilde [*8*]. For this experiment, 6-in. (15.24-cm) long sections were cut from actual power cables. The neutral wires were removed and a 0.5-in. (1.27-cm) wide copper tape was tightly strapped around the SCPE surface on one end of the specimen and electric lead wire was soldered on this tape. The copper tape was then insulated with several

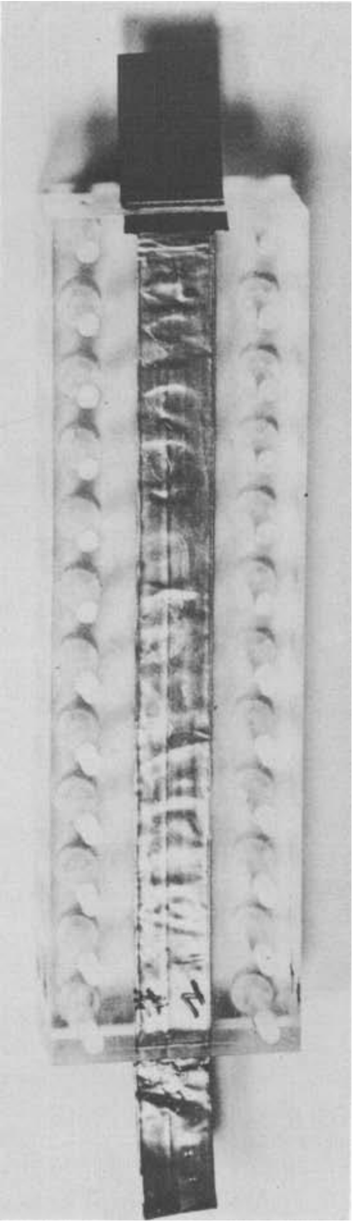

FIG. 3—*Slightly conductive polyethylene electrode.*

layers of black electric tape. A similar thickness of black electric tape was also wound around the other end of the specimen to serve as an insulating spacer. The neutral wires were soldered onto a copper wire ring on both ends forming a circular cage. An electric lead wire was also soldered on one of the wire rings. The neutral wire cage was then positioned around the cable touching only the insulating tape. The cable ends and electric contacts were cast in epoxy resin so that only known surface areas of the electrically isolated components could be exposed to the corrosive liquid (Fig. 4). The cable and neutral wire leads were then connected to a series of switches, which in one position short circuited the galvanic cell through a 12-gage copper conductor, and in another position measured the galvanic current with the zero resistance milliammeter.

All neutral wire electrodes of the cable specimens were cleaned with acetone for 3 min at room temperature before the start of the experiments.

The environments in which the zero resistance milliammeter experiments were conducted are the previously mentioned air containing solutions the soil from Parsippany, N.J. thoroughly saturated with distilled water, and a mixture of 990 cm^3 1 percent NaCl solution with 10 g of agar-agar.

Results and Discussion

The results of the galvanostatic polarization experiments in the pH 2.85, 6.4, 10 solutions and in the moist Parsippany, N.J. soil are listed in Tables 2, 3, 4, and 5, respectively. Although the open circuit potentials (E^{oc}) of the SCPE electrodes reached a stable value after 48-h exposure to the test solution, this potential was as much as 100 mV different from one electrode to another tested under identical conditions. This is not surprising since the polyethylene-carbon mixture in the SCPE may be quite inhomogeneous and the contribution of voltage drop at the electrode surface can be con-

TABLE 2—*Data from galvanostatic polarization measurements in 0.1*M *Na_2SO_2 + 0.01*M *NaCl, pH adjusted to 2.85 with H_2SO_4.*

Solution	Electrode	E_{oc} versus Calomel, V	E_{corr}^{gc} V	i_{corr} μA/cm^2
Air	SCPE	+0.180	−0.492	3.9
Air	Pb/Sn alloy	−0.499		
Air	SCPE	+0.180	−0.047	0.073
Air	Cu	−0.048		
N_2	SCPE	−0.037	−0.430	0.1
N_2	Pb/Sn alloy	−0.431		
N_2	SCPE	−0.037	−0.123	0.0003
N_2	Cu	−0.127		

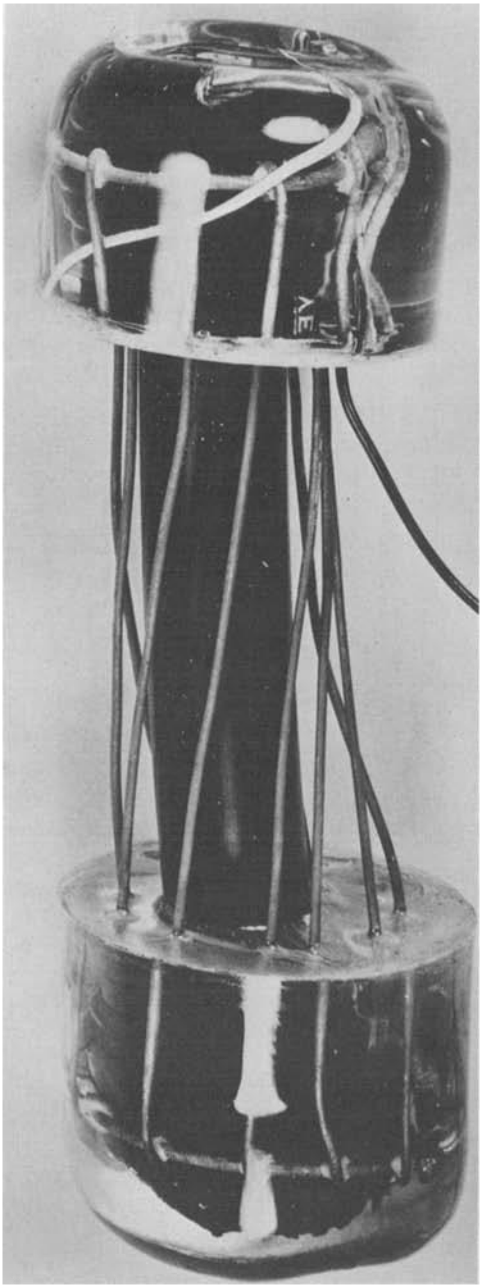

FIG. 4—*Galvanic corrosion specimen made of concentric neutral type power cable.*

TABLE 3—*Data from galvanostatic polarization measurements in 0.1*M *Na_2SO_4 + 0.01*M *NaCl, pH 6.4.*

Solution	Electrode	E_{oc} versus Calomel, V	E_{corr}^{gc} V	i_{corr} μA/cm²
Air	SCPE	−0.006	−0.347	1.91
Air	Pb/Sn alloy	−0.393		
Air	SCPE	−0.006	−0.211	0.042
Air	Cu	−0.228		
N_2	SCPE	+0.025	−0.470	0.21
N_2	Pb/Sn alloy	−0.477		
N_2	SCPE	+0.025	−0.137	0.027
N_2	Cu	−0.154		

TABLE 4—*Data from galvanostatic polarization measurements in 0.1*M *Na_2SO_4 + 0.01*M *NaCl, pH adjusted to 10 with NaOH.*

Solution	Electrode	E_{oc} versus Calomel	E_{corr}^{gc} V	i_{corr} μA/cm²
Air	SCPE	−0.057	−0.348	2.25
Air	Pb/Sn alloy	−0.452		
Air	SCPE	−0.057	−0.133	0.006
Air	Cu	−0.140		
N_2	SCPE	−0.096	−0.450	0.053
N_2	Pb/Sn alloy	−0.465		
N_2	SCPE	−0.096	−0.159	0.0015
N_2	Cu	−0.165		

TABLE 5—*Data from galvanostatic polarization measurements in a soil from Parsippany, N. J.*

Environment	Electrode	E_{oc} versus Calomel, V	E_{corr}^{gc}, V	i_{corr} μA/cm²
Soil	SCPE	+0.019	−0.470	0.029
Soil	Pb/Sn alloy	−0.485		
Soil	SCPE	+0.019	−0.070	0.0004
Soil	Cu	−0.078		

siderable. A similar but smaller (50 mV) inconsistency of E^{oc} on the lead-tin alloy coated copper electrodes was also observed. This can be attributed to the fact that the 50-μin.-thick coating is quite porous, and variation in this thickness can change even further the area of exposed copper at the pore sites. Although the measured potential is primarily due to the lead tin alloy coating, it is also influenced by the mixed potential of the lead-tin alloy-copper galvanic cell. Of the three different electrodes, copper showed the most consistent E^{oc} values from specimen to specimen tested under identical conditions.

Comparison of the open circuit potential of the individual electrodes and the corrosion potential of the galvanic couple ($E_{corr}{}^{gc}$) indicates that the galvanic corrosion reactions in all the environments are cathodically controlled.

The effect of dissolved oxygen in the solution as a cathodic depolarizing agent is obvious when the corrosion current densities (i_{corr}) are compared for the galvanic couples in air containing and deaerated solutions. The presence of oxygen increases the corrosion rate by orders of magnitude in most cases.

As expected, i_{corr} of the SCPE-lead-tin alloy is larger than the SCPE-copper couple in all environments used in this study. The amphoteric lead-tin alloy corrodes at a higher rate in acidic and alkaline solutions than in the neutral solution while the corrosion rate of copper is the highest in the acidic and lowest in the alkaline solution. The relatively low i_{corr} values in the Parsippany, N. J. soil are probably due to the fact that the soil in the galvanostatic polarization experiments was only moist and not saturated with water.

The galvanic corrosion current data, obtained with the zero resistance milliammeter, are listed in Table 6. The galvanic corrosion current densities

TABLE 6—*Galvanic cell currents measured with zero resistance milliammeter on cable specimen.*

Environment	Galvanic Couple	Galvanic Current Density, μA/cm^2
pH 2.85 solution + air	SCPE, Pb/Sn alloy	0.297
pH 2.85 solution + air	SCPE, Cu	0.063
pH 6.4 solution + air	SCPE, Pb/Sn alloy	0.024
pH 6.4 solution + air	SCPE, Cu	0.009
pH 10 solution + air	SCPE, Pb/Sn alloy	0.039
pH 10 solution + air	SCPE, Cu	0.002
Parsippany, N. J. soil	SCPE, Pb/Sn alloy	0.056
Parsippany, N. J. soil	SCPE, Cu	0.033
1% NaCl solution + agar-agar mixture	SCPE, Pb/Sn alloy[a]	0.44

[a] Electrodes are the same type as those used in the galvanostatic polarization experiments.

measured in the solutions are lower than those calculated from the galvanostatic polarization curves. This is partially due to the difficulty of making good electric contact on the SCPE surface of the cable and, partially, because the long term current measurements are conducted with anodes where corrosion products build-up contributes to the polarization of the lead-tin alloy or copper anodes. In the Parsippany, N.J. soil environment the zero resistance milliammeter measurements produced higher current densities than the galvanostatic polarization data, because the former soil specimens were thoroughly saturated with distilled water while the latter soil specimens were only moist. The relative corrosion rates are also indicated in the zero resistance milliammeter measurements; that is, lead-tin anodes corrode at a higher rate in any of the environments than copper and for both types of specimens the corrosion rate is the highest in the acidic solution. The lowest corrosion rate in these experiments is also indicated in the alkaline solution for copper and in the neutral solution for the lead-tin alloy.

Calculations based on Faraday's law indicate that 1 $\mu A/cm^2$ corrosion current density can remove 1.16 mil (2.95×10^{-3} cm) lead-tin alloy or 0.46 mil (1.17×10^{-3} cm) copper in one year. Comparison of these data to the measured corrosion current densities indicate that although galvanic corrosion between SCPE and lead-tin alloy or copper can contribute to the corrosion of the power cable neutral wires, these corrosion rates are too low to cause the type of failures encountered in the field.

The cathodic control aspect of galvanic corrosion of concentric power cable neutrals merit some further discussion in view of the proposal made by Marwick [9] to use SCPE outer jacket over the neutral wires to control corrosion. It is conceivable that such an outer jacket will reduce the number of occurrences of long cell current, stray current, or alternating current leakage induced corrosion. However, at areas where the outer SCPE jacket is damaged, the cathode/anode surface area ratio of the galvanic corrosion cell will be strongly increased and, consequently, the presently negligible galvanic corrosion rate will be increased to the point of playing an important role. Similar type of corrosion failures have been discovered on galvanized high strength steel armor wires jacketed with carbon black containing neoprene [*10*].

Conclusions

1. The galvanic corrosion between SCPE cathode and lead-tin alloy or copper anode is cathodically controlled.

2. Air in the corrosive media acts as a cathodic depolarizer and increases i_{corr} of the galvanic cell compared to the same data measured in deaerated corrosive media.

3. Both the lead-tin alloy and copper anodes of a galvanic cell, with SCPE cathode, corrode at the highest rate in an acidic solution. The corrosion rate of the same type of cells is the lowest in neutral solution for lead-tin alloy and in alkaline solution for copper.

4. Comparison between measured i_{corr} values and calculations based on Faraday's law indicates that although galvanic cells can contribute to the neutral wire corrosion, the currents produced by these cells in the present cable construction cannot explain the failures encountered in the field. However, if the cable is redesigned using a SCPE jacket over the neutral wires, defects on this outer jacket may increase the galvanic corrosion effect by several orders of magnitude. This implies that the neutral wires should be individually surrounded by such a SCPE layer so that at any given defect only one or two neutral wires could be affected.

References

[*1*] McLellan, D. W. and Schick, G., "Corrosion of Concentric Neutrals on Buried Power Distribution Cables—A Preliminary Report," presented at the Institute of Electrical and Electronic Engineers Power Engineering Society Conference and Exposition on Underground Transmission and Distribution, Dallas, Tex., 3 April 1974.

[*2*] Zastrow, O. W., "Copper Corrosion in High Resistivity Soil," U.S. Department of Agriculture, Rural Electrification Administration Staff Report, 31 Oct. 1972.

[*3*] Zastrow, O. W., "Soil Corrosion of Copper Concentric Neutral Wires on Underground Electric Cable," U.S. Department of Agriculture, Rural Electrification Administration Status Report, 8 Aug. 1973.

[*4*] Zastrow, O. W., "Copper Corrosion in Moderate and High Resistivity Soils," presented at the National Association of Corrosion Engineers' Corrosion/74, Chicago, Ill., 4–8 March 1974.

[*5*] Puschel, M. A., "URD Cables Cannot be Buried and Forgotten," presented at the National Association of Corrosion Engineers Corrosion/74, Chicago, Ill., 4–8 March 1974.

[*6*] Marwick, I. J. and McNamara, J. H., *Underground Engineering*, Vol. 2, No. 3, April/May, 1971, pp. 17–24.

[*7*] Fontana, M. and Greene, N. in *Corrosion Engineering*, McGraw-Hill, New York, 1967, p. 342.

[*8*] Henry, W. D. and Wilde, B. E., *Corrosion*, Vol. 27, No. 11, 1971, pp. 479–482.

[*9*] Marwick, I. J., *Electrical World*, Vol. 182, No. 2, 15 July 1974, p. 60.

E. Escalante[1] *and W. F. Gerhold*[1]

Galvanic Coupling of Some Stressed Stainless Steels to Dissimilar Metals Underground

REFERENCE: Escalante, E. and Gerhold, W. F., "**Galvanic Coupling of Some Stress Stainless Steels to Dissimilar Metals Underground,**" *Galvanic and Pitting Corrosion—Field and Laboratory Studies, ASTM STP 576*, American Society for Testing and Materials, 1976, pp. 81–93.

ABSTRACT: Stainless steels, Type 301 half hard and Type 301 full hard, have been found susceptible to failure by hydrogen embrittlement when stressed as low as 40 percent of their yield strength and cathodically charged above 1 $\mu A/cm^2$ by galvanic coupling to a dissimilar metal in four years of exposure at six underground test sites. However, stainless steels Type 304 and alloys 26Cr-1Mo and 26Cr-6.5Ni were resistant under similar conditions. Failures by stress-corrosion cracking were not observed in any of the materials. Electrochemical measurements made periodically above ground are correlated with the subsequent visual examination of the specimens.

KEY WORDS: corrosion, galvanic corrosion, hydrogen embrittlement, soils, stainless steels, stresses, stress corrosion, underground corrosion

Increased interest in the use of stainless steels for underground applications has activated a number of programs directed at learning more about the behavior of these materials in such an environment [*1*,*2*].[2] Data from a 14-year program studying the corrosion of several stainless steels underground has been published by the National Bureau of Standards (NBS) [*3*]. Of particular interest, however, is that situation where the stainless steel is under stress such as can occur, for example, when stainless steel pipe clamps are used to join or repair underground utility services. Often, the circumstances are further aggravated by planned or accidental galvanic coupling of the stainless steel to a dissimilar metal.

This paper is a presentation of some of the work that is being carried out by NBS in order to gather data and develop a better understanding of the

---

[1] Metallurgist and materials engineer, Institute for Materials Research, National Bureau of Standards, Washington, D. C. 20234.

[2] The italic numbers in brackets refer to the list of references appended to this paper.

associated phenomena observed such as the effects of stress and current density on the failure of stainless steel.

Materials

The four types of stainless steel used in this study are listed in Table 1 with their chemical compositions. Table 2 gives the conditions and mechanical properties of the alloys. Austenitic stainless steel Type 301 was exposed in both the half-hard and full-hard condition, exhibiting the highest strength levels of the materials in this portion of the study with tensile strengths well over 150 ksi (1035 MPa). This higher strength for the Type 301 stainless steel is due to the presence of martensite formed during the cold working process. Type 304 austenitic stainless steel was used in the annealed condition and had lower tensile properties. Alloy 26Cr-1Mo, a ferritic single-phase stainless steel, was exposed in the annealed condition

TABLE 1—*Chemical composition of materials major elements*[a], *weight percent.*

Stainless Steel[b]	Cr	Ni	C	Si	S	P	Mn	Mo
301 HH	17.43	7.14	0.10	0.34	0.016	0.030	1.02	0.22
301 FH	16.98	7.23	0.13	0.54	0.013	0.020	0.86	...
304	18.2	9.8	0.048	0.50	0.012	0.030	1.46	0.17
26Cr-1Mo	26.18	0.10	0.002	0.21	0.011	0.010	0.01	0.94
26Cr-6.5Ni	26.5	6.2	0.015	0.40	0.02	0.022	0.49	0.04

[a] Balance iron.
[b] HH = half hard, and
FH = full hard.

TABLE 2—*Mechanical properties and applied stress.*

Stainless Steel	Condition[a]	Tensile Strength, ksi[b]	Yield Strength 0.2% Offset, ksi[b]	% Elongation 5.08-cm gage	Hardness	Applied Stress, % Yield Strength, ksi[b]
301	HH	162	116	25	R_c34	36 42
301	FH	203	175	9	R_c44	22 38
304	annealed	87	46	52	R_B85	93 43
26Cr-1Mo	annealed	72	54	26	R_B88	76 41
26Cr-6.5Ni	partial anneal	132	121	14	R_c31	34 41

[a] HH = half hard, and
FH = full hard.
[b] To convert from ksi to MPa multiply by 6.9.

as was the two-phase stainless steel alloy 26Cr-6.5Ni which had tensile properties almost twice those of the 26Cr-1Mo alloy.

The metals chosen for galvanic coupling to stainless steel were magnesium, zinc, and iron, commercially available in the forms described. A 1.2 m length of extruded magnesium, having a 2 by 1-cm cross section with a 0.3-cm-diameter iron core, was used as an electrode. The zinc electrode was similar in that it too was extruded over a 0.3-cm iron core, but had a 1.5 by 2-cm diamond cross section and was 30 cm long. The iron electrode consisted of a 30 cm length of a cold finished AISI 1017-1018 steel, hexagonal-shaped 2-cm bar.

Soils

Six test sites have been used in this investigation and were selected on the basis of their physical and chemical makeup as being most representative of soils that are found throughout the United States [*4*]. The locations and soil properties of these areas are listed in Table 3. The following is a brief description of the character of each site.

Site A

Sagemoor sandy loam is a well drained alkaline soil with a minimum resistivity of 400 Ω/cm and is typical of that found in vast areas of eastern Washington and Oregon. The soil is consistent in composition to a depth of at least 2 m and supports abundant growth of sage brush.

Site B

Hagerstown loam (soil 55 [*3*]) is a well drained soil representative of the majority of well developed soils found in the eastern part of the United States. The soil consists of a brown loam about 30 cm deep, underlain by reddish-brown clay that extends 1.5 m or more to underlying rock. The soil has an average resistivity of 21 000 Ω/cm.

Site C

Clay is located on a large clay pit on level land consisting of a plastic gray clay to a depth of 15 cm, underlain by a gray clay mixed with patches of brown clay to a depth of 30 cm. This is underlain by a poorly drained, very heavy plastic clay. The soil has an average resistivity of 700 Ω/cm.

Site D

Lakewood sand is a white, loose sand with some black streaks occurring in places. The site is located on a well drained rolling area which is not subject to overflow from the ocean except under unusual flood conditions. The sand supports the growth of beach grasses and has an average resistivity of 39 000 Ω/cm.

TABLE 3—*Properties of soils at test sites.*

Site	Soil	Location	Internal Drainage	Range of Resistivity, Ω/cm	pH	Water Soluble Extract, ppm	
						TDS[a]	H^+
A	Sagemoor sandy loam	Toppenish, Wash.	good	400[b]	8.8	7 080	...
B	Hagerstown loam	Loch Raven, Md.	good	12 600 to 37 300	5.3	...	...
C	clay	Cape May, N. J.	poor	400 to 1 150	4.3	14 640	54
D	Lakewood sand	Wildwood, N. J.	good	13 800 to 57 500	5.7	...	...
E	coastal sand	Wildwood, N. J.	poor	1 320 to 49 500	7.1	11 020	...
G	tidal marsh	Patuxent, Md.	poor	400 to 15 500	6.0	11 580	7.1

[a] Total dissolved solids.

[b] One measurement, water saturated soil.

Site E

Coastal sand is a typical white coastal beach sand located approximately 60 m from the ocean and has an average resistivity of 27 000 Ω/cm.

Site G

Tidal marsh is a soil typical of the poorly drained marsh soils that are found along the Atlantic and Gulf coasts. The site is located along a creek that empties into the Chesapeake Bay. The soil contains hydrogen sulfide and has an average resistivity of 4500 Ω/cm.

Experimental Procedure

Specimen Preparation

Specimens were supplied by several companies in 2.54 by 30.5-cm strips sheared from 0.162-cm sheet with the rolling direction parallel to the long axis of the specimen. The 26Cr-1Mo specimens were also supplied with the rolling direction perpendicular to the long axis. The 26Cr-6.5Ni alloy specimens were prepared with machined edges. Identification numbers were stamped on the specimens on arrival using chromium-plated steel dies. An oblong hole, 0.63 by 1.3 cm, was punched at each end to allow bolting of the specimen in a U-bend configuration. In addition, a 0.24-cm hole was drilled 0.6 cm from the end and side for electrical contact. Insulated 14-gage stranded copper wire was soldered through the small hole on the end, and the solder area was coated with coal tar epoxy. Specimens were bent initially around a 3.2-cm diameter mandrel to about a 20-deg angle, then degreased in trichloroethylene vapor and passivated in 30 percent by volume concentrated (67 percent) nitric acid at 60°C for 25 min. This was followed by rinsing in water and air drying. Finally, the preformed specimens were bent and secured with Type 316 stainless steel fasteners so that the applied strain was in excess of the prestrain, and the sides of the specimen were essentially parallel. Stress determinations were made with the use of strain gages mounted on specimens taken at random from each system. The strain gage was positioned on the flat unstressed stainless steel specimen in such a way that during stressing, the gage was on the outer surface and at the apex of the U-bend where the applied stress was highest. The applied stress for each material is listed in Table 2. Specimens picked for the stress analysis were not used in the burial program.

Stressed stainless steel specimens not coupled to a dissimilar metal were used as controls in the study. The control specimens were prepared in the same manner as those that were to be galvanically coupled.

Electrode Preparation

Electrical connection to the magnesium electrode was made by soldering the electrical lead to a 2-cm extension of the iron wire core and over-coating the joint area. To extend the life of the magnesium electrode, both 2-cm sides were coated so that only the 1-cm sides were exposed to the soil. Electrical contact to the zinc electrode was made in the same manner as with the magnesium. Electrical contact was made to the iron electrode at a point midway between its ends where a small diameter hole was drilled through for inserting and soldering the electrical lead. Again, as in all contact joints, the area was coated with coal tar epoxy. All wires were carefully labeled for identification.

Exposure

Two specimens from each system were buried at every test site about 30 cm apart in trenches approximately 0.8 m deep and 0.6 m wide. The specimens and their corresponding electrodes were placed parallel to the trench and approximately 30 cm apart with the electrical leads extending above ground. The 1.2-cm magnesium anodes were bent into a horseshoe shape with the specimen at its center. The wires were attached to a 10 cm by 10 cm by 2 m wooden post prior to backfilling. After backfilling, the electrical leads were connected to terminal strips on the post and corresponding couples were connected electrically above ground. The stainless steel control specimens had their electrical leads attached to a post, but were not connected to a dissimilar metal.

Electrical Measurements

Electrochemical potentials of the couples versus a copper-copper sulfate (Cu-$CuSO_4$) half cell were measured using a high precision portable pH meter as a millivoltmeter. The half cell was placed in a remote area (approximately 15 m away) and shielded from the light to minimize photopotential effects. Couple currents were measured using a zero impedance circuit employing an operational amplifier (Fig. 1) or a commercially available zero resistance ammeter for larger currents. Electrochemical measurements were made at the time the specimens were buried and three times a year thereafter when possible with the exception of Site A where measurements were usually made once a year. Soil resistivities were also determined regularly at the sites with the 4-pin Wenner bridge [*5*], again, with the exception of Site A where the Shepard cane [*6*] was used.

Removal

On excavation from the soil, the stressed stainless steel specimens were examined for indications of gross fracture failures. Materials were then returned to the laboratory for cleaning and a more careful laboratory examination. In the laboratory the specimens were rinsed in tap water to remove adhering soil particles and visually examined prior to further cleaning. The U-bend specimens were disassembled then by removing the stainless steel fastener and unsoldering the copper wire. Ultrasonic cleaning

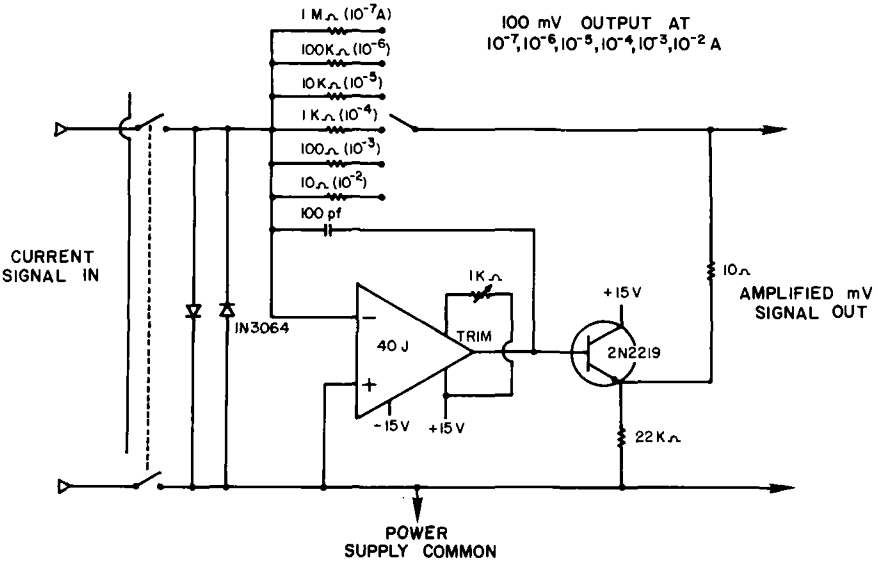

FIG. 1—*Zero impedence current amplifier.*

of the stainless steel in a 10 percent nitric acid solution heated to 50°C for 30 min was followed by rinsing in water and then air drying. After the acid bath, the stainless steel specimens were visually examined thoroughly.

Results and Discussion—Galvanically Coupled Specimens

Potential Measurements

The data obtained from Site G appear in Fig. 2. It illustrates the type of information gathered at each site over the four-year period. The upper portion of the figure shows the average potential versus time for the materials indicated. With this potential measurement the stability of the galvanic couple could be monitored. For example, the potential of the stainless steel-magnesium couple is seen to drop steadily as the magnesium corrodes away within the first year of exposure wih a corresponding drop in galvanic current. On the 16th month, the magnesium wax replaced with a larger electrode which maintained a fairly steady potential of 1.5 V versus Cu-$CuSO_4$ for the remaining 30 months. The same figure reveals that both the zinc and the iron, when coupled to stainless steel, maintained a reasonably steady potential, 1.0 and 0.65 V versus Cu-$CuSO_4$ respectively, with a drop of approximately 100 mV each over the 48-month period. Galvanic current alone is a poor monitor for determining the effectiveness of the galvanic electrode because of its sensitivity to changes in soil characteristics as reflected in the fluctuating galvanic current plots of Fig. 2. This figure is

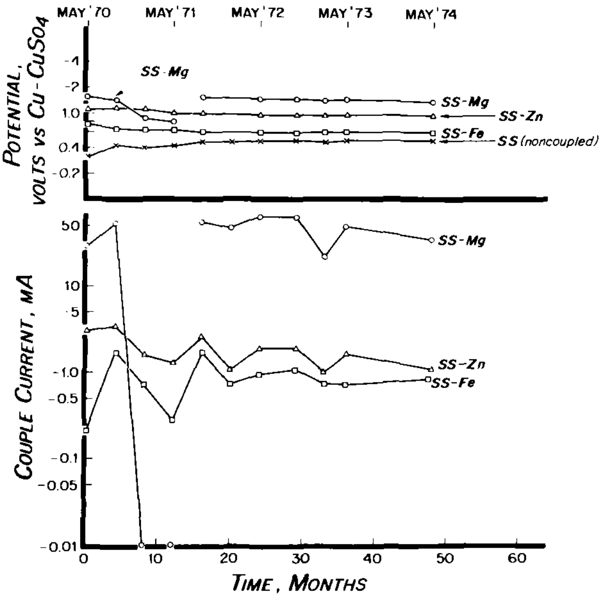

FIG. 2—*Average potential and galvanic current data as a function of time from Site G.*

based on average readings for specimens at Site G and illustrates the effect of time on electrochemical measurements because it was at this site that anode maintenance problems were greatest. Note further that at this site the noncoupled stainless steel specimens in the four year study became progressively more active in potential with time changing from −300 to −500 mV versus Cu-CuSO$_4$ as shown in the upper portion of the figure.

Galvanic Current Measurements

While the potential measurement gave a quick and reliable qualitative evaluation of the condition of the counter electrode connected to the stainless steel, the galvanic current gives a quantitative measurement of the capacity of the couple to generate current and indicates its direction. Table 4 lists the average galvanic current for each material and the number of failures that occurred over the period of exposure at the six test sites. A material was considered failed if inspection disclosed a crack anywhere on the specimen. A hand lens (×7) was generally used for examination, and at questionable areas, a low power binocular microscope (×30) was employed as a final arbiter. From the data obtained it is evident that two of the stainless steel materials in this study, Types 301 full-hard and 301 half-hard, have a tendency to stress crack. It is shown in Table 4 that every stressed Type 301 full-hard stainless steel specimen and all but one of the Type 301 half-hard specimens connected to magnesium failed in the

TABLE 4—*Average[a] couple current versus failure.*

			Site A Washington		Site B Loch Raven		Site C Cape May		Site D Wildwood, dry sand		Site E Wildwood, wet sand		Site G Patuxent	
System	Specimen[b]	Coupled to	μA/cm²	Failures	μA/cm²	Failures	μA/cm²	Failures	μA/cm²	Failures	μA/cm²	Failures	μA/cm²	Failures
82	301 HH[c]	Zn	2.58	0	1.43	2	20	2	0.94	2	1.14	2	10.3	2
83	301 HH[c]	Mg	17.2	1	4.81	2	122	2	3.95	2	34.7	2	237	2
84	301 HH[c]	Fe	0.06	0	0.48	0	1.45	2	0.17	0	0.48	0	4.08	0
85	301 FH[c]	Zn	4.17	0	1.51	2	20.5	2	1.23	2	0.98	2	14.7	2
86	301 FH[c]	Mg	20.5	2	8.66	2	120	2	3.79	2	34.7	2	249	2
87	301 FH[c]	Fe	0.05	0	0.56	0	1.29	2	0.23	0	0.59	0	4.65	1
88	304[c]	Zn	2.57	0	1.86	0	26.3	0	0.96	0	0.71	0	11.5	0
89	304[c]	Mg	25.3	0	6.38	0	117	0	5.25	0	30.2	0	258	0
90	304[c]	Fe	0.09	0	0.45	0	0.99	0	0.06	0	0.59	0	8.27	0
33	26Cr-1Mo[d]	Zn	7.75	0	1.49	0	33.8	0	1.49	0	2.47	0	18.5	0
34	26Cr-1Mo[d]	Mg	22.7	0	3.57	0	133	0	3.77	0	24.0	0	353	0
35	26Cr-1Mo[d]	Fe	4.73	0	0.54	0	0.87	0	0.25	0	2.4	0	−0.21	0
36	26Cr-6.5Ni[d]	Zn	7.30	0	1.72	0	27.8	0	1.31	0	5.01	0	13.1	0
37	26Cr-6.5Ni[d]	Mg	47.4	0	4.0	0	138	0	4.53	0	28.4	0	375	0
38	26Cr-6.5Ni[d]	Fe	0.37	0	0.98	0	1.57	0	0.35	0	0.94	0	6.52	0

[a] Average of two specimens, 16 readings.
[b] HH = half hard, and
FH = full hard
[c] Four-year exposure.
[d] Three-year exposure.

four years of exposure. The Type 301 stainless steel was generally more resistant to failure when connected to iron with failures occurring only at Site C and one at Site G. Zinc generally did cause failure of the stressed Type 301 stainless steel except at Site A where no failures were observed. It is apparent that the likelihood for failure increases with increasing cathodic current on the stainless steel. At any given test site, the largest currents are generated by magnesium, followed by zinc, and then iron. Figure 3 illustrates this current-failure relationship. Note that below 1 $\mu A/cm^2$ no failures occurred for the Type 301 stainless steel alloys. As the current density increases the number of failures increases to the degree that above 8 $\mu A/cm^2$ all Type 301 full-hard specimens failed and above 20 $\mu A/cm^2$ all 301 half-hard specimens failed. The fact that the number of failures increases with increasing cathodic current strongly suggests hydrogen embrittlement as the mode of failure.

As Table 4 indicates, no failures were observed for the stressed Type 304, or alloys 26Cr-1Mo, and 26Cr-6.5Ni stainless steels when coupled to magnesium, zinc, or iron at any of the sites in the times indicated. Figure 4 is included to illustrate clearly the fact that these materials were exposed to the full range of cathodic current with no adverse effects.

The alloys that did not fail were exposed, for the most part, at higher levels of stress as listed in Table 2 than the Type 301 stainless steels that

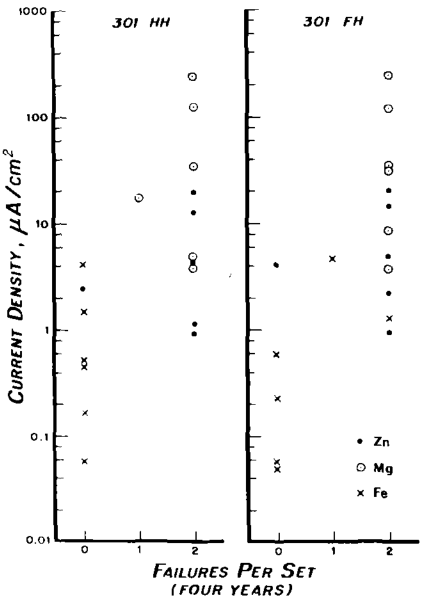

FIG. 3—*Galvanic current density versus failures for Type 301 full-hard and Type 301 half-hard stainless steels. Each data point represents two specimens.*

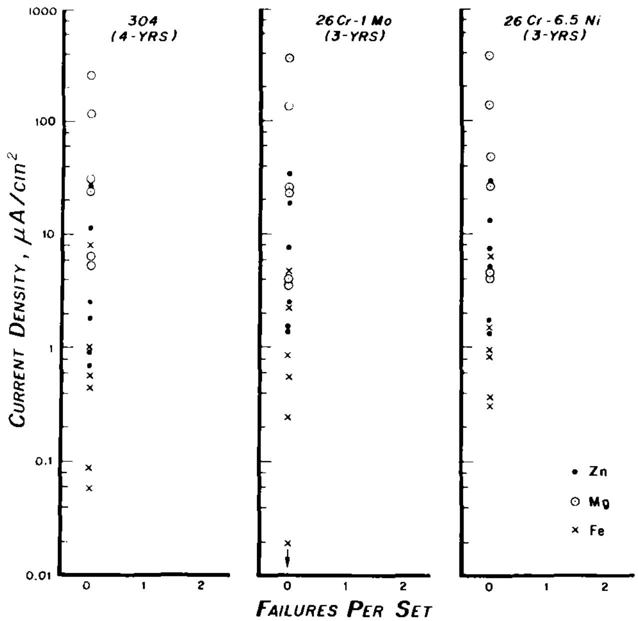

FIG. 4—*Galvanic current density versus failures for Type 304, and alloys 26Cr-1Mo, and 26Cr-6.5Ni stainless steels. Each data point represents two specimens.*

failed. The results indicate that those materials that, in general, did not fail were inherently resistant to cracking under the conditions of this study.

Of course, the site with the lowest soil resistivity develops the highest current densities. Such a situation was noted at Sites C and G where the highest current densities were found. At first glance, Site A did not appear to follow this trend. That is, its resistivity (Table 3) was very low, yet the measured current densities (Table 4) were, likewise, low. The reason for this apparent discrepancy is that the measurement at Site A was made on water saturated soil at a nearby stream, thus, leading to an abnormally low resistance reading. Actually, the resistivity at Site A is quite high because of the semiarid nature of the area which would account for the low galvanic currents observed.

Results and Discussion—Noncoupled Specimens

The noncoupled specimens were of interest not only in their own right, but also because they served as controls for the galvanically coupled specimens. These controls were identical to the coupled specimens in every respect except that they were not connected to another metal. Table 5 reveals that there were no failures observed on any of the specimens in the exposure times given.

TABLE 5—*Results of noncoupled specimens.*

		Site A Washington	Site B Loch Raven	Site C Cape May	Site D Wildwood, dry sand	Site E Wildwood, wet sand	Site G Patuxent
System	Specimen[a]	Failures	Failures	Failures	Failures	Failures	Failures
67	301 HH[b]	0	0	0	0	0	0
70	301 FH[b]	0	0	0	0	0	0
72	304[b]	0	0	0	0	0	0
21	26Cr-1Mo[c]	0	0°	0	0	0	0
30	26 Cr-6.5Ni[c]	0	0	0	0	0	0

[a] HH = half hard, and
FH = full hard.
[b] Four year exposure.
[c] Three year exposure.
[d] One specimen missing.

Summary and Conclusions

The results of this study indicate that the stressed Type 301 half-hard and full-hard stainless steels have a tendency to fail with increasing cathodic charging suggesting failure by hydrogen embrittlement. Certainly there is considerable evidence for this phenomenon as has been observed under laboratory conditions [*7–9*] and at last one reported service failure [*10*]. Furthermore, no failures were observed for the Type 304, or alloys 26Cr-1Mo, and 26Cr-6.5Ni stainless steels under similar conditions of stress and environment. It is also important to note that the noncoupled specimens did not fail, thus, indicating their resistance to failure when at open circuit potential.

Acknowledgments

The authors are grateful for the help and financial support of the American Iron and Steel Institute and the Committee of Stainless Steel Producers.

Special thanks are extended to R. J. Carpenter, Chief of the Electronics Instrumentation Section, NBS, for his design of the current amplifier, and to members of the Corrosion and Electrodeposition Section, specifically W. P. Iverson and W. J. Schwerdtfeger for their helpful discussions and assistance, and B. T. Sanderson and J. L. Fink who have helped gather data at various phases in the program.

References

[*1*] Steinmetz, G. F. and Hoxie, E. C., *Materials Protection and Performance*, Vol. 12, No. 9, 1973, pp. 41–44.
[*2*] Branch, H. C., *Materials Protection and Performance*, Vol. 12, No. 3, 1973, p. 9–14.
[*3*] Romanoff, M., "Underground Corrosion," NBS Circular 579, National Bureau of Standards, Department of Commerce Clearinghouse, April 1957.

[*4*] Romanoff, M., *Journal of the American Water Works Association*, Vol. 56, No. 9, Sept. 1964, p. 1129.
[*5*] Wenner, F., "A Method of Measuring Earth Resistivity," Bulletin 12, National Bureau of Standards, 1915–1916, p. 469.
[*6*] Shepard, E. R., *NBS Journal of Research*, National Bureau of Standards, Vol. 6, No. 4, 1931, p. 683.
[*7*] Rhodes, P. R., *Corrosion*, Vol. 25, 1969, p. 462.
[*8*] Wilde, B. E., *Corrosion*, Vol. 27, 1971, p. 326.
[*9*] Logan, H. L. in *The Stress Corrosion of Metals*, Wiley, New York, 1966, p. 100.
[*10*] Raymond, L. and Kendall, E. G., *Metal Progress*, Vol. 69, Jan. 1968, p. 103.

M. A. Pelensky,[1] *J. J. Jaworski,*[1] *and A. Gallaccio*[1]

Air, Soil, and Sea Galvanic Corrosion Investigation at Panama Canal Zone

---

REFERENCE: Pelensky, M. A., Jaworski, J. J., and Gallaccio, A., "**Air, Soil, and Sea Galvanic Corrosion Investigation at Panama Canal Zone,**" *Galvanic and Pitting Corrosion—Field and Laboratory Studies, ASTM STP 576,* American Society for Testing and Materials, 1976, pp. 94–113.

ABSTRACT: Various combinations of metals are used widely in military and industrial equipment. Many of these are deployed worldwide and in many situations under aggressive natural environmental conditions. The object of this study and this paper relates to the effects of subtropical environment on coupled, dissimilar structural metals of military interest. These include aluminum, brass, magnesium, Monel, steel, stainless steel, and titanium alloys. The environments are the atmosphere at Fort Sherman, soil (burial) at Fort Sherman, and seawater (total immersion) at Coco Solo, Panama Canal Zone. Results of this study should have significance in the selection of materials for design of equipment for use in these environments. The atmospheric specimens are rectangular, directly coupled, and offsetted. Offsetting was employed since this would lead to variability in galvanic effects over the exposed surfaces and edges. End grain attack, particularly at the edges of the tempered and aged light alloys, is of interest. For soil burial and seawater immersion, cylindrical specimens connected through a polyacrylate resin cylinder were used. These were selected as suitable and convenient for this purpose.

The atmospheric specimens were placed at site in April 1973, and the soil and seawater specimens were located during Oct. 1973. Atmospheric tests are expected to continue for a total period of four years and soil, five years; seawater tests are likely to continue for a total of three and one half years.

Atmospheric, soil, and seawater specimens are returned to the laboratory periodically during the test for examination and weight loss determination to assess the effects of each of the environments on the various galvanic couple combinations.

Only limited results are available at this early stage of the investigation. Accordingly, no final determination can be made at this time of the significance of results.

KEY WORDS: corrosion, galvanic corrosion, pitting, crevice, alloys, atmospheric exposure, soil burial, seawater, Panama Canal Zone

---

[1] Chemical engineer, research chemist, and chief, respectively, Materials Applications Branch, Materials Engineering Division, Pitman-Dunn Laboratory, Frankford Arsenal, Philadelphia, Pa. 19137.

Military materiel is deployed and used worldwide under varied and sometimes severe environmental conditions. Consequently, under such use and particularly in tropical or marine environments, significant galvanic corrosion problems usually are encountered.

In the design and fabrication of equipment requiring the joining of dissimilar metals, the use of electrochemically similar metals is desirable. That this is not feasible in many instances because of structural, electrical, or other important design criteria is recognizable and appreciated. But, where efforts are not applied toward mitigating the dissimilar metal (potential) effects, galvanic corrosion is likely to ensue and sometimes with dire consequences.

Specific data relative to galvanic interactions, in tropical and marine environments, of certain metal combinations frequently encountered in military equipment often is incomplete, if not totally lacking. There is a continuing and specific need for this type of information to be made available to the design engineer, to aid him in the selection of metal combinations, to achieve maximum corrosion resistance. This is the intent of this study.

This report, however, is only introductory and preliminary, presenting the limited results available at this early stage of investigation (exposures of eight months and less). Up to four additional years of exposure are anticipated and subsequent reports are planned during the progress of and after completion of this investigation.

Eight different alloys were selected for this investigation: two aluminum alloys, one brass, one magnesium alloy, one Monel, one titanium alloy, one steel, and one stainless steel. The specimens designed for this investigation were machined to provide smooth and close fitting surfaces and equal areas of the coupled members. These were subjected to atmospheric, soil (burial), and seawater (immersion) environments at the U.S. Army Tropical Testing Station, Panama Canal Zone. Seven periods of exposure or inspections were designated, covering a duration period of approximately five years. The extent of corrosion was based on determined weight loss and on observed conditions of the specimen surfaces after removal of the corrosion products. Controls, that is, couples of like metals, also were included.

The form and size of the individual metal specimens and the design and fastening of the dissimilar metal couples are as follows.

1. Atmospheric couples are flat, rectangular parts partially offsetted when coupled. This is considered to offer some variability in surface galvanic effects, both on "free" surfaces, that is, surfaces not in close proximity to the actual contacting surfaces, and the edges closest to the

contact region. End-grain attack at the edges, particularly in the aged light (aluminum or magnesium) alloys is expected to become evident.

2. Couples buried in soil or immersed in seawater consist of members which are cylindrical with flat ends, electrically joined, but separated by means of a polyacrylate resin cylinder.

Experimental

Materials

The alloys included in this study are 6061-T6 and 7075-T6 aluminum, 360 brass, AZ-31 magnesium, 400 Monel, 4340 steel, Type 316 stainless steel, and titanium 6Al-4V.

Atmospheric specimens illustrated in Fig. 1 are flat rectangular plates, about 0.55 by 2.54 by 3.81 cm (0.215 by 1.0 by 1.5 in.), machined from 0.63-cm (0.25-in.) thick flat strips. The plates are coupled by means of an 0.31 cm (0.125 in.) diameter by 5.0 cm (2.0 in.) stainless bolt, through an off center 0.47-cm (0.185-in.) drilled hole, and are in direct contact. (The bolt also serves for mounting the coupled specimen on a mounting bar.) The fastener is insulated from the faces of the specimen by interposing a

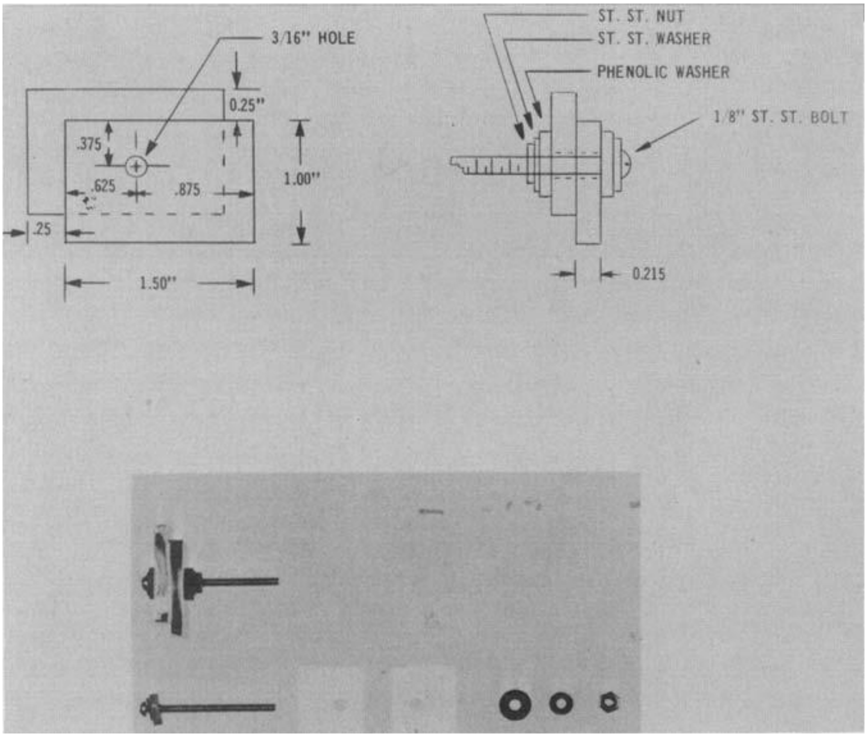

FIG. 1—*Atmospheric specimens.*

1.27 cm outside diameter by 0.31-cm (0.50 by 0.125-in.) reinforced phenolic washer under stainless steel washers at the head and nut side of the fastener. In coupling the atmospheric exposure specimens, the anodic specimen was in all cases positioned on top of the cathodic specimen to avoid contamination of the anode by cathode corrosion products.

Specimens for soil burial and seawater immersion, illustrated in Fig. 2, are 2.54 cm diameter by 1.27 cm (1.0 by 0.5 in.), machined from round bars. One flat face of the cylinder is drilled to provide a cavity of about 0.70 cm diameter by 0.94 cm (0.275 by 0.375 in.) deep, which is tapped to accommodate a 0.67 cm (0.25 in.) diameter cold-rolled, fully threaded steel screw by which the coupling is effected. In the completed coupled assembly, the metal cylinders are separated by a 2.54 cm diameter by 2.54 cm (1.0 by

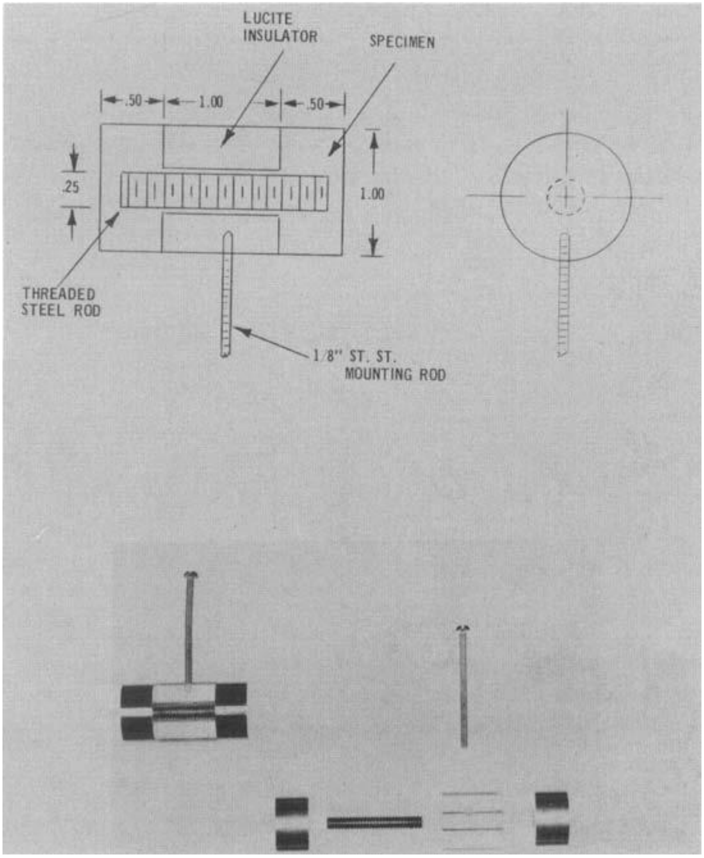

FIG. 2—*Soil burial and seawater immersion specimens.*

1.0 in.) length plexiglass rod, with a lengthwise drilled hole to accommodate the fastening screw. Further, the plastic separator contains a tapped hole to receive a 0.31 by 5.0 cm (0.125 by 2.0 in.) stainless steel screw. This is used for mounting the seawater specimens on a bar for racking. In the case of the soil specimens, a shorter screw, 0.47 cm (0.185 in.), is inserted to which a dacron thread is fastened to space (5.0 cm, 2.0 in.) and maintain sequential arrangement and to facilitate emplacement of the coupled specimens.

All flat and cylindrical metal members were machined from "as-received" stock so as to remove worked or distorted microstructure, and were machine ground to a 20 to 50 μin. scratch free surface finish.

Procedure

Prior to exposure, specimens were degreased with trichlorethylene and individually cleaned according to the procedure in Table 1. Specimen weights were then determined to the nearest milligram.

ASTM exposure test racks fabricated from Monel are employed for the atmospheric exposures. However, aluminum alloy adapter bars were designed and utilized for mounting of couples (5 cm between centers) to the test racks (Fig. 3). The couples on the racks face south and are at a 30-deg angle from horizontal. The atmospheric couples are exposed at the Fort Sherman, Panama Canal Zone, open field site (see Fig.4), approxi-

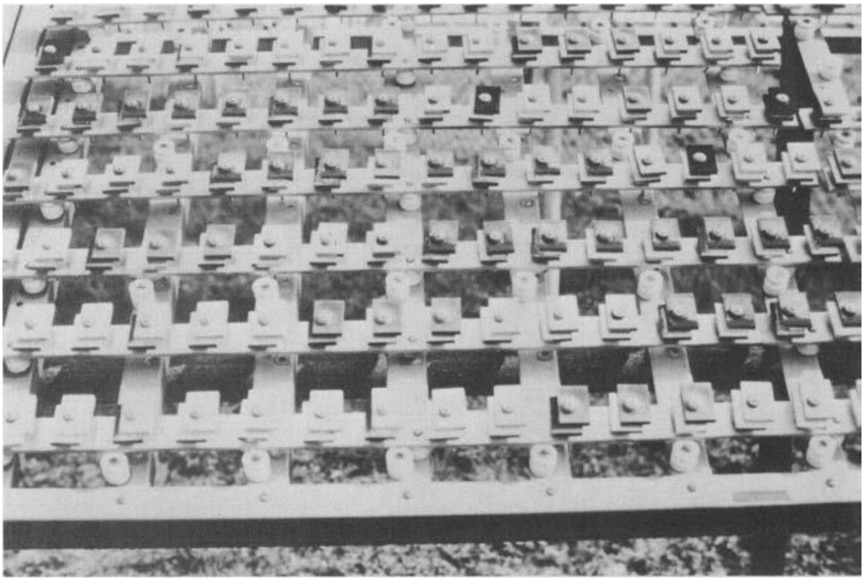

FIG. 3—*Atmospheric exposure rack mounting.*

TABLE 1—*Chemical cleaning of specimens before exposure.*[a]

Material	Pickling Solution	Remarks
AZ31-magnesium	HNO_3 80 ml/1	
Type 316 stainless steel	(litre quantity) HNO_3 400 ml HCl 100 ml H_3PO_4 100 ml CH_3COOH 400 ml	temperature, 140 to 160°F
Ti-6A1-4V	HNO_3 180 ml/1 HF 30 ml/1	time should not exceed 30 s
400 Monel	(litre quantity) H_2O 400 ml H_2SO_4 400 ml HNO_3 200 ml	
6061-T6 aluminum 7075-T6 aluminum	(litre quantity) H_2O 375 ml H_2SO_4 250 ml HNO_3 125 ml H_3PO_4 125 ml CH_2COOH 125 ml	
360 brass	(litre quantity) H_2O 400 ml H_2SO_4 400 ml HNO_3 200 ml	
4340 steel	HCl 300 ml/1	rinse in 5% Na_2CO_3 after pickling and rinsing in water
4340 steel (alternate method)	(litre quantity) HNO_3 100 ml H_2SO_4 200 ml	after pickling and rinsing with water, scrub with cleanser to neutralize acid

[a] Temperatures are room temperatures except where noted.

mately 600 m from the sea at the nearest point and 1250 m away in the direction of prevailing winds. Temperature at this site is fairly constant and uniform, with the average temperature approximately 81°F with a daily range of 9°F. The average relative humidity is 87 percent and the annual rainfall 130 in. with four months dry and eight months rainy. A total of 144 couples are exposed for each exposure period (36 couple combinations, 4 replicates each). This exposure was initiated in April 1973 and 7 exposure periods are planned, namely: 2, 4, 8, 15, 24, 36, and 48 months.

After each exposure period, specimens are returned to the laboratory and cleaned according to the procedure in Table 2 to remove contaminants and corrosion products. Specimens are visually examined for type and uniformity of surface attack, such as etching, pitting, crevice, etc., and

FIG. 4—*Fort Sherman open field site.*

final weights recorded for weight loss determinations, expressed in millimetres per year. Preliminary visual observations and weight loss determinations are included in this report of the 2, 4, and 8 months' atmospheric exposures.

Soil burial couples, approximately 5 cm (2 in.) between couples (Fig. 5) are installed at the water table, buried at a depth of 1.2 m (4 ft) below the soil surface. The soil is clay type with the soil water having a pH of 7.6 and conductivity of 6.88×10^{-5} mho. The soil burial area is adjacent to the atmospheric open field site (Fig. 6). The same number of couples are exposed as for atmospheric exposure. The soil burial was initiated Oct. 1973 and seven exposure periods are planned, namely: 2, 6, 12, 24, 36, 48, and 60 months. Preliminary results are included of the 2 and 6 months' exposures.

Seawater couples are mounted 6.2 cm (2.5 in.) between centers on exfoliation resistant experimental aluminum alloy (MA009) bar frame racks, 0.91 by 1.22 m (3 by 4 ft) (Fig. 7).

The seawater couples are suspended from a concrete pier completely immersed on the racks horizontally suspended and are approximately 1.3 m (4.5 ft) below the water surface at low tide and approximately 1.6 m (5.5 ft) below the surface at high tide in Manzanillo Bay at the Coco Solo Naval Station, Panama Canal Zone (Fig. 8). Water temperature averages approximately 82°F. The same quantity of couples are exposed as for atmospheric and soil burial exposures. The seawater exposure was initiated in Oct. 1973, and seven exposure periods are planned, namely: 2, 4, 7, 12,

TABLE 2—*Methods for cleaning specimens after exposure.*

Material	Chemical	Time	Temperature	Remarks
AZ-31 magnesium	15% CrO_3	1 to 4 h	room	
Type 316 stainless steel Ti-6A1-4V 400 Monel	H_3PO_4 160 ml/1 CrO_3 84 g/1	15 min to 1 h	75°C	
6061-T6 aluminum 7075-T6 aluminum	concentrated HNO_3	1 h	room	if corrosion products persist use 5% H_3PO_4 + 2% CrO_3 at 85 to 90°C for 30 min[b]
360 brass	20% HCl	15 min	room	
4340 steel	H_3PO_4 160 ml/1 CrO_3 84 g/1	1 to 3 h	90 to 100°C	used to initially remove heavy corrosion products
4340 steel	3.5 M HCl 0.2 M $SnCl_2$ Rodine (AMCHEM) No. 213 1 g/1[a]	2 to 4 h	room	used to remove corrosion products from atmospheric specimens and as final treatment for sea and soil exposed specimens
4340 steel (alternate method)	METSO 200 20% (by weight)	10 to 24 h	room	steel specimens, cathode; stainless steel anode; current density 40 to 60 amp/ft^2; used when time is not a factor

[a] *Materials Protection*, Vol. 6, No. 3, pp. 45–46.

[b] ASTM Recommended Practice for Preparing, Cleaning, and Evaluating Corrosion Test Specimens (G 1-67).

18, 28, and 42 months. Preliminary results are included of the 2 and 4 months' exposures.

To adjust for effects of crevice and general corrosion, like metals were coupled and results compared with those of dissimilar metal coupling were taken as galvanic corrosion. It is recognized, however, that crevice and uniform corrosion buildup can affect galvanic corrosion results.

Discussion of Results

Visual Observations

Visual examination of the specimens was made after removal from mounting bars and disassembling of the couples. A large number of the

FIG. 5—*Soil burial specimens.*

atmospheric couples were stuck together by means of a film of corrosion products and had to be forced apart. Steel couples were the most difficult to separate.

Only observations following the most recent exposure period are reported. It can be assumed that the effects for earlier exposure periods are similar but less severe.

AZ31-Magnesium—In the atmosphere, white corrosion products were present on the magnesium specimens in contact with all alloys; the specimens were lightly etched, and pitting was observed on the border of the interface. The sea specimens in contact with Type 316 stainless steel, Monel, and steel were completely consumed after two months. Specimens in contact with the other alloys exhibited a heavily pock-marked surface with penetration ranging from 0.031 in. (0.075 cm) to 0.25 in. (0.64 cm). The soil specimens had the same type of pock-marked surface as the seawater specimens, but not as severe.

Type 316 Stainless Steel—The atmosphere specimens had incipient pitting on the interface. The sea specimens exhibited crevice corrosion attack when coupled to themselves, Monel, and titanium. There was no attack on the soil specimens.

4340 Steel—The atmosphere specimens were etched uniformly showing a pock-marked surface with deep pits along the border of the interface; there was hardly any attack when coupled to magnesium. The sea and soil specimens exhibited a heavily pock-marked surface; hardly any attack

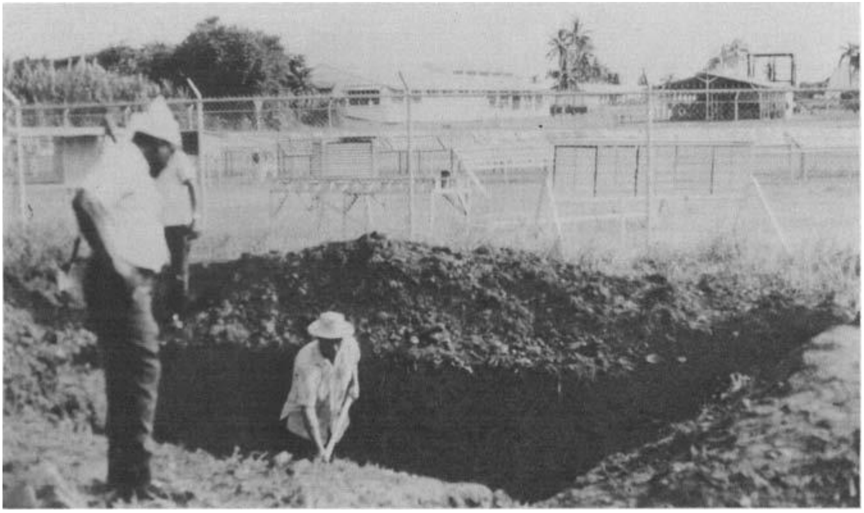

FIG. 6—*Soil burial site.*

appeared when the specimens were coupled to magnesium and the aluminum (6061 and 7075 alloys).

6061-T6 Aluminum and 7075-T6 Aluminum—The 6061-T6 aluminum alloy corroded to a lesser extent than the 7075-T6 aluminum alloy.

White corrosion products were present on the atmospheric specimens; pitting was observed on border of interface of the aluminum specimens in contact with all metals except magnesium and the controls. Pitting occurred in the sea specimens when they were in contact with all alloys except the controls and other aluminum alloy; heavy scaling and exfoliation was observed when the specimens were coupled to magnesium. The soil specimens showed localized pitting.

360 Brass—Surface dezincification and staining was observed in all environments.

400 Monel—The atmosphere specimens exhibited slight staining and the sea specimens, pitting when coupled to themselves, Type 316 stainless steel, and titanium. A slight crevice attack occurred on the soil specimens when the Monel was coupled to itself, Type 316 stainless steel, brass, and titanium.

Ti-6Al-4V—No attack occurred in any of the environments.

Corrosion Weight Losses

The degrees of corrosion are shown in Table 3 for atmospheric exposure, Table 4 for soil burial, and Table 5 for seawater immersion.

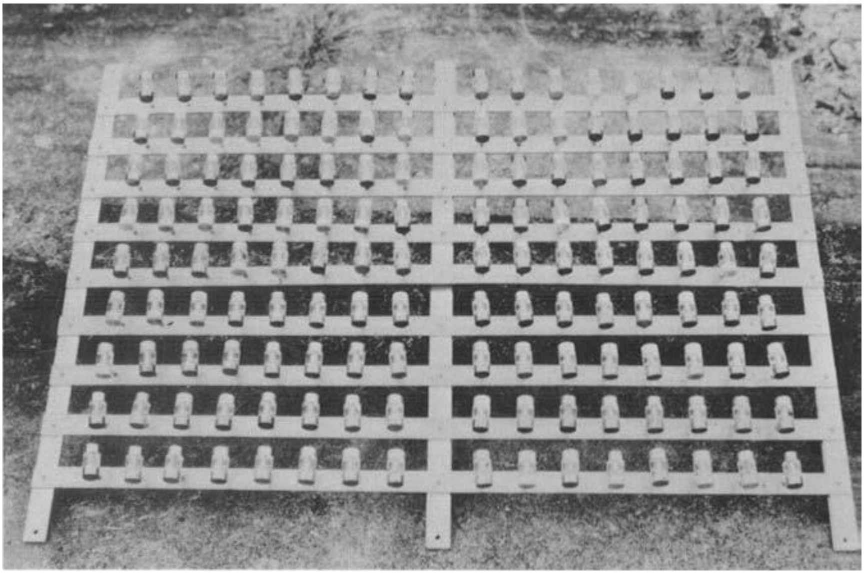

FIG. 7—*Seawater immersion rack.*

From Table 3, atmospheric exposure, little or no attack to date is evident of the Type 316 stainless steel, 6061-T6 aluminum, 7075-T6 aluminum, 360 brass, 400 Monel, or titanium 6Al-4V specimens.

General corrosion of the 4340 steel is evident in all couples but protection to the steel is afforded by coupling with AZ31 magnesium. Galvanic attack of the steel in all couples is not apparent.

Magnesium, as expected, suffers galvanic attack when coupled to each of the other alloys. This attack appears generally to be at a decreasing rate after 8 months of exposure.

From Table 4, soil burial, little or no corrosion is evident of the Type 316 stainless steel, 360 brass, 400 Monel, and titanium 6Al-4V alloys.

General corrosion of the 4340 steel is evident in all couples and the rate of attack appears to be increasing with time. Protection of the steel is afforded by the magnesium, but galvanic attack of the steel appears to occur as a result of coupling to Type 316 stainless steel, 7075-T6 aluminum, 360 brass, 400 Monel, and titanium 6Al-4V.

Magnesium is galvanically attacked by coupling with each of the other alloys. The attack is least in aluminum alloy coupling and greatest in coupling to steel. The galvanic attack in all cases, however, appears to be at a decreasing rate.

Coupling of the 6061-T6 aluminum alloy to brass and Monel results in galvanic attack of the aluminum. Coupling of the 7075-T6 aluminum alloy to Type 316 stainless steel, brass, Monel, and titanium results in

FIG. 8—*Seawater immersion.*

galvanic attack of the aluminum. Coupling of the 6061-T6 and 7075-T6 aluminum alloys to magnesium results in increased attack of the aluminum alloys.

From Table 5, seawater immersion, it may be observed for the magnesium galvanic couples that all the magnesium specimens originally coupled to Type 316 stainless steel, 4340 steel, and 400 Monel were lost and essentially all consumed.

Where coupled to the other alloys, the rate of attack to date appears to be decreasing except where the magnesium is coupled to titanium 6Al-4V.

No galvanic attack of Type 316 stainless steel is indicated. However, crevice attack is evident where the stainless steel is coupled to Monel and titanium. This crevice attack is evident also where stainless steel is coupled to itself. Crevice attack is not apparent when coupled to the more anodic specimens where cathodic protection is afforded to the stainless steel. This cathodic protection tendency with stainless steel galvanic couples in seawater has been investigated and previously reported.[2]

The rate of attack of steel to date appears to be decreasing where coupled with cathodic alloys. Protection is afforded, as expected, by coupling to magnesium and aluminum alloys.

Coupling of 6061-T6 aluminum with the other alloys results in galvanic attack, except when coupled to 7075-T6 aluminum; and the rate of attack

---

[2] Lennox, T. S., Groover, R. E., and Peterson, M. H., *Materials Protection*, Vol. 8, No. 5, May 1969, pp. 41–48.

TABLE 3—*Corrosion weight losses, atmospheric exposure, millimetres per year.*

Months	AZ31-Magnesium	Type 316 Stainless Steel	4340 Steel	A_1, 6061 Aluminum	A_2, 7075 Aluminum	360 Brass	400 Monel	Ti-6A1-4V
				MAGNESIUM				
	upper lower							
2	0.033 0.029	MCR	0.034	0.002	0.003	0.003	MCR	MCR
4	0.043 0.029		0.019	0.001	0.002	0.001		
8	0.041 0.027		0.014	0.001	0.001	0.001		
				STAINLESS STEEL				
2	0.075	MCR	0.072	0.005	0.007	0.009	MCR	MCR
4	0.079		0.051	0.002	0.005	0.004		
8	0.057		0.037	0.001	0.003	0.002		
				STEEL				
			Upper Lower					
2	0.097	MCR	0.064 0.078	0.005	0.009	0.006	MCR	MCR
4	0.070		0.049 0.055	0.006	0.005	0.003		
8	0.064		0.033 0.044	0.003	0.004	0.002		
				A_1				
				Upper Lower				
2	0.046	MCR	0.065	0.002 0.002	0.004	0.005	MCR	MCR
4	0.054		0.056	0.001 0.001	0.002	0.002		
8	0.049		0.039	0.001 0.001	0.001	0.001		

				A₂				
					Upper Lower			
2	0.049	MCR	0.062	0.003	0.004 0.004	0.005	MCR	MCR
4	0.054		0.051	0.001	0.001 0.001	0.002		
8	0.049		0.036	0.001	0.001 0.001	0.001		
				BRASS				
						Upper Lower		
2	0.074	MCR	0-069	0.005	0.010	0.007 0.007	MCR	MCR
4	0.067		0.052	0.003	0.003	0.004 0.003		
8	0.065		0.037	0.002	0.003	0.001 0.001		
				MONEL				
2	0.093	MCR	0.075	0.004	0.006	0.007	MCR	MCR
4	0.078		0.051	0.002	0.003	0.004		
8	0.061		0.037	0.002	0.003	0.002		
				TITANIUM				
2	0.063	MCR	0.074	0.005	0.007	0.008	MCR	MCR
4	0.059		0.058	0.002	0.005	0.004		
8	0.055		0.038	0.002	0.003	0.002		

NOTE—MCR = minimal corrosion rate $\leq$ 0.001 for all exposure periods.

TABLE 4—*Corrosion weight losses, soil burial, millimetres per year.*

Months	AZ31-Magnesium	Type 316 Stainless Steel	4340 Steel	A_1, 6061 Aluminum	A_2 ,7075 Aluminum	Brass	Monel	Titanium
				MAGNESIUM				
2	0.092	MCR	0.005	0.065	0.047	0.004	0.000	MCR
6	0.137		0.009	0.017	0.019	0.001	0.000	
				STAINLESS STEEL				
2	1.399	MCR	0.070	0.003	0.003	0.017	0.001	MCR
6	0.958		0.106	0.008	0.017	0.016	0.009	
				STEEL				
2	1.1920	MCR	0.047	0.002	0.003	0.007	0.001	MCR
6	1.107		0.086	0.001	0.001	0.001	0.000	
				A_1				
2	0.264	MCR	0.049	0.003	0.003	0.006	0.001	MCR
6	0.165		0.088	0.005	0.006	0.001	0.001	

				A_2				
2	0.549	MCR	0.049	0.003	0.003	0.006	0.001	MCR
6	0.234		0.102	0.009	0.009	0.001	0.001	
				BRASS				
2	0.966	MCR	0.058	0.004	0.003	0.005	0.000	MCR
6	0.929		0.145	0.011	0.019	0.007	0.004	
				MONEL				
2	1.320	MCR	0.062	0.002	0.003	0.005	0.001	MCR
6	0.941		0.121	0.013	0.020	0.014	0.005	
				TITANIUM				
2	1.020	MCR	0.058	0.004	0.003	0.005	0.001	MCR
6	0.751		0.093	0.009	0.016	0.012	0.009	

NOTE—MRC = minimal corrosion rate ≤ 0.001 for all exposure periods.

TABLE 5—*Corrosion weight losses, seawater immersion, millimetres per year.*

Months	AZ31-Magnesium	Type 316 Stainless Steel	4340 Steel	A_1, 6061 Aluminum	A_2, 7075 Aluminum	Brass	Monel	Titanium
				MAGNESIUM				
2	1.557	0.000	0.018	0.445	5.162	0.010	0.001	MCR
4	1.293	0.000	0.053	0.786	4.158	0.004	0.002	
				STAINLESS STEEL				
2	23.900 100% consumed	0.098	1.156	0.380	0.467	0.359	0.011	MCR
4	23.900 100% consumed	0.129	0.844	0.276	0.305	0.192	0.025	
				STEEL				
2	23.900 100% consumed	0.000	0.645	0.251	0.340	0.007	0.001	MCR
4	23.900 100% consumed	0.000	0.475	0.176	0.189	0.004	0.001	
				A_1				
2	2.323	0.000	0.018	0.043	0.013	0.007	0.001	MCR
4	2.152	0.001	0.004	0.021	0.009	0.001	0.001	

				A_2				
2	5.019	0.000	0.020	0.050	0.040	0.005	0.001	MCR
4	4.732	0.000	0.024	0.024	0.030	0.002	0.001	
				BRASS				
2	12.070	0.000	1.269	0.438	0.413	0.129	0.003	MCR
4	6.184	0.000	0.808	0.234	0.303	0.111	0.002	
				MONEL				
2	23.900 100% consumed	0.105	1.252	0.385	0.491	0.253	0.035	MCR
4	23.900 100% consumed	0.044	0.827	0.257	0.300	0.198	0.006	
				TITANIUM				
2	7.505	0.088	1.027	0.304	0.614	0.091	0.010	MCR
4	9.166	0.018	0.825	0.198	0.308	0.129	0.007	

NOTE—MCR = minimal corrosion rate ≤ 0.001 for all exposure periods.

appears to be decreasing. The greatest attack of the aluminum is evidenced where coupled to magnesium.

Coupling of 7075-T6 aluminum with the other alloys results in galvanic attack, except when coupled to 6061-T6 where some protection appears to be afforded. The rate of attack in coupling to all the other alloys appears to be decreasing. The greatest attack of the aluminum is evident where coupled to magnesium in which case severe attack and delamination of the 7075-T6 aluminum results.

Galvanic attack, at a decreasing rate, of brass is evident from coupling to Type 316 stainless steel and 400 Monel. Protection is afforded by coupling to AZ31 magnesium, 4340 steel, 6061-T6 aluminum, and 7075-T6 aluminum.

Galvanic attack of the Monel is not apparent to date. However, early pitting of Monel in seawater has been observed in some instances where the Monel is coupled to itself, stainless steel, and titanium. This pitting appears to be only limited and not the high density pitting attack of Monel subjected to seawater reported elsewhere.[3]

No galvanic attack of the titanium is evident.

Heavy buildup of barnacle growth on the seawater immersion specimens develops rapidly. It is expected that this buildup will afford some protection and result in retardation of corrosion as reported elsewhere.[4]

Conclusions

Only limited results are available at this early stage of the investigation; however, some tentative conclusions can be offered.

In general, comparison of the results of atmospheric, soil, and seawater exposures indicates that least attack occurs in the atmosphere and the most attack occurs in seawater. Titanium was not attacked in any of the three test environments. Monel and Type 316 stainless steel were found resistant in the atmosphere and in the soil. Pitting of Monel occurs in seawater but is retarded by coupling with the more anodic alloys (magnesium, aluminum, brass, and steel). Crevice corrosion of stainless steel occurs in seawater but this is also retarded by coupling with the more anodic alloys (magnesium, aluminum, brass, and steel). Based on available data, the 6061 and 7075 aluminum alloys appear to offer sacrificial protection to the steel in seawater, but not in the soil nor in the atmosphere. There is insufficient data at this time to distinguish any difference in the rate of attack of aluminum couples in atmospheric and soil exposures. Magnesium, as expected, affords protection to the other alloys in all three

---

[3] Southwell, C. R. and Alexander, A. L., *Materials Protection*, Vol. 8, No. 3, March 1969, pp. 39–44.

[4] Southwell, C. R., Butterman, J. D., and Hummer, C. W., "Influence of Marine Organisms of the Life of Structural Steels in Sea Water," NRL Report 7672, Naval Research Laboratory, Washington, D. C., 19 March 1974.

environments except where coupled to the 6061 and 7075 aluminum alloys in the seawater in which case severe attack and delamination, especially of the 7075 aluminum, results. The cause of the damaging effect on aluminum is not known but will be investigated.

Acknowledgments

We wish to thank Anthony Gressel, Tropic Test Center, Panama Canal Zone, for his invaluable assistance in assembling exposure racks, in preparation of the soil burial site in installation and subsequent removal of specimens, and in the packaging and return shipment of exposed specimens to this laboratory. Careful packaging has resulted in virtually no physical damage to the coupled specimens returned.

We wish to thank R. S. Haskin of Pitman-Dunn Laboratory, who was extremely helpful in the cleaning, weighing, identification, and assembling of the specimens prior to shipment to Panama Canal Zone for exposure.

Also, we wish to thank W. F. McTeague, also from Pitman-Dunn, for his aid in identifying and assembling the specimens.

Pitting Corrosion

Henry Suss[1]

Localized Corrosion Attack on Carbon Steel—Case Histories of Service Failures

---

REFERENCE: Suss, Henry, "**Localized Corrosion Attack on Carbon Steel—Case Histories of Service Failures,**" *Galvanic and Pitting Corrosion—Field and Laboratory Studies, ASTM STP 576,* American Society for Testing and Materials, 1976, pp. 117–131.

ABSTRACT: Four case histories of service failures attributable to some form of localized corrosion attack are reviewed. The initial case history covers a problem that developed because of the failure to follow operational procedures and because the wrong chemical was used for the inhibitor. The second case history covers an instance where the conjoint actions of the environment and cyclic loading (fatigue) promoted accelerated localized pitting attack rather than the usual loss in fatigue strength generally associated with corrosion fatigue. The third case history presents the potential concerns in using an improperly controlled corrosion protection system. The final case history reveals the perils of allowing systems to remain partially filled with stagnant solutions.

A major concern is the possibility that the same type of failures will recur. An approach for possible actions in programs for the prevention of premature corrosion failures is recommended.

KEY WORDS: corrosion, failure analysis, corrosion prevention, carbon steels, protective coatings control, corrosion fatigue

In an article published recently,[2] the percentage of equipment failures, as related to specific modes of corrosion attack, is listed in Table 1. Much of my experience has been in analysis of many corrosion-related failures, and I agree that the data presented in that article are representative of the type and level of service failures.

To select the more representative case histories for this paper, records from 1958 to the present were reviewed. This review not only recalled many interesting, frustrating experiences but also revealed that the same types of failures keep recurring. To express it in an old cliché, "history tends to repeat itself." Or, as Dr. Mars Fontana of Ohio State University bluntly

---

[1] Principal engineer, Knolls Atomic Power Laboratory, General Electric Company, Schenectady, N. Y. 12301.

[2] "Corrosion and Wear," *Iron Age*, 21 Jan. 1974.

TABLE 1—*Corrosion failure breakdown.*

Form	Percent	
General	31.5	
Cracking		
stress corrosion	21.6	23.4
corrosion fatigue	1.8	
Pitting	15.7	
Intergranular	10.2	
Erosion		
corrosion	7.4	9.0
cavitation	1.1	
fretting	0.5	
Crevice	1.8	
De(metal)ification	1.1	
Two metal	0.0	

NOTE—High temperature, 2.3 percent; weld corrosion, 2.3 percent; cold wall, 1.8 percent; end grain, 1.1 percent; hot wall, 0.5 percent; and hydrogen embittlement, 0.5 percent. Source: DuPont Company.

states, "Virtually all premature corrosion failures occur for reasons well known—and can be prevented."

Case histories and many other equivalent papers are being presented and published continually. Each contains the pertinent data and the means by which equivalent and other types of failures can be prevented or minimized. Yet premature corrosion failures keep recurring at much too high a level. These failures can be attributed to several possibilities: (*a*) available data are overlooked; (*b*) available data may not reach those persons who could benefit most; (*c*) potential use of the available data in minimizing future corrosion problems was not recognized; and (*d*) uncertainty in relating the available data from one failure to stop possible corrosion attack for other applications.

Case histories of service failures that are related to localized corrosion attack (exclusive of stress and intergranular corrosion) are reviewed in this paper. In this effort, I shall explain the means used and the basis for establishing the factors that contributed to these failures, and I shall review some recommended actions to stop or minimize the specific forms of attack. A program that I suggest as essential to reduce the extent of similar premature corrosion failures will conclude this paper.

Case History 1

Through Perforation of Carbon Steel Tubes of a Heat Exchanger

The carbon steel tubes of a heat exchanger, based on studies and available data, had more than adequate corrosion resistance to the environment both through the tubes and on the shell side. The tube resistance on the shell side (outside diameter) required that specific instructions, listed as follows, be followed during operations and shutdown periods.

1. During any shutdown period, the shell side shall either remain completely filled with the solution or completely drained.
2. The chromate levels during operations shall be maintained at 10 to 20 ppm; during periods of stagnancy (inactivity), at 1000 to 2000 ppm.
3. Final instructions covered chemical analyses procedures and the frequency of such analyses.

After about a year in service, perforations developed in the carbon steel tubes (Fig. 1) that affected the usefulness of the heat exchanger. A subsequent investigation and analysis provided the following information.

1. Operators did not follow instructions. The unit was allowed to remain partially filled (note water line in Fig. 2 after the tube bundle was removed) with solution, possibly during shutdown or maintenance periods.
2. Deposits formed on the tube surface because the wrong compound[3] was used to develop the required chromate level. The compound was used at a level equivalent to its maximum solubility, thereby forming a saturated solution. At such concentration levels, chemicals can readily precipitate out locally (Figs. 3 and 4) as a result of actions during heat transfer and drain downs and at water lines.
3. The records indicated that the required number of analyses was conducted and that the chromate levels were maintained within the specified limits.

The end results of the actions, Items 1 and 2, were water-line attack and under-deposit corrosion, both of which are forms of concentration cell corrosion.

This failure, together with the consequences of another similar failure and lack of manpower to ensure maintenance of the required controls for the continued use of carbon steel, was reviewed and resulted in the recommendation that the tubes of the replacement bundle be 90 to 10 or 70 to 30 cupro-nickel. Inspections of similar units in service at that time indicated that the cupro-nickel alloy tubes were resistant to both general and pitting attack in the absence of inhibitors and were not as sensitive to waterline attack. The replacement bundle has been in service for more than eight years with no reported problems.

Case History 2

Leak in Carbon Steel High-Pressure Steam Condensate Bypass Test Line—Corrosion-Fatigue Attack

After five years of service, crack-like indications were observed in the subject pipe (Fig. 5) during radiographic inspection of an adjacent repaired

---

[3] Proprietary inhibitor compound which consisted of about 30 percent chromate, zinc, and polyphosphates. The basis for use of this compound could not be established.

FIG. 1—*Pitting attack carbon steel heat exchanger tube, area of through performation, X10.*

weld. To establish the adequacy of the pipe, the assembly was hydrostatically tested. A pinhole leak necessitated replacement of the pipe section.

After the failed pipe was longitudinally sectioned, similar pits or crack-like indications were evident 4 to 6 in. from each end, in only the three and nine o'clock positions (Figs. 6 and 7). The attack in the nine o'clock position is shown in Fig. 6. The remainder of the pipe indicated no significant evidence of any corrosion attack.

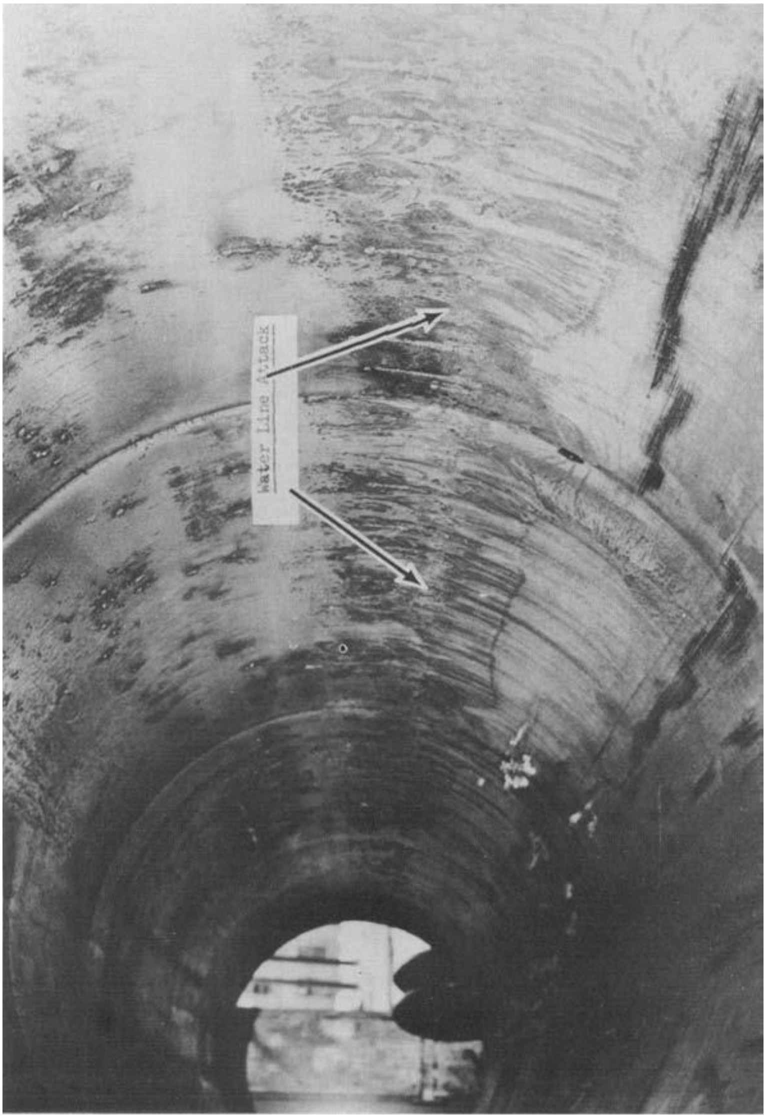

FIG. 2—*Water line attack, inside diameter of shell of heat-exchanger.*

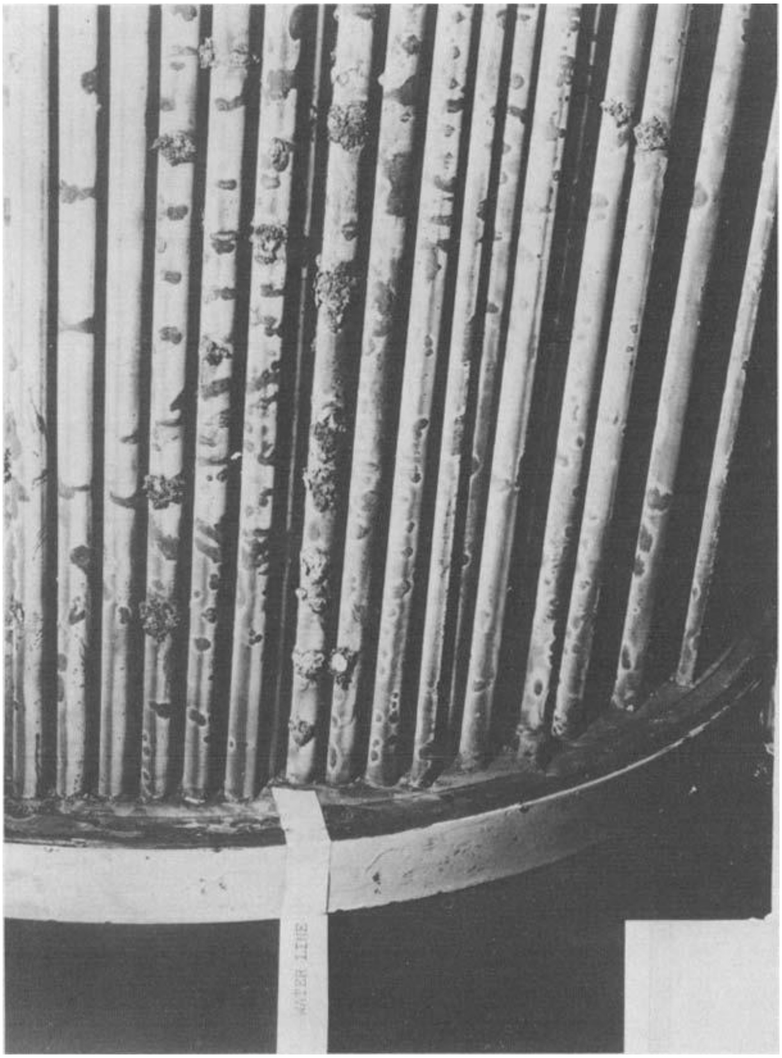

FIG. 3—*Typical nodule distribution on carbon steel tubes.*

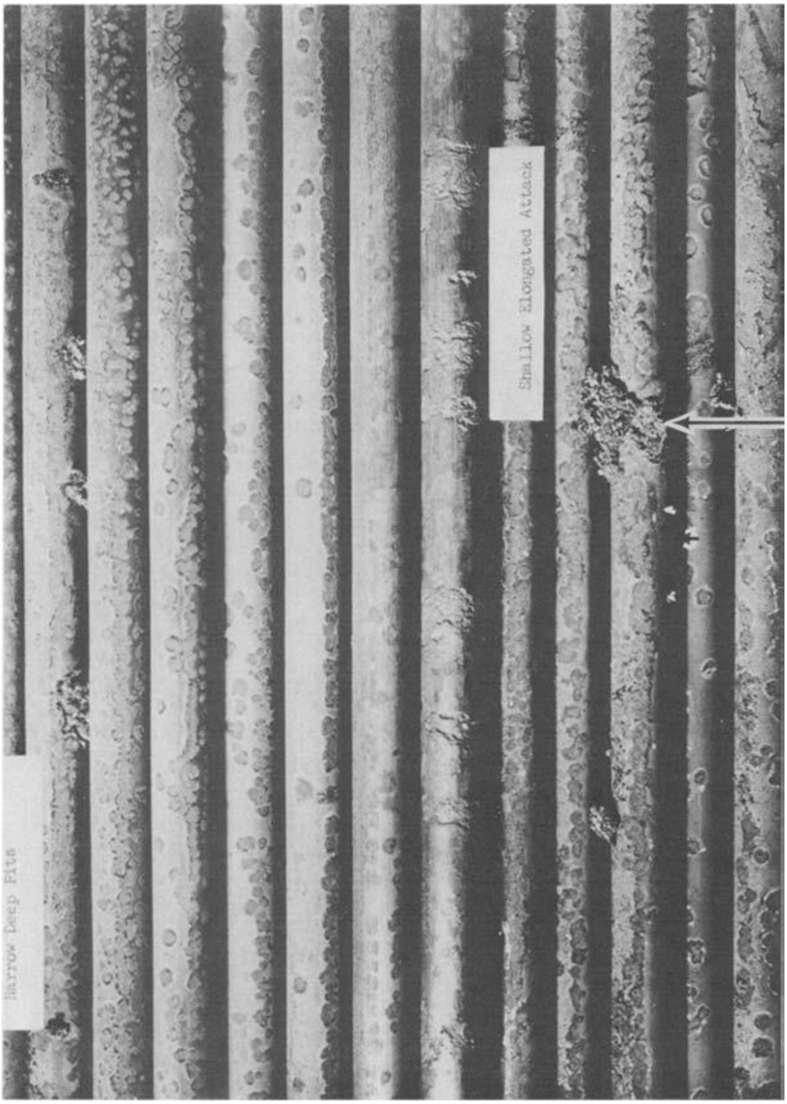

FIG. 4—*Pitting attack, carbon steel heat exchanger tube, narrow deep pits. Note crystal-line appearance of corrosion products.*

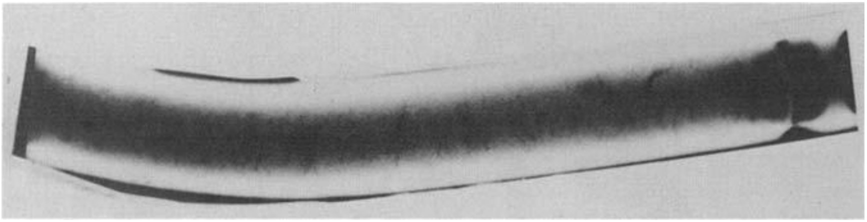

FIG. 5—*High pressure carbon steel steam by-pass line; attack, radiograph inspection.*

A study of the system and a review of the test unit in operation revealed the following indications.

1. The chemistry and temperature of the condensate entering and leaving the pipe were the same. Therefore, the attack could not be attributed directly to the environment.
2. The subject pipe was a by-pass line attached to a larger diameter main pipeline of the test system. With each change (eight to ten times a day) in the test conditions, as required by the program, the main line moved vertically. This movement subjected the by-pass line to a bending moment with peak tensile stresses equivalent to the yield strength of the material.

This case history is the only example in my experience where the combined actions of corrosion and low-frequency cyclic loading promoted accelerated pitting attack rather than the usual loss in the material's fatigue strength (corrosion-fatigue).

To prevent the recurrence of a similar failure, the test unit would have required a major redesign. The changes were not initiated, since the assembly was required for the same test program for an additional six to nine months. The replacement pipe of the same design was considered more than adequate for the desired service period.

Case History 3

Localized Perforation of a Carbon Steel Waste Line

During a routine inspection, a perforation was observed in the twelve o'clock position of a 3-in.-diameter interior coated carbon steel pipe (0.215-in. wall) after about six years in service. The removed pipe section with the failed area was submitted for failure analysis.

A 4-ft length of the pipe was sectioned longitudinally. Most of the inside surface was covered with rust-colored corrosion products. After descaling, the following were observed.

1. Only one area of significant attack, that of the perforation (Fig. 8), was noted.

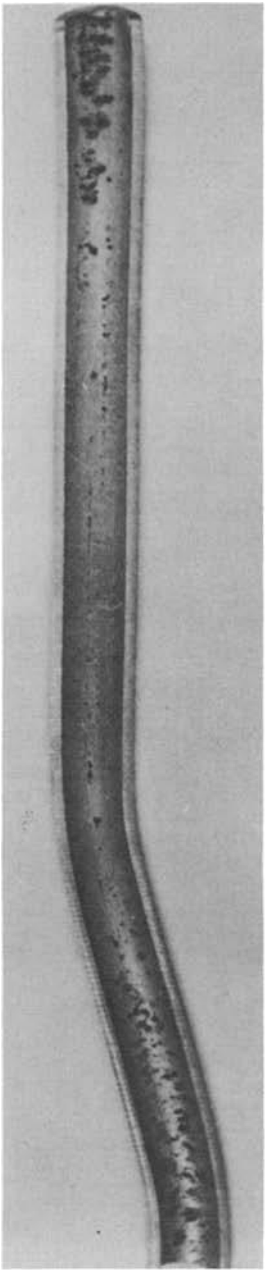

FIG. 6—*Corrosion-fatigue attack, high pressure steam line; inside diameter, pitting attack evident at nine o'clock position, X1/2.*

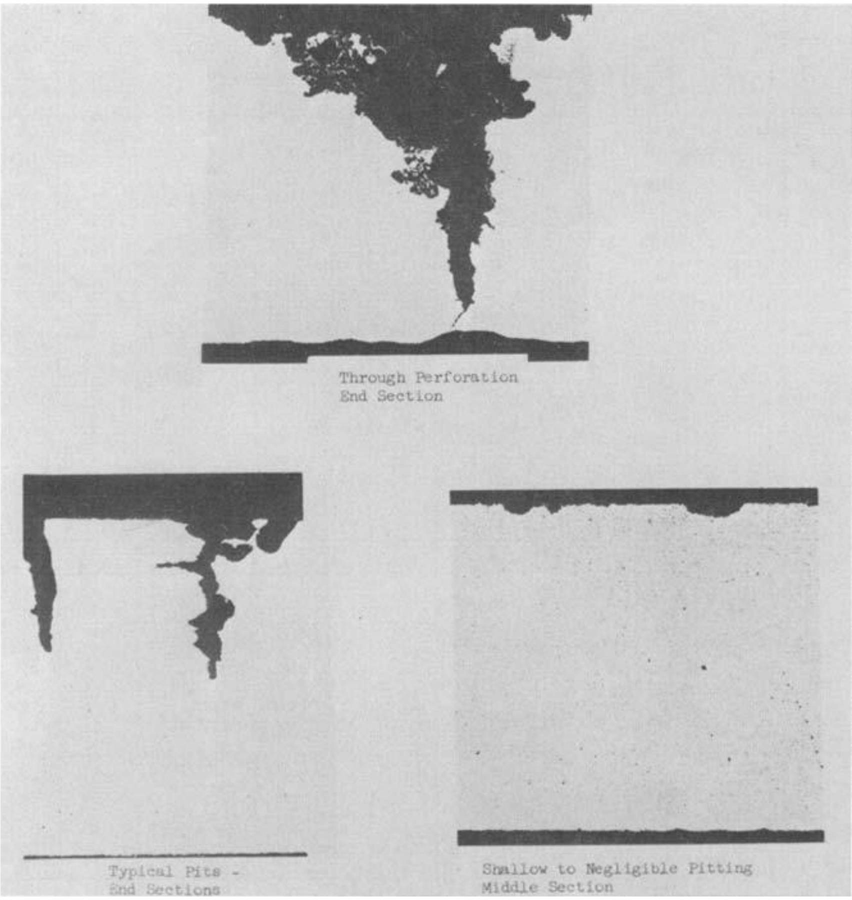

FIG. 7—*High pressure carbon steel steam by-pass line, pitting attack.*

2. In an adjacent area, where a large section of coating had failed, relatively "uniform" metal attack was noted. The typical metal loss was 10 to 20 mils with one localized area reduced by 30 to 40 mils (Fig. 8).
3. The coating protected most of the interior surface, but some areas evidenced the initiation of localized pitting attack (Fig. 9).

The perforation (shown in Fig. 8) is typical of the end result of corrosion attack in areas of localized failure of the protective layers or of holidays (voids) in the coating.

Coatings are a useful means for corrosion protection *but* require continual inspection to detect damage or deterioration. Since such requirements are not practical for inside walls of a pipe, an uncoated pipe would have been the preferred condition.

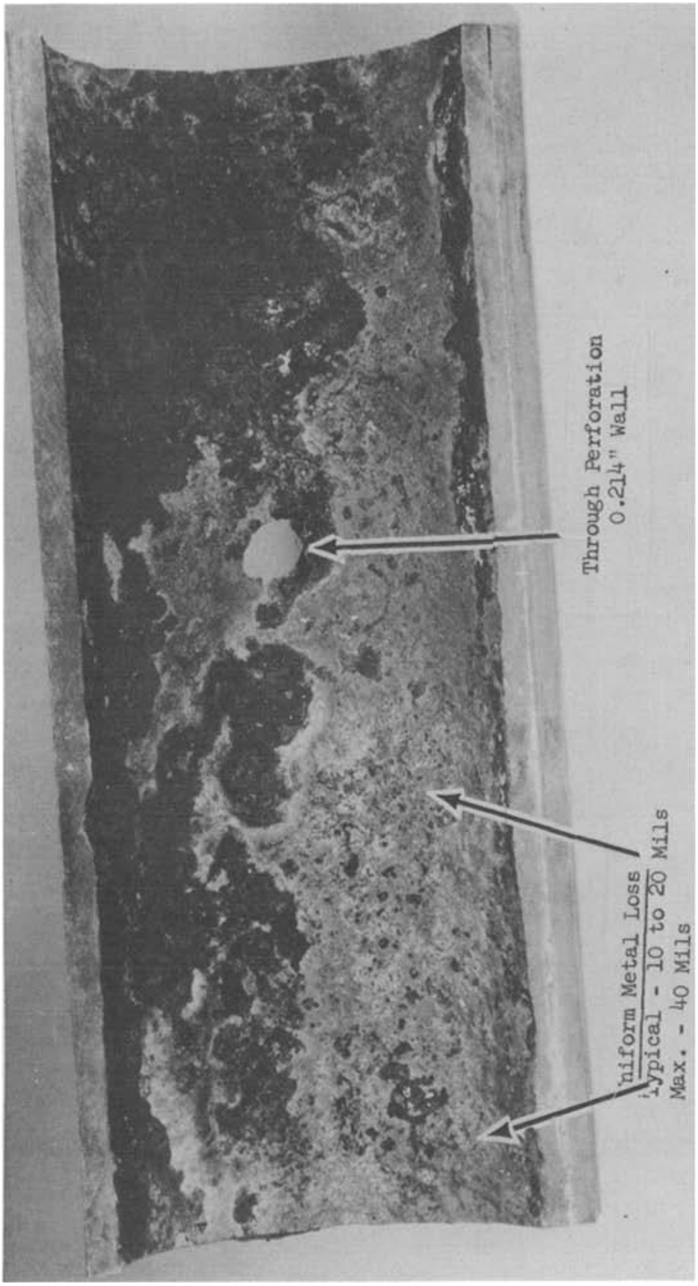

FIG. 8—*Carbon steel drain line.*

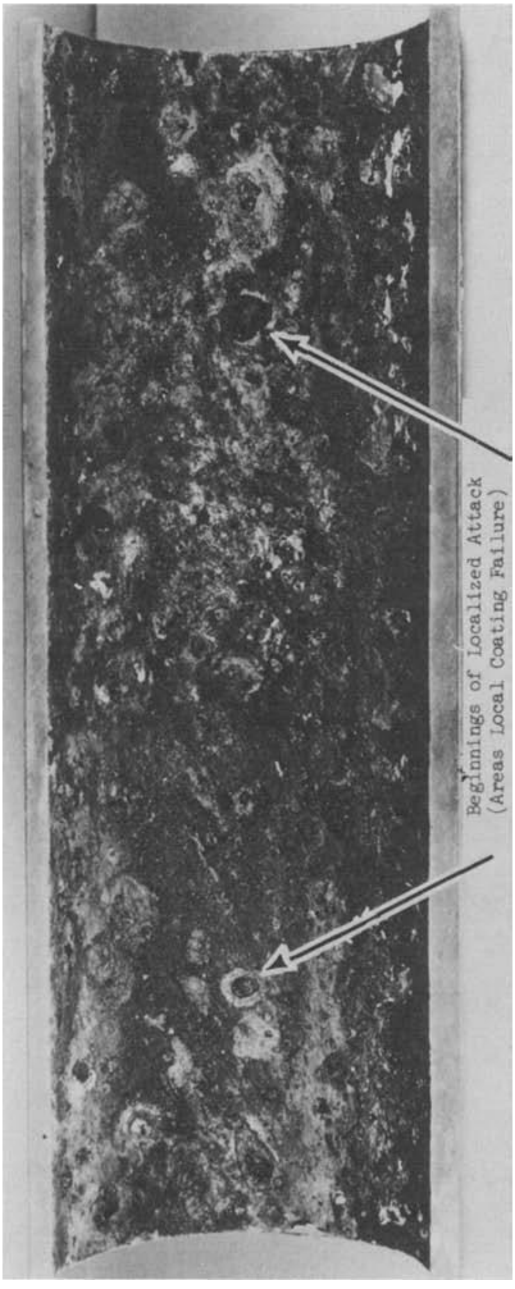

FIG. 9—*Carbon steel drain line.*

Although larger volumes of metal will be lost, with uncoated pipes, the pipe would still be functional. Also, the possibility of a localized perforation developing before detection would be lessened. Routine spot checking by nondestructive techniques could detect wall thinning that approaches unsafe limits. To detect areas with localized attack before perforation occurs would require either 100 percent inspection of the surface or repeated hydrostatic testing.

The use of improperly maintained protection systems can create more concerns than if protective systems were omitted.

Case History 4

Localized Pitting Attack in Steam Generator Carbon Steel Blow-Down Lines

Based on experience and laboratory tests, carbon steel possesses more than adequate corrosion resistance for service as blow-down lines during periods of stagnancy. Yet, in one unit, severe pitting attack was detected in some horizontal lines after less than four years in service.

After the pitted pipe was removed and sectioned, it was evident that the attack was restricted to the bottom section, five to seven o'clock (Fig. 10). Available data revealed that carbon steel pipe can exhibit pitting attack in the environment when allowed to remain only partially filled with the solution with air in the vapor phase. A subsequent analysis of the blow-down system indicated that the pitting attack was restricted to specific horizontal lines. In each instance, these lines remained partially filled with the solution during periods of stagnancy because of the valve closing sequence used.

Oxygen, the corrosion accelerant, is continually available in the vapor phase of most partially filled systems. In a completely filled system, the low dissolved levels of oxygen dissipate relatively rapidly, resulting in a solution that remains nonaggressive. To avoid attack in the replacement pipes, the valve closing sequence was therefore modified to ensure that all lines would be, and remain, filled completely during periods of inactivity.

Corrosion Prevention Programs

In reviewing the report issued by the government-sponsored National Committee on Materials Policy (NCMP),[4] I quote the following paragraph:

> One of the most obvious opportunities for materials economy is control of corrosion. It has been estimated that the Nation's annual corrosion cost is $15 billion. One third of this cost can be saved by applying techniques presently developed and available. Engineers and designers can make more extensive use of anticorrosion techniques. To this end, pertinent information must be widely disseminated. Research and development can provide additional means of controlling corrosion.

[4] Staehle, R. W., *Corrosion*, Vol. 31, No. 2, 1970, p. 41.

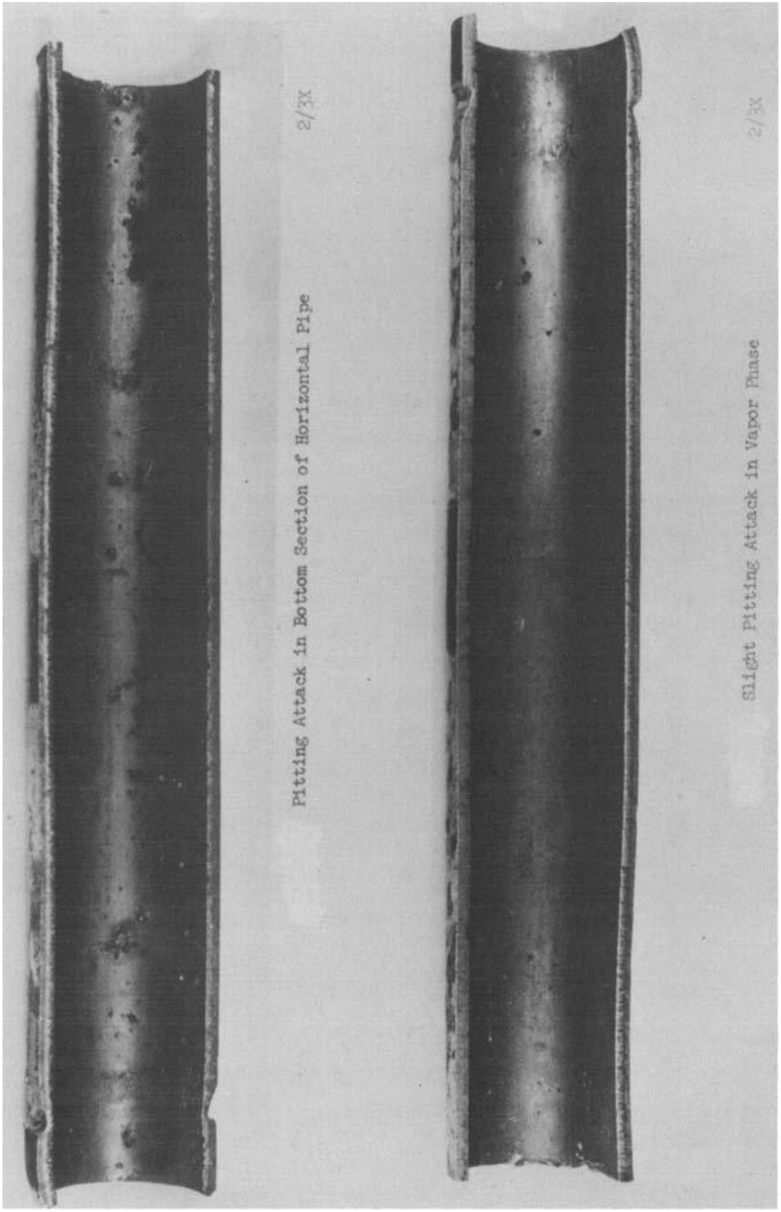

FIG. 10—*Pitting attack in carbon steel blow-down line.*

With the increasing equipment complexity, the consequences of premature failures, and the data from corrosion failure analyses, a major effort was initiated within my division several years ago to develop programs for corrosion prevention and to adopt the best available means for their implementation. In planning the study, it was recognized that one of the more important approaches was similar to the recommendation prescribed in the foregoing quotation: dissemination of pertinent information to all engineering disciplines including an understanding of all forms of premature corrosion attack and available anticorrosion methods.

Following this study, a company-sponsored engineering-oriented corrosion course was developed and presented. Data and experience from prior failure analyses are an important part of the course content, and, as a result of this program, interest among all engineers has increased. With the consequences of this greater understanding, there has been a marked increase in the means for prevention of corrosion failures. With this background of tangible results, management is now requesting that new courses be developed and offered and is encouraging an increase in the level of attendance.

The importance of engineering-oriented corrosion courses cannot be overemphasized. If such efforts are not expanded throughout industry, then other corrosion engineers will report similar case histories, express concerns relative to their recurrence, or will report that many failures did occur for reasons that were known but that could have been prevented.

J. W. Spence[1] *and F. H. Haynie*[1]

Pitting of Galvanized Steel in Controlled Clean Air Environments

---

REFERENCE: Spence, J. W. and Haynie, F. H., "**Pitting of Galvanized Steel in Controlled Clean Air Environments,**" *Galvanic and Pitting Corrosion—Field and Laboratory Studies, ASTM STP 576*, American Society for Testing and Materials, 1976, pp. 132–146.

ABSTRACT: Specimens of galvanized steel sheet were exposed to polluted and clean air in controlled environmental chambers having the capability to simulate diurnal conditions. Corrosion of the zinc films was essentially a linear function of time for each exposure condition. The range of weight losses for the polluted and clean air environments were unexpected approximately the same. However, uniform corrosion of the zinc occurred in the polluted exposures whereas pitting corrosion of the zinc was observed in the clean air exposures.

Scanning electron microscopy/microprobe analysis of the galvanized zinc surface was used to study the mechanism of initiation and propagation of pitting corrosion. Corrosion products were observed to localize and form a barrier that could accentuate an acidic condition within the pit. Pitting corrosion is thus accelerated by the difference in pH within and outside the pit. During the pollutant exposures pitting corrosion is prevented because the drastic difference in pH within and outside the pit. During the pollutant exposures pitting corrosion is prevented because the drastic difference in pH did not occur.

KEY WORDS: corrosion, metals, galvanized steel, exposure chamber, clean air, sulfur dioxide, statistical analysis

For the past several years the Environmental Protection Agency (EPA) has been conducting field and laboratory investigations to assess the detrimental effects of air pollution on materials [*1–5*].[2] The ultimate objective of these studies has been to develop predictive dose-response relationships for various classes of materials. This information is needed to serve as input for cost-benefit studies and as criteria for developing secondary air quality standards.

Accelerated degradation of materials by pollutants is generally measured by conducting controlled environment laboratory exposures with and

---

[1] Research chemist and chief, Materials Section, respectively, National Environmental Research Center, Environmental Protection Agency, Research Triangle Park, N. C. 27711.

[2] The italic numbers in brackets refer to the list of references appended to this paper.

without pollutants and comparing the observed effects. Thus, a statistically designed study involving the exposure of economically significant materials to controlled environments containing pollutants (sulfur dioxide, nitrogen dioxide, and ozone) as well as clean air was performed. The results of the polluted and clean air exposures for similar environmental conditions were compared in order to assess material damage. Over 20 000 h of exposure time, which includes 4000 h of clean exposure, were accumulated.

Experimental Procedure

This exposure study was conducted in five environmental chambers that were designed to operate continuously with each chamber having independent control of temperature, humidity, lighting intensity, and concentration of pollutant gases [6]. Before initiating this study, differences in chamber lighting and pollutant distribution, as well as the control capability of the environmental variables within the five chambers, were adjusted to be below 10 percent variation for 95 percent of the measurements.

The environmental chambers (Fig. 1) are equipped with a cap that houses a xenon arc lamp for simulating sunlight. Each chamber also contains a chill rack (Fig. 2) upon which the material specimens are mounted to

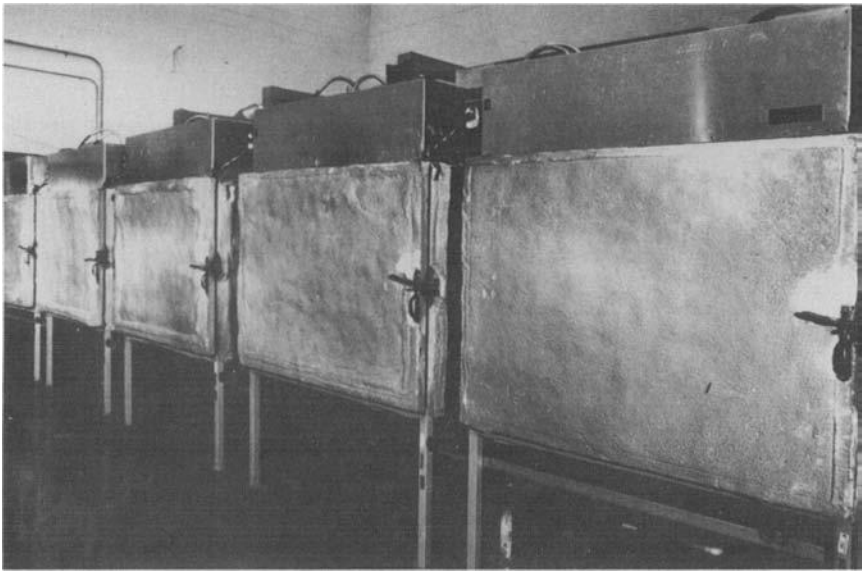

FIG. 1—*Environmental chambers.*

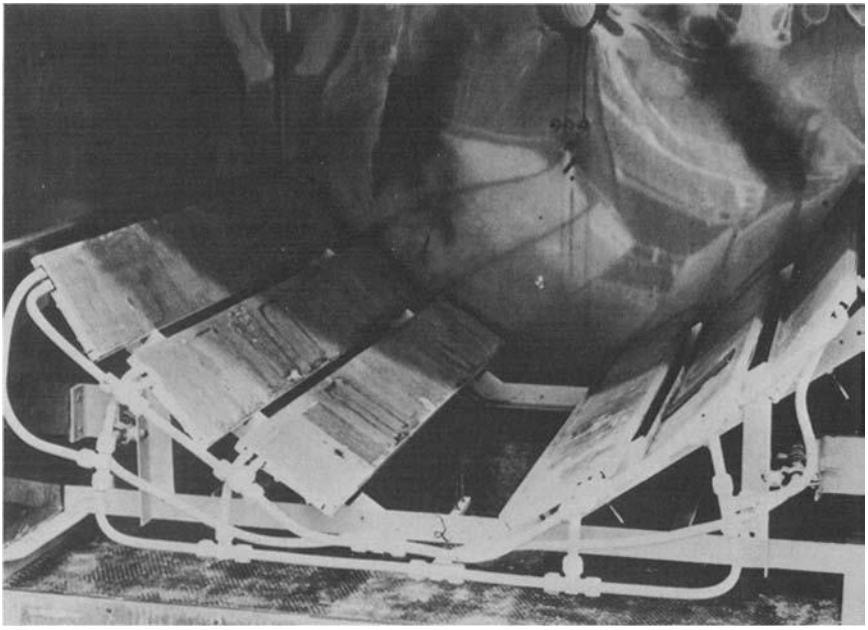

FIG. 2—*Specimen chill rack.*

enhance dew formation. Diurnal conditions are simulated as each chamber features a controllable dew/light cycle. This mode of exposure allows the surfaces of test materials to absorb and concentrate gaseous pollutants as they do in real world environments.

Temperature-time profiles (Fig. 3) were obtained by monitoring specimen temperatures during the dew/light cycles for each set of chamber conditions (temperature and relative humidity). The temperature and relative humidity of the air flowing into the chambers were maintained at desired levels. However, the temperature of the specimens continually varied during the dew/light cycle, thus changing the local relative humidity. Moisture condensed on the specimens when the temperature was below the dew point. Since the moisture content of the air is constant (set by feed air conditions), the relative humidities at the specimens as a function of time were calculated using the cycling temperature data. Visual detection of condensation on the specimens occurred at or above a calculated relative humidity of approximately 85 percent. Thus, at corresponding temperatures (Fig. 3) the specimens were considered to be wet.

Time of wetness per cycle and geometric mean specimen temperatures when wet were calculated from the data and are given in Table 1. Previous studies have shown that the corrosion of metallic materials occurs only

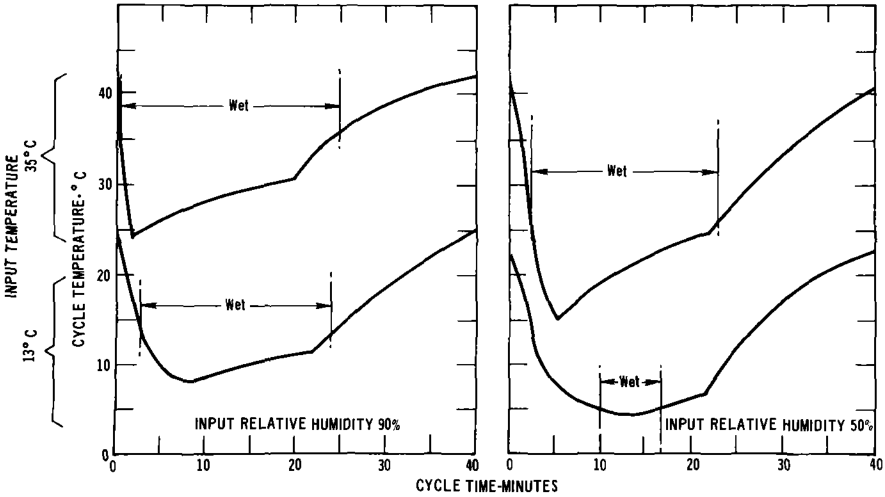

FIG. 3—*Temperature-time profiles.*

TABLE 1—*Cycle time of wetness and geometric mean specimen temperature when wet.*

Input Temperature of Feed Air	Input Relative Humidity	
	90%	50%
35°C	24.5 min 302.4 K	20.7 min 293.4 K
13°C	22.0 min 283.2 K	7.0 min 277.6 K

NOTE—Geometric mean specimen temperatures were reported in degrees Kelvin (K) for use in Arrhenius relationship.

when the specimens are wet [*7*,*8*]. Therefore, exposure data obtained from this study should be analyzed in terms of the expected times of wetness.

Commercial 18-gage galvanized steel with an approximate 25 μm zinc coating was one of several economically important materials selected for simultaneous exposure in these experiments. The sheet was cut into 7.6 by 12.7-cm exposure panels. The panels were scrubbed in a warm detergent solution, rinsed in distilled water, and degreased in acetone. Initial panel weights were measured on an analytical balance.

For each exposure condition, six galvanized panels were randomly mounted on the chill racks with thermally conducting silicone paste which also served to protect the contact surface from corrosion. After exposure periods of 250, 500, and 1000 h, two panels were removed randomly from the environmental chambers. The silicone paste was removed mechanically. The corrosion products were dissolved by immersing the panels for approximately 10 min in a 10 percent aqueous ammonium chloride solution maintained at 72 to 80°C, followed by scrubbing and rinsing in water and a final rinse in acetone. The galvanized steel panels were then reweighed and corrected for the estimated amount of zinc metal lost during cleaning.

The weight loss measurements expressed as grams per panel were converted to zinc film thickness loss in micrometres (μm) using the multiplication factor of 14.98. Units of film thickness are normally used in estimating and comparing product life.

Results

As was theoretically expected, corrosion of the zinc film was essentially a linear function of time for each of the environmental exposure conditions. Thus a least square fit of the following relationship was obtained for each set of exposure conditions

$$CORR = bt$$

where

$CORR$ = zinc lost in micrometers (μm),
t = exposure time in years, and
b = coefficient representing the corrosion rate.

For the polluted exposures, the corrosion rates ranged from a low of 3.18 μm/year and to a high of 33.27 μm/year. Based on analysis of variance and regression analysis, the corrosion rate with pollutants present was primarily a function of sulfur-dioxide concentration and input relative humidity.

Clean air corrosion rates ranged from a low of 1.14 μm/year to a high of 37.17 μm/year for the respective extremes of input relative humidity and temperature. Thus, unlike other materials exposed in this study, calculated galvanized steel corrosion rates for both polluted and clean air exposure conditions showed the same approximate range.

The surfaces of panels exposed to both polluted and nonpolluted conditions were examined after removal of the corrosion products. Panels exposed to polluted environments (Fig. 4) showed no pitting, thus indicating uniform corrosion; the entire surface of each panel developed a dull appearance. For the clean air exposures the panels developed pitting (Fig. 5); however, much of the surface area of each panel retained its original shiny metallic appearance.

FIG. 4—*Cleaned galvanized steel panel exposed to polluted air* (*X9.4*).

The pitting corrosion, expressed as a uniform thickness loss, fits the relationship

$$CORR = t_w e\left[30.53 - \frac{16{,}020}{\mathrm{RT}_M}\right]$$

where

$CORR$ = amount of pitting corrosion (μm),
t_w = time of wetness, years, and
T_M = geometric mean specimen temperature when wet, K.

At 25°C, the corrosion rate is equivalent to a current density of 2.2 μA/cm^2 over the total specimen surface. Measured pit depths were approximately 25 μm for the most severe conditions (1000 h, high temperature, and high relative humidity). This rate of corrosion is equivalent to approximately 22 μA/cm^2. Therefore, the estimated cathode to anode area ratio is 10.

Apparently, different corrosion mechanisms take place during the clean air and pollution exposures. Electron microscopy/microprobe analysis was used to investigate the corrosion mechanisms of the zinc film.

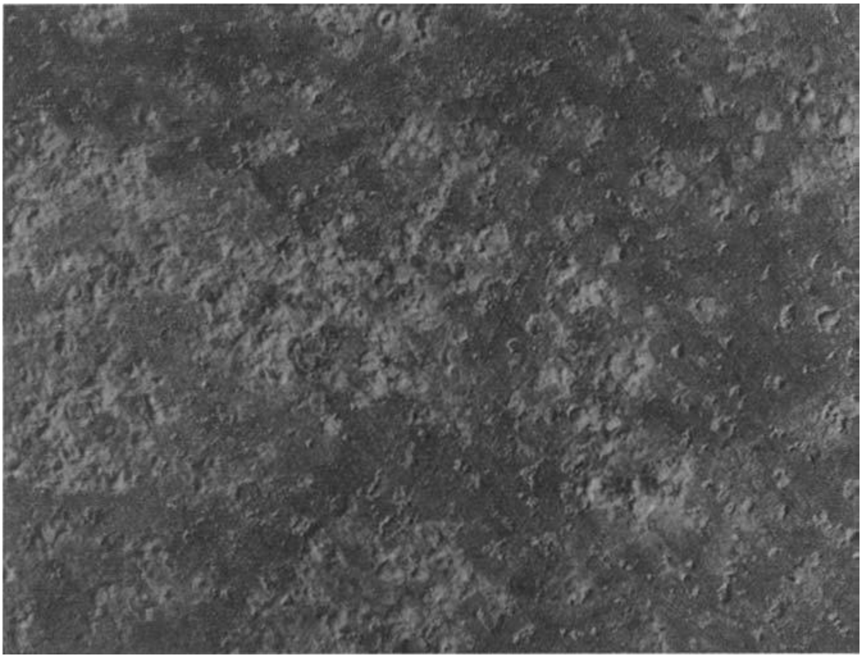

FIG. 5—*Clean galvanized steel panel exposed to clean air* (*X9.4*).

Discussion

Clean Air Exposure

The mechanism of pitting involves both initiation and propagation. Conditions must exist for both phases to occur. These conditions may be associated with the metal, the environment, or both.

Pitting corrosion of zinc has been reported [*9–10*] to occur when oxygen was not replenished or freely available. A critical oxygen level was proposed to exist below which pitting is initiated and propagated by the formation of concentration cells on the zinc surface. These investigations suggest that not only the rate of zinc corrosion but also the type of corrosion, uniform versus pitting, is controlled by the supply and diffusion of oxygen through the corrosion products.

In our exposure study no attempt was made to remove the oxygen or carbon dioxide gases. During the dew cycle, a thin layer of moisture condensed on panel surfaces; oxygen and carbon dioxide, therefore, were readily available to react with the zinc film in both the clean air and polluted exposures. Therefore, the critical oxygen level mechanism for pit initiation was not likely.

Initiation of pits probably occurred around some inclusion or defect on zinc surfaces. Scanning electron photomicrographs (Fig. 6) of unexposed galvanized steel panels revealed minor inclusions that were identified by microprobe scans (Fig. 7) as metallic lead. Inclusions that could definitely serve as active sites (such as iron-aluminum intermetallics) were not found. The lead inclusions, although not normally expected to be a problem, possibly could have served as pitting-initiation sites when exposed to this unique clean air environment.

An environmental factor that may have contributed to the initiation of pits was the relatively short dry-wet cycle. Some moisture nucleation sites on the galvanized surface may have stayed wet longer than the remaining surface area. Possibly such sites may have never dried completely or may have had a very short dry period compared with the remainder of the surface. Under such conditions, a protective zinc carbonate film may not have had time to form. As a result, a large cathode-to-anode area ratio would have occurred, thereby producing a very high localized current density at these active sites and subsequent formation of pits. Chemically, zinc goes into solution as ions around the sites while hydroxide ions form on the passive cathode surface. During migration the zinc ions react with

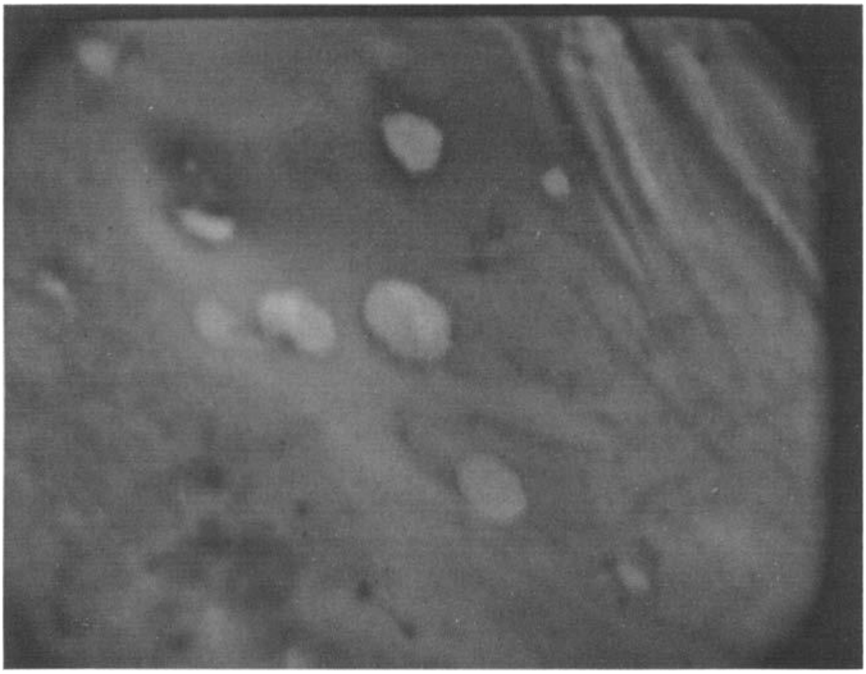

FIG. 6—*Scanning electron microscopy of unexposed galvanized steel panel (X5000).*

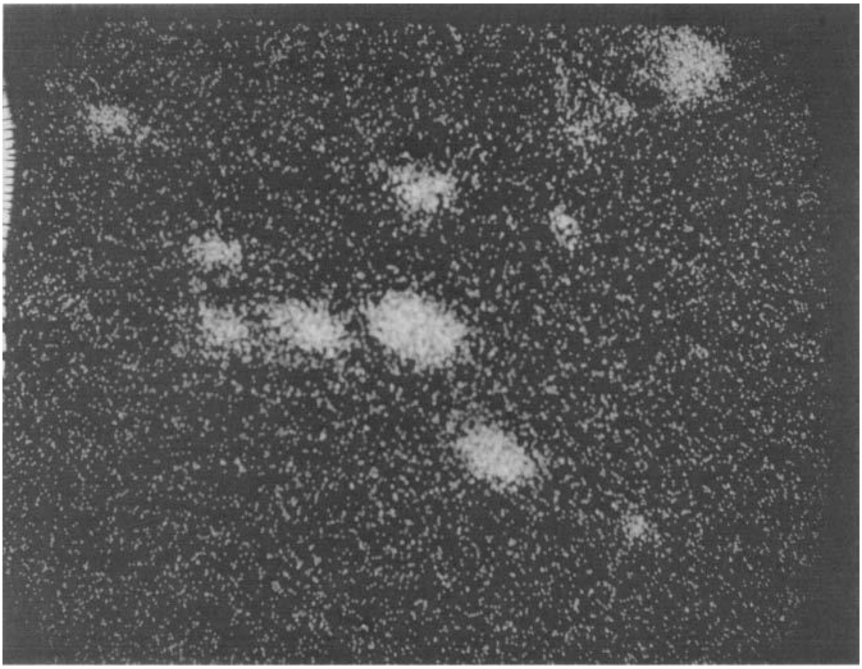

FIG. 7—*Microprobe scan of unexposed galvanized steel panel* (*X5000*).

water to form zinc hydroxide. This process produces hydrogen ions which migrate toward the cathode and become neutralized. During the neutralization process, the corrosion products tend to precipitate about the active site and produce a barrier that enhances pit formation.

Scanning electron photomicrographs (Figs. 8 and 9) of the corrosion products formed during the clean air exposures revealed a localized, circular buildup of an amorphous substance on the zinc surface. This pattern of corrosion products is characteristic of pitting corrosion. X-ray diffraction identified the corrosion products as primarily zinc oxide with a secondary phase of zinc carbonate. Zinc hydroxide, although not identified as a corrosion product, was formed during the dew cycle. However, since the pH of the dew on an inert surface was acidic (4.5) because of dissolved carbon dioxide, the zinc hydroxide probably reacted to produce zinc carbonate. Also, zinc hydroxide probably decomposed to zinc oxide [*11*] as the panel dried during the light cycle. The pH of the dew formed on the corroding panels during the exposure was 7.5. This level of pH suggests that the corrosion rate was near minimum [*12*] and a passive protective film had formed on most of the surface; nevertheless, pitting corrosion occurred.

FIG. 8—*Scanning electron microscopy of galvanized steel corrosion products from clean air exposure (X50).*

Other scanning electron photomicrographs (Figs. 10 and 11) show a cross-sectional view of the exposed panels. Corrosion products, which completely surround and cover the pits, apparently serve as a barrier that hinders diffusion and causes highly acidic conditions to develop in the pits by enhancing the concentration of hydrogen ions. This process is autocatalytic in that as more localized corrosion occurs, conditions become more favorable for pitting corrosion.

Pollution Exposures

Uniform corrosion of the zinc film was observed (see Fig. 12) for the exposures containing the three gaseous pollutants at various concentrations. Scanning electron photomicrographs of the corrosion products (Fig. 13) revealed primarily crystalline materials uniformly dispersed over the zinc surfaces. X-ray diffraction patterns were very complex and indicated one or more unidentifiable hydrated corrosion products. However, microprobe scans revealed sulfur atoms, probably in the form of sulfate, to be uniformly distributed over the zinc surface.

In the polluted exposure experiments, dew collected on an inert substrate measured quite acidic with a pH of 3.2; collected on the galvanized panels

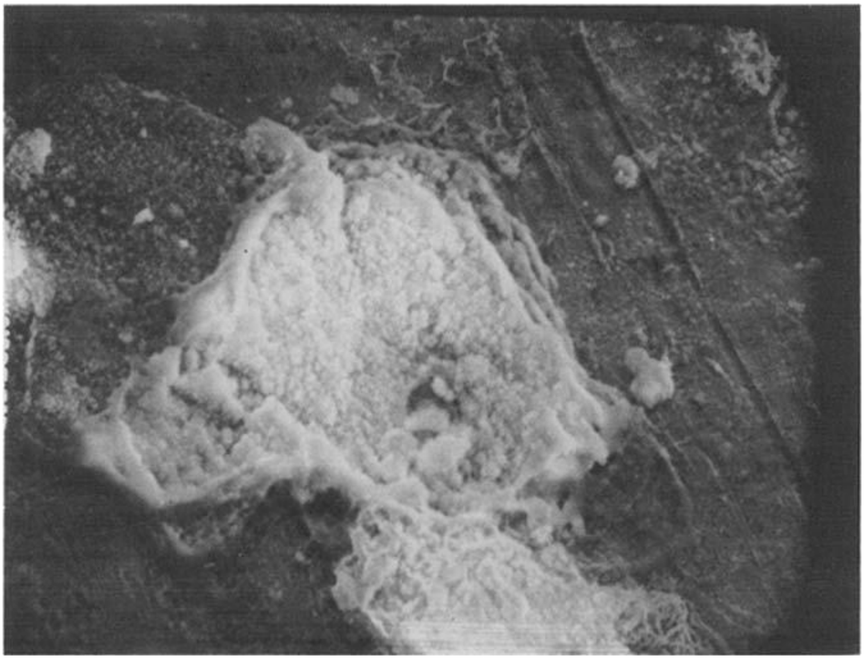

FIG. 9—*Scanning electron microscopy of galvanized steel corrosion products from clean air exposure (X1000).*

the dew remained acidic but with a pH of 5.6. Apparently, the acidic medium prevents the formation of a highly passive protective film, as well as localized cells at possible pitting initiation sites. The acidic dew dissolves and reacts with the corrosion products, resulting in the uniform distribution of these products across the galvanized surface. This process occurred during each cycle of dew and light.

The conditions of corrosion, immunity, and passivation of zinc (Fig. 14) as a function of pH and electrical potential have been reported [*13*]. This figure shows the influence of pH on the corrosion of zinc in aqueous solutions containing carbon dioxide. The dotted line represents the stability limit of water.

The influence of pH on the potential of zinc galvanized steel panels with two different aqueous media on the surface of each panel has been added to Fig. 14. These measurements were recorded using a calomel reference electrode with liquid junction (readings adjusted to hydrogen (H_2) electrode potential) and a glass miniature pH electrode. The deionized water used to prepare this solution was not boiled and, therefore, contained dissolved oxygen and carbon dioxide. With deionized water containing sulfur dioxide, a potential of -0.763 V at a pH of 4.2 was initially recorded. Over

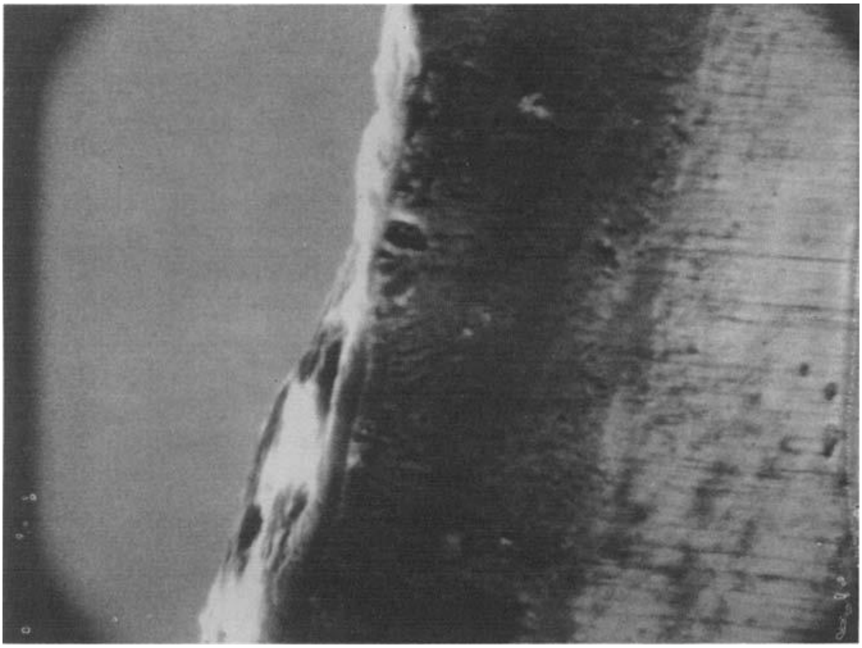

FIG. 10—*Scanning electron microscopy of cross section of galvanized steel panel from clean air exposure (X2000).*

a period of 24 h the pH moved into the passivation region (8.2) of the diagram (Fig. 14) and the potential leveled off at −0.799 V. The solution on the panel remained clear; however, the panel had a dull stained appearance over its entire surface. These panels resembled the galvanized panels exposed to the polluted environmental conditions. For the other condition with deionized water containing carbon dioxide, a potential of −0.823 V was initially recorded at a pH of 4.2. After 24 h the pH moved into the passivation region (8.0 in Fig. 14); however, the potential shifted to −0.690 V. This shift in potential was due to the formation of a passive film over most of the surface. The appearance of a milky color solution gave evidence that corrosion products had developed. Removal of the liquid and products from the panel revealed localized pitting corrosion similar to that observed for the clean air environmental exposures.

Conclusion

Galvanized steel revealed two different mechanisms of corrosion depending on whether the metal was exposed to clean air or polluted environments. During exposure to the clean air environments programmed with short

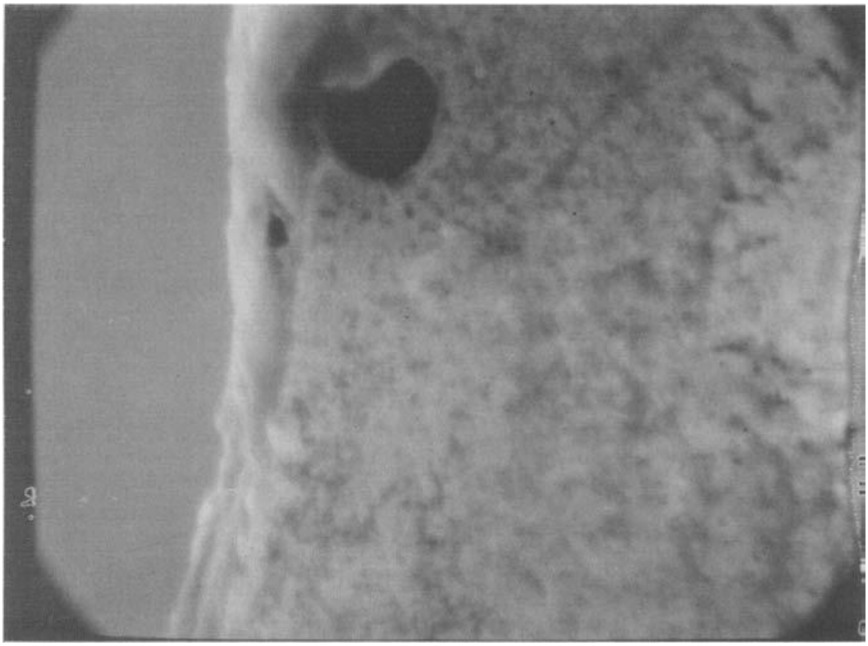

FIG. 11—*Scanning electron microscopy of cross section of galvanized steel pane from clean air exposure (X5000).*

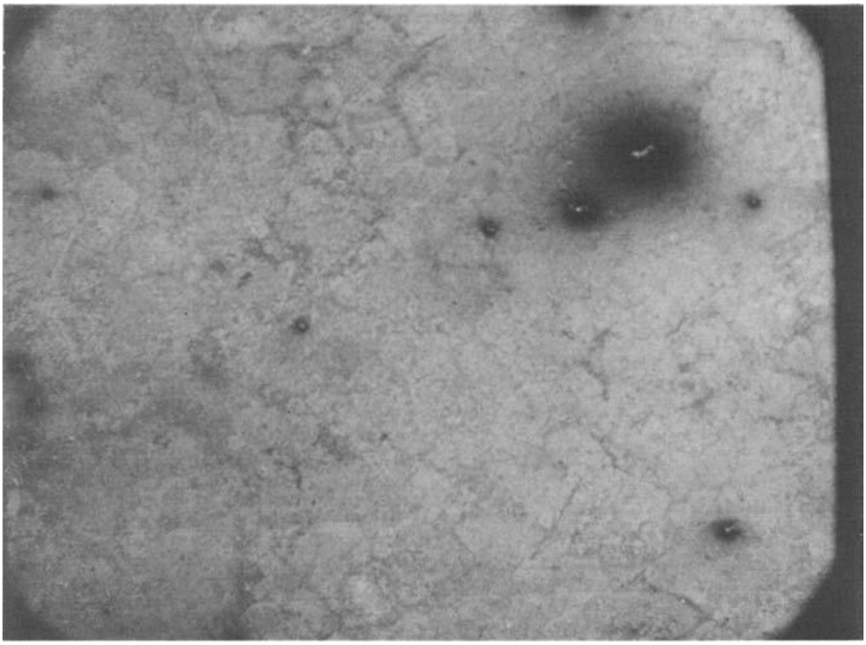

FIG. 12—*Scanning electron microscopy of galvanized steel corrosion products from polluted air (X50).*

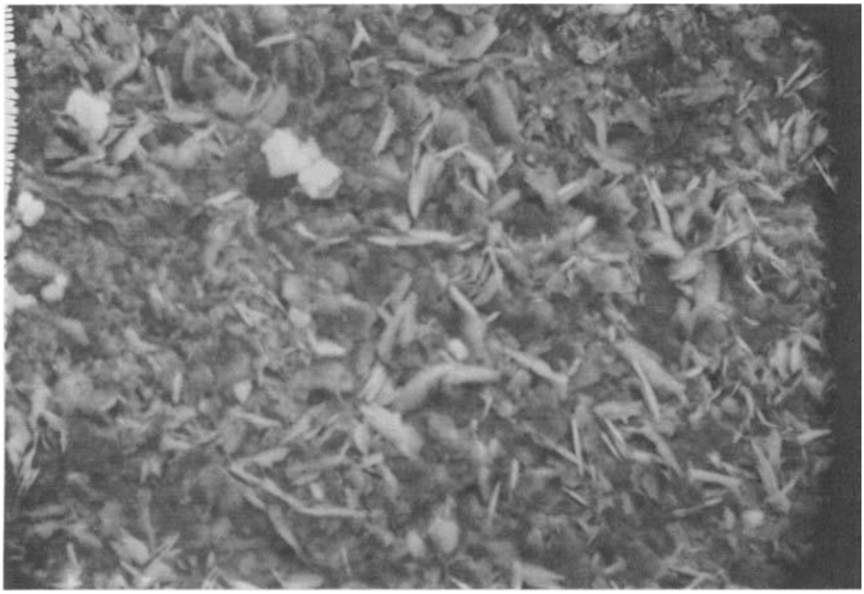

FIG. 13—*Scanning electron microscopy of galvanized steel corrosion products from polluted air (X1000).*

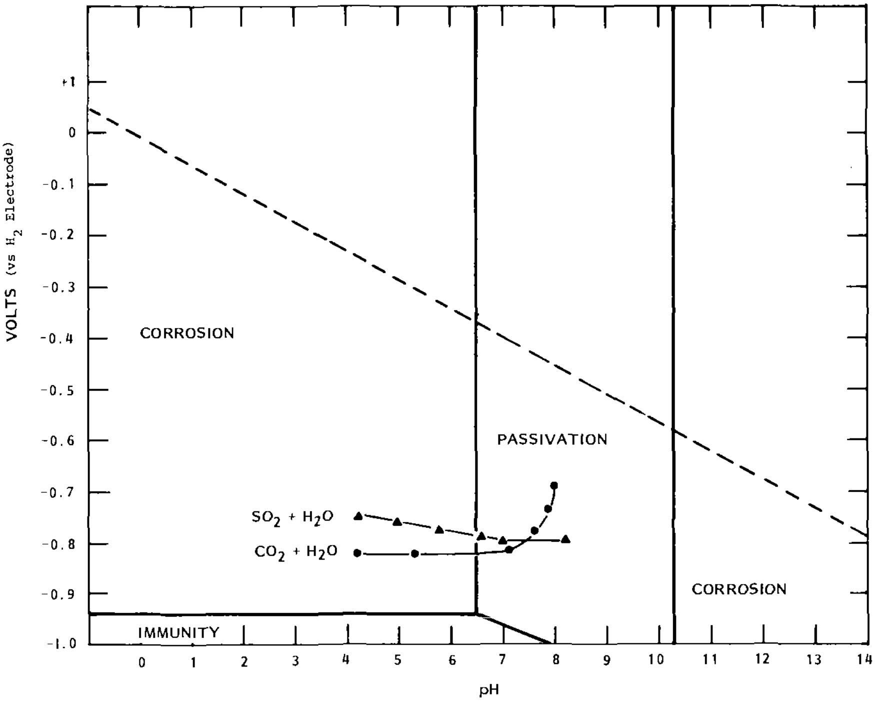

FIG. 14—*Potential-pH behavior of galvanized steel compared with thermodynamic relationships for the zinc-water-carbon dioxide system.*

wet-dry cycles, moisture nucleation sites on the zinc surface remained active and initiated pitting corrosion. Propagation of pits occurred with the formation of diffusion barriers over active sites. Pitting corrosion resulted because the pH (7.5) of the dew on the surface of panels minimized corrosion product solubility while the pH within the pits was more acidic and conducive to corrosion product solubility. For the polluted exposures, the surface dew was acidic and prevented the formation of a highly passive corrosion film as well as the formation of local active sites. Therefore, the corrosive effects of polluted environments on galvanized steel are not additive to the corrosive effects of these unique clean conditions and thus should not be compared. The effects of different levels of pollutants, however, are comparable and meaningful. Galvanized steel that becomes only partially dry during exposure to clean air environments in the real world could develop the type of pitting that was observed in this study.

References

[*1*] Campbell, G. G., Schurr, G. G., Slawikowski, D. E., and Spence, J. W., *Journal of Paint Technology*, Vol. 46, No. 593, June 1974, pp. 59–71.
[*2*] Beloin, N. J., *Textile Chemist and Colorist*, Vol. 4, No. 3, March 1972, pp. 77–82.
[*3*] Beloin, N. J., *Textile Chemist and Colorist*, Vol. 5, No. 7, July 1973, pp. 128–133.
[*4*] Haynie, F. H. and Upham, J. B., *Materials Protection and Performance*, Vol. 9, No. 8, Aug. 1970, pp. 35–40.
[*5*] Haynie, F. H. and Upham, J. B., *Materials Protection and Performance*, Vol. 10, Nov. 1971, pp. 18–21.
[*6*] Spence, J. W. and Haynie, F. H. in *Corrosion in Natural Environments, ASTP STP 558*, American Society for Testing and Materials, 1974, pp. 279–291.
[*7*] Guttman, H. and Sereda, P. J. in *Metal Corrosion in the Atmosphere, ASTM STP 435*, American Society for Testing and Materials, 1968, pp. 326–359.
[*8*] Guttman, H. in *Metal Corrosion in the Atmosphere, ASTM STP 435*, American Society for Testing and Materials, 1968, pp. 223–239.
[*9*] Bengough, G. D., Stuart, J. J., and Lee, A. R., *Transactions*, American Society of Mining, Metallurgical, and Petroleum Engineers, Vol. 83, 1929, pp. 29–46.
[*10*] Evans, U. R. and Davies, D. E., *Corrosion*, Vol. 8, 1952, p. 165–170.
[*11*] Gilbert, P. T., *Journal of the Electrochemical Society*, Vol. 99, No. 1, 1952, pp. 16–21.
[*12*] Roetheli, B. E., Cox, G. L., and Littreal, W. B., *Metals and Alloys*, Vol. 3, 1932, p. 73–76.
[*13*] Pourbaix, M. in *Establishment and Interpretation of Potential-pH Equilibrium Diagrams, Atlas of Electrochemical Equilibria in Aqueous Solutions*, Pergamon, Oxford, England, 1966, p. 406.

L. C. Covington[1]

Pitting Corrosion of Titanium Tubes in Hot Concentrated Brine Solutions

REFERENCE: Covington, L. C., "**Pitting Corrosion of Titanium Tubes in Hot Concentrated Brine Solutions,**" *Galvanic and Pitting Corrosion—Field and Laboratory Studies, ASTM STP 576*, American Society for Testing and Materials, 1976, pp. 147–154.

ABSTRACT: Pitting problems have been encountered in titanium tubes in heat exchangers handling hot saturated brines. These pits appear to be of two types. One type results in symmetrical holes about one-fourth inch diameter. These are associated with scratches in which iron is found to have been smeared into the titanium surface. The second type results in large irregular shaped holes. These are believed to be associated with salt plugs. This second type of pitting is believed to be initiated by the galvanic couple between the titanium tubes and the Monel tube sheets. Use of titanium tube sheets might eliminate the pitting problem but could introduce a crevice corrosion problem unless the tubes are welded into the tube sheet. An alternate solution is the use of titanium alloy tubing that is resistant to pitting attack.

KEY WORDS: titanium, pitting, corrosion, brines, heat exchangers

The salt industry has been troubled by pitting failures of titanium tubes in salt evaporators. These salt evaporators are a tube and shell heat exchanger consisting of titanium tubes roller expanded into Monel tube sheets. A saturated brine flowing through the tubes is heated to 268°F by steam on the shell side at 276°F. The brine carries solid salt particles, including flakes, that are large enough to plug a tube if they get turned just right. This happens frequently enough that every few months the units must be opened and the plugged tubes washed out. Occasionally, following a cleaning operation, it will be noted that some of the tubes are leaking. An examination of the tube will usually reveal the presence of one or two pits that have perforated the tube. Sometimes these leaks develop after the tube has been in service for five or six years, and sometimes the tubes fail within a few weeks after installation.

[1] Senior research engineer, Titanium Metals Corporation of America, Henderson, Nev. 89015.

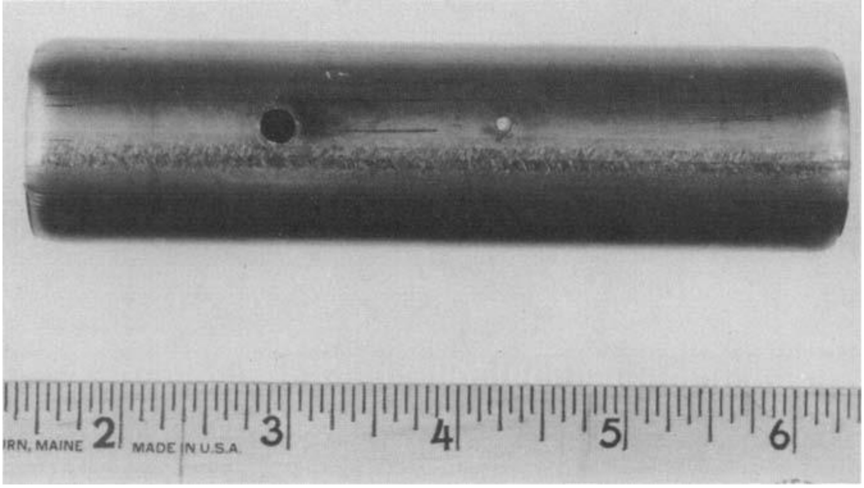

FIG. 1—*Small sharply defined pits.*

This paper describes an investigation that was made of this pitting problem and the conclusions that were reached regarding the probable causes.

Experimental

Samples of the pitted tubes were obtained. Photographs were made of the pitted areas, and electron probe analyses of the pitted areas were conducted.

Autoclave tests were conducted with specimens of titanium tubing in saturated brine solutions in an attempt to reproduce the pitting observed in the salt evaporators. These tests were conducted at 300°F for 500 h.

Results and Discussion

The pitting corrosion of titanium has been studied extensively. The observations and conclusions reported here are consistent with the known characteristics of pitting corrosion as reported by various investigators [*1-4*].[2] Figures 1 and 2 show views of some of the pits. These failures appear to be of two types. Pits of the type shown in Fig. 1 are usually located within 4 in. of the tube end and are associated with scratches. Pits of the type depicted in Fig. 2 may appear anywhere along the length of a tube, and scratches have not been associated with this type of pit.

---

[2] The italic numbers in brackets refer to the list of references appended to this paper.

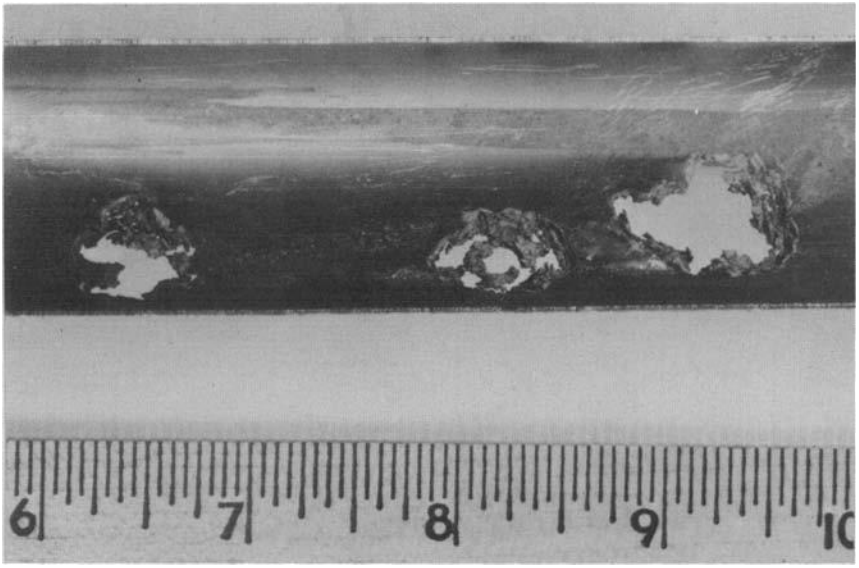

FIG. 2—*Large irregular shaped pits.*

It should be pointed out that titanium is operating in a borderline condition as far as pitting is concerned in these salt evaporators. Figure 3 shows the temperature and chloride concentration ranges in which titanium has been observed to pit.[3] This chart is derived from industrial experience as well as experimental data. At the temperature and brine concentration present in a salt evaporator, titanium would be in the pitting possible zone of this chart. Under these conditions tight crevices or scratches could be expected to initiate pitting. Pitting is not observed in the tube to tube sheet crevice, however, because of the presence of nickel and copper ions from the tube sheet which passivate the titanium [5]. Galvanic corrosion is also reduced in the crevice area by the presence of the nickel and copper ions because these ions act as cathodic depolarizers and tend to shift the potential of the titanium in the positive direction, thus, reducing the potential difference between the Monel tube sheet and the titanium tubes.

Mechanism of Pitting Attack

Figures 4 and 5 are examples of pits resulting from scratches. Electron probe analysis revealed traces of iron in the scratches. This suggests the scratches were made by a piece of iron.

Temperature wise, 268°F is believed to be a borderline condition for pitting to initiate in unalloyed titanium exposed to a saturated brine. At

---

[3] This chart was prepared by N. G. Feige and T. J. Murphy, Titanium Metals Corporation of America, West Caldwell, N. Y. 07006.

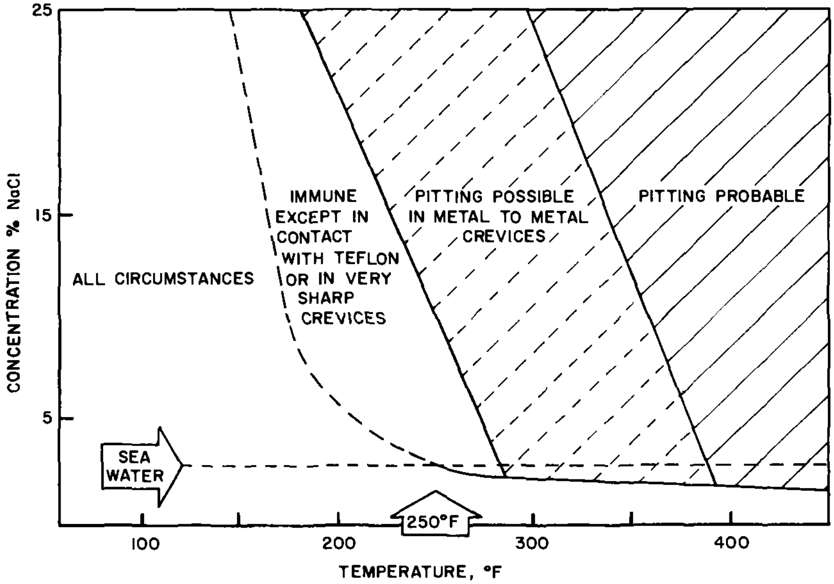

FIG. 3—*Immunity of titanium from pitting in neutral chloride brine (ASTM Grade 2 materials).*

this temperature any defect in the protective oxide film can serve as the nucleating site for a pit. The titanium-dioxide (TiO_2) film is very resistant to attack by chloride ions; however, a small fragment of iron abraded into the surface by contact with a steel implement might rupture the film. The presence of the iron particle would prevent the TiO_2 film from healing. Since iron is readily attacked by chloride ions, the iron particle would provide a site for corrosion to initiate [*6*].

Once chloride ions have penetrated to the titanium metal surface, an electromechanical cell is established in which the metal in the pit becomes anodic to the surrounding oxide covered surface. According to Uhlig [*2*], "The anodic sites do not spread along the metal surface because the resulting high galvanic currents cathodically protect the immediate metal surrounding the anode and prevent additional pits from initiating."

The titanium chlorides formed would tend to hydrolyze [*3*] on contact with the solution, generating hydrogen ions and forming insoluble TiO_2. The TiO_2 would form a slightly porous cap over the pit which would limit the diffusion of the brine into the pit. Because of hydrogen ion generation, the solution in the pit would become highly acidic, greatly accelerating the attack on the metal.

Because of the effect of the galvanic current, the attack on the metal would be limited to the area directly under the cap of corrosion product. The result would be a corrosion pit filled with TiO_2 that would continue to propagate until the pit perforated the metal.

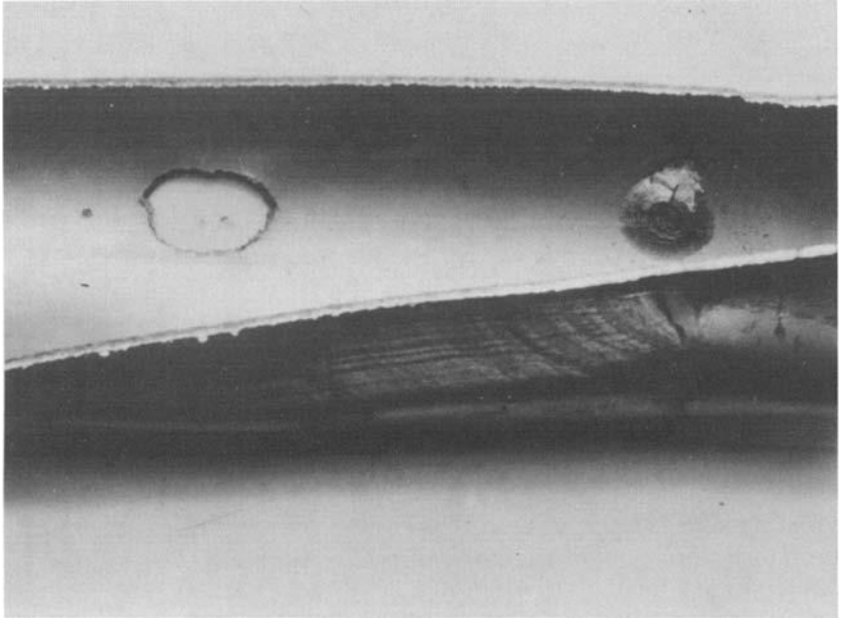

FIG. 4—*Inside diameter of tube showing two pits connected by scratch.*

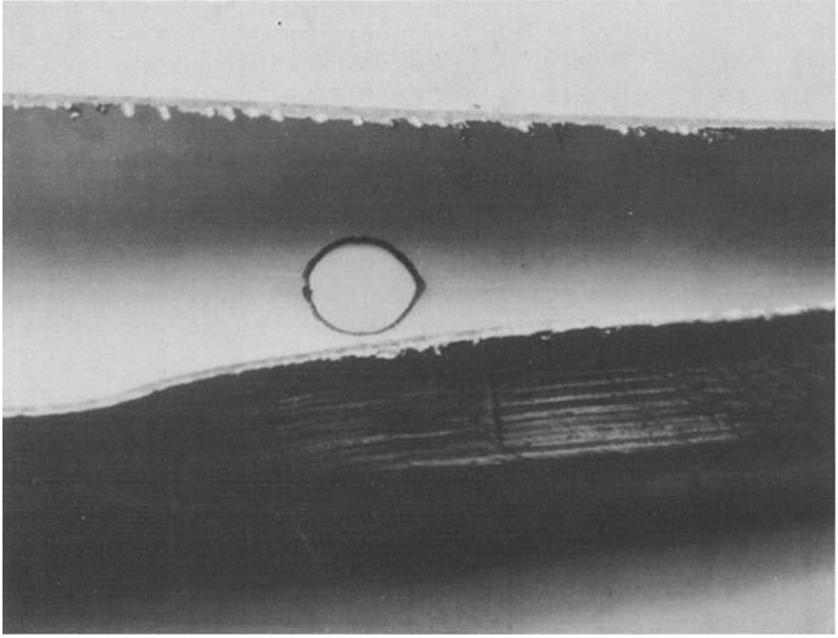

FIG. 5—*Hole resulting from perforation of the tube by a pit associated with a scratch.*

The small symmetrical pits associated with scratches as shown in Figs. 4 and 5 seem to be fully explained by the foregoing mechanism. In Fig. 4, we even have an example of a pit still tightly plugged with a corrosion product. When this plug was scraped away, a hole very similar in size and shape to the one on the left was revealed. This would explain why tubes containing pits of this type are not found to leak until after a cleaning operation. Indeed it appears that unless the plug is dislodged the tube may operate for considerable time without leaking.

The second type of large irregular pit is shown in Fig. 3. This type is believed to be associated with salt plugs that develop during the operation of the evaporators. The effect would be to produce a tight crevice in which the stagnant brine would rise to a temperature equal to that of the steam on the outside of the tube. In the stagnant crevice, acidic conditions would develop [7] until a pH is reached at which the protective oxide film is no longer stable. Pits would then develop and perforate the tube wall underneath the salt plug.

Attempts were made unsuccessfully to reproduce pitting attack in the laboratory. Specimens of unalloyed titanium tubing (ASTM Grade 2) were exposed to a saturated brine at 300°F for 500 h. The tube was packed in solid salt to simulate a salt plug, but pits did not develop. In reviewing the exposure conditions in a salt evaporator, it was noted that the titanium tubes are expanded into a Monel tube sheet so that a galvanic couple exists with titanium being the cathodic member of the couple. The potential difference between Monel and titanium at 300°F in saturated brine was measured and found to be 210 mV. This would result in accelerated attack on the Monel with hydrogen being generated on the titanium. The potential difference is not considered to be large enough to cause a serious galvanic corrosion problem. However, it was decided that the test should be repeated again, this time with Monel coupled to the titanium tubes to duplicate the galvanic conditions.

This time pitting was observed as can be seen in Figs. 6 and 7. The metal strips crimped to the edges of the tube are Monel. No corrosion occurred under the Monel clips, but a very definite crevice corrosion type of attack has occurred at other areas on the tube as shown in Fig. 6. Note the similarity between this attack and the pits shown in Fig. 2. Figure 7 shows two pits that have perforated the tube although they are still filled with a plug of a corrosion product. These are examples of pits of the first type resulting from iron contamination. The tube was cut off with a hacksaw, and two scratch marks were made by the saw while getting the cut started. Pits initiated in both marks.

In order to be certain that the galvanic couple triggered the pitting reaction, the experiments were repeated with the same results. No pitting was observed without the galvanic couple. With the galvanic couple, severe pitting was obtained.

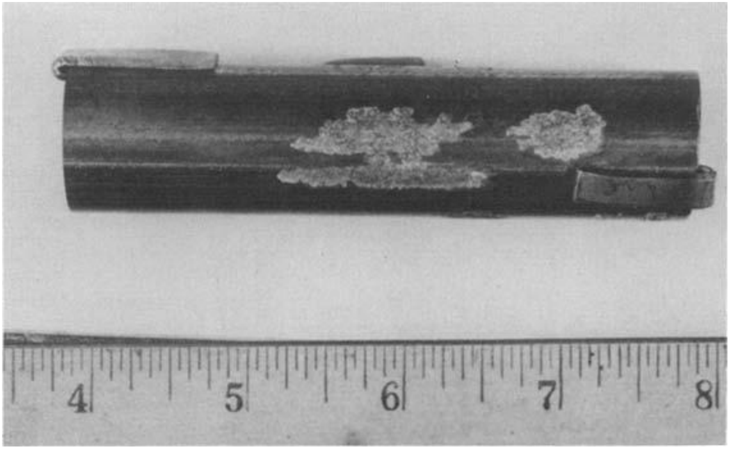

FIG. 6—*Pitting test with Monel coupled to titanium tube.*

Apparently the galvanic couple between the titanium and the Monel is involved in the pit initiation under salt plugs. Since the galvanic couple would result in small amounts of hydrogen being generated on the titanium surface it may be that patches of hydride would form. Titanium hydride is not as stable a compound as TiO_2 and in the stagnant confined areas covered by the salt plug, this film would decompose allowing the chloride ions to react with the underlying titanium metal. A corrosion cell would then be set up in which highly acidic conditions would develop and an accelerated attack on the metal in the pit would occur.

The question arises as to why pits associated with scratches are nearly perfectly round, while salt-plug pits are irregularly shaped. This is probably due to the fact that the pits associated with scratches initiate at a small particle of iron embedded in the titanium and are, therefore, highly localized in nature. The pits that are associated with salt plugs, on the other hand, initiate as a crevice corrosion attack and involve a much greater area. Turbulence near the tube sheet is not believed to be a factor in the shape of the pits. It is generally agreed that corrosion occurs because of the development of acidic conditions in the pit. This is promoted by stagnant conditions. The fact that the round pits are nearly always found in the area adjacent to the tube sheet is probably due to the fact that this area is most likely to be scratched during installation of the tubes.

It appears the Monel tube sheet may trigger the reaction that causes these tube failures. Use of titanium tube sheets may eliminate this problem, but it would require that the tubes be welded into the tube sheet to eliminate any crevices. Under the conditions involved in this application, severe crevice corrosion could be expected if any crevices existed. This is not a

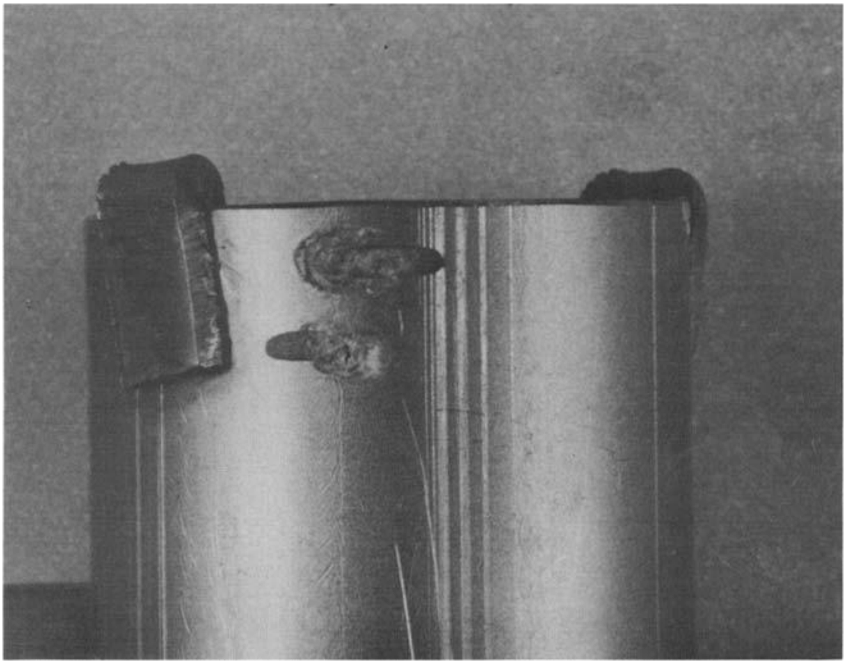

FIG. 7—*Pits resulting from Monel couple.*

problem with the Monel tube sheet because the nickel and copper ions from the tube sheet inhibit crevice corrosion [5].

The alternate to replacing the tube sheet may be to use tubes of a titanium alloy resistant to attack under these conditions.

References

[*1*] Posey, F. A. and Bohlmann, E. G., "Pitting of Titanium Alloys in Saline Waters," paper presented at the Second European Symposium on Fresh Water from the Sea, Athens, Greece, 9–12 May 1967.

[*2*] Uhlig, H. H. *Materials Protection and Performance*, Feb. 1973, pp. 42–44.

[*3*] Brown, B. F., *Corrosion-NACE*, Vol. 26, No. 8, 1970, pp. 249–250.

[*4*] Greene, N. D. and Judd, G., *Corrosion-NACE*, Vol. 21, Jan. 1965, pp. 15–18.

[*5*] Covington, L. C. in *Titanium Science and Technology*, Vol. 4, R. I. Jaffee and H. M. Burte, Eds., Plenum, New York, 1973, p. 2395.

[*6*] Cotton, J. B., *Chemical Engineering Progress*, Vol. 66, No. 10, Oct. 1970, pp. 57-62.

[*7*] Griess, J. C., *Corrosion-NACE*, Vol. 24, April 1968, pp. 96–109.

F. J. Cornwell,[1] *G. Wildsmith,*[2] *and P. T. Gilbert*[2]

Pitting Corrosion in Copper Tubes in Cold Water Service

REFERENCE: Cornwell, F. J., Wildsmith, G., and Gilbert, P. T., "**Pitting Corrosion in Copper Tubes in Cold Water Service,**" *Galvanic and Pitting Corrosion—Field and Laboratory Studies, ASTM STP 576,* American Society for Testing and Materials, 1976, pp. 155–179.

ABSTRACT: The occurrence of pitting corrosion in copper tubes carrying cold supply waters has been investigated in relation to (*a*) carbon residues in the bore of the tube from the bright annealing operation, (*b*) the hardness and composition of the metal, and (*c*) water composition. The electrode potential of tubes in several supply waters has been used to assess their susceptibility to pitting corrosion. It is concluded that pitting occurs only in certain types of water with a low level of organic matter in tubes containing more than a critical amount of carbon residue in the bore. Hardness of the metal appears to have little effect on susceptibility to pitting corrosion, but the addition of about 1 percent tin to the copper substantially reduces the rate of pitting for a given level of carbon contamination in the bore. The significance of these findings is reviewed in the light of service experience with copper water tubes in the United Kingdom.

KEY WORDS: corrosion, pitting, copper, tubes, domestic supply waters, carbon residues

Copper tubes (usually phosphorus deoxidized, for example, copper 122) are widely used in water distribution systems where they generally give reliable performance and have a very long life [*1–6*].[3] Not unexpected for a material in widespread use in a variety of environmental conditions, corrosion problems occasionally arise. In many countries the most troublesome problem occurs in cold waters originating from deep wells or boreholes in the presence of carbon residues on the tube surfaces. This type of localized corrosion was first described by Campbell [*7*] and has since been identified in tubes in service in Belgium, Germany, Holland, New Zealand, the United Kingdom, and the United States [*3,8–10*]. Failures are

---

[1] Technical manager, Yorkshire Imperial Metals Limited, Kirkby, Liverpool, England.

[2] Manager, Metallurgical Services and Research, and technical director, respectively, Yorkshire Imperial Metals Limited, Leeds LS1 1RD, England.

[3] The italic numbers in brackets refer to the list of references appended to this paper.

often comparatively rapid, many occurring within the first year or two of service.

Investigations by a number of organizations during recent years have indicated that several factors affect the incidence of this type of attack. These can be briefly summarized as follows.

1. The presence of carbon residues on the tube surfaces produced during manufacture affect attack. If the amount of carbon residue is sufficiently low, pitting does not occur.
2. The nature of the water is another factor. In surface-derived waters, attack does not normally occur, even in tubes containing carbon films. Campbell [7] attributed this to the presence of a naturally occurring organic corrosion inhibitor. However, if such waters are treated to remove organic matter (for example, by alum flocculation treatment) they may be capable of supporting pitting in tubes containing carbon. Lucey [*11*,*12*] has suggested that several inorganic constituents (Cl^-, NO_3^-, SO_4^{2-}, Na^+, O_2) are important in determining the pitting propensity of a water and that pH is also a major factor, the pitting propensity increasing with decreasing pH in the range 9.4 to 7.0. His analysis of the situation does not take any direct account of the presence of organic substances, but there may be interrelated effects since organic matter can stabilize the pH value at a higher figure than would otherwise occur.
3. Another factor is the temper of the copper tube. It has been reported [*13*] that other things being equal (including carbon contamination), hard tubes (though not entirely immune to failure) are more resistant than half-hard tubes, which are, in turn, more resistant than annealed tubes. The reasons for these differences have not been elucidated.
4. The composition of the copper can influence attack. Modifications to the composition of the copper can improve the resistance to pitting in the presence of carbon residues. Small additions of aluminum and tin are claimed to be beneficial [*13*].
5. The effect of tube wall thickness is another factor. Devroey and Depommier [*13*] have reported that the rate of penetration falls off with time in Brussels water, and they concluded that there was a limiting wall thickness above which perforation of the tube would not occur however high the carbon contamination.

The authors have investigated most of these factors during the past five years, together with other factors, such as the use of different types of tube-drawing lubricants, the use of various final cleaning processes, and the application of protective treatments. This paper gives some of the results obtained, particularly those relating to the effects of carbon residues, water composition, and the temper and composition of the copper. Reference is made to laboratory investigations, field trials, and service experience in the United Kingdom.

Experimental

Copper and copper alloy tubes were exposed to supply waters in test rigs situated at two pumping stations, one in Yorkshire (Bramham) and one in Lincolnshire (Barrow Park), and in the company's Leeds laboratory. The test site at Bramham is supplied with both hard (untreated) borehole water and base-exchange softened borehole water (public supply). Preliminary trials established that both the untreated and softened supplies were capable of supporting pitting corrosion of copper in the presence of carbon residues, but the results presented in this paper are for copper tubes exposed only to the softened supply. The test facility at Barrow Park is supplied with hard, untreated, borehole water. Both sites are in areas where pitting corrosion is experienced in service. The Leeds water is mainly derived from surface sources and pitting failures do not occur in this area.

It has been established that the electrode potential of the copper tubes during exposure shows a significant correlation with pitting behavior, and potential/time curves were plotted for tubes exposed at Bramham and in the laboratory. Progress of pitting was followed using an eddy current technique, and the time taken for tubes to be perforated was recorded at each site.

Preparation of Tube Specimens

Half-Hard Temper Tubes—Half-hard copper tubes were manufactured to British Standard Specification for Light Gauge Copper Tubes (light drawn) (B.S. 659:1967), ½ in. Table A (now British Standard Specification for Copper and Copper Alloys Tubes, Part 1, Copper Tubes for Water, Gas, and Sanitation (B.S. 2871: Part 1: 1971), 15 mm Table X), from extruded shells. In the course of manufacture the tubes are cold drawn to the penultimate size and then bright annealed. A final sinking pass increases the hardness to the "half-hard" temper (80 to 100 VHN5 kg load). At final size, the bore of the tube may be more or less contaminated with carbon residues arising from: (*a*) graphite in the extrusion lubricant, (*b*) breakdown of lubricant during drawing, or (*c*) decomposition of residual bore lubricant during the bright annealing operation.

In the course of normal production within the authors' company, ½-in. or 15-mm half-hard copper tubes (the most commonly used size) are given a final abrasive cleaning treatment using air-borne alumina or iron grit. The exposure trials have included both cleaned and uncleaned tubes.

Copper alloy tubes have been manufactured for trial purposes by basically similar procedures. Such tubes are somewhat more difficult to produce than copper, but could be of interest if resistant to pitting corrosion in the uncleaned condition. If cleaning were necessary they would probably have no advantage over ordinary copper. Therefore the alloys were tested in the uncleaned condition.

Hard-Temper Tubes—Hard-drawn copper tubes were manufactured to British Standard Specification for Hard-Drawn Thin Wall Copper Tubes (B.S. 3931: 1965), ½ in. (now B.S. 2871: Part 1: 1971, 15 mm Table Z) from extruded shells. These tubes are not annealed at penultimate size and the level of carbon residues in them is usually low. Occasional failures occur in service when, for one reason or another, an abnormally high amount of carbon residue is present in the bore.

Carbon Determination

Before installation in the test rigs the level of carbon contamination was assessed using the carbon black (CB) test devised by Devroey and Depommier and described by Campbell [*14*]. Briefly this test entails taking a tube specimen (internal surface area 20 cm^2), the outside surface of which is filed clean. This is immersed in nitric acid and boiled for about 3 min. The specimen is then removed and washed with distilled water. The solution (including washings) containing the carbon residues from the tube bore is filtered under suction through a standard micropore filter paper, 20 mm in diameter. The residue on the filter paper is washed with distilled water and methylated spirit, allowed to dry, and compared with a set of standard disks to establish the CB number. An increase of one in the CB number corresponds to a doubling of the amount of carbon. A limitation of the test is that it gives an average value for the level of contamination and it gives no information about local variations over the 20 cm^2 of surface tested.

The CB number of an uncleaned half-hard tube can vary considerably along its length, a typical range being CB 2 to 5.[4] Normal abrasive cleaning reduces the contamination to the range CB 1 to 2. However, if the tube is initially abnormally heavily contaminated or if the abrasive cleaning process is not operated effectively or both, the CB numbers for the" cleaned" tube will be higher, and there will then be a significant risk of failure if the tube enters service in a water capable of supporting pitting attack.

The one-half inch size of hard-drawn tubing normally has CB numbers in the range 1 to 2, though occasionally higher figures are encountered. The general degree of contamination is not high enough to make it necessary to apply the abrasive cleaning process to this product.

Description of Test Rigs

Site Test Rigs—The corrosion rigs at the Bramham and Barrow Park sites have been described in detail elsewhere [*15*]. A general view of the

---

[4] These figures refer to standards established for Yorkshire Imperial Metals Limited. Others, though using similar methods for carrying out the test, do not necessarily obtain identical results, possibly because of variations in the standards used. Therefore, the CB numbers quoted here are not necessarily directly comparable with those obtained in other laboratories.

corrosion rig at Bramham is shown in Fig. 1. The tubes (about 5 m long) were tested in sets of four in parallel (a bank) with common water inlet and outlet pipes. Water flowed in a particular bank when a time switch opened a solenoid valve positioned in the outlet pipe.

At both Bramham and Barrow Park, the time sequence was set to allow water to flow for 35 s once an hour, every hour for 12 h, to change the water in the tubes completely every hour. The water flowed to waste after passing through the tubes. During the remaining 12 h, the water remained stagnant in the tubes. This flow/stagnation sequence was used to simulate the day/night conditions in domestic water systems.

Corrosion Rigs in the Laboratory—Two laboratory corrosion rigs, each containing four tubes, were constructed. One rig was supplied with laboratory tap water (which does not support pitting), the other with water brought regularly from Bramham. In both rigs, water from a large header tank flowed into a smaller tank fitted with an automatic siphon, which operated when the water in the small tank reached a critical level. The feed from the header tank was adjusted so that the siphon operated once every hour and the header tank contained sufficient water for the siphon to operate for 12 h. Water (and some air bubbles) flowed from the siphon

FIG. 1—*Corrosion rig at the Bramham site.*

tank into another small tank situated immediately below it. This tank allowed the air bubbles to be expelled before the water flowed through the test tubes. Water was maintained in the tubes during the periods of water flow by a 15-cm head at the outlet. The rig had the same flow/stagnation sequence as the Bramham and Barrow Park rigs.

Potential Measurements

Previous work [*15–17*] has shown that pitting of copper occurs when the electrode potential of the copper exceeds a critical value of about 100 to 170 mV (all potentials will be given on the saturated calomel scale).

The electrode potential of the tubes was measured periodically throughout the exposure periods using a silver/silver chloride reference electrode. The tube to be examined was completely removed from the test rig, and the reading was taken before the tube had time to dry out. The reference electrode was held in the center of the tube bore by plastic couplings which also included an inlet for the supply water. The water flowed over the reference electrode and along the bore of the tube, which was inclined so that the water had to flow up a slight incline thereby ensuring that the tube was filled with water. The experimental technique adopted ensured that the measurements were taken in the dark since both Lucey [*18*] and Pourbaix [*16,17*] have demonstrated that the potential is affected by illumination of the specimen. The reference electrodes were calibrated against a saturated calomel electrode before use, and the experimental results have been converted to the saturated calomel scale.

Eddy-Current Examination

In order to follow the development of pitting, the tubes were eddy-current tested periodically during exposure. An external coil, energized with alternating current, was pulled slowly along the axis of the tube; changes in electromagnetic response caused by the presence of pits produced electrical signals which were amplified to actuate a recorder. The instrument was calibrated by passing the coil over standard defects machined into a tube of the same size and composition as those on test. The sensitivity was adjusted so that the output obtained from the standard defects produced specific sizes of deflections on the eddy-current recorder.

Composition of Supply Waters

Typical analyses for Bramham, Barrow Park, and laboratory (Leeds) waters are given in Table 1. To assess the relative amounts of organic matter present, a technique based on that described by Campbell [*19*] was used, in which a sample of water is illuminated with ultraviolet light and the degree of fluorescence compared with a standard sample illuminated at the same time. The Leeds laboratory tap water has been adopted as standard as this gives reasonably constant fluorescence, although slight

TABLE 1—*Typical water analyses (results in ppm where appropriate).*

		Water Supply		
		Bramham (Public Supply)	Barrow Park	Laboratory (Leeds)
pH		7.4	7.5	8.5
Total dissolved solids dried at 180°C		553	506	198
Total dissolved solids ignited at 600°C		490	433	178
Carbonate (temporary) hardness	$CaCO_3$	174	219	30
Noncarbonate (permanent) hardness	$CaCO_3$	Nil	147	40
Total hardness	$CaCO_3$	174	367	70
Total alkalinity	$CaCO_3$	298	219	30
Calcium	Ca	37	140	22
Magnesium	Mg	20	3.7	4.0
Sodium	Na	150	18	38
Iron	Fe	0.22	0.06	0.08
Aluminum	Al	0.36	0.03	<0.02
Copper	Cu	<0.025	<0.025	<0.025
Lead	Pb	<0.10	<0.10	<0.10
Manganese	Mn	<0.005	<0.005	<0.005
Chloride	Cl	48.5	41.8	29.0
Sulfate	SO_4	103	98	75
Ammoniacal nitrogen	N	<0.02	<0.02	0.04
Nitrate nitrogen	N	7.2	6.4	1.9
Nitrite nitrogen	N	<0.02	<0.02	<0.02
Silica	SiO_2	4	3	4
Free carbon dioxide	CO_2	15.8	13.2	<0.01
Free chlorine	Cl	<0.01	<0.01	0.05
Dissolved oxygen	O	8.2	12.6	9.5
Fluorescence fraction of laboratory supply water		1/8	1/4	1

variations do occur. The laboratory water is diluted with deionized water (zero fluorescence) in order to reduce its level of fluorescence to that of the supply water under test. The intensity of fluorescence of this water is then expressed as a fraction of that of the standard water.

Experimental Results

The results of early trials suggested that pits are initiated more readily when water is left stagnant in the tubes for a period before switching to the regular flow/stagnation sequence. Subsequent trials have not entirely supported this conclusion, but the majority of the trials described in this paper have included an initial period of one month during which water was left stagnant in the tubes. No potential measurements were taken during this period.

Effect of Carbon Residues on the Incidence of Pitting

Trials at Bramham—Exposure trials were carried out at Bramham with 12 uncleaned half-hard tubes (CB numbers in the range 2 to 6), 12 tubes abrasively cleaned with iron grit for 0.5 s (CB numbers in the range 1 to 5), and 23 tubes abrasively cleaned with either iron or alumina grit for 5 to 30 s. Ten of these 23 tubes were manufactured using excessive amounts of lubricant during drawing in order to deliberately produce a tube heavily contaminated with carbon in the bore before abrasive cleaning. These tubes were abrasively cleaned with iron grit for 5 s. The remaining 13 tubes were manufactured using normal lubrication procedures and abrasively cleaned for a minimum of 7 s. The CB numbers of all 23 abrasively cleaned tubes were in the range 1 to 3, although, in general, the CB number of those manufactured with excessive lubricant was higher within this range than that of tubes produced using normal lubrication.

The initial potential of the 12 uncleaned tubes was approximately −40 mV. After the initial stagnation period the potentials increased steadily into the range 270 to 350 mV. Potential/time curves typical of those obtained with uncleaned tubes are shown in Fig. 2. Rapid pitting occurred and all the tubes were perforated within five months.

The 12 tubes abrasively cleaned for 0.5 s had potential/time curves similar to those of the uncleaned tubes except that the peak potential attained was generally somewhat lower. Typical curves are shown in Fig. 3. Eight of these tubes were perforated within 4 to 16 months. Eddy-current

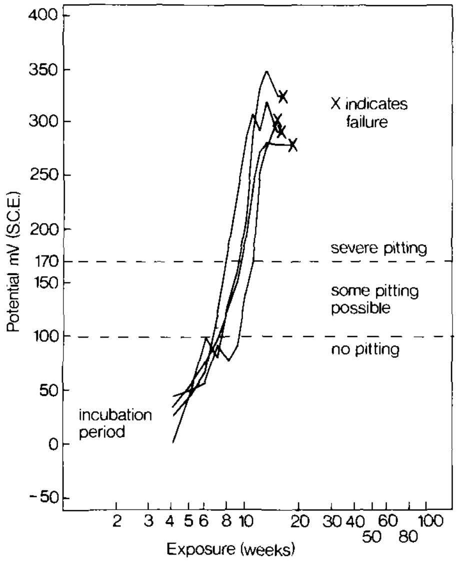

FIG. 2—*Potential/time curves obtained with uncleaned copper tubes exposed to a water that supports pitting.*

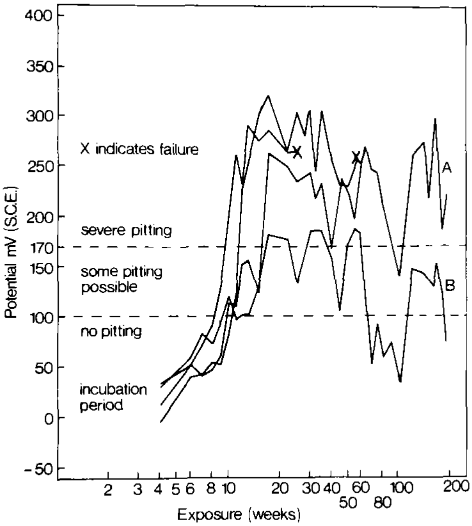

FIG. 3—*Potential/time curves obtained with inadequately cleaned copper tubes exposed to a water that supports pitting.*

inspection of the remaining four tubes indicated that all were severely pitted, but no failures had occurred in 42 months. The potentials of these four tubes fell after approximately 18 months from the range 188 to 274 mV to the range 33 to 140 mV. The potentials were relatively low, in some cases for about 18 months before increasing again to higher potentials. Curves A and B in Fig. 3 show this fall and rise in potential for two of the tubes.

The ten tubes manufactured with excessive carbon residues and abrasively cleaned with iron grit for 5 s also exhibited this cyclic effect in their potential/time curves, as shown in Fig. 4. For the first 6 months' exposure the potentials of all ten tubes remained low. After 7 to 12 months the maximum potentials observed were in the range 40 to 154 mV. The tubes with potentials above 100 mV continued to have potentials > 100 mV for a further 12 months, after which time they fell below 100 mV. The potentials of all ten tubes remained below 100 mV for a further 8 to 16 months before increasing during the next 12 months to peak values in the range 108 to 205 mV. The tube that attained a potential of 205 mV failed after 36 months' exposure.

Tubes manufactured by the normal production methods and abrasively cleaned for a minimum of 7 s gave potential/time curves as shown in Fig. 5. The potentials remained low (less than 100 mV) throughout the whole of the exposure period and no pitting occurred.

Trials at Barrow Park—Similar trials were carried out at Barrow Park with 16 uncleaned and 24 abrasively-cleaned tubes. Potential measurements here were taken only at irregular intervals during the 38 months'

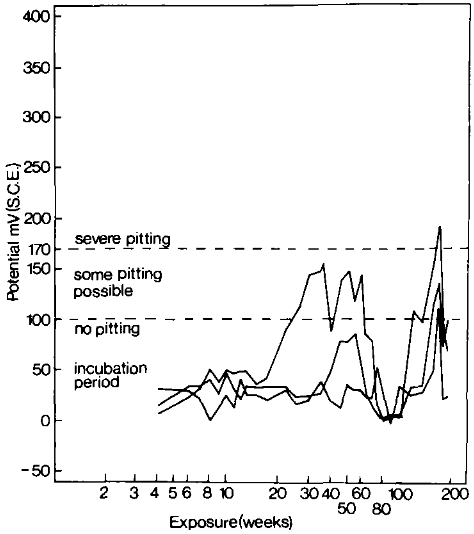

FIG. 4—*Potential/time curves obtained with abrasively-cleaned copper tubes manufactured with excessive carbon residues when exposed to water that supports pitting.*

exposure period. All 16 uncleaned tubes had potentials in excess of 170 mV but the highest value measured (270 mV) was somewhat lower than the maximum value occurring at Bramham. Severe pitting of all the tubes was detected by the eddy-current inspection, and nine failed within 6 to 31 months.

The potentials of the 24 abrasively-cleaned tubes never rose above 100 mV, and no pitting occurred during the 38 months' exposure.

Effect of Water Composition on the Incidence of Pitting

The results of exposure trials at Bramham and Barrow Park suggest that there is a correlation between the pitting behavior and the organic content of the supply water (as shown by fluorescence under ultraviolet light), as well as the degree of carbon contamination of the bore. For example, the most rapid failures in uncleaned half-hard copper tubes exposed at Barrow Park (one-fourth fluorescence of laboratory supply) occurred in about 9 months, whereas similar tubes exposed at Bramham (one-eighth fluorescence of laboratory supply) failed in 3 months. Furthermore, it has been found that Bramham water will induce pitting in tubes with CB number 3 (for example, tubes abrasively cleaned for only 0.5 s) whereas this level of contamination is insufficient to cause pitting at Barrow Park. As mentioned earlier, pits do not develop at Bramham if abrasive cleaning has reduced the CB number to 2 or less.

The use of water treatments to remove organic matter is increasing, and, if such treatments reduce the level of corrosion inhibitor in a water, an

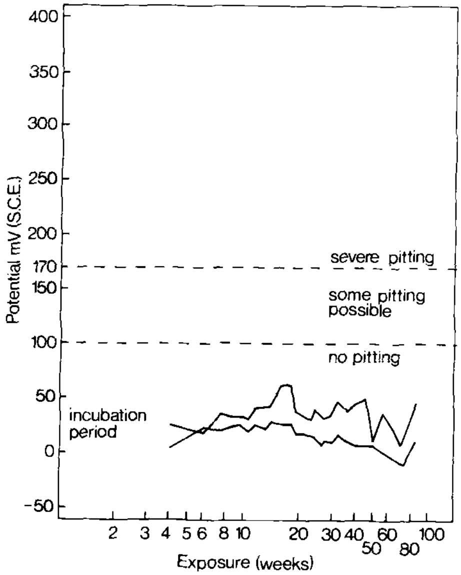

FIG. 5—*Potential/time curves obtained with copper tubes manufactured by normal production methods.*

increased pitting propensity may result. It is therefore of interest to determine the behavior of carbon-contaminated tubes, originally supplied with water that does not support pitting when the water is changed to one that does support this type of corrosion. It is also of interest to determine whether a change to a water containing inhibitor is able to cause stifling of pits that were previously developing actively. The following trials were carried out to investigate these aspects.

Uncleaned Tubes Exposed Initially to a Water That Supports Pitting, Then to One That Does Not—The potential of four uncleaned tubes with CB numbers in the range 3 to 5 exposed at Bramham increased steadily to >350 mV (Fig. 6). An eddy-current examination indicated that after 2.5 months, severe pitting was occurring in all four tubes. Each tube was cut into two equal lengths and one half brought to the laboratory without being allowed to dry out. Two of the halves were installed in the laboratory rig supplied with Bramham softened water and two in the laboratory rig supplied with laboratory tap water. The results were as follows.

Tubes left at Bramham—Three out of four half-tubes left at Bramham failed within a few days of the transfer. The fourth tube was perforated after a further two weeks' exposure (giving a total exposure of 3 months).

Tubes transferred to the laboratory rig supplied with Bramham water—Before transfer to the laboratory rig, the tubes had potentials >350 mV. Although the potentials fell slightly after transfer (Fig. 7), the two half-tubes failed after one and four weeks in the laboratory rig.

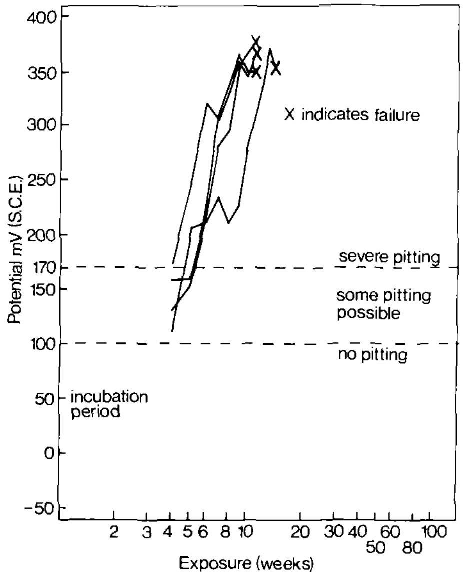

FIG. 6—*Potential/time curves for uncleaned copper tubes exposed at Bramham to water that supports pitting.*

Tubes transferred to the laboratory rig supplied with laboratory water—Before transfer, these tubes also had potentials >350 mV. Within one week of being supplied with laboratory water the potentials of the two half-tubes had fallen to less than 20 mV (Fig. 8). The tubes were exposed to the laboratory supply for nine months without failure, and no further significant changes in potential occurred.

Uncleaned Tubes Exposed Initially to a Water That Does Not Support Pitting and Then to One That Does—Two uncleaned copper tubes, with CB number 4, were exposed in the laboratory rig supplied with laboratory tap water. After five months' exposure the potential had never exceeded 54 mV. The tubes were transferred to the Bramham rig without being allowed to dry out, and their potentials then increased steadily to >300 mV (Fig. 9). The tubes were perforated after 4 and 4.5 months' exposure at Bramham.

These experiments demonstrated that with carbon-contaminated tubes changes in water composition can promote pitting when it was not previously occurring, or stifle it when it was. Furthermore, the potential taken up by the tubes is determined by the character of the water.

In a previous section it was stated that the potential of abrasively-cleaned tubes with marginal levels of contamination exhibited periodic variations in corrosion potential on prolonged exposure to Bramham water. It is considered that this type of variation in potential probably results from

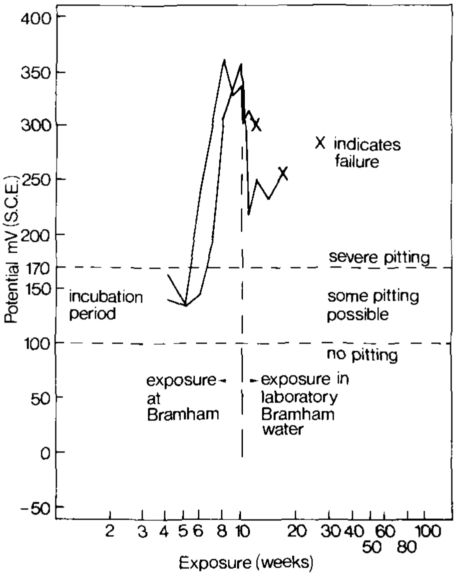

FIG. 7—*Effect of transferring uncleaned copper tubes undergoing pitting at Bramham to Bramham water in the laboratory.*

relatively slight variations in water composition. There is evidence that pits become stifled when the tubes have a potential <100 mV, but continue developing when the potential rises significantly above 100 mV.

Effect of Temper on the Incidence of Pitting

Hard-drawn tubes have been found to behave well generally in field trials, and this is in accordance with practical experience, which is that failures in such tubes are rare. As previously indicated, this type of tubing is not normally abrasively cleaned. After the final plug-drawing pass, residual lubricant remains in the bore, and this may not be completely removed even when steam-cleaning or detergent-washing processes are applied. It is possible that residual (uncarbonized) drawing lubricant may give some protection against the development of pitting in service in some circumstances, though, in general, the CB numbers for hard-drawn tubes are so low that pitting would not be expected to develop anyway.

In field trials with six relatively clean (CB numbers 1 to 2) hard-drawn tubes at the Bramham site and six rather less clean (CB numbers 1.5 to 5) hard-drawn tubes at the Barrow Park site, no pitting developed and all the tubes had low potentials throughout the exposure periods (14 months at Bramham and 9 months at Barrow Park).

To eliminate any complications due to possible presence of residual uncarbonized drawing lubricant in hard-drawn tubes, the effect of varying the temper of the copper was investigated by exposing sheet specimens.

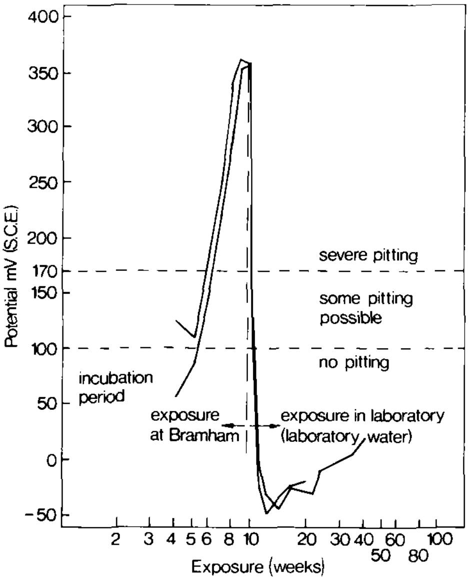

FIG. 8—*Effect of transferring uncleaned copper tubes undergoing pitting at Bramham to the laboratory (Leeds water).*

These were prepared by the British Non-Ferrous Metals Research Association (BNFMRA now the BNF Metals Technology Centre) as part of a larger program carried out under International Copper Research Association sponsorship. Phosphorus-deoxidized copper plate ¼ in. thick was cold-rolled to 0.1 in. thick and then bright annealed to give a hardness of 40 VHN5. Varying amounts of further cold-rolling were carried out to give specimens with hardnesses of about 60, 80, 100, or 125 VHN5. All the material was chemically cleaned in a nitric acid/acetic acid mixture, and on certain specimens carbon was deposited from the vapor phase to give two levels of surface contamination (*a*) lightly contaminated corresponding approximately to CB number 1.5 and (*b*) fairly heavily contaminated corresponding approximately to CB number 4.

Specimens in all tempers, with and without carbon deposits, were exposed at the Bramham site. Figure 10 shows the experimental arrangement.

Figure 11 shows the potential/time curve obtained with three specimens having a hardness of 80 VHN5 and with CB numbers 0, 1.5, and 4. The plots are typical of those obtained for these levels of contamination and similar graphs are obtained irrespective of specimen temper. Figure 12 shows the peak potentials attained by the individual sheet specimens during the exposure period. Only the most highly contaminated specimens reached potentials greater than 100 mV, and there was no systematic variation of

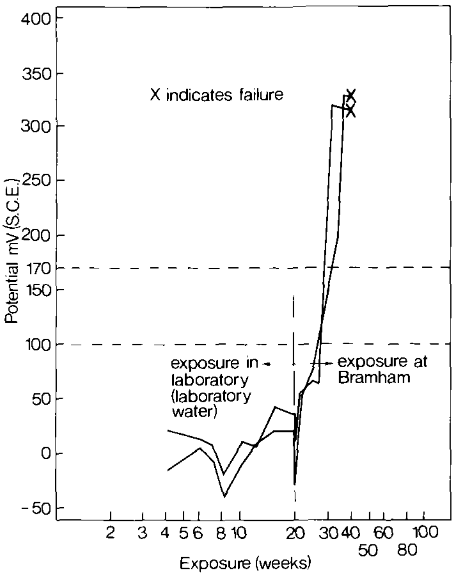

FIG. 9—*Effect of transferring uncleaned copper tubes from the laboratory (Leeds water) to Bramham.*

peak potential with hardness. The results obtained with these artificially contaminated sheet specimens indicate, therefore, that hardness in itself does not affect the pitting behavior of copper.

Effect of Alloying on the Incidence of Pitting

In an attempt to find a copper alloy with an increased resistance to pitting in the presence of carbon residues, a number of special tubes, in the half-hard condition, uncleaned, with CB numbers generally in the range 4 to 5, were tested at the Bramham and Barrow Park sites. The following eight materials were evaluated: (*a*) special coppers: Cu-1Sn, Cu-1Al, Cu-0.7Al-0.4As, Cu-0.25Fe, Cu-0.5Fe; and (*b*) special brasses: Cu-15Zn, Cu-10Zn-1.0Al, Cu-10Zn-0.5Sn. Their performance was compared with that of uncleaned (CB numbers 3 to 4) half-hard copper tubes, which, as already indicated, usually attain high potentials (300 to 350 mV) at Bramham and are generally perforated in 3 to 12 months. Similar tubes tested at Barrow Park do not attain such high potentials, the maximum being about 270 mV and the most rapid failures occurring in about 9 months.

With the iron-bearing alloys and the Cu-0.7Al-0.4As alloy at the Bramham site, the electrode potentials increased rapidly and attained similar values to those for uncleaned copper. Failures occurred in the iron-bearing alloys within 7 months, and in the Cu-0.7Al-0.4As alloy tubes within 15 months. No failures occurred after 18 months' exposure in the Cu-1Al

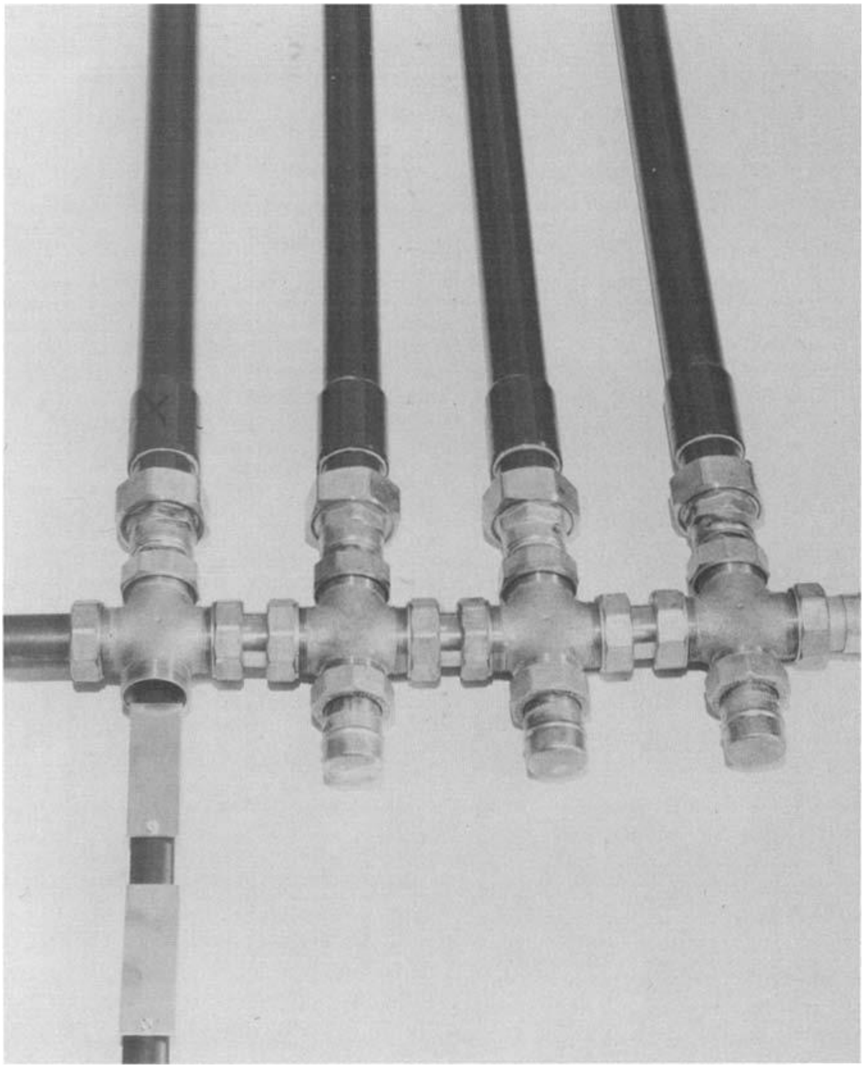

FIG. 10—*Experimental arrangement for exposure of sheet specimens.*

alloy tubes at Bramham, but deep pits (up to 50 percent through the wall) had developed.

No failures occurred in the Cu-1Sn alloy tubing exposed at Bramham or Barrow Park for 39 and 25 months, respectively. Peak potentials were about 150 mV and examination of tubes after trial showed that only relatively shallow pitting had occurred.

Most of the Cu-15Zn and Cu-10Zn-0.5Sn tubes failed within 16 months when exposed at Barrow Park. Although none of the Cu-10Zn-1Al tubes

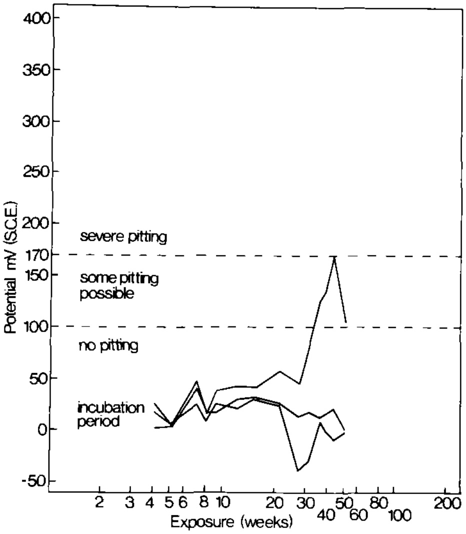

FIG. 11—*Potential/time curves obtained with three sheet specimens having a hardness of 80 VHN5 and CB numbers 0, 1.5 and 4.*

failed at this site after 25 months, extensive deep pitting occurred in all the specimens exposed.

On the basis of these trials, therefore, alloying the copper can give some improvement in resistance to pitting in the presence of carbon residues. The best addition was 1Sn, the other materials being less good, with several of them no better than ordinary copper (for equal CB numbers). Even the best material showed some attack, however, and it is doubtful whether it would be wise to supply it for general service in the uncleaned condition. Bearing in mind also the increased processing costs in manufacture, the use of alloys instead of phosphorus-deoxidized copper for seamless water tubing does not appear to be an attractive proposition.

Service Experience in the United Kingdom

Pitting corrosion of copper became a serious problem in the United Kingdom in the 1950's, when the practice of bright annealing was becoming increasingly used in preference to an oxidizing anneal followed by a pickling operation. Once it had been demonstrated that pitting corrosion was associated with carbon films, British manufacturers began to introduce cleaning operations designed to remove the deleterious films from the bores of copper tubes. Abrasive cleaning using water-borne alumina and cleaning using a variety of air-borne abrasives were processes that became widely used. Campbell [*8*] analyzed the failures received by the BNFMRA and by two large British tube manufacturers involving tubing installed

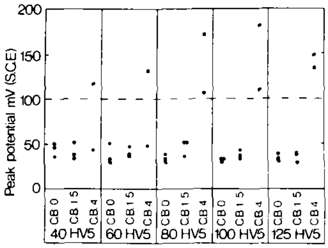

FIG. 12—*Peak potentials attained by individual sheet specimens during exposure at Bramham.*

between 1956 and 1962. The analysis led to the conclusion that a practical solution to the problem had been found in abrasive cleaning.

Variation in the annual rate at which failures have been received by the authors' company for investigation, for the years between 1958 to 1973, is shown schematically in Fig. 13. Most of these failures involved half-hard temper tubing in the one-half inch nominal size. Following the introduction of cleaning with water-borne alumina in Nov. 1959, the number of failures investigated fell to acceptable levels in 1964 and remained almost constant for the next two years. This is in line with Campbell's analysis of the situation in 1962.

In 1966, however, the British Standard Specification for Light Gauge Copper Tubes for Water, Gas, and Sanitation (B.S. 659: 1963) was amended

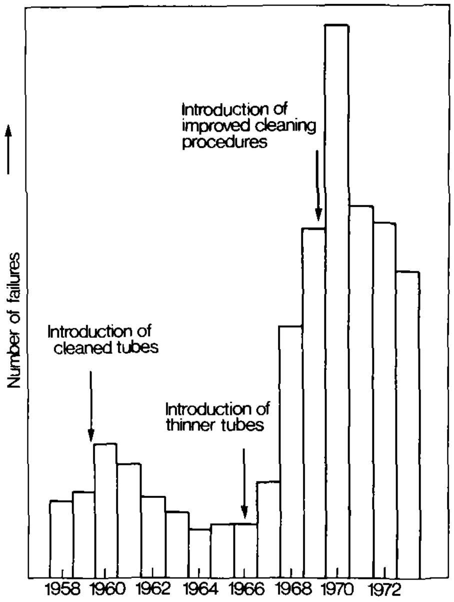

FIG. 13—*Variation in the annual rate at which failures have been received for investigation.*

and tubing with a reduced wall thickness was introduced; in 1967 a substantial increase in the number of service failures was observed. The service failures increased dramatically during the next three years (Fig. 13), and it transpired that the abrasive-cleaning procedures that had hitherto been satisfactory were no longer adequate. In the middle of 1969, more efficient air-borne abrasive-cleaning treatments and tighter quality control procedures were introduced, and as a result the number of service failures started to decrease (Fig. 13).

Figure 14 shows the cumulative number of pitting failures per million metres for ½ in. (or 15 mm) half-hard tubing manufactured in 1967, 1969, and 1971. These graphs confirm that the situation has improved considerably since the introduction of abrasive-cleaning practices that are more effective in removing carbon residues than the earlier treatments.

Summary

The results presented in this paper show that in certain water supplies the presence of carbon residues in the bores of copper tubes causes the potential of the surface to increase above a critical value and that rapid pitting of the copper then occurs. Abrasive cleaning is one means of reducing the level of carbon contamination to such an extent that the potential does not rise above the critical value and pitting does not occur. The results of service experience in the United Kingdom show that the numbers of failures in bright-annealed half-hard tubing have been greatly reduced by the use of effective abrasive cleaning techniques.

In surface supply waters that are believed to contain organic corrosion inhibitors, carbon residues do not give rise to high potentials and pitting does not occur. However, if the water in a carbon-contaminated tube is changed from one that does not support pitting to one that does, pits will develop. Conversely, active pits can be stifled by changing from an aggressive water to one in which pits cannot be initiated.

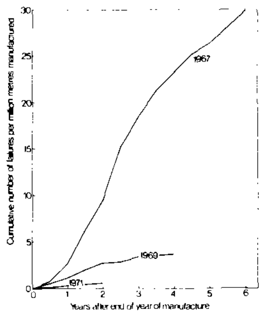

FIG. 14—*Cumulative number of pitting failures per million metres for 1/2-in. (15-mm) half-hard tubing manufactured in 1967, 1969, and 1971.*

Experience with hard-drawn tubing is that it normally gives good service performance and pitting failures are rarely encountered. This is due to the fact that such a tube normally contains only small amounts of carbonaceous residues; in addition, thin films of residual drawing lubricant may give a degree of protection in some circumstances.

Copper containing about 1 percent of tin or aluminum (particularly the former) are more resistant than ordinary coppers to pitting in the presence of carbon residues. It appears, however, that these materials do not give an economic answer to the problem of eliminating pitting in cold, organically pure supply waters.

Acknowledgments

The authors wish to thank the directors of Yorkshire Imperial Metals Limited for permission to publish this paper. Thanks are also due to the Claro and North Lindsey Water Boards (now part of the Yorkshire and East Anglia Water Authorities, respectively) for providing sites for the corrosion test rigs, without which the work would not have been possible. The preparation of the sheet specimens by the BNF Metals Technology Centre is also gratefully acknowledged.

References

[*1*] Campbell, H. S., *Chemistry and Industry*, 1955, p. 692.

[*2*] Hatch, G. B., *Journal of the American Water Works Association*, Vol. 53, 1961, p. 1417.

[*3*] Schafer, G. J., *New Zealand Plumbing Review*, Sept. 1964, p. 5

[*4*] Gerth, D., *Sanitar-installation, Blechberarbeitung, Zentralheizungsbau, Lufttechnik*, Vol. 20, No. 19, 1965, p. 350.

[*5*] Rambow, C. A. and Holmgren, R. S., Jr., *Journal of the American Water Works Association*, Vol. 58, 1966, p. 347.

[*6*] Gilbert, P. T. and Cairns, J. H. in *The Technology of Heavy Non-Ferrous Metals and Alloys*, Newnes, London, 1967, p. 144.

[*7*] Campbell, H. S., *Journal of the Institute of Metals*, Vol. 77, 1950, p. 345.

[*8*] Campbell, H. S., *Proceedings*, Second International Congress on Metallurgical Corrosion, National Association of Corrosion Engineers, 1963, p. 237.

[*9*] Schafer, G. J., *Australian Corrosion Engineering*, Vol. 6, 1962, p. 5.

[*10*] von Franque, O., *Werkstoffe und Korrosion*, Vol. 19, No. 5, 1968, p. 377.

[*11*] Lucey, V. F., "Pitting Corrosion of Copper in Supply Waters—The Effect of Water Composition, First Report," Research Report No. A 1692, British Non-Ferrous Metals Research Association, June 1968.

[*12*] Lucey, V. F., "Pitting Corrosion of Copper in Supply Waters—The Effect of Water Composition, Second Report," Research Report No. A 1723, British Non-Ferrous Metals Research Association, April 1969.

[*13*] Devroey, P. and Depommier, C., unpublished work.

[*14*] Campbell, H. S., "The Resistance of Hard Drawn Copper Tubes to Pitting Corrosion," Technical Memorandum 209, British Non-Ferrous Metals Research Association, May 1966.

[*15*] Cornwell, F. J., Wildsmith, G., and Gilbert, P. T., *British Corrosion Journal*, Vol. 8, 1973, p. 202

[*16*] Pourbaix, M., *Corrosion*, Vol. 25, 1969, p. 267.

[*17*] Pourbaix, M., *Corrosion Science*, Vol. 12, 1972, p. 183.

[*18*] Lucey, V. F., *British Corrosion Journal*, Vol. 2, 1967, p. 175.

[*19*] Campbell, H. S., *Journal of Applied Chemistry*, Vol. 4, 1954, p. 633.

DISCUSSION

Arthur Cohen[1]—The authors have prepared a detailed report on a problem that has been underway on a semicontinuous basis for the past 25 years in both Britain and the United States. This study originated in the late 1940's during Britain's massive reconstruction of war-damaged housing when a serious epidemic of pitting corrosion in England was circumstantially associated with the presence of heavy films of carbon inside copper water tube. The paper by Hector Campbell of the British Non-Ferrous Metals Research Association publicized this circumstantial evidence and as a result of Campbell's investigation, production practices were adopted by British brass mills that were intended to produce tubes "free from . . . deleterious films in the bore".

While it is scientifically sound to associate the presence of carbon films in the bores of copper water tube with the occurrence of pitting corrosion, we are convinced that carbon films have never been demonstrated to be the cause of pitting corrosion in copper water tube. More important, neither has it been demonstrated that special procedures to produce tubes free of carbon films solve the problem of pitting by aggressive water because it can and has been demonstrated that an aggressive water can cause pitting of copper in the absence of such films.

But most important, we are certain that pitting of copper water tube cannot occur without exposing the tube to an aggressive water in the first place, irrespective of surface condition or degree of cleanness.

It is surely true that if there were carbon present on the inside surface of a tube it would, in theory, provide the electrochemical conditions that would favor pitting. However, we maintain that no direct evidence has ever been established showing a direct cause and effect relationship between carbon films and pitting corrosion. Nor has it been shown that complete absence eliminates the problem. For example, in laboratory experiments conducted at a Belgian brass mill, hard drawn tube with appreciable amounts of carbon on the inside surface were found to resist pitting corrosion, while annealed tube with the same amounts of carbon present suffered failures.

This experience has been verified in both the United States and Britain where pitting corrosion by an aggressive water has occurred even in the absence of carbon films as, for example, in hard drawn tube. Even though the British tube producers have introduced aqua- or dry-blasting cleaning techniques, they still experience pitting corrosion.

---

[1] Standards engineering manager, Copper Development Association, New York, New York.

A recent paper by Cruz and Pomeroy[2] also confirms the fruitlessness of work to try to establish that carbon films cause pitting. Their data also clearly show that pitting corrosion has occurred in carbon-free tubes.

Also supporting the position that the presence of carbon films is unnecessary for pitting corrosion to occur is the report of the British Non-Ferrous Metals Research Association.[3] It illustrates that copper hot water cylinders or combination tanks fabricated from carbon-film-free copper sheet have given completely trouble-free service except for a few districts which are supplied with aggressive hard or moderately hard deep well waters. The pitting that has been experienced has occurred in the cold water section of these tanks.

A paper by Lyman and Cohen[4] rejected the British position of carbon film as being responsible for pitting corrosion and established how it is the chemistry of water that determines whether or not pitting will occur. The paper also pointed out how tube production methods differ in the United States and Britain. Regrettably, this paper has not been referenced despite its familiarity to the authors. Also regrettably omitted by the British authors is any reference to the work of Rambow and Holmgren which demonstrated how water chemistry controls whether or not pitting occurs and how pitting can be eliminated by simply treating an aggressive water to increase the pH and drive out the free carbon dioxide.[5] The British authors cite Rambow and Holmgren (Ref 5 of paper) but only in passing in the first sentence of their paper and for the purpose of establishing that "copper tubes are widely used . . . and have very long life."

Information received from a number of U.S. water companies have confirmed that the solution to overcome pitting corrosion has been and continues to be to treat the aggressive water. This is accomplished by the addition of either lime or caustic soda.

In the United States, treatment of well waters to control their corrosivity to plumbing materials is a common practice. We are convinced that this is the route to follow rather than to follow the suggestion of the British and introduce another operation in the tube manufacturing process, an operation whose quality control cannot be reproduced (and for which no standards exist) despite repeated efforts by numerous laboratories on both sides of the Atlantic.

Attempts at controlling the operation by measuring the level of carbon contamination in a carbon black (CB) test devised by Devroey and

---

[2] Cruz, H. and Pomeroy, R. D., "Corrosion of Copper Pipe, *Journal of the American Water Works Association*, Aug. 1974.

[3] "Copper Cylinders and Combination Tanks for Long Service," British Non-Ferrous Metals Research Association.

[4] Lyman, W. S. and Cohen, A., "Service Experience with Copper Water Tube," *Materials Protection and Performance*, Feb. 1972.

[5] Rambow, C. A. and Holmgren, R. S., *Journal of American Water Works Association*, Vol. 58, 1966, p. 347.

Depommier in Belgium, have been fruitless. In one study with which we are familiar, seven independent laboratories conducted several round-robin tests to determine whether it was possible to achieve uniformity of laboratory results in the determination of the CB numbers. The data were completely nonreproducible and, in fact, so were the colors which ranged from black to gray to brown despite rigorous adherence to the prescribed procedure.

The one significant contribution of the authors' paper is the tests where tubes were exposed to an aggressive pitting water at Bramham and then moved to Leeds where they were exposed to a nonaggressive water, and vice versa. The tubes which were exposed to the nonpitting water initially and then to a pitting water, experienced no failure in the first water and then failed in four to four and one-half months after transfer to the pitting water. Similarly, those tubes which were exposed first to a pitting water and then to a nonpitting water experienced failure in the first water but no further failures after transfer to the nonaggressive water because the pitting progression through the tube wall became stifled.

The British authors seem to be offering us a solution to pitting which their own and other data show to be unreliable. We would propose to them a simple solution that has been demonstrated to work everytime; treat the water to render it nonaggressive. Since the British promote water treatment to control dezincification of the brasses they choose to use in their water systems, it is strange indeed that they do not take the same approach to pitting problems.

F. J. Cornwell, G. Wildsmith, and P. T. Gilbert (authors' closure)—In reply to Cohen's contribution the authors wish to make the following points.

1. It is agreed that pitting of copper occurs only in certain waters that support this form of attack.

2. The relationship between pitting corrosion and presence of carbon residues on tubes as installed, in waters that support this form of attack, has been demonstrated both by direct experiment and by analysis of overall operating experience in the United Kingdom.

Clean (well-abraded) copper tubes suffered no pitting at the Bramham test site and had consistently low potentials (see Fig. 5 of paper), whereas tubes containing carbon residues assumed high potentials (see Fig. 2 of paper) and failed rapidly by pitting when tested in the same water at the same time.

Analysis of service failures in the United Kingdom over many years and correlation with production control data recorded by the authors' company has shown that over a period of some years about 1 percent of the tubes manufactured had rather higher levels of carbon residues than normal, and these gave rise to over 90 percent of the failures occurring. Effective removal of carbon residues by dry abrasive cleaning with iron grit has practically eliminated the failures previously occurring. Almost all the failures still experienced are in tubes made prior to the introduction of this process (see Fig. 14 of paper).

3. Hard-drawn (unannealed) tubes can contain carbon residues as there are other possible sources of carbon besides decomposition of residual drawing lubricant during bright annealing (such as use of graphitic lubricants during extrusion and decomposition of lubricant during drawing). In general, however, hard-drawn tubes have low levels of carbon residues as produced, and work, in United Kingdom and in Belgium, has shown that this is the main reason why such tubes behave relatively well, any effect of temper as such being secondary. No doubt the widespread use of hard temper tubes in the United States is one reason why pitting corrosion has been a less severe problem than in the United Kingdom where most of the tubing used is of half-hard temper.

4. The CB test is certainly far from ideal. However, when used under strictly standardized conditions by a single organization it has proved a most useful aid to quality control. On the basis of this control the authors' company has reduced the incidence of pitting failures in half-hard tubes to a few percent of those previously occurring.

5. After a period of service carbon residues become incorporated in the general corrosion product films on the tube surfaces and can then be readily removed by treatment with dilute citric acid solution. This cleaning process has been applied to several large-scale installations in which pitting corrosion was occurring. In each case trouble then ceased, showing that the removal of carbon was an effective remedy; there was no change in the nature of the supply water at any stage.

6. The role of carbon in promoting pitting corrosion in certain types of water has been recognized and accepted, to the authors' knowledge, by authorities in Belgium, France, Germany, Holland, New Zealand, South Africa, and Sweden as well as the United Kingdom, and no doubt in other countries as well.

7. There are many factors that influence the development of pitting of copper under nodules of corrosion product in cold supply waters, including the nature of the supply water, the condition of the metal surface, and the geometrical features that affect disposition of copper corrosion products. This last factor can explain why copper cylinders can suffer corrosion in certain waters whereas clean copper tubes do not.

8. In the paper by Cruse and Pomeroy it is interesting to note that the three specimens containing least carbon (Specimens 24, 40, and 41) suffered no pitting. All the other specimens for which a carbon figure is given contained enough to account for the observed attack. The paper by Lyman and Cohen, though valuable in other respects, has only limited information

on pitting corrosion. It deals with only a few cases and gives no information on carbon contamination.

9. It is encouraging that in the United States pitting has been successfully overcome by treating the water. The authors look forward with interest to hearing of further evidence from the United States of the successful application of this technique.

Florian Mansfeld[1]

Pitting Caused by Chlorides or Sulfates in Organic Media

REFERENCE: Mansfeld, Florian, "**Pitting Caused by Chlorides or Sulfates in Organic Media,**" *Galvanic and Pitting Corrosion—Field and Laboratory Studies, ASTM STP 576*, American Society for Testing and Materials, 1976, pp. 180–202.

ABSTRACT: The pitting behavior of titanium and titanium alloys, pure nickel, aluminum 6061, and stainless steel Type 304 has been studied using electrochemical techniques in methanol in the presence of sulfates or chlorides. An important factor is the water content of these solutions. In anhydrous solutions of methanol and hydrochloric acid (HCl), passivation cannot occur for titanium and high corrosion rates are observed. Addition of water at a concentration as low as 0.6 percent leads to passivation. The passive region is limited to noble potentials by the pitting potential which, up to 2.5 percent water, increases linearly with water content and is more or less independent of water content for higher concentrations. Similar observations are made for methanol containing sulfuric acid (H_2SO_4). Aluminum 6061 suffers from severe pitting when polarized anodically in methanol with 0.1 or 1.0 *N* H_2SO_4. Pitting was observed also for nickel after anodic polarization experiments in 2 *N* H_2SO_4 in methyl alcohol (CH_3OH). Iron, on the other hand, could not be passivated and pitting, therefore, did not occur. Pitting occurred for stainless steel Type 304 in 0.1 *N* H_2SO_4 in CH_3OH at rather noble potentials in the transpassive region. These results indicate that the solvent can have a large influence on the pitting susceptibility of metals. Titanium is very resistant in aqueous media, but shows pitting behavior similar to aluminum in organic media. It is also found that sulfates which do not cause pitting in aqueous media, where they even might be used as inhibitors, cause severe pitting in organic media for certain materials. Perchlorates have also been found to induce pitting in methanol. Phosphates lead to passivation by formation of a film of high electronic resistance. While pitting occurs on titanium in methanol containing 0.1 *N* H_2SO_4, no localized attack was observed under the same conditions in ethanol, ethylene glycol, or isopropanol.

KEY WORDS: corrosion, chlorides, sulfates, pitting, passivation, perchlorates, phosphates, methanol

Most studies of localized corrosion in the form of pitting have been carried out in aqueous media and have led to the conclusion that the halide ions, especially the chloride ion, are very dangerous in promoting failure

---

[1] Member of technical staff, Science Center, Rockwell International, Thousand Oaks, Calif. 91360.

of a wide variety of materials. Other types of anions, such as sulfates, nitrates, perchlorates, and chromates, seem to inhibit pitting when present in solutions containing halides as shown by Uhlig et al for iron [*1*],[2] 18Cr-8Ni stainless steel [*2*], and aluminum [*3*].

The susceptibility of metals and alloys to localized corrosion in nonaqueous solutions is of interest since Mori et al [*4*] have shown that stress corrosion cracking (SCC) of titanium occurs in methanol containing hydrochloric acid (HCl) or sulfuric acid (H_2SO_4), while zirconium cracked in methanol containing HCl or H_2SO_4 and in ethanol containing HCl. Small additions of water were shown to inhibit SCC of zirconium or titanium.

In order to obtain further information concerning localized corrosion in nonaqueous media, the author has recently studied the effect of water on passivity and pitting of titanium in solutions of methyl alcohol (CH_3OH) and HCl [*5*] and the passivation and pitting behavior of titanium, aluminum, nickel, stainless steel, and other materials in CH_3OH containing H_2SO_4 [*6*]. More recent studies [*7*] include the corrosion behavior of titanium in CH_3OH containing perchloric acid ($HClO_4$), nitric acid (HNO_3), and phosphoric acid (H_3PO_4) and comparison of polarization behavior in methanol, ethanol, ethylene glycol, and isopropanol containing sulfuric acid.

Experimental Procedures

Anhydrous solutions of CH_3OH-HCl were prepared by saturating methyl alcohol (nanograde, Mallinckrodt) with HCl gas. These solutions were then diluted by adding more methyl alcohol to give a certain concentration of HCl which was measured by titration. Aqueous solutions ofCH_3OH + HCl were prepared by adding water to anhydrous solutions of CH_3OH + HCl or by adding certain amounts of concentrated hydrochloric acid to pure methanol. Due to the water content of concentrated HCl, a solution of 1 *N* HCl in CH_3OH contains about 6.3 percent water (H_2O).

Unlike the case of methanolic solutions containing HCl, anhydrous solutions of CH_3OH + H_2SO_4 cannot be prepared. The solution of 0.1 *N* H_2SO_4 in CH_3OH used for most tests contains, however, only 0.04 percent H_2O, while a solution of 1.0 *N* H_2SO_4 in CH_3OH contains 0.4 percent H_2O as determined by Karl Fischer titration. Pure titanium (iodide), commercially pure titanium (Ti-75A containing about 4000-ppm total interstitial impurities), or Ti-6Al-4V were machined to cylindrical electrodes (about 2 cm^2 geometric surface) and connected to a holder so that only the electrode, Teflon, and glass were in contact with the solution. The electrode was degreased in boiling benzene at 80°C for 5 min, then etched in a solution of 30 percent HNO_3-20 percent hydrofluoric acid (HF)-20 percent

[2] The italic numbers in brackets refer to the list of references appended to this paper.

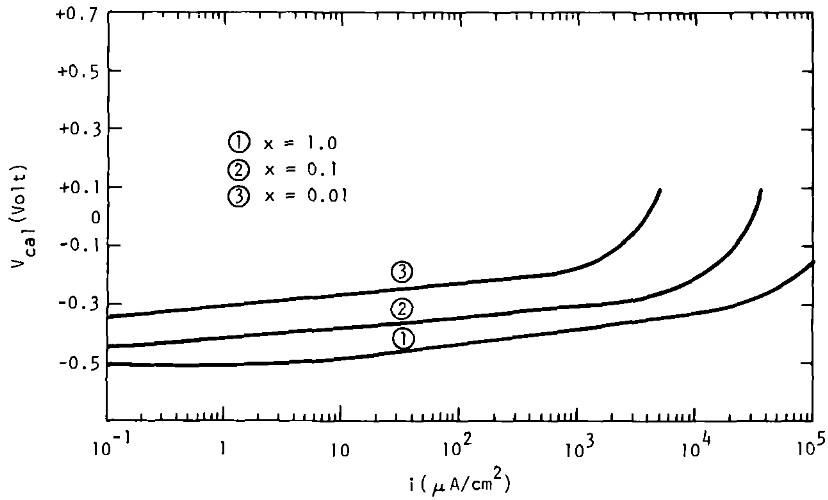

FIG. 1—*Potentiostatic anodic polarization curves for titanium 75A in solutions of* CH_3OH + xN *HCl anhydrous* (x = *1.0, 0.1, or 0.01*).

H_2SO_4-H_2O for 30 s, washed thoroughly in pure methanol, and then immediately immersed in the test solution, which was either air saturated (but unstirred) or deaerated and stirred with argon. The reference electrode was an aqueous saturated calomel electrode (SCE).

All potentials refer to SCE. After the rest potential had become constant, the potential was changed in steps of 10 mV/min using a potentiostat. In most experiments, a cathodic polarization curve was recorded first, the potential was then made more positive, and an anodic curve was recorded. At higher potentials when no pitting was observed, the rate of potential change was 50 mV/5 min. Since methanol solutions of hydrogen chloride of H_2SO_4 have high electrical conductivity due to the anomalously high mobility of the methoxonium ion $CH_3OH_2^+$, no major experimental problems concerning ohmic drops were encountered.

Results

Titanium in CH_3OH + *HCl*

Figure 1 shows potentiostatic polarization curves for Ti-75A in anhydrous $CH_3OH + xN$ HCl for $x = 1.0$, 0.1, or 0.01.[3] The effect of HCl concentration is clearly seen. The curves are shifted parallel in the noble direction with decreasing HCl concentration, and no active-to-passive transition is observed up to the highest currents studied. For comparison,

---

[3] Due to the water content of pure methanol (≈0.02 percent) these "anhydrous solutions" contain a small amount of water.

Fig. 2 shows polarization curves in methanol to which sufficient concentrated HCl was added to give aqueous solutions of CH_3OH + xN HCl for $x = 1.0, 0.1$, or 0.01. Again, the rest potential has the most noble value for the lowest HCl concentration, but surprisingly, passivity is observed in the solution with the highest HCl concentration (1.0 *N*, 6.3 percent H_2O) but not for the solution with the lowest HCl concentration (0.01 *N*, 0.06 percent H_2O). For the solution which contains 0.1 *N* HCl, the region of passivity is small due to pitting, the occurrence of which was confirmed by microscopical observation. In these aqueous HCl-CH_3OH solutions, the H_2O content increases with increase of the HCl content, because of the water content of concentrated HCl (37 percent HCl).

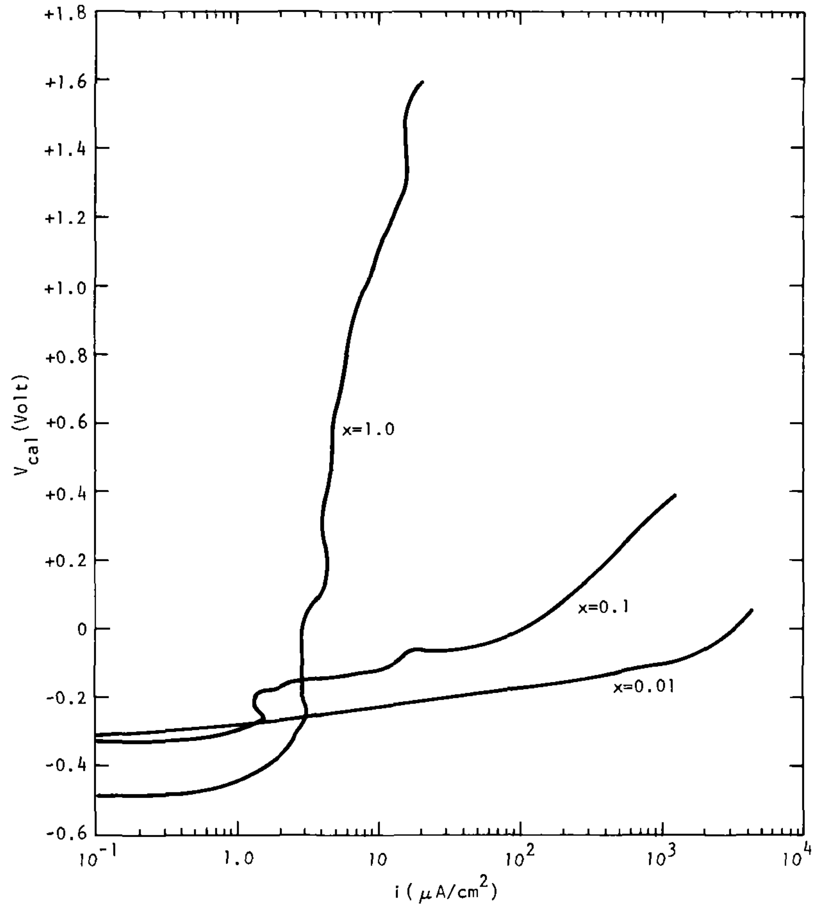

FIG. 2—*Potentiostatic anodic polarization curves for titanium 75A in solutions of* CH_3OH + xN *HCl aqueous* (x = *1.0, 0.1, or 0.01*).

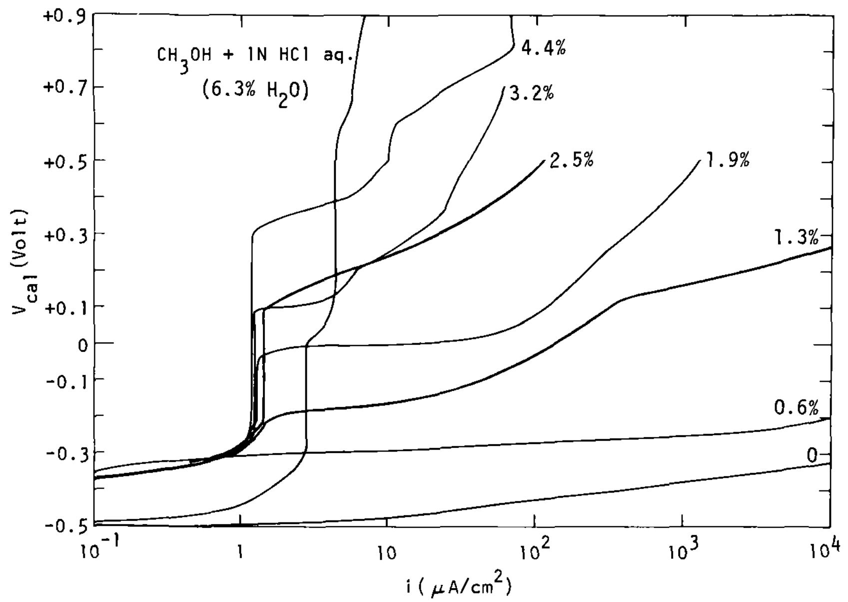

FIG. 3—*Potentiostatic anodic polarization curves for titanium 75A in solutions of* CH_3OH + *1* N *HCl anhydrous* + H_2O.

In the experiments of Fig. 3, increasing amounts of H_2O were added to a solution of anhydrous 1 *N* HCl-CH_3OH. In the absence of H_2O no active-passive transition is observed; the addition of 0.63 percent H_2O shifts the polarization curve in the noble direction, and a small region of passivity is observed limited by breakdown of passitivity through pitting. With an increase in H_2O content, the region of passivity is extended, the passive current density being about 1.3 μA/cm². The passive region is limited by the critical potential for pitting V_c' which becomes more noble as the H_2O content increases. After each run the specimen was investigated under a microscope to make sure that pitting had indeed occurred. At higher water contents, establishment of V_c' from polarization curves was very difficult. In aqueous 1 *N* HCl-CH_3OH (about 6.3 percent H_2O), no precise value of V_c' could be established. For this reason, the following two different experiments were carried out to determine more precisely the steady-state value, V_c, of the critical pitting potential.[4] In the first experiment, a constant current density of about 50 μA/cm² was applied to the test electrode and the potential-time curve recorded. This technique has been recently used by Tsinman et al [*8*]. Figure 4 shows the results for CH_3OH + 1 *N* HCl + 4.4 percent H_2O. After application of the constant

---

[4] The notation by Leckie and Uhlig [*9*] is used here to distinguish between short time (V_c') and steady state (V_c) critical pitting potentials.

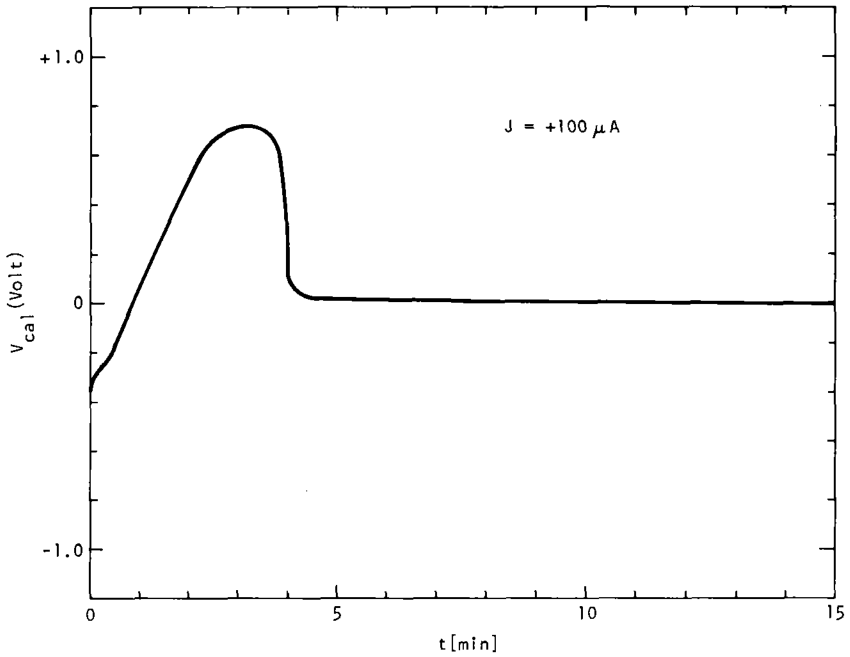

FIG. 4—*Changes of potential at a constant anodic current of 100 μA in* CH_3OH + *1* N *HCl anhydrous* + *4.4 percent* H_2O.

current density, the potential increased slowly to more noble values. When the maximum value was reached, small fluctuations of the potential, which were probably due to formation of the first pits, were observed. The potential then decayed fast to a constant value, which has been called the activation potential by Tsinman [*8*]. Microscopic observation of the electrode after the test showed occurrence of a number of pits. In the next experiment this constant potential was applied to a fresh electrode immediately after immersion into a fresh solution and the current-time curve recorded. If the potentiostatically applied potential was below the critical pitting potential V_c, the current decayed continuously due to passivation of the surface and no pits were observed (Curve A, Fig. 5). The potential was then increased by 15 or 25 mV. If V_c was exceeded, the current increased after an initial decrease and pitting was observed (Curve B). Critical pitting potentials estimated from polarization curves (V_c') and measured more precisely at a constant potential (V_c) are plotted in Fig. 6. While V_c' seems to increase linearly with water content, values for V_c seem to level off after a H_2O content of 2.5 percent H_2O. Values of V_c in solutions of CH_3OH + 3.15 percent H_2O + xN HCl (x = 0.01, 0.1, 1.0) are shown in Fig. 7, which shows an increase of about 0.3 V when [HCl] is decreased by a factor of 10.

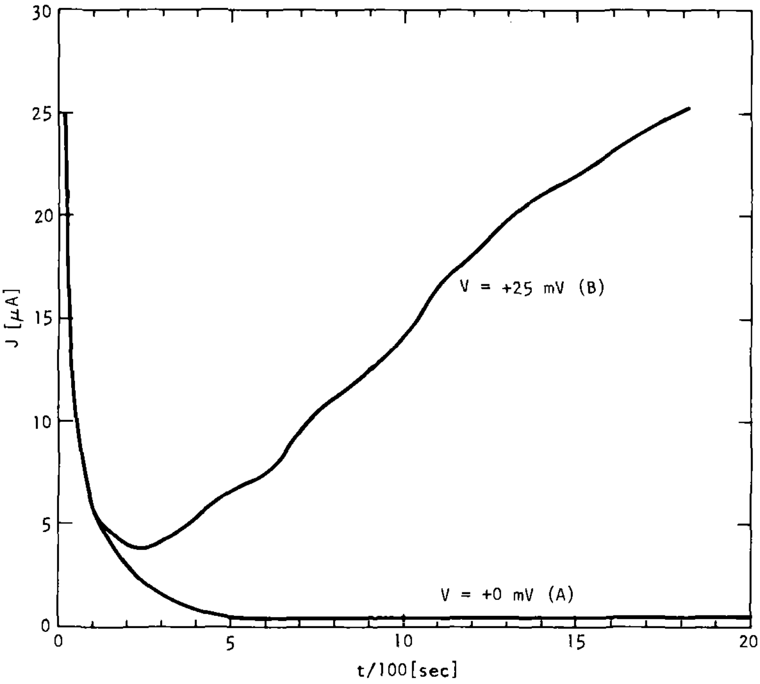

FIG. 5—*Changes of current at constant potential in* CH_3OH + *1* N *HCl anhydrous* + *4.4 percent* H_2O.

Various Materials in $CH_3OH + H_2SO_4$

Titanium and Titanium Alloys—Polarization curves were obtained for pure titanium (iodide), Ti-75A, and Ti-6Al-4V. No significant differences in the polarization behavior were observed for different alloy compositions. Figure 8 shows polarization curves for pure titanium in 0.1 *N* H_2SO_4 in CH_3OH. In the absence of water starting from the corrosion potential, a cathodic polarization curve has been obtained with a Tafel slope of $b_c \approx$ 0.09 V. This cathodic polarization apparently resulted in reduction of the surface oxide and a lowering of the hydrogen overvoltage as can be seen from the cathodic curve obtained on shifting the potential in the more noble direction. This effect might also result from formation of titanium hydrides which are assumed to have a hydrogen overvoltage lower than oxide covered titanium [*10*]. On the anodic branch of the curve, a short region of passivity can be detected, at about −0.24 V versus SCE, a sharp increase of the current occurs. Examination of the electrode after the experiment showed that localized attack in the form of pitting had occurred (Fig. 9).

When 1 percent of water was added to the test solution, the titanium electrode apparently was in the passive state. The anodic current remained

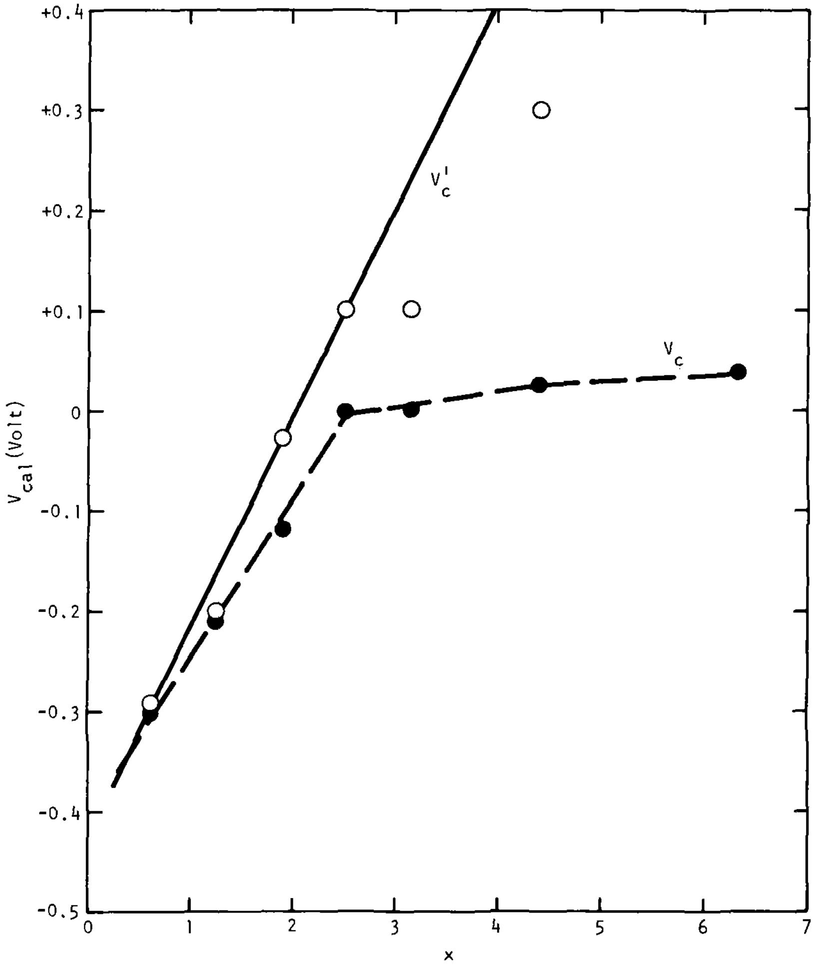

FIG. 6—*Dependence of pitting potential on water content of* CH_3OH + *1* N *HCl anhydrous* + x *percent* H_2O.

small and constant up to about +0.7 V (Fig. 8). At higher potentials the current increased steadily, but not as sharply as in water-free solutions.

Nickel—Figure 10 shows the effect of water on the polarization behavior of pure nickel (99.9 percent) in 0.1 *N* H_2SO_4 in CH_3OH. The cathodic branches and the anodic branches of the polarization curves were identical up to +0.2 V for solutions with 1 percent H_2O and without added H_2O. A decrease of the current was observed upon further anodic polarization indicating passivation in the solution containing added water, while only a very small decrease of the current was observed at +0.35 V in solutions where no water had been intentionally added. These results show that

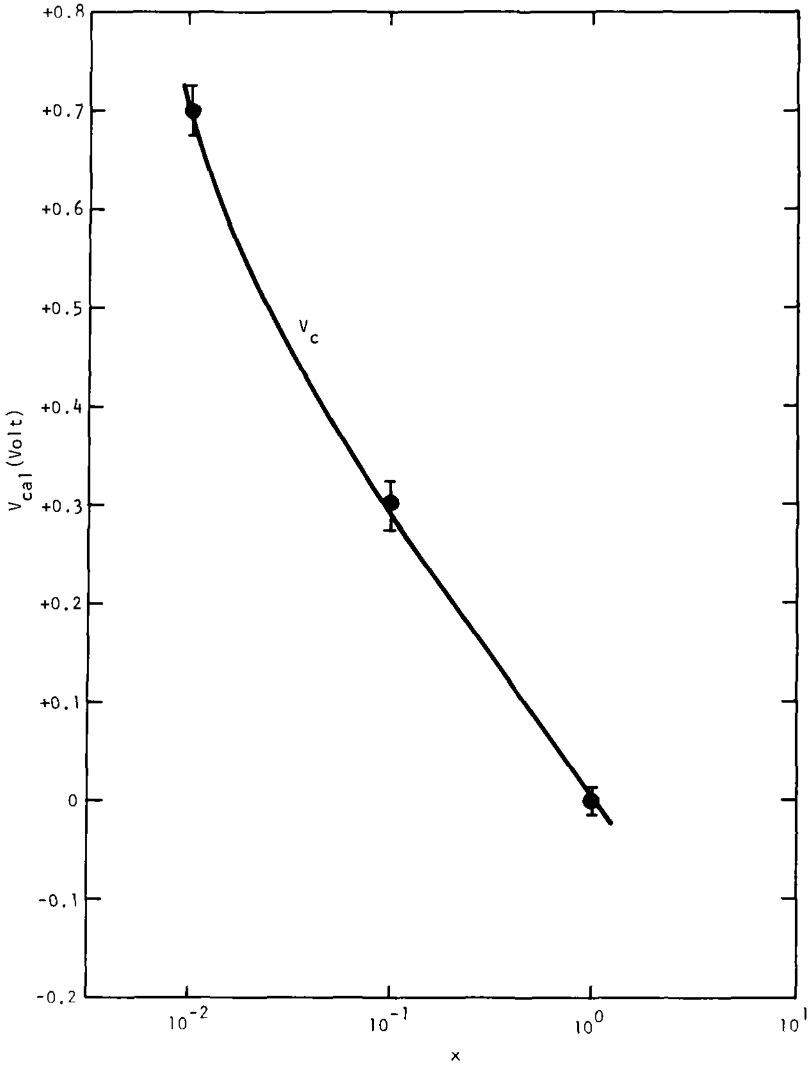

FIG. 7—*Dependence of pitting potential on concentration of HCl anhydrous in solutions of CH_3OH + 3.15 percent H_2O +* xN *HCl* (x = *1.0, 0.1, or 0.01*).

water has no influence on the kinetics of the hydrogen evolution reaction (HER) and on active dissolution. The water plays, however, a decisive role in passivation. Figure 11 shows the effect of H_2SO_4 concentration in methanol. While an increase in acid concentration leads to an increase in the critical current density for passivation, it also leads to a decrease of the passive current density. The latter effect most likely results from the higher water content inherent in the solution of 2 *N* H_2SO_4 in CH_3OH. Pitting of

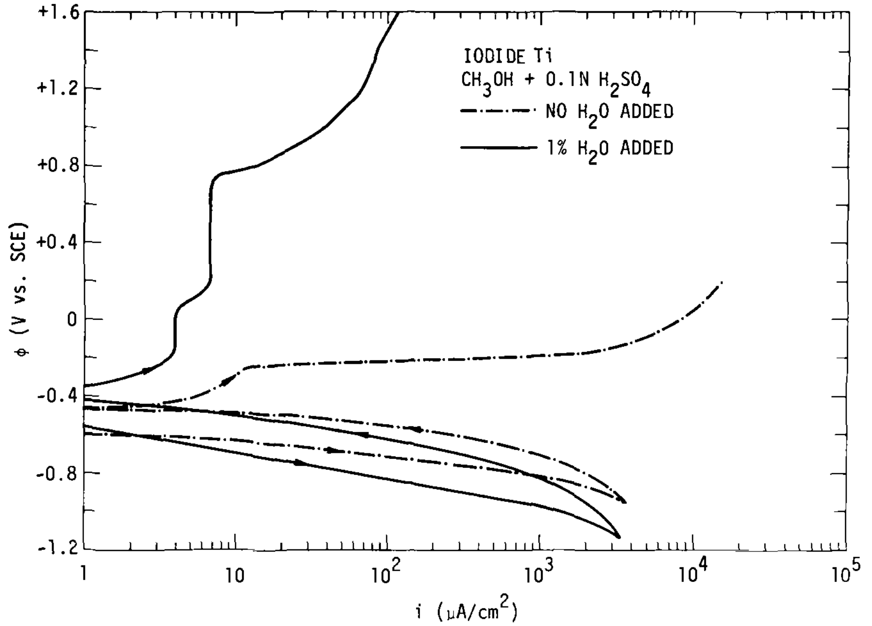

FIG. 8—*Potentiostatic polarization curves for pure titanium on 0.1* N *H_2SO_4 in CH_3OH, argon stirred.*

the electrode was observed after the anodic polarization experiments in 2 *N* H_2SO_4 in CH_3OH (Fig. 12).

Stainless Steel Type 304—Stainless steel Type 304 is readily passivated at rather low potentials in 0.1 *N* H_2SO_4 (Fig. 13) or 1.0 *N* H_2SO_4 in CH_3OH. The active to passive transition in Fig. 13 is only observed after cathodic reduction of the surface film formed in air or in solution. At potentials higher than +1.1 V versus SCE, a rapid increase of the current was observed. Microscopic observation of the surface of the specimen showed that pitting had occurred (Fig. 14*a*). The area around the pits appears to be attacked as shown in Fig. 14*b* in a different pattern than observed for titanium, aluminum, and nickel.

Aluminum 6061—The corrosion rate of aluminum 6061 in 0.1 *N* H_2SO_4 in CH_3OH was low (about 0.2 mg/dm²/day (mdd)). The potentiostatic polarization curve is shown in Fig. 15. When the specimen is polarized in the cathodic direction, the current starts to increase continuously with time at potentials more negative than −1.0 V. This leads to the loop in the cathodic polarization curve shown in Fig. 15. Upon anodic polarization, the aluminum alloy is in the passive state up to about 0.0 V when the current increases very sharply due to pitting. Gas evolution from the pits is observed under these conditions. Very large pits are observed as shown

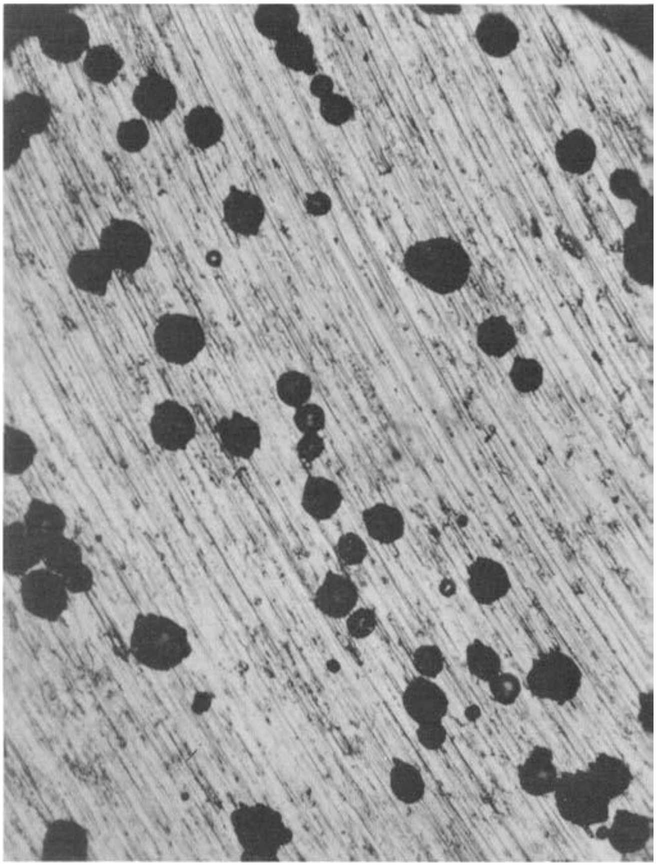

FIG. 9—*Pits on surface of titanum after anodic polarization in 0.1* N H_2SO_4 *in* CH_3OH *without water addition, magnification approximately* ×*180.*

in Fig. 16. Similar results were obtained in 1.0 *N* H_2SO_4 in CH_3OH. The effect of water additions has not yet been studied.

Iron—For pure iron, no passivation occurred in 0.2 *N* H_2SO_4 or 2 *N* H_2SO_4 in methanol up to a potential of +0.8 *V* versus SCE. The effect of water addition is different than that in the case of titanium or nickel. Additions of water up to 10 percent did not produce passivation upon anodic polarization, but increased the rate of anodic dissolution reaction (Fig. 17). The corrosion rate of iron in 0.1 *N* H_2SO_4 in CH_3OH was very high compared to that of titanium or nickel in the same medium. Using polarization resistance measurements and extrapolation of potentiostatic polarization curves to the corrosion potential, an average corrosion current density of 0.32 mA/cm^2 was measured for iron, which corresponds to 800 mdd.

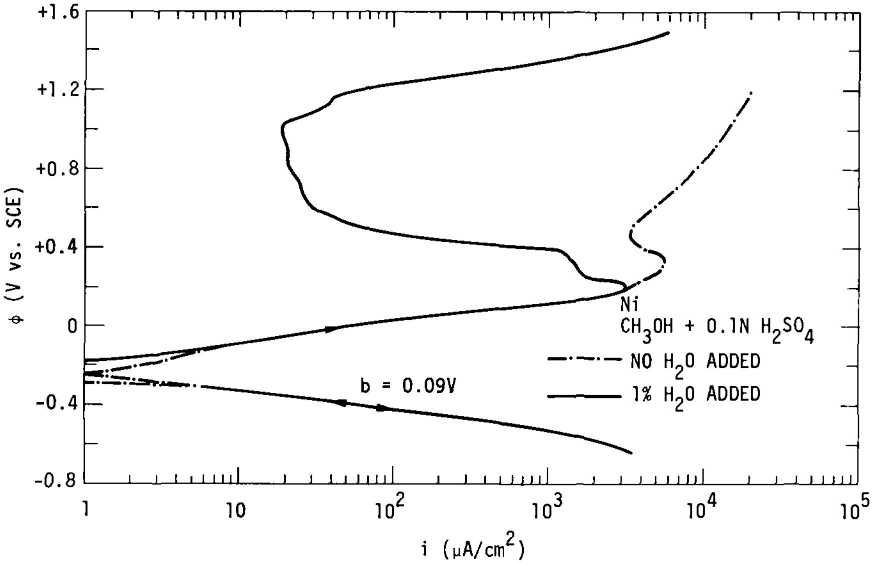

FIG. 10—*Potentiostatic polarization curves for nickel in 0.1* N *H_2SO_4 in CH_3OH with and without addition of 1 percent H_2O, argon stirred.*

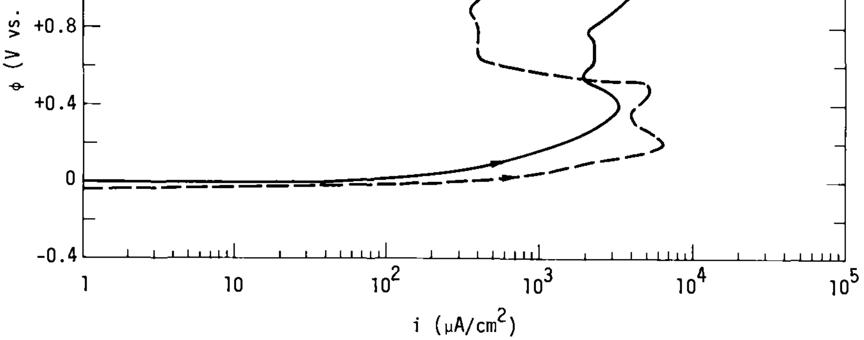

FIG. 11—*Potentiostatic polarization curves for nickel in 0.1,* N *H_2SO_4 in CH_3OH and 2* N *H_2SO_4 in CH_3OH.*

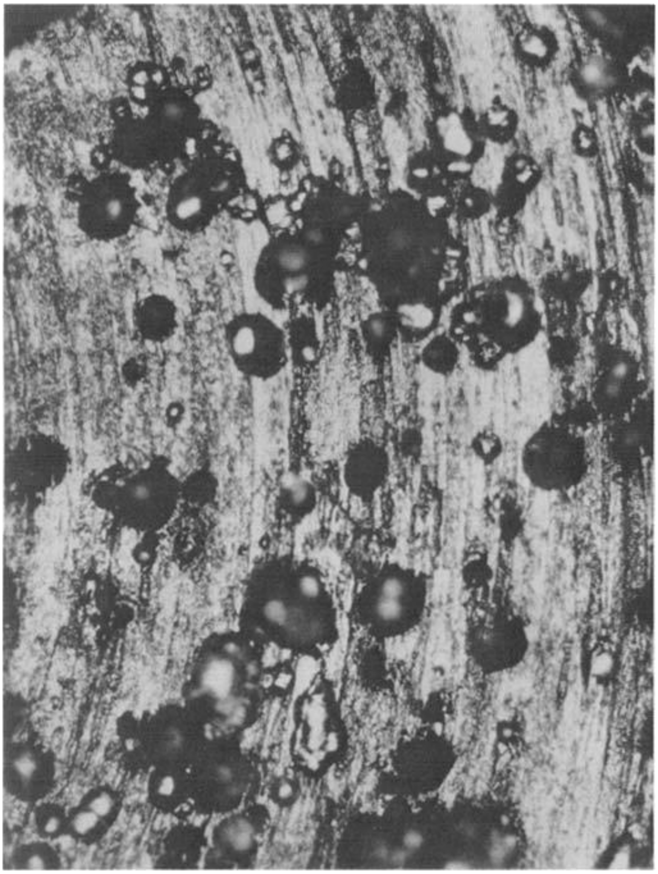

FIG. 12—*Pitting on nickel after test in 2* N *H_2SO_4 in CH_3OH; magnification approximately ×180.*

Copper—The anodic polarization curve for copper (Fig. 18) was similar to that observed in aqueous H_2SO_4. No active-passive transition was observed up to an applied potential of +2.0 V. The anodic current at potentials more noble than about 0.0 V versus SCE increased when the solution was stirred by argon, indicating that the anodic process is limited by mass transport in this potential region.

Platinum—Experiments on platinum were carried out in order to investigate the stability of the electrolyte. Figure 19 shows a polarization curve which was started at −0.8 V versus SCE. Tafel behavior with a Tafel slope of b_c = 45 mV is observed over 4 decades; the deviations at higher current density are most likely due to uncompensated ohmic drop. The anodic current remains low up to about +1.0 V from where it increases continuously. This is most likely due to oxidation of methanol as also ob-

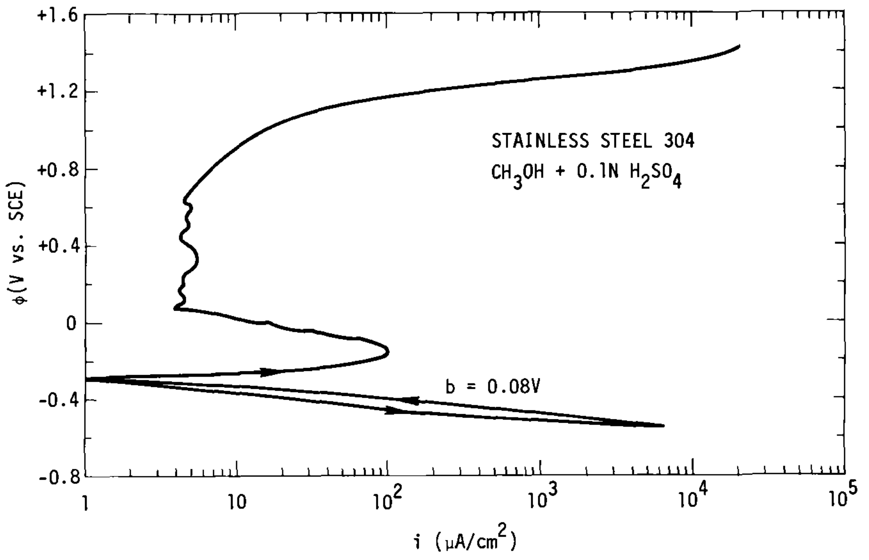

FIG, 13.—*Potentiostatic polarization curves for Type 304 stainless steel in 0.1* N *H_2SO_4 in CH_3OH, argon stirred.*

served by Stolica on platinum in lithium chloride (LiCl)-CH_3OH-H_2O solutions [*11*]. No oxygen evolution has been observed on platinum or any other metals studied.

Titanium in CH_3OH Containing Different Acids

In order to study further the effect of different anions on passivity and pitting in methanol, potentiodynamic polarization curves have been obtained in CH_3OH containing $HClO_4$, HCl, H_2SO_4, HNO_3, or H_3PO_4 with an anion concentration of one (Fig. 20). The different water content of these solutions makes it difficult to obtain a quantitative evaluation of anion effects. The occurrence of pitting in solution containing $HClO_4$ is, however, very surprising since the perchlorate ion in aqueous solutions usually is much less damaging to passive films. It is remarkable, in addition, that pitting is most pronounced in CH_3OH + 1 *N* $HClO_4$ since this solution has the highest water content. The absence of pitting in solutions containing H_2SO_4 or HCl is expected due to the high water content (Figs. 3 and 8). A film of very high resistance seems to form on the titanium surface in CH_3OH + H_3PO_4 as shown by alternating current impedance measurements [7]. This film protects the surface in the passive region and slows down the reduction reaction in the cathodic region. The rate of the reduction reaction is the highest in the presence of nitric acid, probably due to reduction of the nitrate ion.

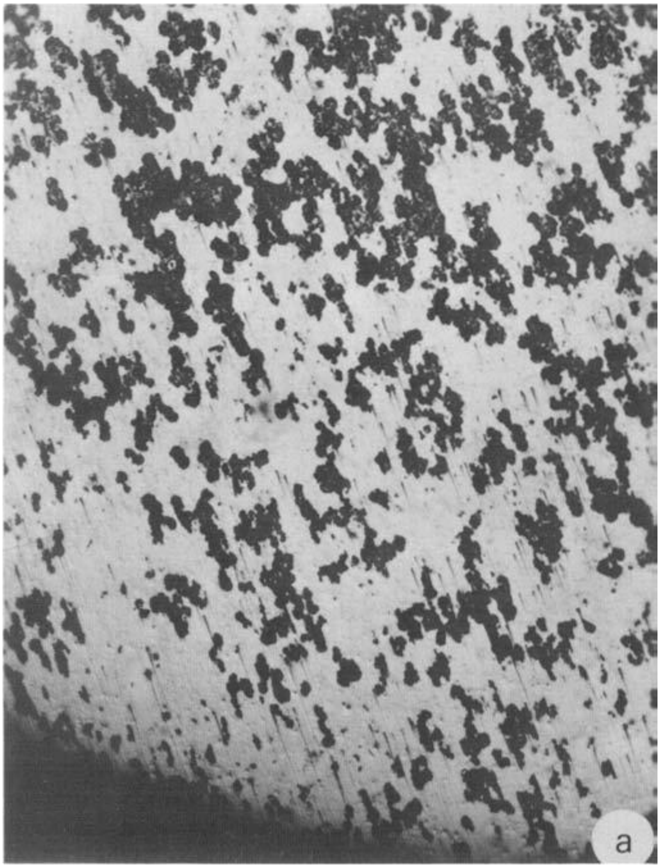

FIG. 14—*Pitting on Type 304 stainless steel after anodic polarization in 0.1* N H_2SO_4 *in* CH_3OH *(Fig. 13):* (a) *magnification approximately ×45, and* (b) *magnification approximately ×180.*

Titanium in Different Organic Solvents Containing H_2SO_4

The effect of water on passivity and pitting of titanium in organic solvents has been studied further for water contents between 0 and 100 percent in methanol, ethanol, isopropanol, and ethylene glycol in the presence of HCl or H_2SO_4 [7]. Figure 21 presents an example obtained for titanium 75A in solvents containing 0.1 *N* H_2SO_4 (0.04 percent H_2O). Pitting as evidenced by the sharp rise of the current at a characteristic potential in the passive region is only observed in methanol, in which the corrosion potential has the most active value. In ethanol, an increase of the current is observed at the most noble potentials, while in ethylene glycol, the typical active-passive passivation is observed in the polarization curve. In isopropanol the most noble corrosion potential and passive behavior in the entire potential region studied are observed.

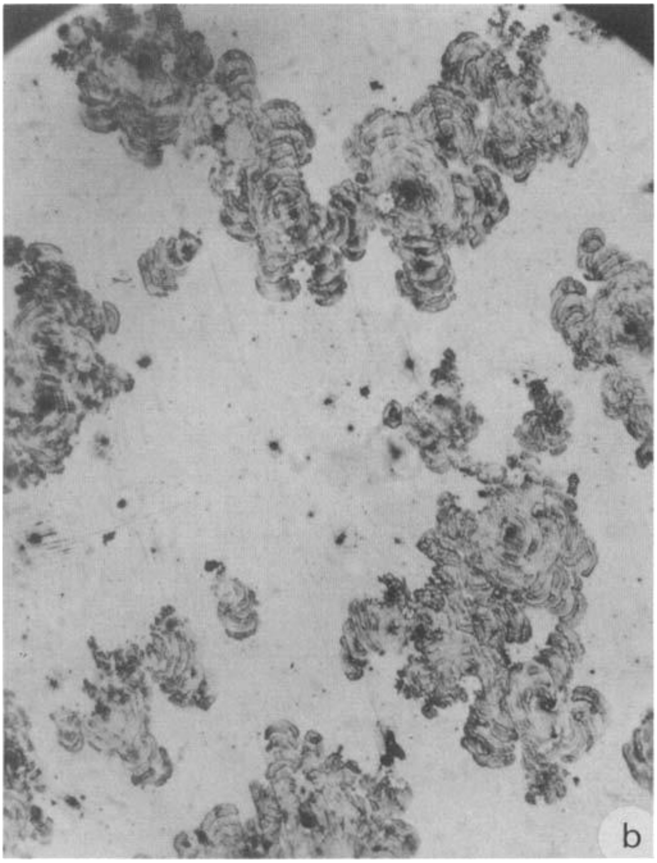

FIG. 14—(*Continued*).

Discussion

Passivating Effect of Water

The results obtained in this investigation have shown clearly that passivation of titanium cannot occur in CH_3OH-HCl in the absence of water. In anhydrous solutions anodic dissolution occurs following Tafel behavior. The polarization curves are shifted parallel in the noble direction as the HCl concentration decreases. Addition of water to the anhydrous electrolyte leads to passivation at a concentration as low as 0.6 percent water although the extent of the passive region is very small. This results from the fact that the critical pitting potential V_c' is only slightly noble to the corrosion potential. It has to be considered at this point that the surface concentration of water might be different from that in the bulk due to double-layer effects and solvation of dissolved metal ions. The latter effect would

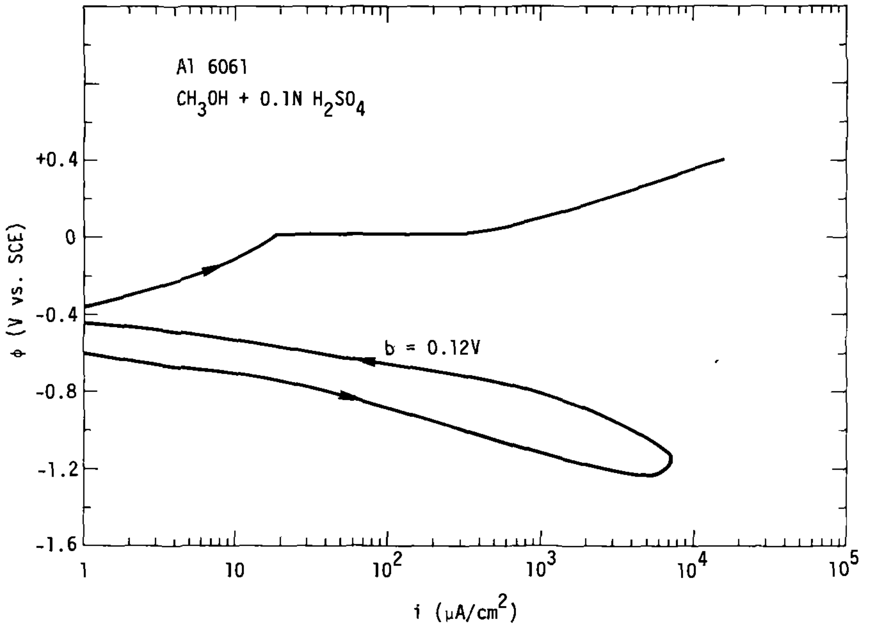

FIG. 15—*Potentiostatic polarization curves for aluminum 6061 in 0.1* N *H_2SO_4 in CH_3OH, argon stirred.*

decrease the amount of water available for passivation. No information is available concerning double-layer effects in the solutions studied. Increasing additions of water lead to a broader region of passivity in which the current is independent of potential. At a certain potential (the critical pitting potential) chloride ions are absorbed strongly enough to displace the adsorbed water molecules and penetrate the passive film. As more water is added to the electrolyte the passivating species (presumably the oxygen of water) is more strongly absorbed and V_c is shifted to more positive values. When a sufficient amount of water is added to produce a sufficient concentration of the passivating species at the surface of the metal, the critical pitting potential increases only very slightly. At a sufficiently high, constant water content, the pitting potential becomes more noble as the chloride ion concentration decreases, as observed for many metals in aqueous electrolyte.

These findings also explain the initially surprising results of Fig. 2, where the electrode was polarized in the anodic direction in solutions prepared from pure methanol and concentrated hydrochloric acid containing a constant ratio of water to chloride ion. In the solution of CH_3OH + 0.01 *N* HCl the water content is too small to allow formation of a passive film. In the solution containing 0.1 *N* HCl, enough water is present in the bulk to passivate the surface. However, the passive film is not very stable and therefore penetrated by chloride ions at a relatively low potential. In

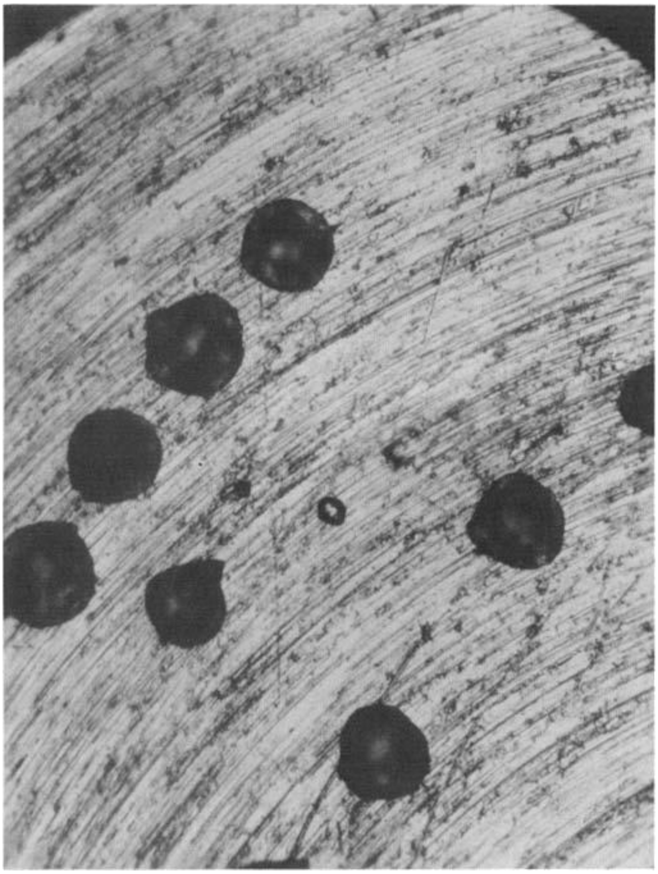

FIG. 16—*Pitting on aluminum 6061 after anodic polarization in 0.1* N *H_2SO_4 in CH_3OH, argon stirred; magnification approximately ×45.*

CH_3OH + 1 *N* HCl, enough water is present to protect the surface from pitting up to rather noble values. The film becomes more and more stable when the electrode is polarized slowly in the noble direction.

Experiments on titanium in 0.1 *N* H_2SO_4 in CH_3OH (Fig. 8) show that water also has a passivating effect in these solutions. It cannot be decided unambiguously whether the small region of passivity observed in 0.1 *N* H_2SO_4 in CH_3OH containing about 0.04 percent H_2O results from adsorption of the oxygen from the sulfate or from the water. By analogy with the results obtained in HCl-CH_3OH solutions and because of the large effect of the addition of 1 percent H_2O on passivity, it seems logical that the initial step in the passivation reaction on titanium is

$$Ti + H_2O \rightarrow Ti \cdot O_{ads} + 2H^+ + 2e^- \qquad (1)$$

where $Ti \cdot O_{ads}$ represents oxygen absorbed on titanium.

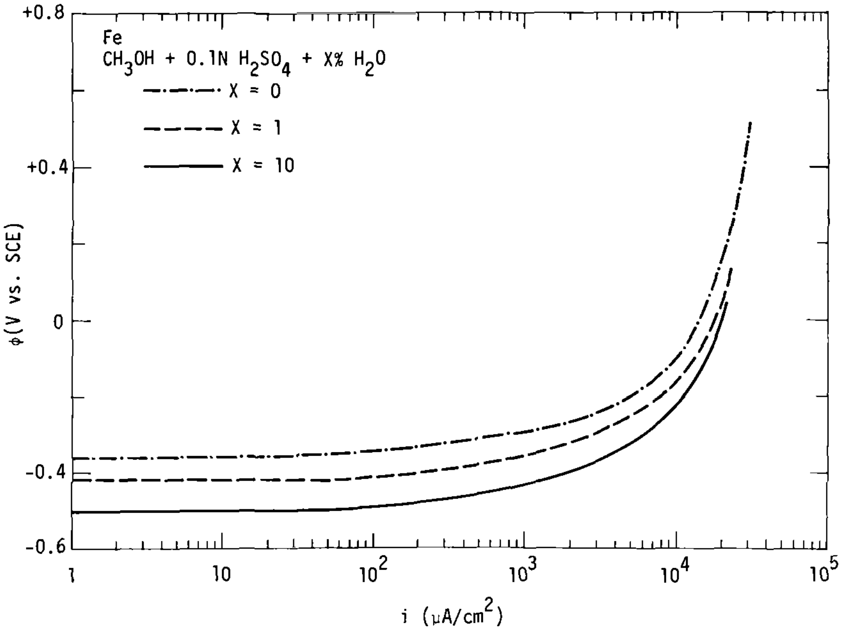

FIG. 17—*Potentiostatic polarization curves for iron in solutions of 0.2* N H_2SO_4 + x *percent* H_2O (x = *0, 1, or 10) in* CH_3OH.

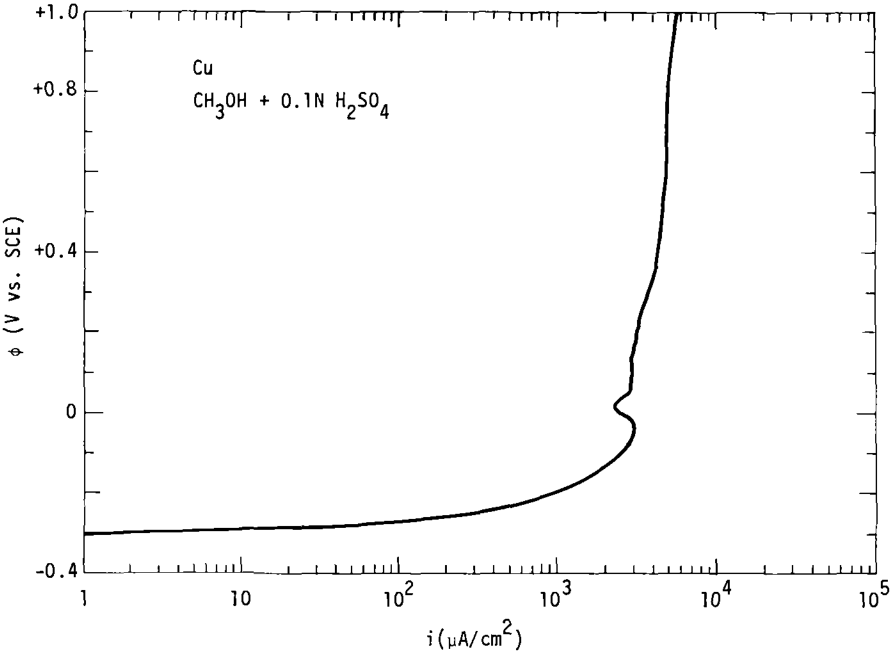

FIG. 18—*Potentiostatic polarization curve for copper in 0.1* N H_2SO_4 *in* CH_3OH, *deaerated.*

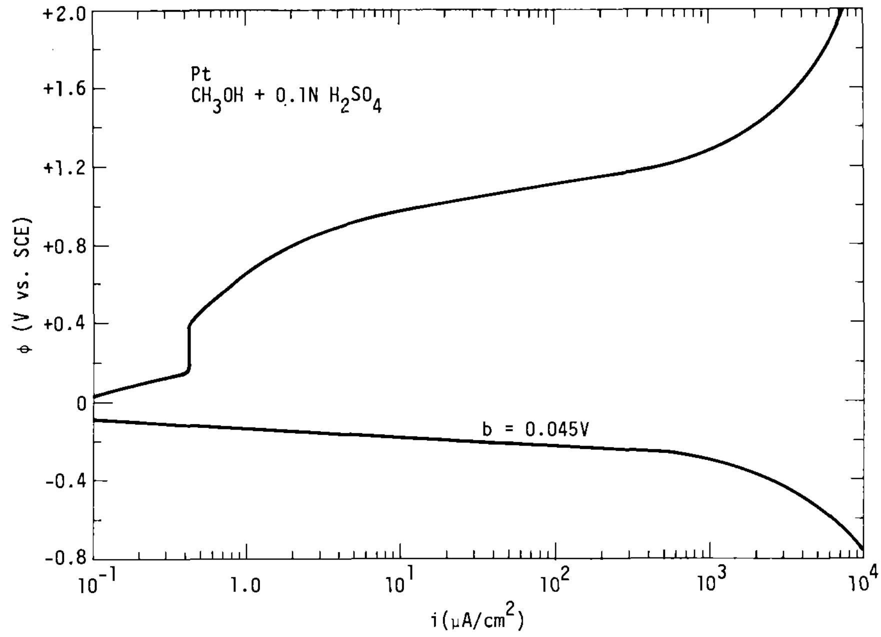

FIG. 19—*Potentiostatic polarization curves for platinum in 0.1* N *H_2SO_4 in CH_3OH, argon stirred.*

The results obtained for nickel (Figs. 10 and 11) support the assumption that water is responsible for passivation. For stainless steel Type 304 it was found in the present study (Fig. 13) that very small amounts of water (about 0.04 percent) are sufficient for passivation. For iron, on the other hand, no passivation could be observed even with water additions of up to 10 percent (Fig. 17). Additions of water in fact increased the anodic dissolution current in the potential range studied. A similar behavior was found by Kiss et al [*12*] for iron in acetic acid containing 0.5 M sodium acetate (HC_3COONa) or 0.5 M $HClO_4$. Additions of water in each case accelerated the rate of active dissolution. The authors concluded that in sodium acetate solutions passivation occurs only in the presence of water, while in solutions containing perchloric acid passivation occurred only in the absence of water. These results show that many factors determine the ability of a metal to passivate. These may include the electronic structure [*13,14*], the relative affinity to oxygen,[5] and the characteristics of ion pairs formed in solution [*12*].

When the results for nickel and iron are compared, it becomes evident that water molecules also have a different effect on the region of active dissolution of these metals. While the rate of the anodic dissolution reaction is not affected by water in the case of nickel (Fig. 10), it increases with increasing water content in the case of iron (Fig. 17). An increase in

---

[5] Evans, U. R., private communication.

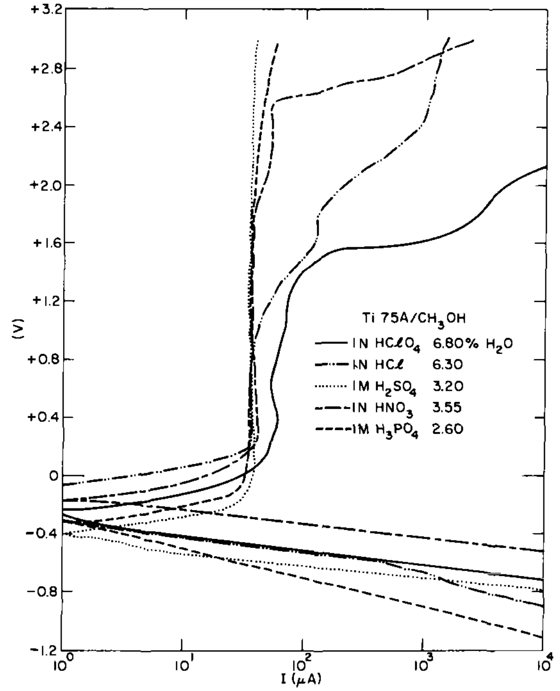

FIG. 20—*Potentiostatic polarization curves for titanum 75A in CH_3OH containing $HClO_4$, HCl, H_2SO_4 HNO_3, or H_3PO_4.*

the acid concentration apparently increases the rate of anodic dissolution of nickel and the critical current density for passivation (Fig. 11). In the passive region, the passivating effect of the higher water concentration is stronger than the activating effect of the higher acid concentration in 2 *N* H_2SO_4 in CH_3OH.

Pitting Produced by Sulfate Ions—It has been observed in this investigation that all metals which undergo passivation also suffer from localized attack in the form of pitting. This is a very surprising result since pitting is usually observed only in the presence of halides, especially chloride ions. Anions like sulfates, nitrates, perchlorates, and chromates have been shown to inhibit pitting of iron [*1*], 18Cr-8Ni stainless steel [*2*], and aluminum [*3*] in aqueous solutions containing halides. Toušek [*15*] recently pointed out, however, that there is no apparent reason why some of these anions should not lead to pitting. It was shown [*15*], that under certain conditions pitting can be produced by sulfates on iron and nickel in aqueous acid solutions containing both sulfate and chloride ions. Toušek also mentions briefly that "some sort of pitting corrosion" by sulfate ions occurs in a solution of 2 *N* H_2SO_4 and 2 percent H_2O in CH_3OH resulting in a polarization curve which is similar to that shown in Fig. 8.

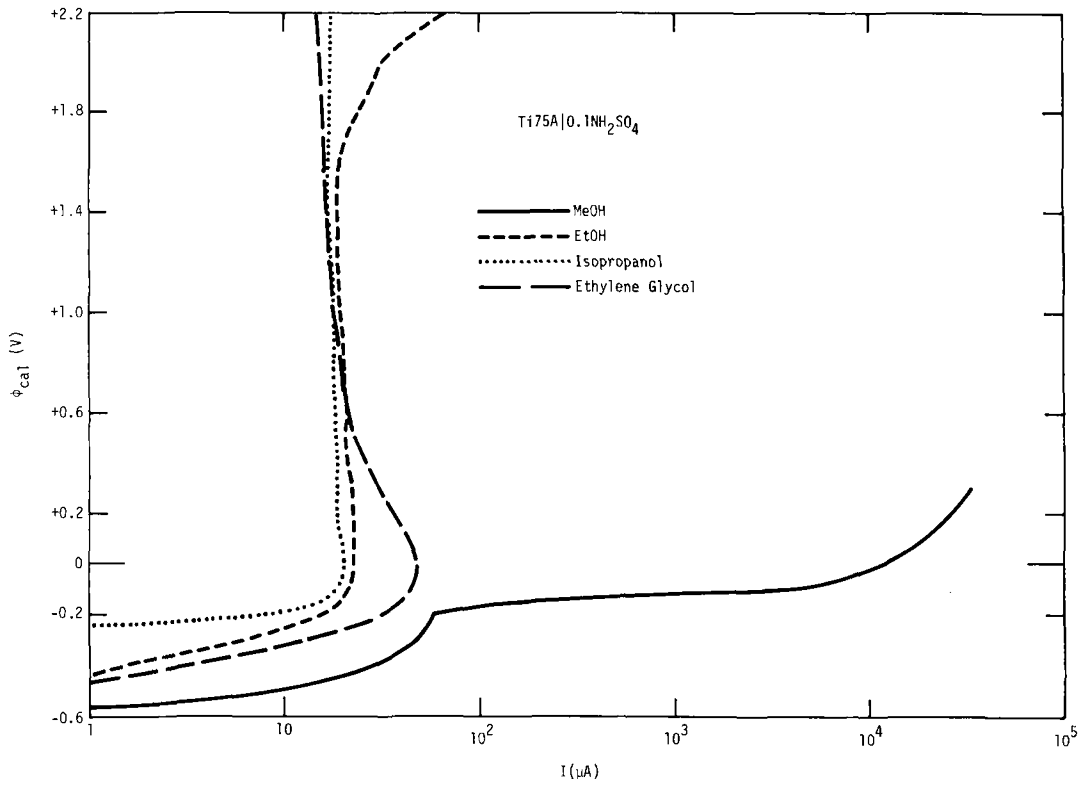

FIG. 21—*Potentiostatic anodic polarization curves for titanum 75A in methanol, ethanol, ethylene glycol, or isopropenol containing 0.1* N *H_2SO_4.*

Since pitting on nickel and stainless steel is observed at potentials where methanol decomposition occurs ($\phi > 1.0$ V) as shown on platinum (Fig. 19), it cannot be concluded solely from the increase of the anodic current that localized attack has occurred. Microscopic observation (Figs. 12 and 14) has confirmed, however, that pitting occurred in both cases. The possibility of reaction between oxidation products of methanol (HCHO, HCOOH) and the passive film has not yet been studied.

It is quite remarkable that titanium, which is so resistant to pitting in aqueous solutions containing halides, is more susceptible to pitting than aluminum 6061, nickel, and stainless steel in H_2SO_4-CH_3OH. The degree of susceptibility of titanium is similar in H_2SO_4-CH_3OH and HCl-CH_3OH. Although this author does not believe that SCC results from a pitting-type attack, there is a striking resemblance in the susceptibility of titanium to pitting and SCC in these solvent systems. This behavior suggests that the nature of the passive film and its rate of formation is different in aqueous solutions (sodium chloride) (NaCl) and methanolic solutions containing small amounts of water. Recent results by Smith and Mansfeld [*16*] have shown however, no differences of film properties in the two media as measured by ellipsometry.

Acknowledgments

The author thanks D. H. Hern and J. V. Kenkel for help in carrying out many of the experiments.

References

[*1*] Matsuda, S. and Uhlig, H. H., *Journal of the Electrochemical Society*, Vol. 111, 1964, p. 156.

[*2*] Uhlig, H. H. and Gilman, J. R., *Zeitschrift für Physikalische Chemie*, Vol. 226, 1964, p. 127.

[*3*] Böhni, H. and Uhlig, H. H., *Journal of the Electrochemical Society*, Vol. 116, 1969, p. 906.

[*4*] Mori, K., Takamura, A., and Shimose, T., *Corrosion*, Vol. 22, 1969, p. 29.

[*5*] Mansfeld, F., *Journal of the Electrochemical Society*, Vol. 118, 1971, p. 1412.

[*6*] Mansfeld, F., *Journal of the Electrochemical Society*, Vol. 120, 1973, p. 188.

[*7*] Mansfeld, F. and Kenkel, J. V., to be published.

[*8*] Tsinman, A. I., Kuzub, V. S., and Katrevich, A. N., *Soviet Electrochemistry*, Vol. 2, 1966, p. 513.

[*9*] Leckie, H. P. and Uhlig, H. H., *Journal of the Electrochemical Society*, Vol. 113, 1966, p. 1262.

[*10*] Armstrong, R. D., Harrison, J. A., Thirsk, H. R., and Whitfield, R., *Journal of the Electrochemical Society*, Vol. 117, 1970, p. 1003.

[*11*] Stolica, N. D., *Proceedings*, 5th International Congress on Metallic Corrosion, Tokyo, May 1972, p. 318.

[*12*] Kiss, L., DoNgoc, L., and Varsanyi, M. L., *Collection of Czechoslovak Chemical Communications*, Vol. 36, 1971, p. 914.

[*13*] Uhlig, H. H., *Zeitschrift für Elektrochemie*, Vol. 62, 1958, p. 626.

[*14*] Mansfeld, F. and Uhlig, H. H., *Journal of the Electrochemical Society*, Vol. 117, 1970, p. 427.

[*15*] Toušek, T., *Corrosion Science*, Vol. 12, 1972, p. 15.

[*16*] Smith, T. and Mansfeld, F., *Journal of the Electrochemical Society*, Vol. 119, 1972, p. 663.

L. C. Rowe[1]

Measurement and Evaluation of Pitting Corrosion

REFERENCE: Rowe, L. C., "**Measurement and Evaluation of Pitting Corrosion,**" *Galvanic and Pitting Corrosion—Field and Laboratory Studies, ASTM STP 576,* American Society for Testing and Materials, 1976, pp. 203–216.

ABSTRACT: Pitting is a destructive form of localized corrosion that requires careful analysis and evaluation. Metal surfaces are examined first to identify and determine the extent of pitting, which may be described in terms of standard charts. Nondestructive tests may be used, but they have limitations. Pit depths provide more meaningful information and can be determined by microscopic measurement, depth gages, and other techniques. Statistical methods can be used to show the probability of pitting to estimate maximum pit depths or to show the relationship with time. The change in mechanical properties may also provide useful information.

KEY WORDS: pits, pitting, corrosion, pitting evaluation, pit depth measurement, microscopic pit-depth measurement, nondestructive tests, pitting probability, statistics

Pitting is a form of localized corrosion that affects only small portions of a metal surface but causes a rapid change in metal thickness at these areas because of the accelerated corrosion rate within the cavities that are formed. Pits can produce early service failure because they may provide sites for crack initiation, may decrease the mechanical strength of a material, or may penetrate the metal wall and allow leakage of a contained gas or liquid. Thus, it is important to be able to determine the extent of pitting, either in a service application where it is necessary to predict the remaining life in a metal structure or in laboratory test programs that are used to select the most pitting resistant materials for service.

A number of different techniques have been used to measure and evaluate pitting corrosion. A recommended practice on this subject was prepared by a task group under ASTM Subcommittee G01.05 on Laboratory Corrosion Tests and was the basis for this review. (Much of the supple-

---

[1] Supervisory research chemist, Physical Chemistry Department, General Motors Research Laboratories, Warren, Mich. 48090.

mentary information from this review was used in a subsequent revision of the recommended practice to improve and to expand its content.)

Identification and Examination of Pits

Visual Methods

The initial examination of a corroded metal surface can provide useful information and should receive careful attention. The surface is examined visually under ordinary light, with or without the use of a low power magnifying glass. It is often advisable to photograph the corroded surface so that it may be compared with the clean surface after removal of corrosion products. If there is some doubt about the cause of pitting or the environmental exposure conditions, the corrosion products should be removed carefully following a recommended procedure, such as the National Association of Corrosion Engineers (NACE) Recommended Practice on Collection and Identification of Corrosion Products (RP-01-73). In some cases an analysis of pit sites before cleaning can be helpful in identifying the cause of pitting. An example of this is shown in Fig. 1 where the electron microprobe analysis of an aluminum surface shows a direct association between a pit site and the presence of a high concentration of iron particles. After the preliminary examination has been completed and sufficient corrosion products have been reserved for analysis, the remaining corrosion products should be removed by proper cleaning procedures, such as those given in ASTM Recommended Practice for Preparing, Cleaning, and Evaluating Corrosion Test Specimens (G 1-72).

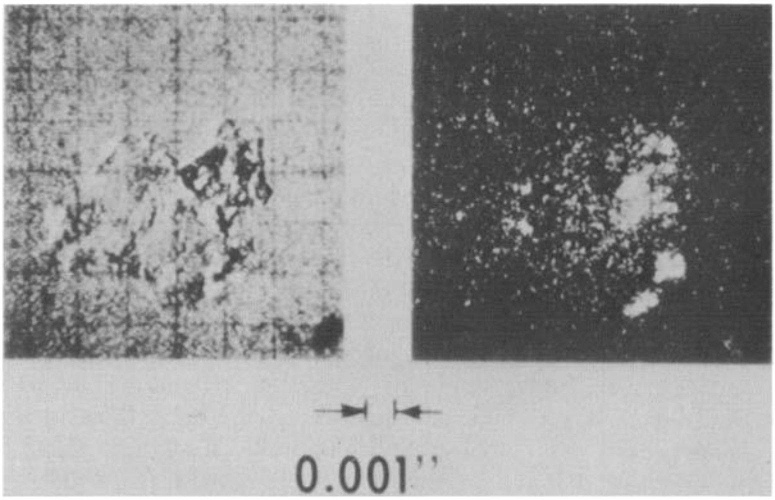

FIG. 1—*Electron microprobe analysis of a pit in aluminum. The high concentration of iron at the pit site is shown by light areas in the photograph on the right.*

The approximate size and distribution of pits are determined by visual examination, followed by a more critical and detailed examination through a microscope to determine the exact size, shape, and density of pits. The true shape and depth of a pit are not always evident from an examination of the surface because the pit cavity may have enlarged in a lateral direction beneath the surface (Fig. 2). If this should be the case, it is necessary to make a cross section of the specimen through the pit to determine its true shape and depth.

It is a tedious and time-consuming job to determine pit density, but the use of a plastic grid will be of some help. The grid, containing 3 to 6-mm (1/8 to 1/4-in.) squares, is placed on the metal surface. By counting and recording the pits in each square, one can readily determine a density. In addition, eye strain is minimized when this procedure is used because the eyes can be taken from the field of view without fear of relocating the area of interest.

If the relationship between pitting and microstructure is of interest, a portion of the specimen must be mounted metallographically and etched according to recommended procedures, such as those provided in ASTM Preparation of Metallographic Specimens (E 3-62). The etched specimen is

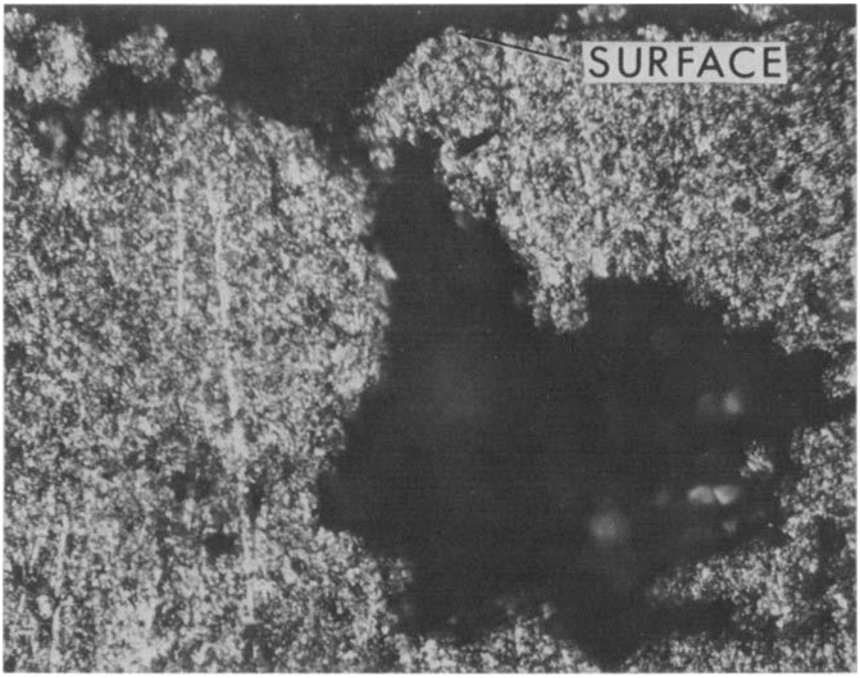

FIG. 2—*Cross section of a pit in aluminum showing the undercutting beneath the metal surface. The size and depth of the pit would not be evident from the surface,* ×*200.*

examined through the microscope to show the relationship between pits and microstructure.

Nondestructive Methods

There are a number of techniques that have been developed to assist in the detection of cracks or cavities in a metal surface without destroying the product [*1*].[2] These nondestructive methods are less useful than the visual methods previously discussed for the identification and evaluation of pits. but they merit attention because they can often be used *in situ.*

Radiographic—Radiation, such as X-rays, are passed through the object. The intensity of the emergent rays varies with the thickness of the material. Imperfections may be detected if they cause a change in the absorption of X-rays. Detectors or films are used to provide an image of interior imperfections. The technique is used for both ferrous and nonferrous castings. The metal thickness that can be inspected is dependent on the available energy output. Pores or pits must be at least as large as one-half percent of the metal thickness to be detected. The technique has only slight application to pitting evaluation, but it might be a useful means to compare specimens before and after corrosion to determine whether pitting has occurred and whether it is associated with previous porosity.

Electromagnetic—Eddy currents can be used to detect defects or irregularities in the structure of electrically conducting materials. When a specimen is exposed to a varying magnetic field, produced by connecting an alternating current to a coil, eddy currents are induced in the specimen; and they, in turn, produce a magnetic field of their own. Materials with defects will produce a magnetic field that is different from that of a reference material without defects; differences can be determined by the use of an appropriate detection instrument.

Another approach is the induction of a magnetic field in ferromagnetic materials. Discontinuities that are transverse to the direction of the magnetic field cause a leakage field to form above the surface of the part. Ferromagnetic particles are placed on the surface to detect the leakage field and to outline the size and shape of the discontinuities. Rather small imperfections can be detected in these materials by this method. However, the method has some limitations: the required directionality of defects to the magnetic field, the possible need for demagnitization of the material, and the limited shape of parts that can be examined.

Sonics—One approach is based on the use of ultrasonics. Pulses of sound energy are transmitted through a couplant, such as oil or water, onto the metal surface where waves are generated. The reflected echoes are converted to electrical signals that can be interpreted to show the location of flaws or pits. Both contact and immersion methods are used. The test has

---

[2] The italic numbers in brackets refer to the list of references appended to this paper.

good sensitivity and provides instantaneous information about the size and location of flaws. However, reference standards are required for comparison, and training is needed to properly interpret results.

In another method, acoustic emissions are used to detect flaws in metals. Imperfections, such as pits, generate high-frequency emissions under thermal or mechanical stress. The frequency of emission and the number of occurrences per unit time determine the presence of defects.

Penetrants—Defects opening to the surface can be detected by the application of a penetrating liquid that subsequently exudes from the surface after the excess penetrant has been removed. Defects are located by spraying the surface with a developer that reacts with a dye in the penetrant, or the penetrant may contain a fluorescent material that is viewed under black light. The size of the defect is shown by the intensity of the color and the rate of bleedout. This technique provides only an approximation of the depth and size of pits.

None of these nondestructive tests provide satisfactory detailed information about pitting. They may locate pits and offer some information about their size. But they generally are not able to distinguish small pits, and there can be confusion between the identification of pits and other surface blemishes. When more detailed information is required, it is necessary to use other methods of measurement.

Determination of the Extent of Pitting

Weight Loss

Metal weight loss is not very satisfactory as a measure of the extent of pitting unless the overall corrosion is small, and even in this case it provides no information about variations in depth of pitting. When uniform corrosion is significant, the contribution from pitting to the total weight loss is too small to provide meaningful information. However, there are several other methods that can be used to provide more precise pitting measurements, and weight loss data may aid in assessing the results from these measurements.

Pit Depth Measurements

Metallographic—The specimen is sectioned vertically through a preselected pit, and the cut surface is mounted metallographically and polished. The depth of the pit is measured by the use of a microscope with a calibrated eyepiece. A typical pit is shown in Fig. 3, and the depth can be seen to be 0.006 in. (0.152) mm). This method has several disadvantages: (*a*) it is time consuming, (*b*) it offers no assurance that the deepest pit has been selected, and (*c*) it is difficult to section the pit at the deepest point of penetration.

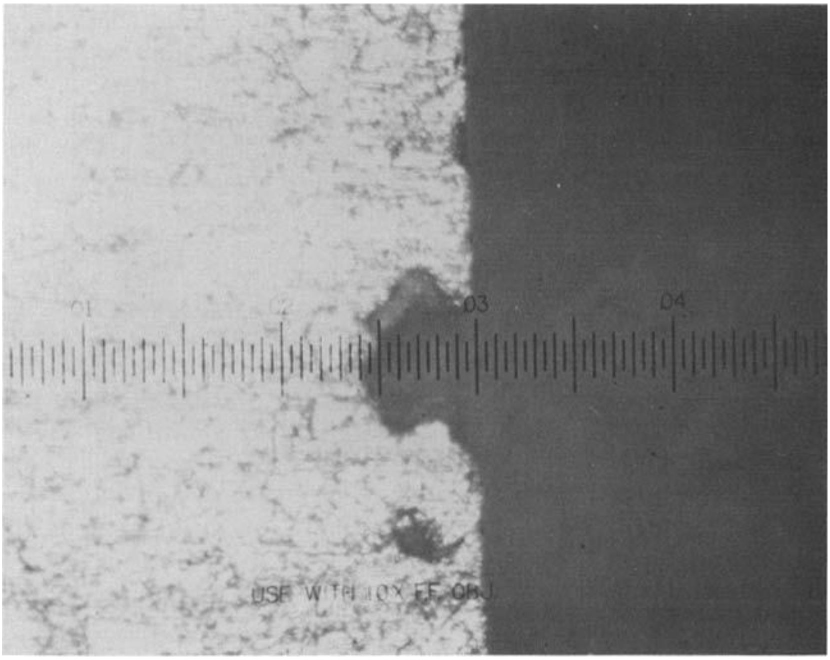

FIG. 3—*Cross section of a pit showing how a microscope with a micrometer reticle may be used to measure pit depth; one scale division = 0.0005 in. (13 μm), ×100.*

Machining—This method requires a specimen that is somewhat regular in shape, and it involves the destruction of the specimen [*2,3*]. An unaffected portion of the metal is selected to measure the original thickness. One side of the specimen is machined with a lathe until the last trace of a pit has disappeared. The thickness between the machined surface and an unaffected portion on the opposite side is measured and subtracted from the original thickness to give the depth of the deepest pit. The procedure is repeated on the unmachined side.

This procedure can also be used to determine the number of pits that reach specific depths. The surface is machined away in measured stages, and the visible pits are counted at each stage. The difference between the number of pits at any stage and the number at the previous stage gives the number of pits at each depth of cut.

Micrometer or Depth Gage—A pointed needle is attached to a micrometer or calibrated depth gage. The instrument is zeroed in on an unaffected area at the lip of the pit. The needle is inserted in the pit until it reaches the base where a new measurement is taken. The distance traveled by the needle is the depth of the pit. It is best to use a spring tension instrument to avoid excessive penetration of the metal by the needle. This method is only applicable to pits that are wide enough to allow the needle to penetrate the pit without obstruction.

In a variation of this method, the probe is attached to a spherometer and connected through a micrometer and battery to the specimen [*3*,*4*]. When the probe touches the bottom of the pit, the circuit is completed, and the depth of probe movement is a measure of pit depth. This method is limited to very regularly shaped pits because any contact with the side of the pit would give a false reading.

Microscopic—This method is valuable when pit openings are too narrow to allow penetration with a probe. However, it can only be used when the microscope can be focused on the base of the pit; this eliminates pits where undercutting has occurred.

A microscope with a magnification range in the order of 50 to 500 and a calibrated fine focusing knob (for example, 1 division = 0.001 mm) is required for this method. The pit is centered under the objective lens at low magnification, which is increased until the pit area, including the lip, fills most of the field of vision. The microscope is focused first on the lip of the pit and then on the base of the pit. The difference in the two recorded readings from the fine focusing knob is the depth of the pit. Repeatability of measurements improves with increasing magnification, as shown in Table 1. The method is limited to the depth of pits that are within the range of movement of the fine focusing knob on the microscope. This method is time consuming and fatiguing, particularly if many pits have to be measured. If specific pits are to be measured, it is often necessary to mark them with a stain before attempting to locate them under the microscope.

In a variation of this technique, the interference microscope is used [*5*]. In this method a beam of light is split so that one portion of the light is projected on the specimen and the other on a reference mirror surface. When the reflected light from the two surfaces is recombined, interference fringes are formed that provide a topographical map of the specimen surface. The fringes provide a measure of the vertical deviations on the metal surface.

Evaluation of Pitting Corrosion

Standard Charts

Some procedure is often needed to quantitatively describe or classify the extent of pitting. One such procedure is to rate the pits in terms of their density, size, and depth on the basis of standard charts, such as those used by Champion [*3*] and shown in a modified form in Fig. 4. Columns A and B relate to the extent of pitting at the surface of the metal (that is, Column A is a means for rating the number of sites per unit area, and Column B is a means for showing the average size of these sites). Column C rates the intensity or average depth of attack. A typical rating might be A-3, B-2,

TABLE 1—*Microscopic pit depth measurement of pit in Fig. 3.*

Magnification	Pit Depth, mm
65	0.183
	0.159
	0.179
	0.174 avg
132	0.159
	0.160
	0.155
	0.159
	0.159 avg
200	0.149
	0.157
	0.150
	0.153
	0.152 avg
370	0.151
	0.151
	0.151
	0.152
	0.151 avg

C-3, representing a density of 500 pits/dm^2, an average pit opening of 2.0 mm^2, and an average pit depth of 1.6 mm. This system offers a means of communication between those who are familiar with the standard charts, and it is a simple method for storing data for comparison with other test results. However, it does not show the full impact of pitting because it is concerned with averages. The determination of the average pit depth is not highly recommended because of the time involved in making measurements and the difficulty associated with measuring the depths of all pits.

Metal Penetration

The depths of the deepest pits are usually more significant than the average depth of all pits, particularly if a hole through the wall of a metal enclosure for a gas or liquid could lead to a loss of fluid. Therefore, metal penetration is often expressed in terms of the maximum pit depth or the average depth of several of the deepest pits. It is often advisable to use both methods because the maximum pit depth may indicate a greater severity of pitting than that shown by other pitting.

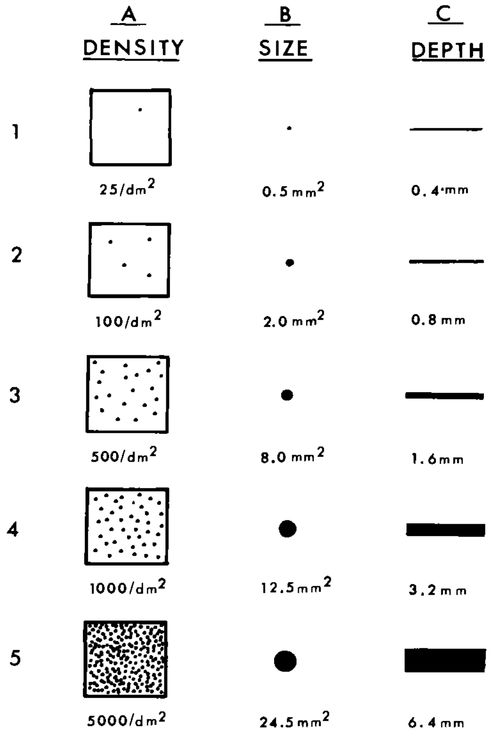

FIG. 4—*Charts for rating pits according to their density, size, and depth.*

Metal penetration may also be expressed in terms of a pitting factor. This is the ratio of the deepest metal penetration to the average metal penetration, determined from weight loss, as shown in the following relationship.

$$\text{pitting factor} = \frac{\text{deepest metal penetration}}{\text{average metal penetration}}$$

A pitting factor of one represents uniform corrosion; the larger the number, the greater is the depth of penetration.

Statistical

Pitting is usually divided into two stages, initiation and propagation. Many pits are stifled after initiation and fail to propagate, while others continue to propagate to varying depths. A pitting probability test can be conducted to determine the susceptibility of metals to pitting, but it will not provide information about the rate at which pits propagate. The pitting probability (*P*) after the exposure of a number of specimens to a particular set of conditions can be expressed in percent as follows (taken from Ref *6*)

$$P = \frac{N_p}{N} \times 100$$

where

N_p = number of specimens that pit, and
N = total number of specimens.

The pitting probability for a metal will vary with conditions of exposure, such as the corrosivity of the environment, the specimen area, and the length of exposure.

Aziz and Godard [*7*] demonstrated the importance of specimen area on the determination of aluminum pitting probability. In their experiment, large aluminum specimens were subdivided with wax into various rectangular areas. A drop of test solution was placed in each subdivision, which was kept wet by exposure to 100 percent relative humidity. The subdivisions showing any evidence of pitting were counted at the end of the test. The results showed that the probability of pitting increased with the area of metal exposed, and the probability of finding only one pit per subdivision was a maximum for an area of one square centimetre.

Several methods have been developed to show the relationship between pit depth and area or time of exposure. For example, Scott and others [*8–10*] found the following relationship between the maximum pit depth (d) and area (A) of a pipeline exposed to soil.

$$d = bA^a$$

In the equation a and b are constants that are obtained from the slope and the y-intercept of a straight line curve obtained by plotting the logarithms of the mean pit depths for successively increasing areas against the logarithms of the corresponding areas.

Godard [*6,11*] found that the maximum pit depth of aluminum exposed to various waters was a function of the cube root of time as expressed by the following relationship

$$d = Kt^{1/3}$$

where

d = maximum pit depth,
t = time, and
K = a constant that is a function of the composition of the water and alloy.

It was found that this relationship applied to several aluminum alloys exposed to different waters. One example is the pitting rate of 5052 aluminum alloy pipeline in Arvida, Quebec. When the maximum pit depths were plotted against the cube root of time, Pathak [*6*] found a straight line relationship, as shown in Fig. 5.

Summerson et al [*12*] used a statistical approach to analyze pit depth measurements on aluminum. By plotting the square root of the pit depth against frequency, a reasonable normal distribution was obtained. From these curves, the mean square root of the pit depth, the standard deviation, and the probability error could be determined. This approach required the measurement of many pits. But once it was established that a normal frequency distribution was a function of the square root of the pit depth, a sampling procedure could be developed that would allow the measurement of a smaller number of randomly selected pits to give a predetermined confidence level.

Extreme value probability statistics have been applied successfully to maximum pit depth data to estimate the maximum pit depth of a large area of material after examination of a small portion of that area [*3,6,11*]. Gumbel [*13*] is given credit for the original development of this method, but Aziz [*14*] simplified its use by plotting data on extreme value probability paper.

The procedure is to measure maximum pit depths on several replicate specimens that have pitted, and then arrange the pit depth values in order of increasing rank. A plotting position for each order of ranking is necessary, and this is obtained by substituting in the relationship

$$M/(n + 1)$$

where

M = order of ranking, and
n = total number of specimens or values.

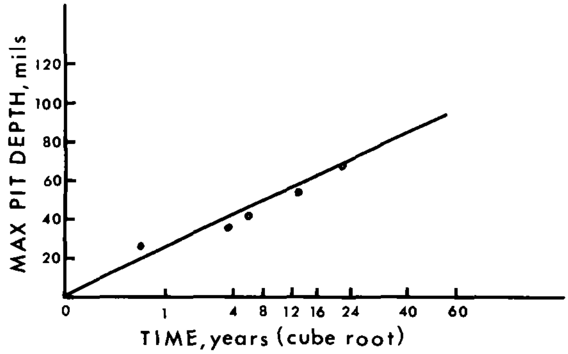

FIG. 5—*Pitting rate curve for 5052 aluminum alloy pipeline showing the relationship between maximum pit depths and the cube root of time* (*taken from Ref* 6).

For example, the plotting position for the second value out of 10 would be $2/(10 + 1) = 0.1818$. These values are plotted on the ordinate of extreme value probability paper versus their respective maximum pit depths. If a straight line is obtained, it shows that extreme value statistics apply. Extrapolation of the straight line can be used to determine the probability that a specific depth will occur or the number of observations that must be made to find a particular pit depth.

Figure 6 shows an example of how this approach was used by Pathak [6] to estimate the maximum pit depth of a 610-m (2000-ft) pipeline by the measurement of maximum pit depths on a segment of the line. The 13-year data are based on the determination of maximum pit depths for an 18-m (60-ft) length of pipe divided into 1-m (3-ft) sections. A smaller segment of the same pipeline was used for the 22-year data. By extrapolation of the lines to the point on the return period of the graph representing the entire length of the pipeline [666 for (*A*) and 1000 for (*B*)], the estimated maximum pit depth was 90 mils after 13 years and 99 mils after 22 years.

Loss in Mechanical Properties

The mechanical properties of a material may change because of pitting corrosion, and the amount of change may be used as a means for evaluating the degree of pitting. Typical properties that are often considered for this

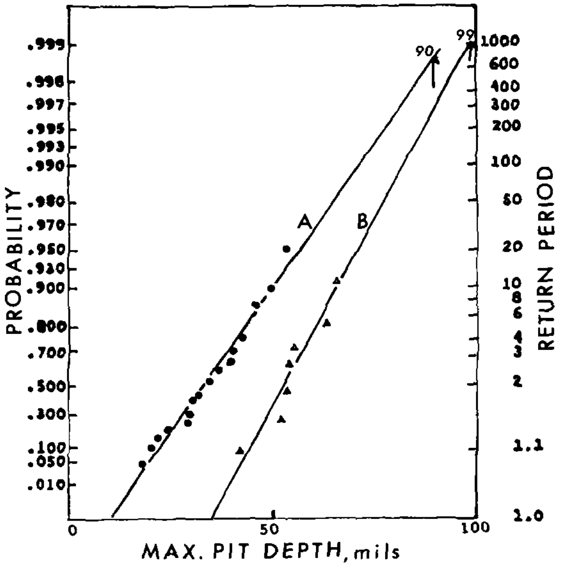

FIG. 6—*Straight line curves obtained when maximum pit depths from 5052 alloy pipeline are plotted on extreme probability paper. Curve A is based on data from the subdivision of an 18-m (60-ft) section after 13 years; Curve B is based on a 6-m (20-ft) section after 22 years (taken from Ref 6).*

purpose are tensile strength, elongation, fatigue strength, impact resistance, and burst pressure. The use of this method is often more suitable for other forms of localized corrosion, and it has had particular application to intergranular or stress corrosion. Summerson [*12*] found that the measurement of changes in tensile strength and elongation were not satisfactory for aluminum because the changes due to pitting were usually small. So this must be considered if these techniques are to be used.

The precautions that must be taken in the use of these procedures are well defined in most standard methods and need no further discussion here. What must be stressed is the importance of using as nearly replicate specimens as possible for both the exposed and unexposed specimens. This means consideration should be given to edge effects, direction of rolling, surface conditions, etc. Representative specimens of the metal are exposed to the same conditions except the corrosive environments. The mechanical property of the exposed and unexposed specimens is measured after the exposure, and the difference between the two results is because of corrosion. It may be difficult to separate the effects due to pitting and those from other forms of localized corrosion, but this must be determined by the investigator.

Baboian [*15*] measured the burst pressure of metal tubes to determine whether a subsurface layer of stainless steel would decrease the depth of pitting through terne-coated steel. This was a reasonable approach because burst strength is dependent on metal thickness, and a reduction in thickness at even a small area will affect pressure retention. The change in burst strength was determined with time on successive specimens exposed to salt spray, and it was found that the stainless steel caused a reduction in the depth of pitting.

Summary

1. Metal surfaces are examined visually and under low magnification to identify pits and to determine their number.
2. Nondestructive methods can be used to locate pits, although other metal defects may interfere. There is a limit to the size of pit that can be detected.
3. Metal weight loss alone is not a satisfactory procedure for the determination of the extent of pitting.
4. Pit depths can be determined by the following techniques: (*a*) microscopic measurement of a cross-sectioned pit that has been mounted metallographically, (*b*) determination of the difference in metal thickness before and after machining a specimen to the bottom of a pit, and (*c*) measurement of a pit depth by the use of a micrometer, pit depth gage, or a microscope that has a graduated focusing knob.
5. Standard charts can be used to describe the degree of pitting in terms of density, size, and depth of pits.

6. The measurement of the maximum pit depth or the average of a number of the deepest pits is often a more meaningful way to show the extent of pitting.

7. Statistical methods can be used to show the probability of pitting occurring, to show the relationship between pit depth and time of exposure, and to estimate the maximum pit depth on the basis of an examination of a portion of the exposed metal surface.

8. The change in a particular mechanical property of a metal can be used to show the effect of pitting under some conditions, but this approach is often more applicable to other forms of localized corrosion.

Acknowledgments

The author is indebted to R. L. Chance and M. S. Walker for their helpful suggestions during the preparation of this paper.

References

[*1*] Mock, J. A., *Materials Engineering*, Vol. 69, June 1969, p. 60.
[*2*] Bengough, G. D. and Wormwell, F., *Journal of the Iron and Steel Institute*, Vol. 3, 1935, p. 168.
[*3*] Champion, F. A. in *Corrosion Testing Procedures*, 2nd ed., Wiley, New York, 1965, p. 205.
[*4*] Thornhill, R. S., *Journal of the Iron and Steel Institute*, Vol. 146, 1942, p. 90P.
[*5*] Saur, R. L., *Plating*, Vol. 52, July 1965, p. 663.
[*6*] Pathak, B. R. in *Handbook on Corrosion Testing and Evaluation*, W. H. Ailor, Ed., Wiley, New York, 1971, p. 553.
[*7*] Aziz, P. M. and Godard, H. P., *Journal of the Electrochemical Society*, Vol. 102, Oct. 1955, p. 577.
[*8*] Scott, G. N., *Proceedings*, American Petroleum Institute, Vol. 14, 1934, p. 204.
[*9*] Romanoff, M., "Underground Corrosion," Circular 579, National Bureau of Standards, U. S. Government Printing Office, Washington, D. C., 1957, p. 71.
[*10*] Denison, I. A. in *Corrosion Handbook*, H. H. Uhlig, Ed., Wiley, New York, 1948, p. 1048.
[*11*] Godard, H. P., *Canadian Journal of Chemical Engineering*, Vol. 38, Oct. 1960, p. 1671.
[*12*] Summerson, T. J., Pryor, M. J., Keir, D. S., and Hogan, R. J. in *Metals*, *ASTM STP 196*, American Society for Testing and Materials, 1957, p. 157.
[*13*] Gumbel, E. J., "Statistical Theory of Extreme Values and Some Practical Applications," Series 33, U. S. Department of Commerce Applied Mathematics, Washington, D. C., 1954.
[*14*] Aziz, P. M., *Corrosion*, Vol. 12, Oct. 1956, p. 495t.
[*15*] Baboian, R., "Corrosion-Resistant, High-Strength Clad Metal System for Hydraulic Brake Line Tubing," Preprint 720290, Society of Automotive Engineers, Detroit, Mich., 1972.

D. L. Crews[1]

Interpretation of Pitting Corrosion Data from Statistical Prediction Interval Calculations

REFERENCE: Crews, D. L., "**Interpretation of Pitting Corrosion Data from Statistical Prediction Interval Calculations,**" *Galvanic and Pitting Corrosion—Field and Laboratory Studies, ASTM STP 576*, American Society for Testing and Materials, 1976, pp. 217–230.

ABSTRACT: The National Bureau of Standards data for pitting corrosion of ductile iron and steel pipe in four soils and gray cast iron and 3-in. Bessemer steel pipe in one soil have been treated by statistical methods to obtain the prediction intervals of estimated pit depths as a function of time. In the nonaggressive soils which are representative of most pipe installations, these ductile iron and gray iron pipe exhibited less corrosion than the companion steel pipe.

Prediction interval calculations are useful for quantitative analysis of corrosion data which has considerable inherent scatter and where service life is determined by the failure at relatively few points.

KEY WORDS: corrosion, pitting, statistical analysis, nodular iron, gray iron, steels

Corrosive attack on buried ferrous materials is characterized by pitting; total attack, as measured by weight loss, may be moderate in specimens in which severe pitting has developed.

In underground pipes conveying liquids or gases, the termination of service life by corrosive attack is characterized by pits which have perforated the pipe wall. At the time of failure, the overall decrease in bursting strength or loss in weight may be minimal. It is obvious then that the evaluation of corrosive attack or determination of service life under such circumstances must be based on measurements of pit depth.

In representative conditions of actual service, corrosion proceeds quite slowly; service life usually exceeds the professional life span of an individual observer. Accelerated tests which utilize highly corrosive environments or aggressive soils are of questionable validity. Extrapolation of pit depth measurements therefore becomes an essential part of an evaluation

---

[1] Research consultant, Clow Corporation, Coshocton, Ohio 43812.

of pipe materials or environments or both which seeks to represent actual service conditions.

The method of statistical treatment of the data should be carefully chosen to avoid errors in interpretation. A method which provides a calculation of the distribution of pit depths for extrapolated periods of exposure, rather than an average pit depth, includes the element of probability.

The technique of measuring pitting attack consists of exhuming specimens which have been buried in selected environments and measuring the penetration of the pits into the metallic material. Since the products of corrosion cannot escape, they accumulate on the exposed surface; hence, it is necessary to completely clean the specimens before it is possible to make measurements of pit depth. Obviously, a specimen which has been measured cannot be returned to the environment for further exposure. An adequate number of specimens must be buried initially, then a selected number are exhumed at intervals of time.

It is a characteristic of underground pitting corrosion that a wide range of pit depths exists at any moment in time. Any particular specimen of practical size can contain only a small fraction of the total population of all pits or even the deepest pits. It has been a practice in evaluating specimens to measure only a selected number of the deepest pits, since such pits eventually produce failure. This small sample size, compared to the population, accounts for the observed result that the data from a series of pit depth measurements over a period of time exhibit considerable dispersion and apparent anomalies; some increments of time result in a decrease in the measure pit depth.

Due to this statistical scatter, interpretation of pitting corrosion is difficult. Most commonly, the position of different materials or environments are merely placed in rank; no quantitative interpretation of the data is attempted, either as to relative attack at any point in time or a projection of expected service life.

Data Treated

The most extensive tests of underground corrosion have been conducted by the National Bureau of Standards (NBS).[2] These tests were initiated in 1922; the most recently reported data are those of ductile iron pipe and carbon steel pipe, which had completed 8 years exposure in 1966.[3] The maximum exposure in the earlier NBS tests is reported as 18 years. By comparison, the service life of cast iron pipe is expected to be in excess of

---

[2] See National Bureau of Standards Circulars 450 and 579.

[3] Romanoff, Melvin, *Journal of the American Water Works Association*, Vol. 60, 1968, pp. 645–655.

100 years. The recent tests provided data for four exposure periods (1, 2, 4, and 8 years); the earlier data provided, typically, six exposure periods. The data of the recent series consist of the average of the deepest pits measured on four 12-in.-long specimens; only 5 of the 6 test sites survived for 8 years; two of these 5 exhibited instances of perforation of the pipe wall, so that some bias exists in the data. All of the published data of the NBS tests identify the data as "an average of the maximum pit depths of four specimens." Table 1 reproduces the data reported for the recent series of tests.

Calculation of the regressions relationship between pit depth and time can be made from a series of test values using the accepted exponential equation and utilizing the logarithms of the variables to obtain a straight line. However, a regression value is merely an estimate of the central tendency; half of the population values are expected to fall below the regression value and half above.

More relevant is an estimate of the distribution of the pits in the population. The scatter of the measured data about the regression is an expression of the width of the distribution band; the greater the deviation of the data values from the regression relationship, the wider is the distribution band of the population values.

The distribution of the population is termed, in statistical inference, the prediction interval; this is in distinction to the confidence limits. Of the total prediction interval, the deepest pits are the ones which are relevant to estimates of longevity.

Manual statistical calculations are particularly laborious, which may be the reason that they have been used so infrequently in the analysis of pitting corrosion data, despite the demonstrable need. That difficulty has been removed by the development of computers and prepared computer programs which can make the required calculations with a feasible investment of time and effort. Compared to the effort required to produce the original tests data, the effort of the calculation becomes minimal.

Prediction Intervals

The statistical treatment in this paper utilizes a prepared computer program which provides calculated values of both the regression and the distribution, expressed as prediction intervals, of pit depths for times both within the exposure period of the test and extrapolated exposure times. Specifically, the values were calculated for times of 4, 7, 10, 20, 40, 70, 100, and 400 years. The data were entered as the logarithms of the experimental values. Since the computer program provided the normal distribution, the resulting distribution is log-normal. The extreme-value distribution is believed to provide the most accurate representation of pit depth but the log-normal distribution is similarly skewed and is judged by the writer to

TABLE 1—*Average*[a] *loss in weight and maximum pit depth of carbon steel and ductile cast iron in different soils.*

	Soil			Carbon Steel		Ductile Iron	
	Type	Location	Exposure Time, years	Weight Loss, oz/ft²	Maximum Pit Depth, mil	Weight Loss, oz/ft²	Maximum Pit Depth[b], mil
A	Sagemoor sandy loam	Toppenish, Wash.	1.0	0.9	39	0.3	45
			2.0	2.5	66	1.7	66
			4.0	3.0	55	1.1	60
			8.0	4.4	71	1.4	102[b]
B	Hagerstown loam	Loch Raven, Md.	1.0	0.9	18	1.3	49
			2.1	1.5	20	2.0	68
			4.1	2.2	53	2.2	81
			8.1	3.4	60	3.1	97
C	clay	Cape May, N. J.	1.0	1.0	12	2.4	61
			2.0	3.3	12	4.7	108
			5.0	7.6	30	5.9	114[b]
			8.0	42.7	121[b]	13.8[c]	231[b]
D	Lakewood sand	Wildwood, N. J.	1.0	1.4	19	0.7	50
			2.0	1.8	33	1.4	44
			4.0	2.6	54	2.1	43
			8.0	4.0	45	2.3	52
E	coastal sand	Wildwood, N. J.	1.0	0.3	13	1.8	35
			2.0	0.6	8	3.8	49
G	tidal marsh	Patuxent, Md.	0.9	1.1	12	2.7	63
			1.8	2.0	14	3.4	56
			3.9	34.3	136[b]	10.3	142[b]
			7.8	40.0	128[b]	17.6	190[b]

[a] Average of four specimens.

[b] One or more specimens perforated by corrosion.
Pipe wall thickness: carbon steel, 145 mil; ductile iron, 250 mil.

[c] Average of three specimens; one specimen not recovered.

approximate the extreme-value distribution of the interval used for this interpretation of the data and the estimate of service life.

As an illustration of the proposed statistical procedure, the prediction interval was calculated for the NBS data of ductile iron and steel pipe exposed concurrently in four test sites representing a range of corrosivity from very mild to extremely aggressive soils (300 to 30 000 Ω/cm resistivity); the prediction intervals chosen were 50, 80, 90, 95, and 99 percent. The results of the calculation are shown in graphical form in Figs. 1 through 8, with the omission of the 99 percent interval and, in the case of Figs. 7 and 8, the omission of the lower limits, which are redundant for estimates of service life. The regression line is marked "0".

The interpretation of the prediction interval is that the indicated fraction of the population pit depths lies between the limits shown. For example, 90 percent of the deepest pits lie between the upper and lower 90 percent lines and 5 percent lie above the upper 90 percent prediction line.

The wall thickness of the specimens is also shown in these figures. As a practical index of service life, whose magnitude corresponds in general to actual experience, the upper 90 percent line was chosen for purposes of interpretation. Figures 9 through 12 show the upper 90 percent line of the two materials, carbon steel and ductile iron, for four soil environments.

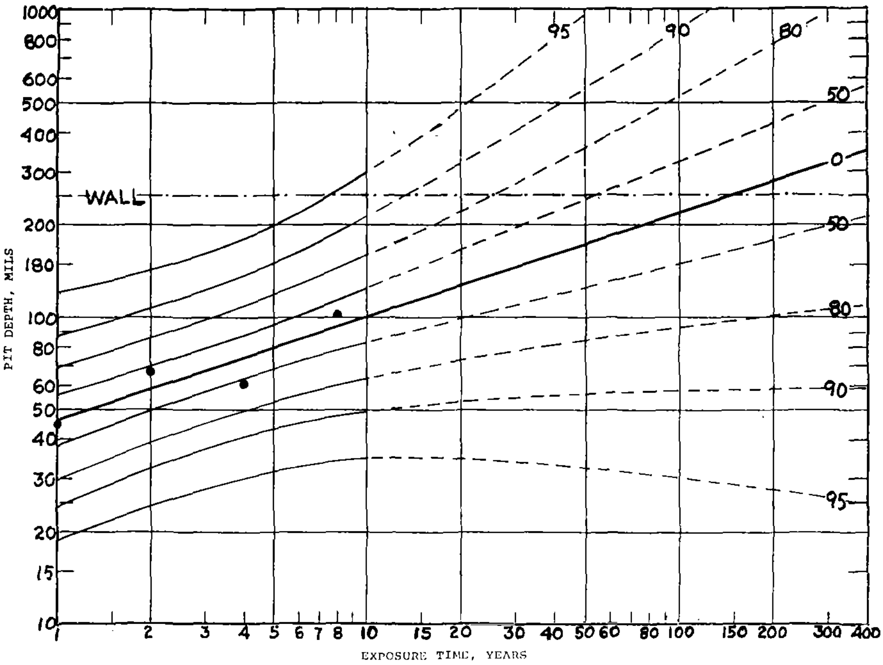

FIG. 1—*Ductile iron pipe, Site A; prediction intervals of pit depth versus exposure time.*

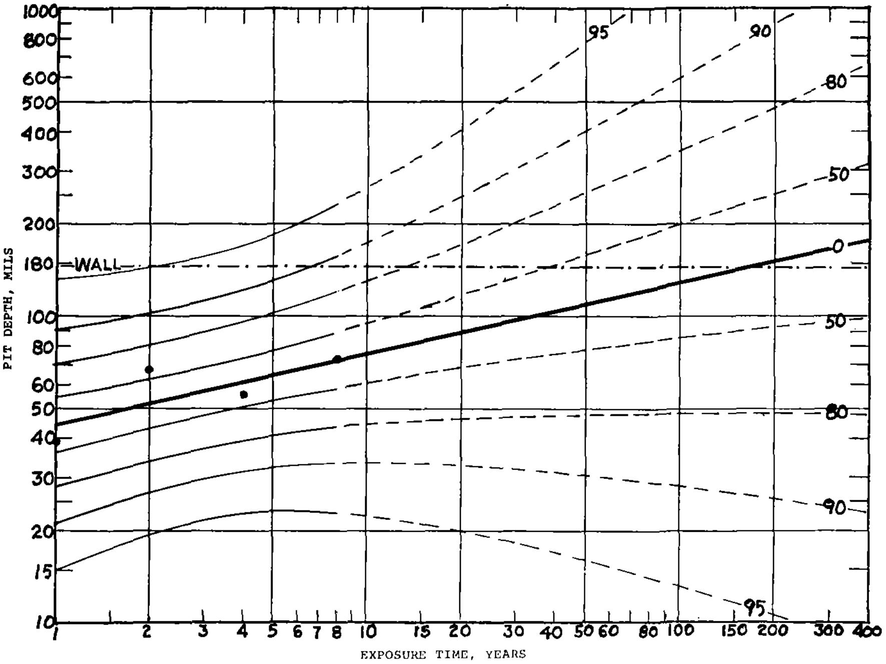

FIG. 2—*Steel pipe, Site A; prediction intervals of pit depth versus exposure time.*

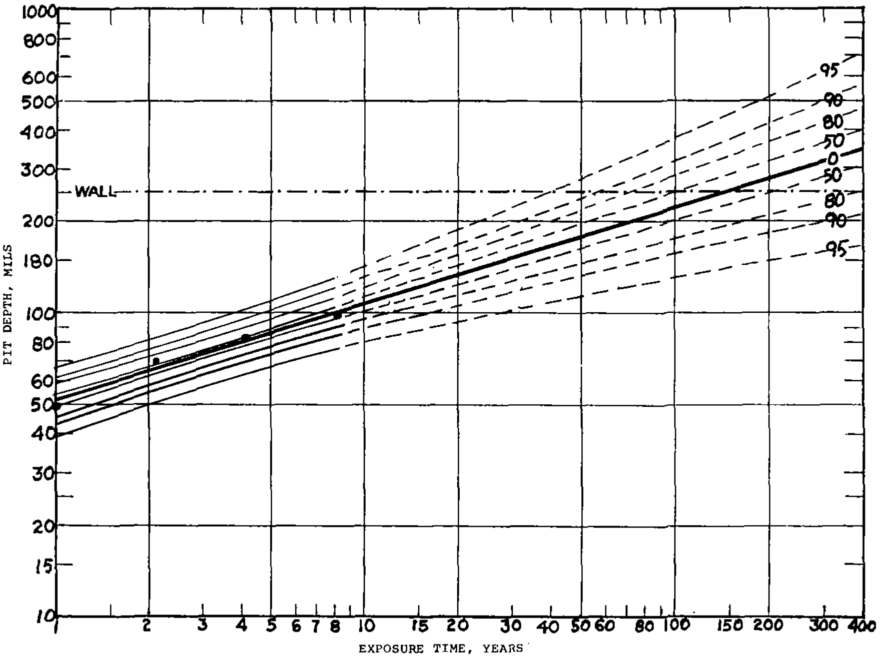

FIG. 3—*Ductile iron pipe, Site B; prediction intervals of pit depth versus exposure time.*

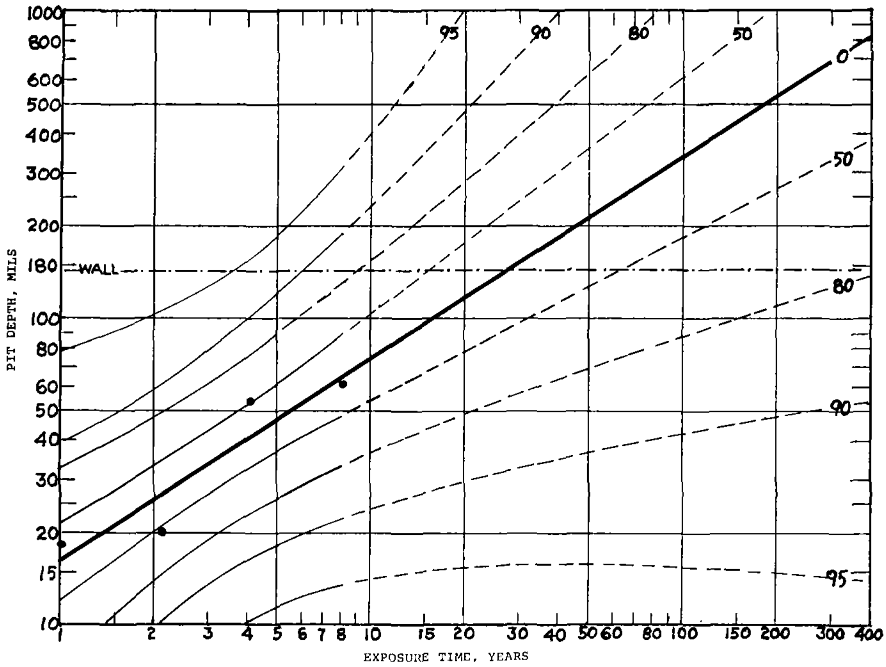

FIG. 4—*Steel pipe, Site B; prediction intervals of pit depth versus exposure time.*

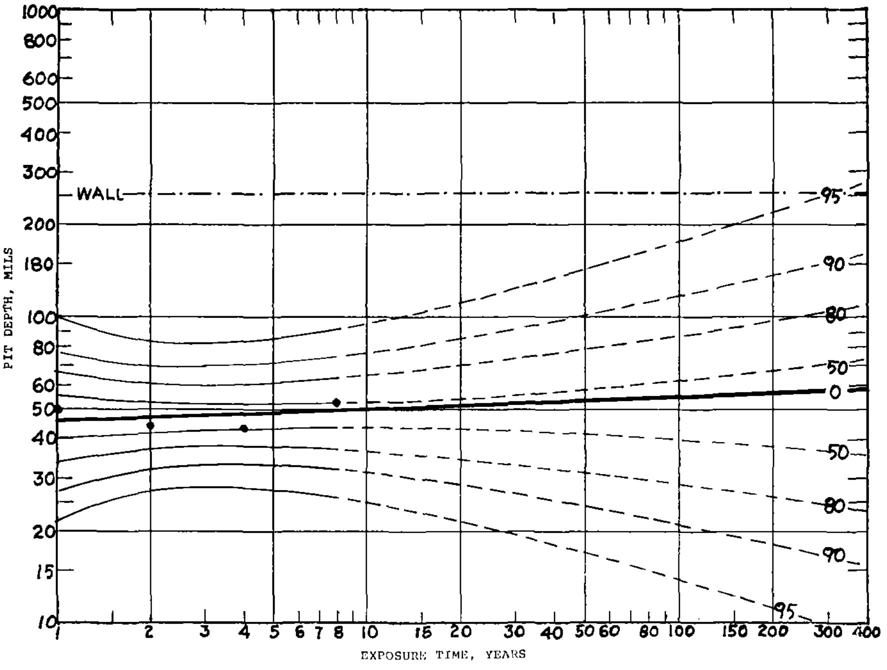

FIG. 5—*Ductile iron pipe, Site D; prediction intervals of pit depth versus exposure time.*

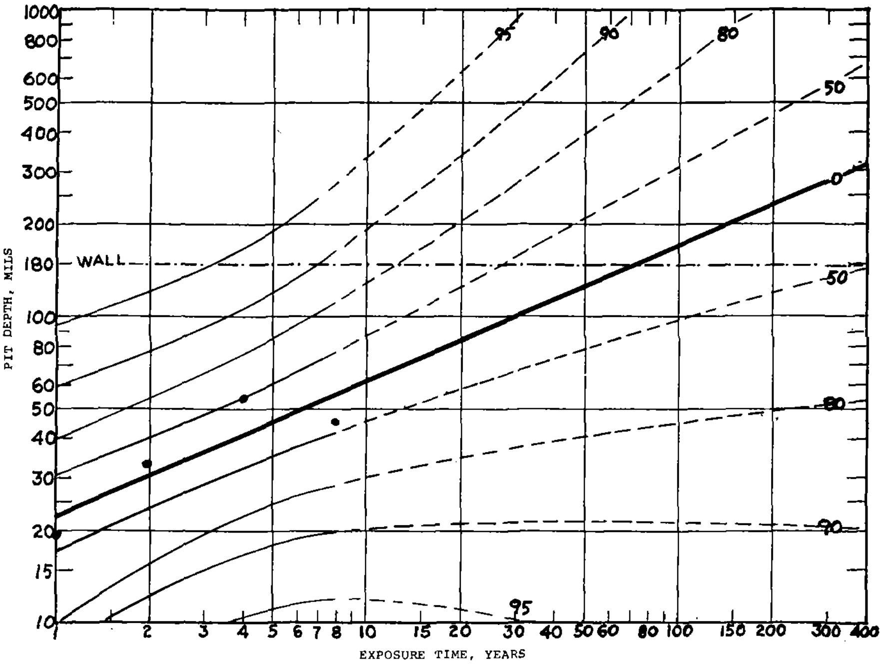

FIG. 6—*Steel pipe, Site D; prediction intervals of pit depth versus exposure time.*

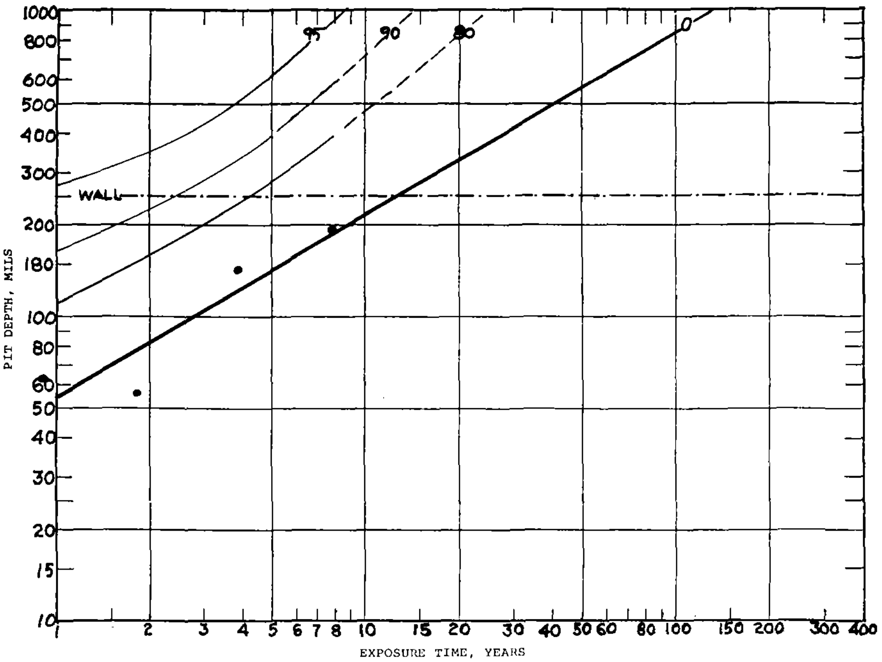

FIG. 7—*Ductile iron pipe, Site G, prediction intervals (upper limit only) of pit depth versus time.*

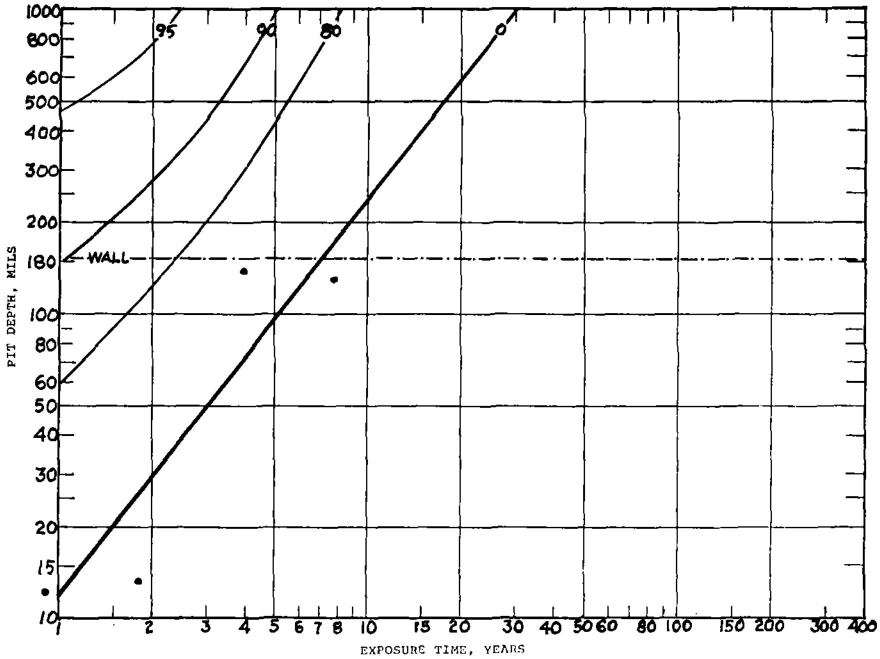

FIG. 8—*Steel pipe, Site G; prediction intervals (upper limit only) of pit depth versus time.*

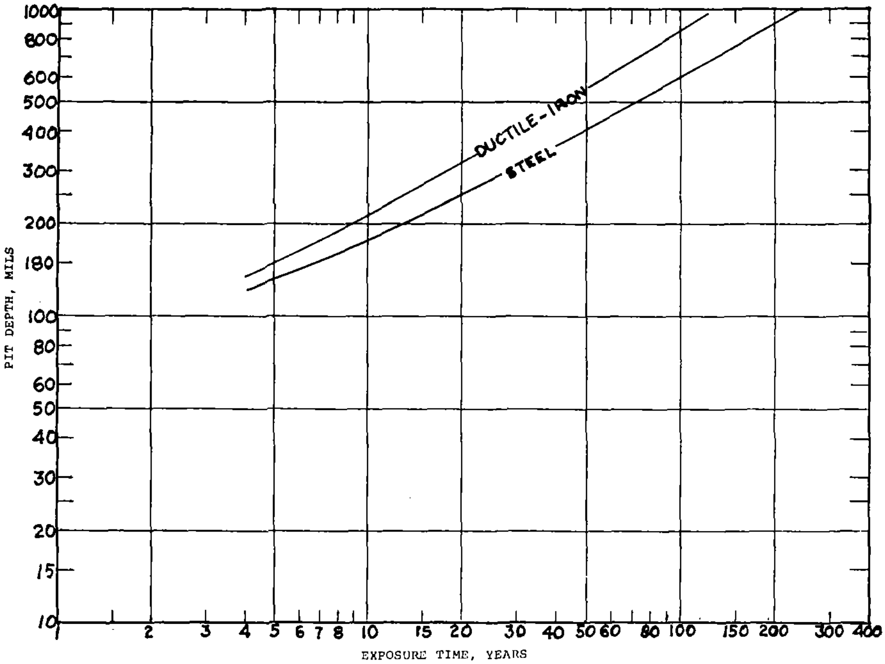

FIG. 9—*Five percent of the deepest pits (the upper 90 percent prediction interval line) of ductile iron and steel pipe, Site A.*

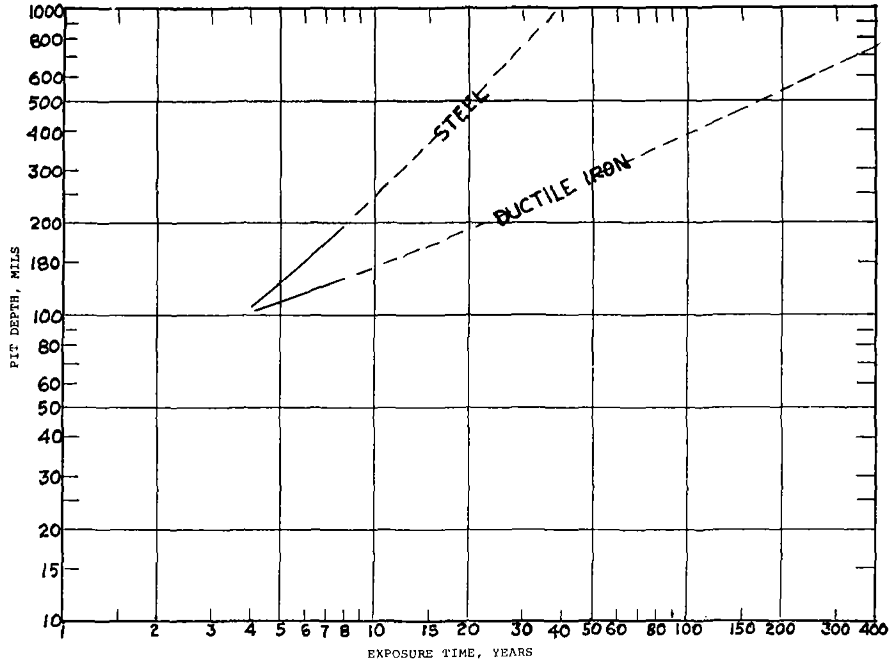

FIG. 10—*Five percent of the deepest pits (the upper 90 percent prediction interval line) of ductile iron steel pipe, Site B.*

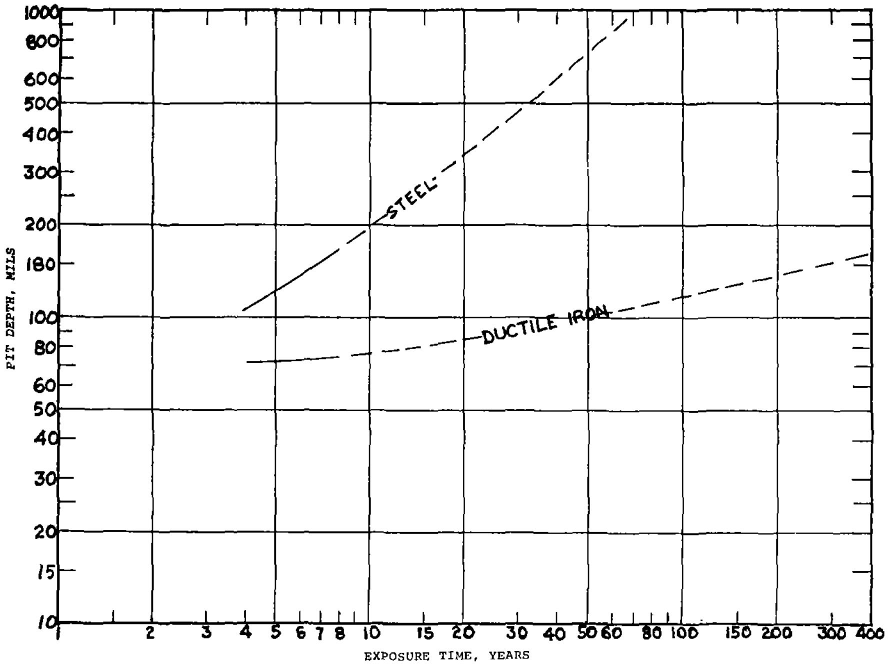

FIG. 11—*Five percent of the deepest pits (the upper 90 percent prediction interval line) of ductile iron and steel pipe, Site D.*

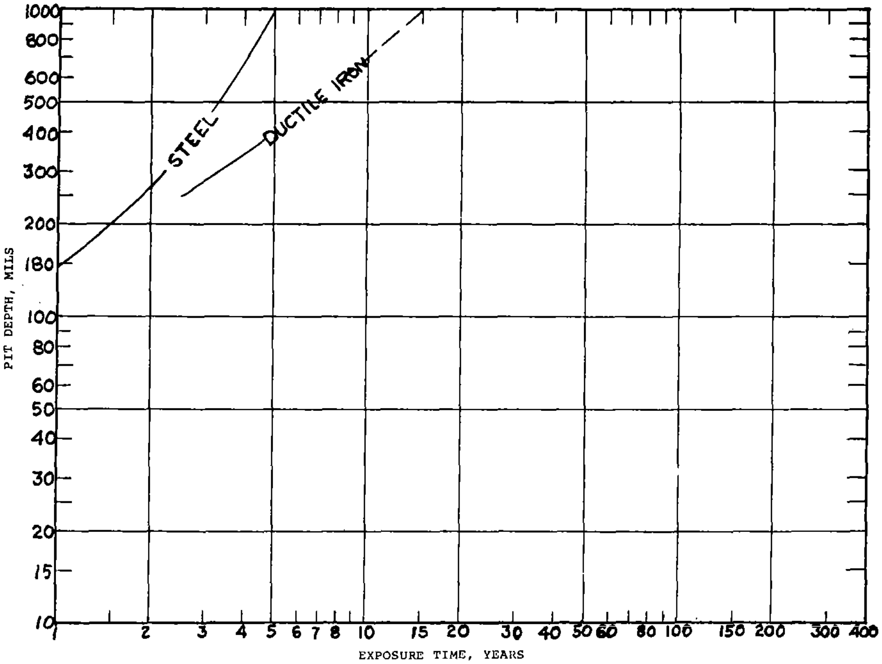

FIG. 12—*Five percent of the deepest pits (the upper 90 percent prediction interval line) of ductile iron and steel pipe, Site G.*

Estimation of Service Life

From these upper 90 percent lines, estimates of service life and rates of corrosion can be made which have the same magnitude as service experience. Numerical values are shown in Table 2, in which service life is expressed in years for 5 percent of the deepest pits to perforate the pipe wall. Pitting corrosion rate provides a comparison which eliminates the effect of the differences in wall thickness of the two materials, ductile iron and steel (0.25 in. for ductile iron pipe and 0.145 for steel pipe) and can be expressed as exposure in years for 5 percent of the measured pits to be equal to or greater than some specified depth; for this tabulation 0.25 and 0.50 in. were chosen.

The absolute values of longevity and corrosion rate in some of the NBS tests, as they relate to service conditions generally, may be open to question; soils of 300 or 400 Ω/cm do not represent realistic service conditions (in practice, pipe in such soils, which are infrequently encountered, would be provided with some type of external protection, such as coating or wrapping). However, relative longevity may be useful since the materials which were tested concurrently have experienced the same environmental circumstances. Soils A and G are examples of highly aggressive soils which might

TABLE 2—*Estimated service life and pitting corrosion rate of carbon steel, ductile iron, and gray cast iron in different soils.*

		Service Life	Pitting Corrosion Rate	
Site	Material	Years to 5% Perforation	Years to 5% at 0.25 in. Depth	Years to 5% at 0.50 in. Depth
A, Sagemoor loam	ductile	14	14	43
400 Ω/cm, 8.8 pH	steel	6½	21	74
B, Hagerstown loam	ductile	52	52	300
5 200 Ω/cm, 5.8 pH	steel	6	10½	21
D, Lakewood sand	ductile	2 500	2 500	10 000
30 000 Ω/cm, 7.3 pH	steel	7	14	33
G, Tidal, marsh	ductile[a]	2½	2½	6½
300 Ω/cm, 7.1 pH	steel[a]	1	1.9	3¼
11, Hagerstown loam	gray cast iron metal mold	1 000	350	2 000
11 000 Ω/cm, 5.3 pH	Bessemer steel 3-in. pipe	26	37	140

[a] Biased data

be employed to provide accelerated testing but which do not actually yield estimates of representative service life.

In Soil B, which may be considered representative of soils encountered in normal practice, the relative status of ductile iron versus carbon steel in these tests falls within a range of about 5 to 15 for rate of corrosion and about 8 for longevity, ductile iron pipe being the more resistant to corrosion.

A major deficiency in the recent NBS series is the omission of gray iron pipe, which has been the principal underground piping material for several centuries. A comparison of the expected service life of ductile iron with gray cast iron is of major practical importance; no direct comparison is possible from NBS data, since concurrent testing of these two materials was not conducted.

The NBS reports data in Hagerstown loam for gray cast iron produced in a metal mold and Bessemer steel pipe (see footnote 2). The prediction intervals for these two materials are shown graphically in Figs. 13 and 14 and the upper lines alone in Fig. 15. The ratio of the rates of corrosion, as shown in Table 2, fall within a range of about 10 to 15, gray cast iron being the more resistant.

Summary

The statistical treatment of pitting corrosion data which calculates the prediction intervals of pit depth for exposure periods greater than the test

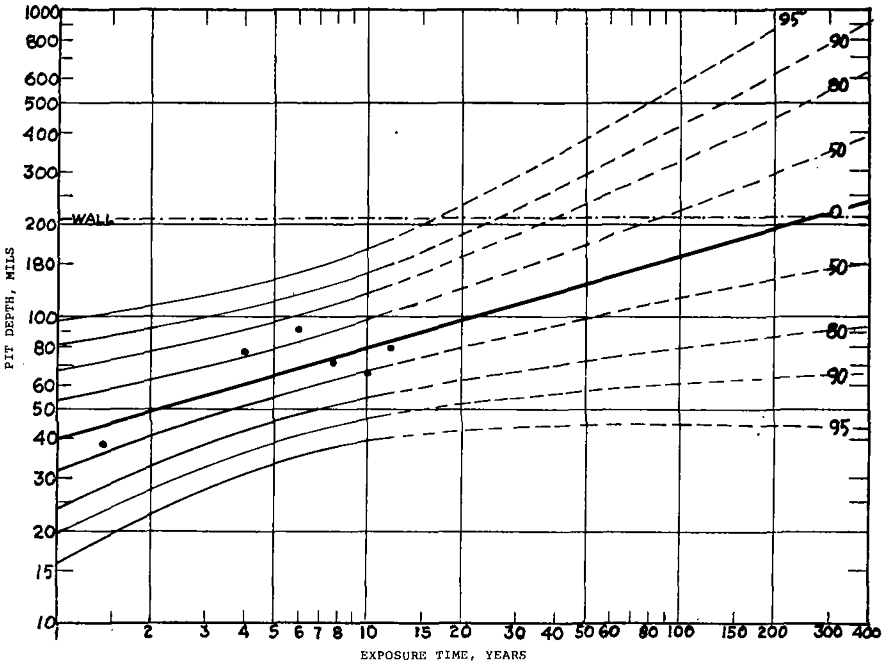

FIG. 13—*Bessemer steel pipe (3-in. pipe), Site 11, prediction intervals of pit depth versus time.*

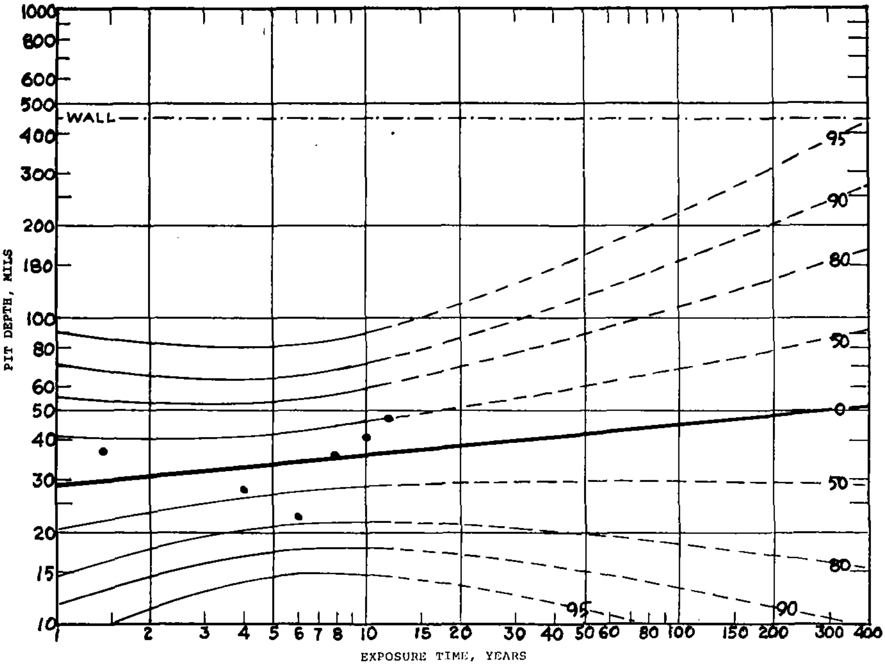

FIG. 14—*Gray cast iron pipe (metal molds), Site 11, prediction intervals of pit depth versus time.*

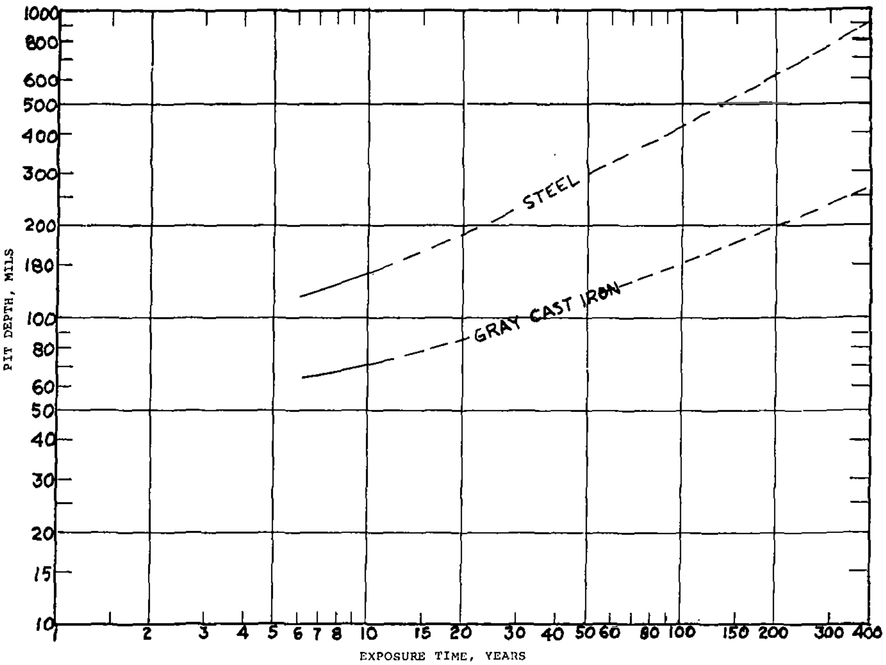

FIG. 15—*Five percent of the deepest pits (the upper 90 percent prediction interval line) of gray cast iron and 3-in. Bessemer steel pipe, Site 11*

periods is proposed as a means for obtaining quantitative estimates of service life or corrosion rate in normally encountered environments; adequate statistical interpretation has been notably absent in the past. The examples of longevity which are contained herein are relevant to commercially important underground piping materials.

D. B. Anderson[1]

Statistical Aspects of Crevice Corrosion in Seawater

REFERENCE: Anderson, D. B., "**Statistical Aspects of Crevice Corrosion in Seawater,**" *Galvanic and Pitting Corrosion—Field and Laboratory Studies, ASTM STP 576*, American Society for Testing and Materials, 1976, pp. 231–242.

ABSTRACT: The natural variability in incidence and severity of oxygen concentration cell crevice corrosion in seawater systems has been shown to follow prescribed statistical patterns. These considerations have been used to develop a viable multiple crevice test method for assessing comparative alloy capabilities and for isolating specific geometrical and environmental effects. Test data developed by this method have also provided interesting insight into the corrosion mechanisms involved.

KEY WORDS: corrosion, concentration cell corrosion, pitting, seawater corrosion, corrosion tests, stainless steels, nickel alloys

Crevice corrosion is generally recognized as the limiting corrosion phenomenon in seawater systems determining serviceability of stainless steels and a variety of other commonly used marine materials which exhibit marked susceptibility to localized corrosion induced by either oxygen or metal-ion concentration cells. Crevices can be built in from gaskets, O-rings, lap seams, etc. or can develop in service from sediments, fouling, etc.

Unfortunately, the severity of attack often defies prediction ranging from no apparent attack to superficial etching to catastrophic failure. The inherent variability in both occurrence and intensity of attack, plus the frequency with which seawater crevice corrosion test data reflect the particulars of the evaluation method, compound the problem of trying to accurately assess the merits and capabilities of candidate materials for a specific application without resorting to unduly complex evaluations.

Consistent trends indicative of comparative alloy capabilities (for example, Type 316 stainless steel is generally considered more resistant to

---

[1] Project manager, The International Nickel Company, Incorporated, New York, N. Y. 10004.

crevice corrosion than Type 304) can be derived from critical comparisons of data from a variety of sources and from tests involving extended exposures of a reasonable number of specimens and specimen configurations. However, comparisons based on limited data or data developed for different alloys using different test methods are all too often inconclusive or misleading.

Development of Statistical Test Method

Attempts to introduce a "standard" crevice capable of providing consistent and reproducible data for seawater corrosion studies have been notably unsuccessful. The variability observed suggests the potential usefulness of a cumbersome statistical approach involving exposures of large numbers of specimens with varying exposure periods. The use of a reduced number of specimens, each exposed with a large number of duplicate crevices, has been evaluated as a reasonable alternative.

Several criteria were considered of primary importance in the development of a viable test method using the multiple crevice approach.

1. The required test period must be reasonably short, both to salve researcher anxiety and to reduce conflicting interactions due to fouling attachments, seasonal temperature variations, etc.
2. The test method must be capable of clearly demonstrating recognized differences in alloy capabilities (that is, properly rank Types 304 and 316 stainless steel).
3. The test method must be capable of providing a clear assessment of the merits of highly corrosion-resistant alloys for use in critical applications requiring corrosion immunity.
4. The test method must be adaptable to specimens of various thicknesses, shapes, and surface conditions and not entail modification or destruction of "as-received" surfaces.
5. The test should not require electrochemical stimulation or chemical alteration of the environment.

The basic test method which evolved exposes flat panel specimens with multiple crevices formed by two grooved acetal resin washers as shown in Fig. 1. A 4 by 6 in. (10 by 15 cm) specimen size was selected out of convenience. Subsequent tests, described as follows, showed important effects which can be studied by introducing specimen size as a controlled variable. A typical grooved washer is shown in Fig. 2. Each washer has 20 grooves and plateaus, providing 40 crevices per specimen. Grooves are typically 0.020 in. (0.5 mm) deep and 0.040 in. (1.0 mm) wide, but these dimensions are not critical variables except to provide a minimum creviced/exposed surface area ratio of at least 1:10 to assure sufficient cathode area to

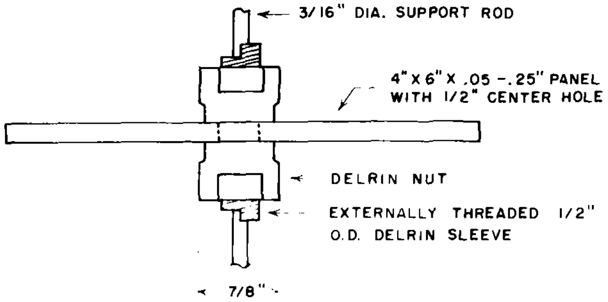

FIG. 1—*Multiple crevice test assembly.*

prevent interference between crevices. The selection of the washer material was based on the attractive combination of mechanical properties and dimensional stability in seawater. Other nonmetallics with similar properties should be equally suitable.

Specimens are prepared by degreasing and pickling using pickling solutions appropriate for the materials involved. Generally, three specimens of each alloy are provided to produce a good statistical base of 120 crevices per alloy. Specimens are exposed vertically (to reduce silting) in a wooden flume where gravity flow of fresh, well aerated seawater produces a constant velocity of 2 ft/s. Exposure periods vary, depending upon the relative corrosion resistance of the materials being evaluated. For most stainless steel alloys, the optimum exposure period has generally been found to be one to three months.

Analyses of the particular alloys used in these investigations are given in Tables 1 and 2.

TABLE 1—*Alloy compositions.*

	%					
Alloy	Fe	Ni	Cr	Mo	Cu	Other
Type 304 stainless steel	68	10	19	...	...	...
Type 316 stainless steel	65	12	17	2.5	...	...
6X	48	24	20	6.5	...	...
Incoloy alloy 825	30	42	22	3	2	...
Inconel alloy 625	3	61	22	9	...	Cb, Ta
Hastelloy alloy C	5	56	15	16	...	W, Co
65:35 Ni-Cu	1	67	...	...	32	...
70:30 Cu-Ni	0.5	30	...	...	69	Mn
Copper (electrolytic tough pitch)	...	...	...	...	99.9	...

TABLE 2—*Crevice corrosion of centrifugally cast stainless steel alloys in sea water.*[a]

Stainless Steel Alloy	%				Heat Treatment, °F	Probability, %			Pitting, mil
	Ni	Cr	Mo	Mn		Corrosion Initiation	10-mil Attack	>50-mil Attack	
CA-15	0.8	13	0.6	0.8	1800/1350	100	98	52	160
21-8-9	8	21	0.1	9	1950	45	38	9	135
Cast T-202	5	19	0.1	8	1950	89	63	9	95
CF-8M	10	22	2.8	0.8	1950	25	5	1	0
IN-862[b]	24	20	5.0	0.3	2150	0	0	0	0
Wrought T-316[c]	13	18	2.6	1.6	. . .	19	6	0	0

[a] 30-day exposure, seawater temperature = 60 to 80° F (18 to 27°C), creviced/boldly exposed surface area ratio = 1:85.

[b] Laboratory heat.

[c] Wrought alloy control.

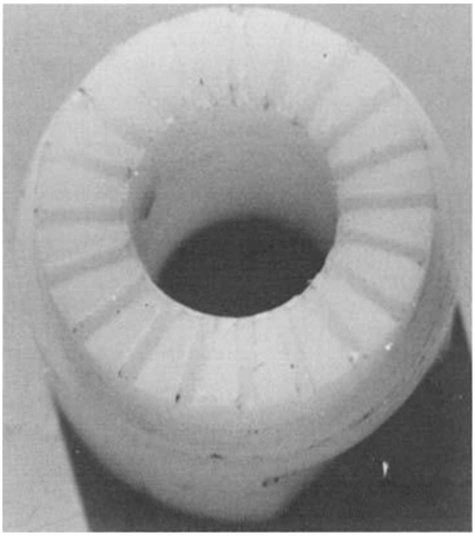

FIG. 2—*Grooved acetal resin washer.*

Test Results

The creviced area on a typical cast stainless steel specimen is shown in Fig. 3. Despite precautions to make the individual crevices as uniform as possible, a random pattern persists. Four distinct degrees of corrosion are evident: (1) no attack, (2) uniform shallow attack, (3) accelerated "pit-in-crevice" resulting from buildup of acidic corrosion products, and (4) catastrophic attack. Although the corrosion appears to follow a random pattern, statistical evaluations reveal consistent trends. Probability plots (ASTM Recommended Practice for Applying Statistics to Analysis of Corrosion Data (G 16-71)) of tabulated depths of attack measured in each crevice area on multiple specimens provide clear alloy comparisons. A typical probability plot, comparing two cast stainless steel alloys is shown in Fig. 4. These data indicate a 100 percent probability of corrosion initiation (zero probability of no corrosion) for alloy CA-15 and a 50 percent probability of crevice corrosion penetrating greater than 30 mil. The higher level of corrosion resistance to be expected for alloy CF-8M is delineated by a 25 percent probability of corrosion initiation with only a 2 percent change of corrosion penetration to >30 mil. Thus the probability curve can be used to assess alloying effects on resistance to both corrosion initiation and corrosion propagation.

The probability curves in Fig. 4 follow two distinct slopes for each alloy, one associated with crevices where uniform corrosion occurred (Type 2 in Fig. 3) and the second where accelerating pit-in-crevice attack

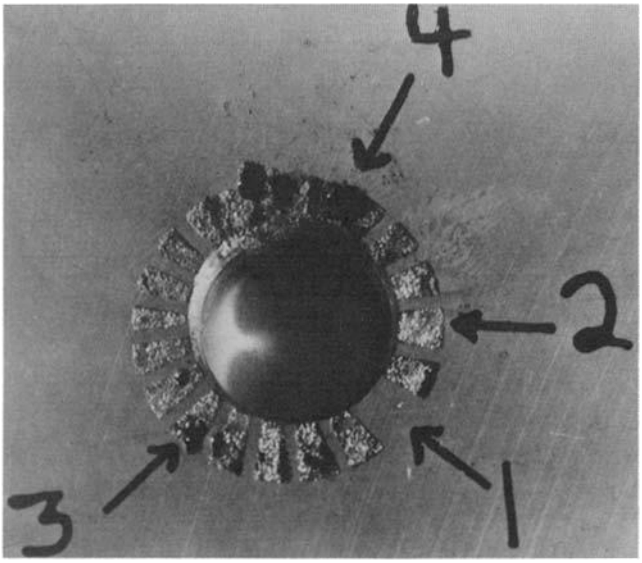

FIG. 3—*Four stages of crevice corrosion observed on single cast stainless steel specimen exposed with multiple crevices, 30-day exposure.*

developed (Type 3). Where Type 4 or catastrophic corrosion occurs, a third steeper slope is frequently observed. Only alloy CA-15 suffered any pitting (that is, localized corrosion not associated with known crevices), and typical for many of the tests, the maximum pit depth exceeded the maximum depth of crevice attack.

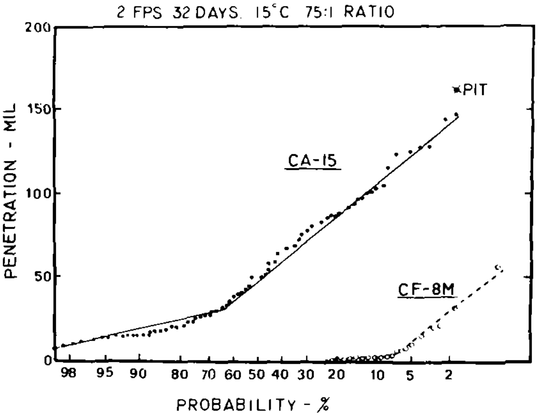

FIG. 4—*Probability of crevice corrosion for cast stainless steels; exposure conditions: 32 days, 59°F (15°C), 75:1 bold/shielded area ratio.*

Table 2 summarizes data developed for a series of cast alloys. Alloying appears to have equal effects on corrosion initiation and the various stages of crevice corrosion. However, it is of interest to note that all of the alloys containing <0.6Mo suffered distinct pitting while alloys containing >2.6Mo did not, even though two of the three alloys in the latter category did incur significant crevice corrosion. Only the development alloy IN-862,[2] containing 5Mo, provided immunity to both pitting and crevice corrosion. This is a clear indication of the different alloying requirements for control of pitting and crevice corrosion in seawater.

Area Ratio Effects

Initial tests on wrought alloys have concentrated on three alloys: Types 304 and 316 stainless steel and Incoloy alloy 825, alloys which have been recognized through field experience to provide three different levels of inherent resistance to crevice corrosion in the seawater system.

Specimen size was introduced as a second variable in these studies to assess the effects of creviced/exposed surface area ratio (that is, anode/cathode area ratio), a factor previously shown to be important in determining severity of crevice corrosion in seawater.[3] Various area ratios were created by varying both specimen size and by machining different sized plateaus on the washers. Figure 5 shows creviced areas on typical specimens from a one month exposure. The importance of area ratio is evident, both in relation to the corrosion initiation and corrosion propagation stages.

Area ratio effects have been isolated for these two stages in Figs. 6 and 7. Variability provides considerable overlap in both instances, but the consistent differences in the relative merits of the three alloys are readily apparent.

The highest area ratio used in these studies was 580:1. The marked effect of increasing area ratio suggests that even higher ratios could be used effectively to reduce the exposure period required to induce significant attack.

Metal-Ion Versus Oxygen Concentration Cell Corrosion

Similar studies have been conducted with copper, copper-nickel, and nickel-copper alloys to provide comparative data for metal-ion concentration cell corrosion to contrast the oxygen concentration cell corrosion

---

[2] Forbes-Jones, R. M., *AFS Transactions*, American Foundrymen's Society, Vol. 81, 1973, pp. 349–352.

[3] Ellis, O. B. and LaQue, F. L., *Corrosion*, Vol. 7, 1951, pp. 362–364.

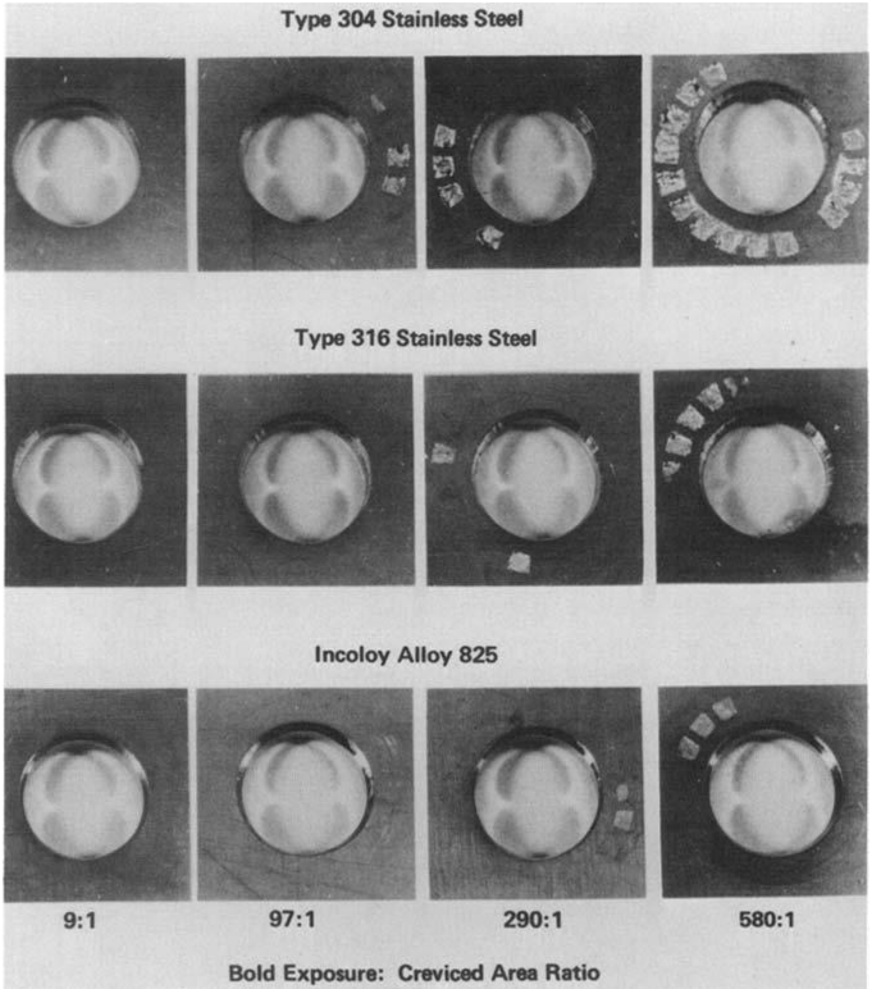

FIG. 5—*Area ratio effects on oxygen concentration cell corrosion in seawater, one month exposure.*

studies described previously. Crevice areas from a three-month test are shown in Fig. 8. Following the classic pattern for metal-ion cells, corrosion developed adjacent to, rather than within, the creviced areas. The lack of any apparent statistical pattern is also apparent. Neither copper nor copper-nickel showed any sensitivity to area ratio effects (Fig. 9) reflecting reduced cathodic control in metal-ion concentration cell corrosion. The nickel-copper alloy exhibited an apparent mixed mode between oxygen and metal-ion cell control.

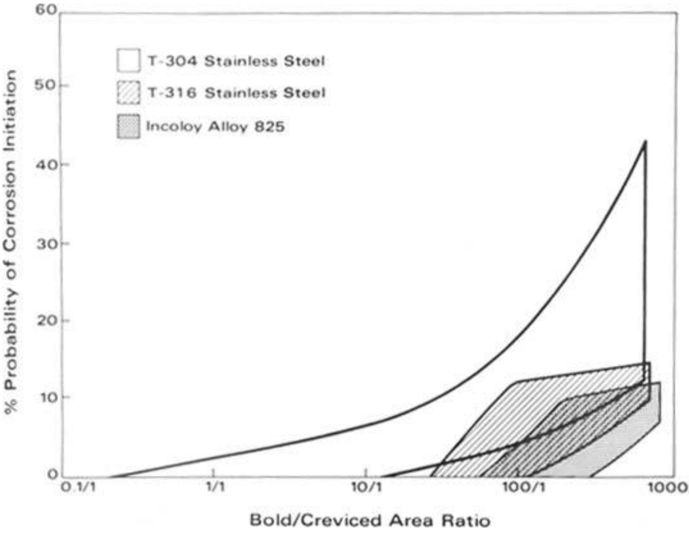

FIG. 6—*Probability of crevice corrosion initiation, one month exposure in flowing seawater.*

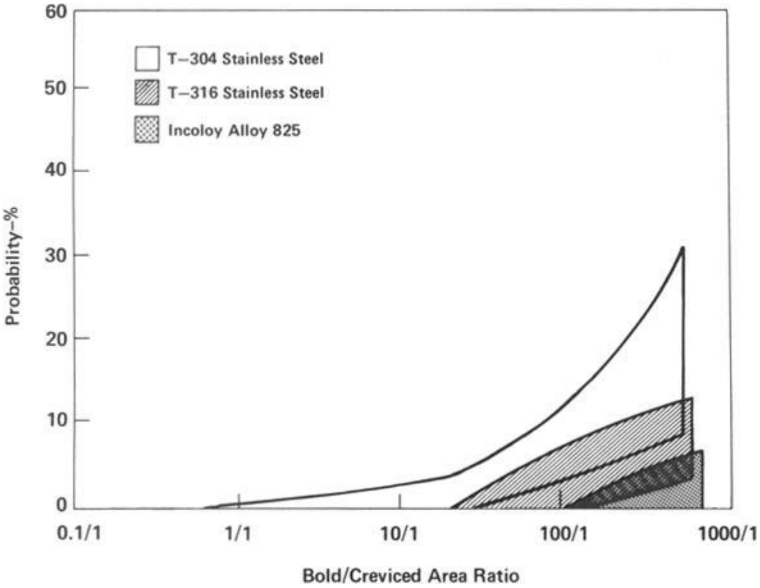

FIG. 7—*Probability of crevice corrosion penetration to 10 mil in one month.*

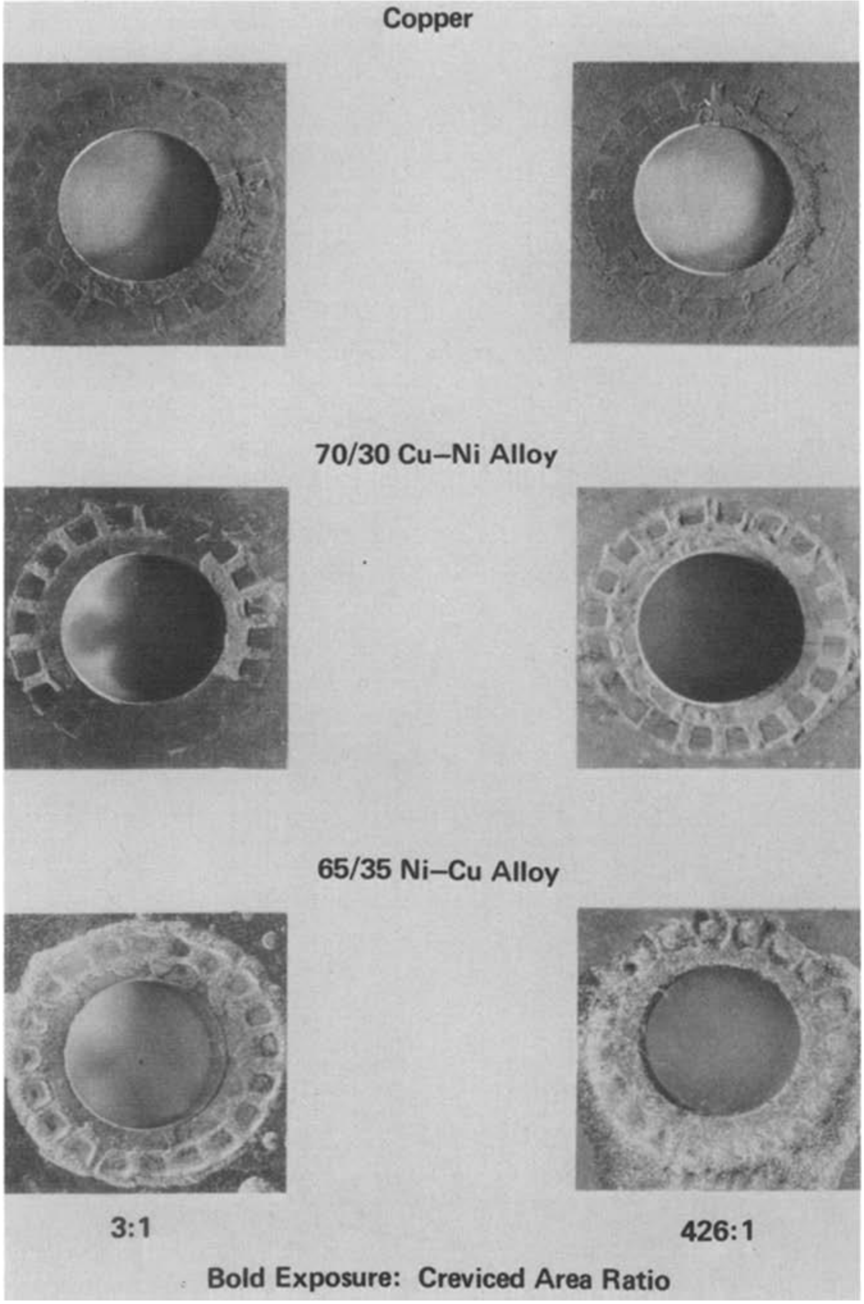

FIG. 8—*Area ratio effects on metal-ion concentration cell corrosion in seawater, three month exposure.*

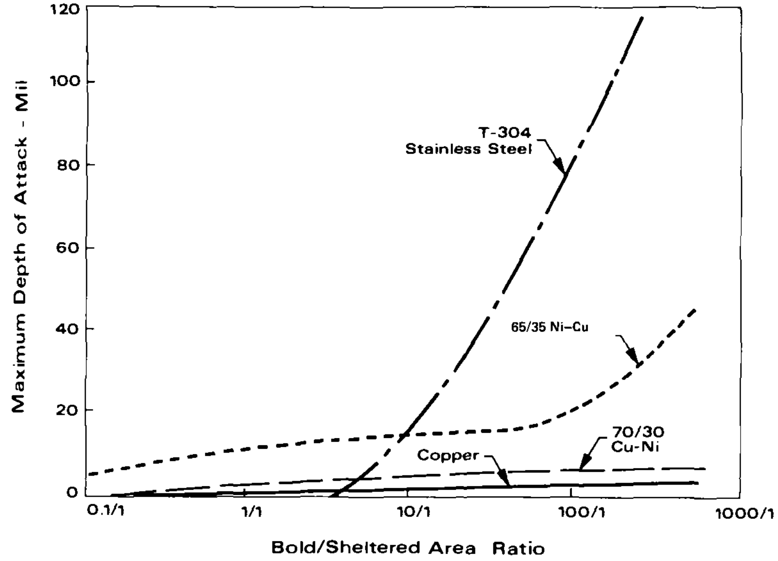

FIG. 9—*Area ratio effects on depth of attack in tight crevices, three month exposures in flowing seawater.*

Evaluation of Highly Corrosion Resistant Alloys

The use of highly corrosion resistant alloys in critical applications requires assurance of virtual corrosion immunity, that is, demonstration of an exceptionally high probability of resistance to corrosion initiation, or assuming extreme conditions permit some corrosion to initiate, resistance to active corrosion penetration to any significant depth. Table 3 shows typical data for one year (as contrasted to the one month exposures in Table 2) for three highly corrosion resistant alloys which are finding increasing acceptance for a variety of marine applications. Of the three

TABLE 3—*Crevice corrosion of wrought corrosion resistant alloys.*[a]

		Probability, %		
Alloy	Corrosion Initiation	1-mil Attack	10-mil Attack	Pitting
6X	0	0	0	0
Inconel alloy 625	23	1	0	0
Hastelloy alloy C	0	0	0	0

[a] One year tests, seawater temperature = 40 to 90°F (4 to 32°C), creviced/exposed surface area ratio = 1:89.

alloys only alloy 625 incurred any visible corrosion in this particular test, but it is important to consider the exceptional resistance to corrosion penetration exhibited by this alloy as is evidenced by the 1 percent probability indicated for corrosion penetration deeper than one mil.

Summary

Statistical evaluation of data developed through the multiple crevice approach provides a useful basis for isolating geometrical and environmental factors affecting oxygen concentration cell crevice corrosion in seawater. The method also provides a useful laboratory test for detailed assessment of inherent capabilities of a variety of candidate alloys for marine service.

C. W. Petersen[1]

Solution Chemistry of Pitting of Iron in Artificial Seawater

REFERENCE: Petersen, C. W., "**Solution Chemistry of Pitting of Iron in Artificial Seawater,**" *Galvanic and Pitting Corrosion—Field and Laboratory Studies, ASTM STP 576*, American Society for Testing and Materials, 1976, pp. 243–260.

ABSTRACT: The mechanism of pitting corrosion in carbon steel in a simulated seawater environment was studied by obtaining data on the chemical changes which occur with time in the pit and cathode solutions. Quantitative measurements were made of pH; sodium, magnesium, calcium, iron, chlorine, sulfate concentrations, and weight loss. The solutions used in the analysis were generated by using a recently developed artificial pit which not only provided a sufficient amount of solution but also made it possible to obtain specimens from specific locations in the cell itself. The results show a depletion of magnesium, calcium, chlorine, and sulfate in the cathode region while sodium and hydroxyl ion concentrations increased. Inside the pit the chlorine, iron, and hydrogen ion concentrations rose while the calcium, magnesium, and sodium concentrations dropped. Based on the results of these tests, it is shown that the decrease in pH in the pit is greatly enhanced by the magnesium and calcium reactions occurring at the cathode and by the formation of iron colloids ($Fe(OH)_4^-$ and $Fe(OH)_2^+$).

KEY WORDS: corrosion, corrosion tests, pitting tests, artificial pit, seawater attack, solution chemistry, carbon steel pitting, evaluation, pitting mechanism

Many people have studied pitting corrosion [*1–3*][2] and have compiled a vast amount of data. Unfortunately, as stated by Parsons, Cudd, and Lochte [*4*] in 1941, "while theories regarding the mechanism of . . . pitting have been well developed . . . this has been done largely without the aid of chemical analysis of the solutions enclosed within the pit." This point was reiterated by Szklarska-Smialowska [*3*] in her 1970 review of pitting corrosion research, "knowledge of the composition of the solution within the pit, and it changes during pitting, would throw more light on the mechanism of processes occurring in the pits. Unfortunately, there are only a few quantitative references concerning that problem." For this

---

[1] Senior engineer, Bettis Atomic Power Laboratory, Westinghouse Electric Corporation, West Mifflin, Pa. 15122.

[2] The italic numbers in brackets refer to the list of references appended to this paper.

reason a study was conducted to determine the changes in the solution chemistry of a pit during its growth.

Experimental

Test Apparatus

A macropit developed in an earlier study [*5*] was used to provide sufficient pit solution for chemical analyses. Figure 1 shows the test cell and the entire test apparatus. The test cell consisted of a ¾ by 1⅝-in.-diameter cylinder made of low carbon steel clamped between two plexiglass disks. The interior portion of the cylinder was partially filled with the electrolyte. A pressure vessel was used to house the cells during testing. Figure 2 shows how the pit formed and denotes the cathode and anode areas as well as the sampling areas.

Procedures

Each specimen was polished to a standard surface using 320 grit emery paper. The polished specimen was dipped in hydrochloric acid, cleaned in acetone, rinsed in alcohol, and dried. The specimen was weighed, clamped between the plexiglass disks, and partially filled with a test electrolyte. The complete test cell was then placed in the pressure vessel which was subsequently sealed and charged with oxygen. The oxygen pressure (500 psi) was used to accelerate attack and to set up a concentration cell.

The progress of each run was monitored visually, and photographs were taken or sketches were made of the test cell appearance during the test and at the completion of each run. The vessel was then depressurized, the cells removed, and the chemistry specimens taken. The solutions were saved for chemical analysis and the specimen itself was reweighed to determine weight loss.

The sampled solutions were analyzed using atomic absorption and wet chemistry techniques. They were tested only for the major anions and cations. In so doing, the composition of the solution was monitored both as a function of time and as a function of location in the cell.

Results

There were many electrolytes used in the tests conducted for this study [*6*], varying from 0.535 *M* sodium chloride to an ASTM sea salt (according to ASTM Specifications for Substitute Ocean Water (D 1141-52)). Although much valuable information was gained from all of these tests, only the results of those tests which were designed to determine the roles of the ions during pit formation in the artificial seawater will be discussed. The solution used was prepared according to ASTM Method D 1141-52, Table 1, Section 4, Formula A.

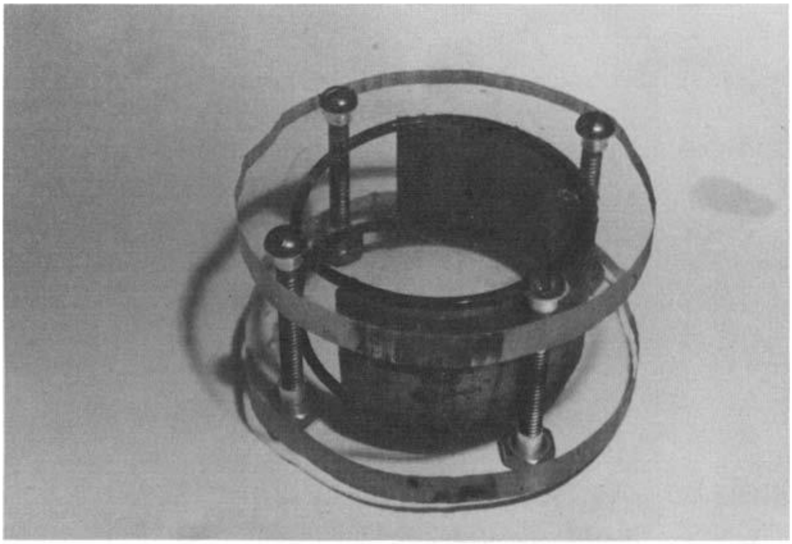

TEST CELL

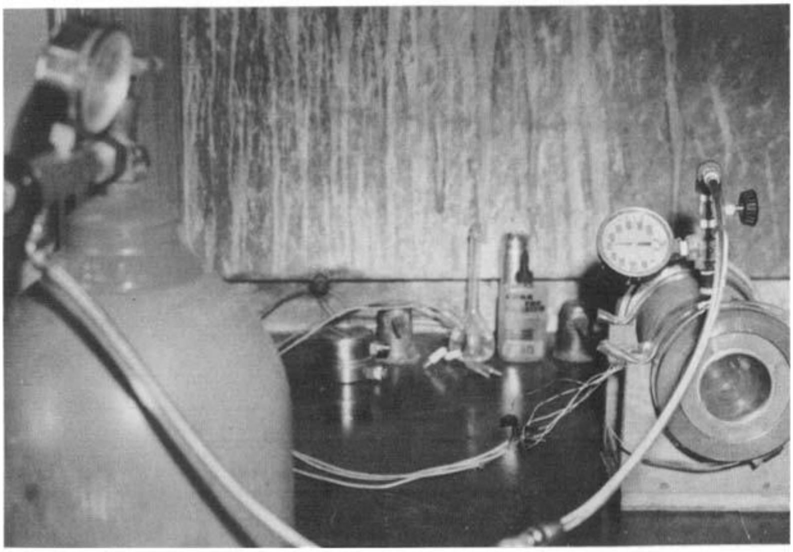

TEST APPARATUS

FIG. 1—*Test cell apparatus.*

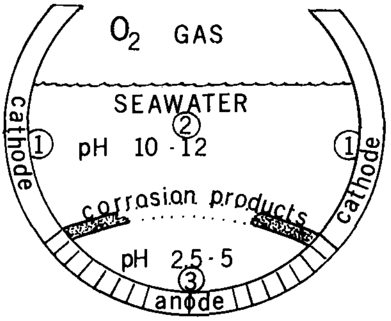

FIG. 2—*Cell formation and sampling locations.*

Changes in the Solution Chemistry

The results reported in the following pages were obtained by analyzing specimens from three locations in the cell: (*a*) along the cell wall near the cathode, (*b*) in the middle of the top bulk solution, and (*c*) at the very bottom of the cell near the anode (below the layer of corrosion products which formed across the pit) (Fig.2). Each test was run in triplicate, and the averages are plotted for each ion in Figs. 3 to 10 as a function of time in the life of the cell.

X-ray Results

A qualitative fluorescence analysis of the corrosion products revealed the presence of iron, calcium, and manganese in the products. Elements with an atomic number less than 20 could not be detected by the equipment available. The lighter elements were, however, detected by emission spectrographic analysis, and these results are shown in Table 1. X-ray diffraction yielded amorphous patterns with no distinct peaks.

In Situ *pH Measurements*

The pH variations during pitting proved to be very important. On selected time series experiments, *in situ* measurements were made prior to sampling of the electrolyte by carefully lowering a micro-pH electrode into the test cell at various locations. Readings were taken at the cathode surface, on a vertical line through the center of the cell, and at the anode surface. This allowed precise pH determinations at pinpoint locations which would otherwise be missed in testing extracted specimens. The results are presented graphically in Fig. 11. It should be noted that in the early stages of the cell formation the pH was constantly decreasing from top to bottom. After products began to form, however, there was a pH inversion in the pit solution and the pH actually rose slightly as the electrode approached the anode surface.

TABLE 1—*Results of elemental analysis.*

	Cathode Material[a]	Bridge Material	Pit Material
X-ray fluorescence	Fe Ca Mn	Fe Ca Mn	Fe Mn

Emission spectrography (bridge material only), %[b]

Na,	0.1 to 10	Cr	0.0001 to 0.001
Mg,	0.1 to 1	Mn,	0.01 to 0.1
Al,	0.001 to 0.1	Fe,	>10
Si,	0.0001	Cu,	0.0001 to 0.001
Ca,	0.01 to 0.1	Zr,	0.001 to 0.01
K,	none detected		

[a] Cathode material was scraped from cathode wall and combined with white floc obtained by centrifuging the cathode solution.

[b] Results based on dried crushed samples; instrumentation = 3.4 m Ebert Mark IV Spectrograph.

Discussion of Results

The quantitative results show the changes in ion concentrations within the electrolyte. There are some general trends which seemed to affect all ions. The changes were: (*a*) every ion in solution experienced a period of instability during the first 6 h; (*b*) the period from 6 to 41 h was a period of transition, with large changes occurring; and (*c*) the period from 41 h until the end of the test was a period of stabilization and solution equilibrium.

Instability

The fluctuations in ion concentrations (Fig. 12) coincided with fluctuations in the potential of the solution (see Appendix) and were due undoubtedly to the changes occurring on the cell surface itself. For the ions initially in solution, the instability took the form of temporary depletions. The cell has many anodes and cathodes spread over the whole surface, the anodes generating iron ions and the cathodes generating hydroxyl ions. This was evidenced by the rise in iron concentration in all areas. Initially these sites are close together, and there is rapid interaction between the iron and hydroxyl ions produced at these sites, causing the formation of basic salts which remove ions from the solution. As the anodic and cathodic regions grow, the iron and hydroxyl ions must migrate farther as a part of the corrosion current before reacting, and there is less chance of a rapid interaction trapping other anions and cations. Thus, as the metal surface stabilized into localized anodes and cathodes, the behavior patterns of the ions also stabilize.

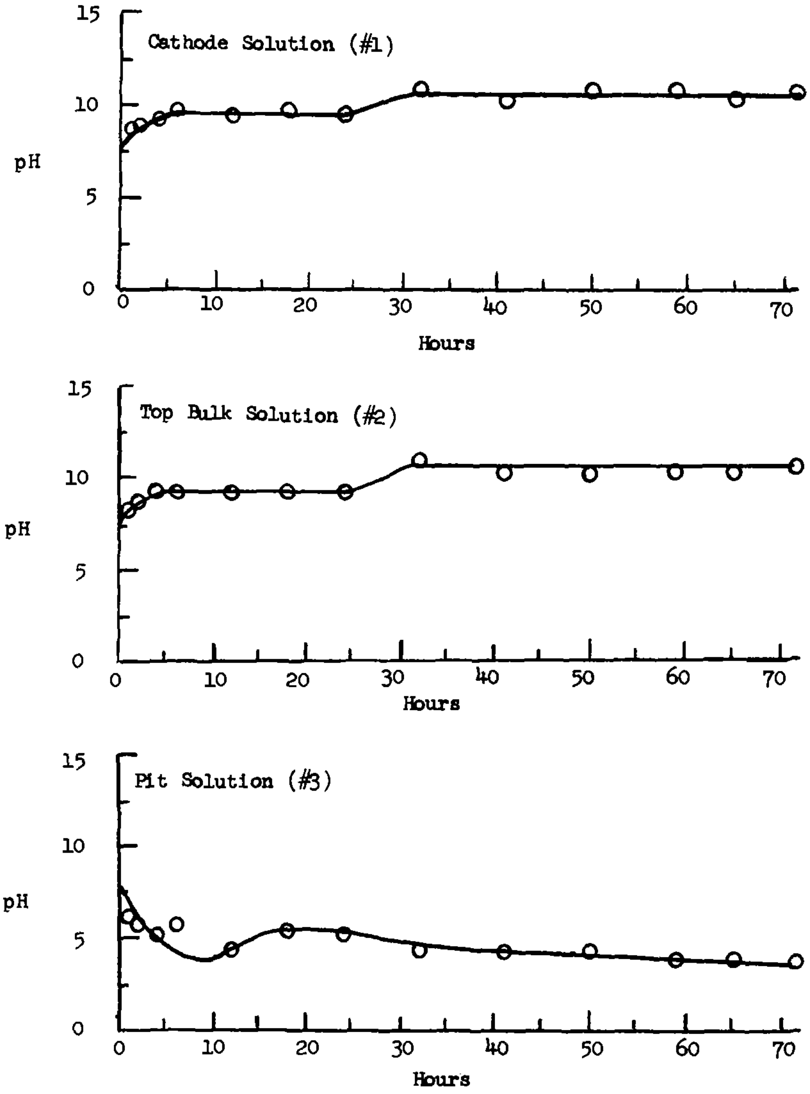

FIG. 3—*Hydrogen concentration as a function of time.*

Transition

During the 6 to 41-h period there were a variety of changes in ion concentrations. The changes encountered in the top solution will be discussed first since they play an important part in what occurs elsewhere in the cell.

Magnesium experienced a rapid depletion in the upper region. Calculations indicate that the solubility of magnesium hydroxide was exceeded at a pH of approximately 9.5. Thus, the equilibrium between hydroxyl genera-

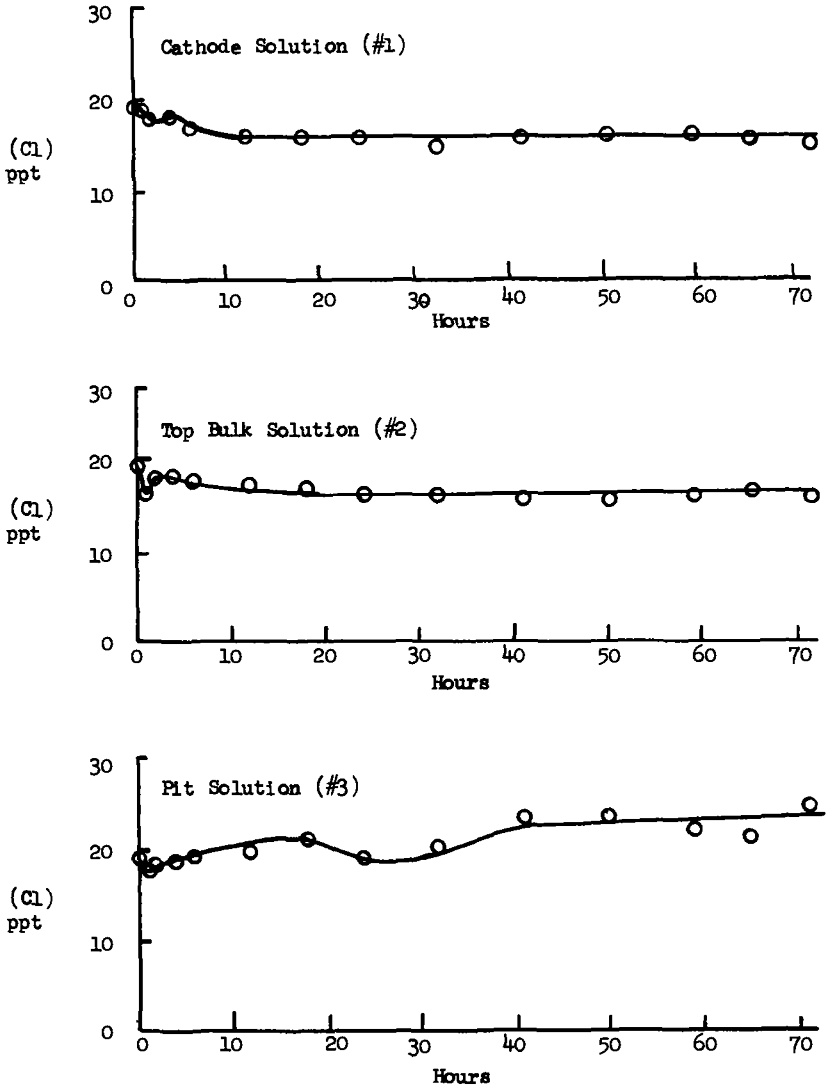

FIG. 4—*Chloride concentration as a function of time (ppt = parts per thousand).*

tion and magnesium depletion accounts for the first plateau in the pH curve. The formation of magnesium hydroxide prevented some hydroxyl from reaching the pit region. The actual precipitate which formed was white and quite voluminous. Because of its nontenacious character, the product accumulated at the interface between the pit and upper solution rather than adhering to the walls. During this time the magnesium concentration in the pit slowly decreased.

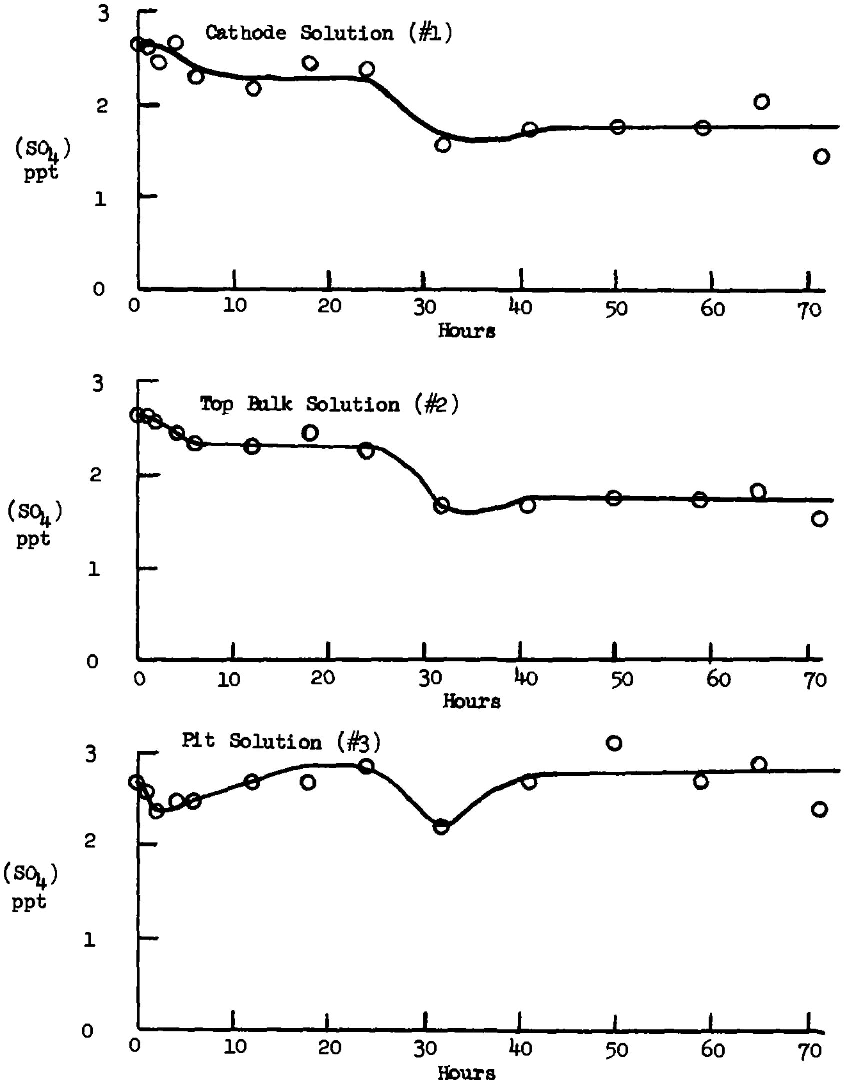

FIG. 5—*Sulfate concentration as a function of time.*

Once the magnesium was depleted in the top solution, however, the hydroxyl was able to enter the solution as free ions, and the pH increased. This rise in pH in Areas 1 and 2 was accompanied by large changes in the chemistry of the pit solution. After 24 h the slow decrease in magnesium was altered, and there was a rapid drop in concentration. Since the magnesium did not show up in either Area 1 or 2, it must have been removed from solution either in the pit or at the interface between the pit and the

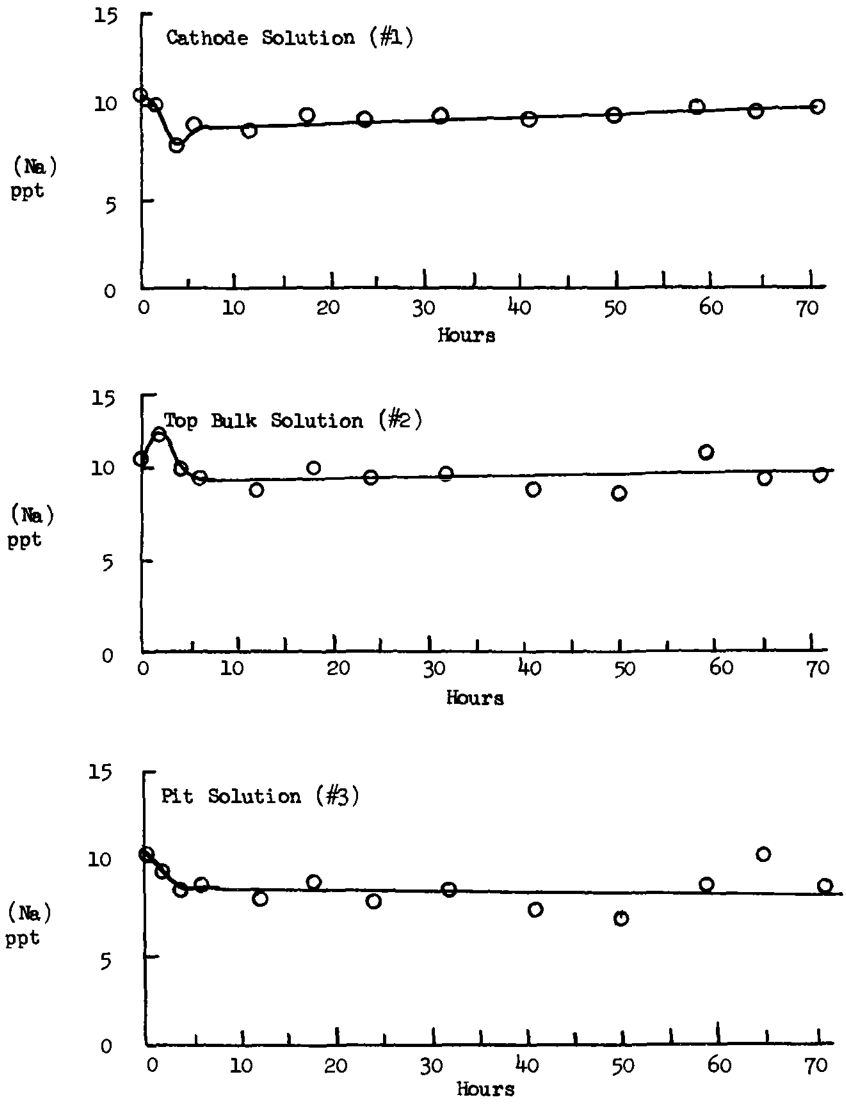

FIG. 6—*Sodium concentration as a function of time.*

upper solution. Also, since none of the solubilities of magnesium compounds was exceeded in the pit, the magnesium removed from solution must have been incorporated into the structure of other precipitates as an impurity. The rise in pH in the pit at 24 h was accompanied by a rapid drop in iron and chloride-ion concentrations as well as magnesium. Rapid precipitation of iron could have trapped the magnesium and chloride into the

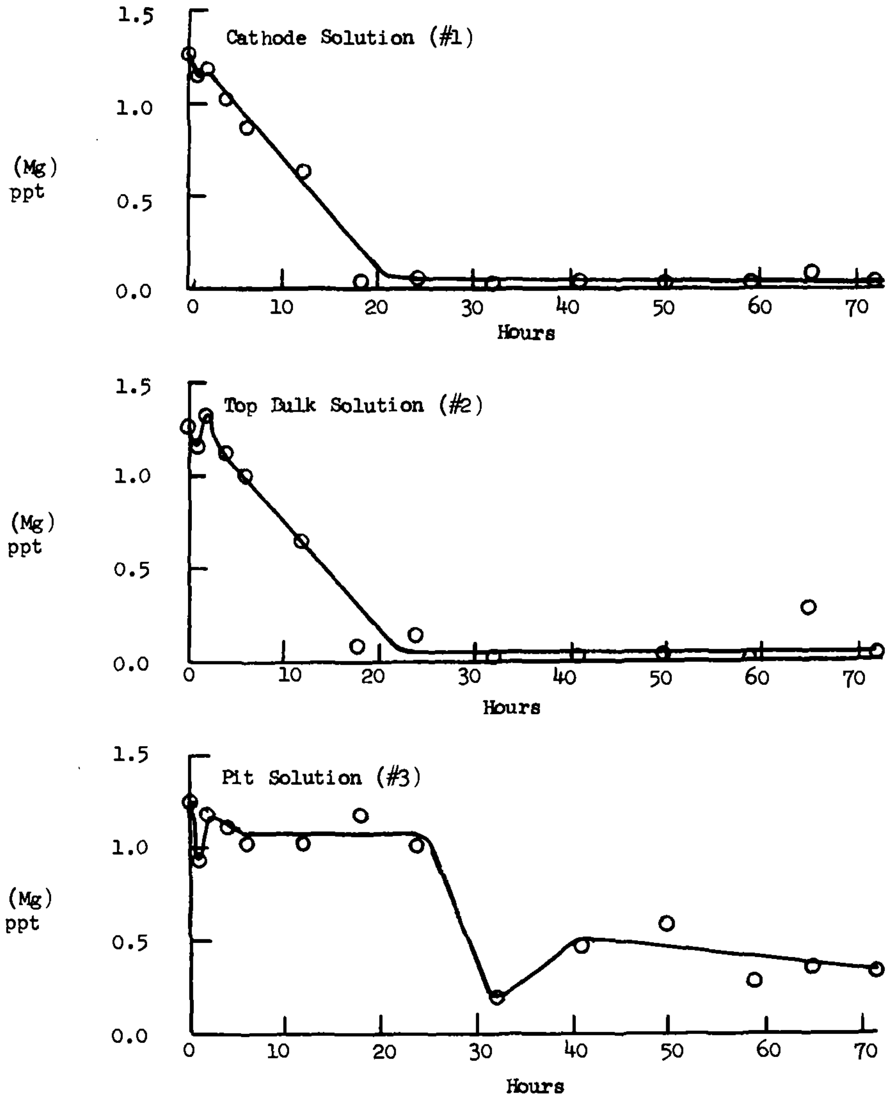

FIG. 7—*Magnesium concentration as a function of time.*

products. It is interesting to note that emission spectrometry identified magnesium as an element in the bridge. At this same period when iron, magnesium, and chloride decreased, the first signs of a layer (bridge) of corrosion products began to appear at the anode/cathode interface. Unfortunately, no analysis was made of the pit products by emission spectrometry. It is interesting to note that the weight loss increased sharply

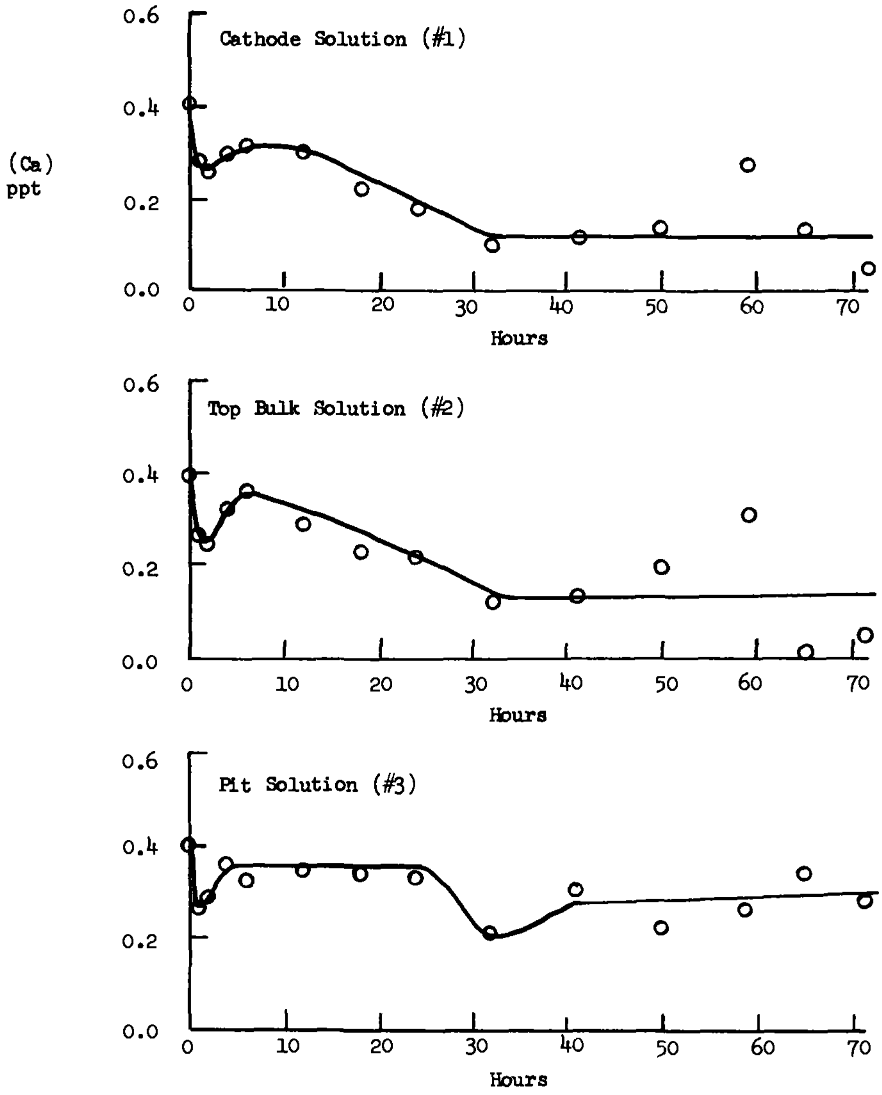

FIG. 8—*Calcium concentration as a function of time.*

between 32 and 41 h, as did the amount of iron in solution. These increases could be explained by a depolarization of the anode due to the decrease of iron in the pit solution between 24 and 32 h.

Calcium experienced a slower reduction in concentration in all areas than did magnesium. Calculations show that the solubility of calcium hydroxide was not exceeded; therefore, its formation is not a major factor in calcium depletion. Calculations do show, however, that the solubility of calcium

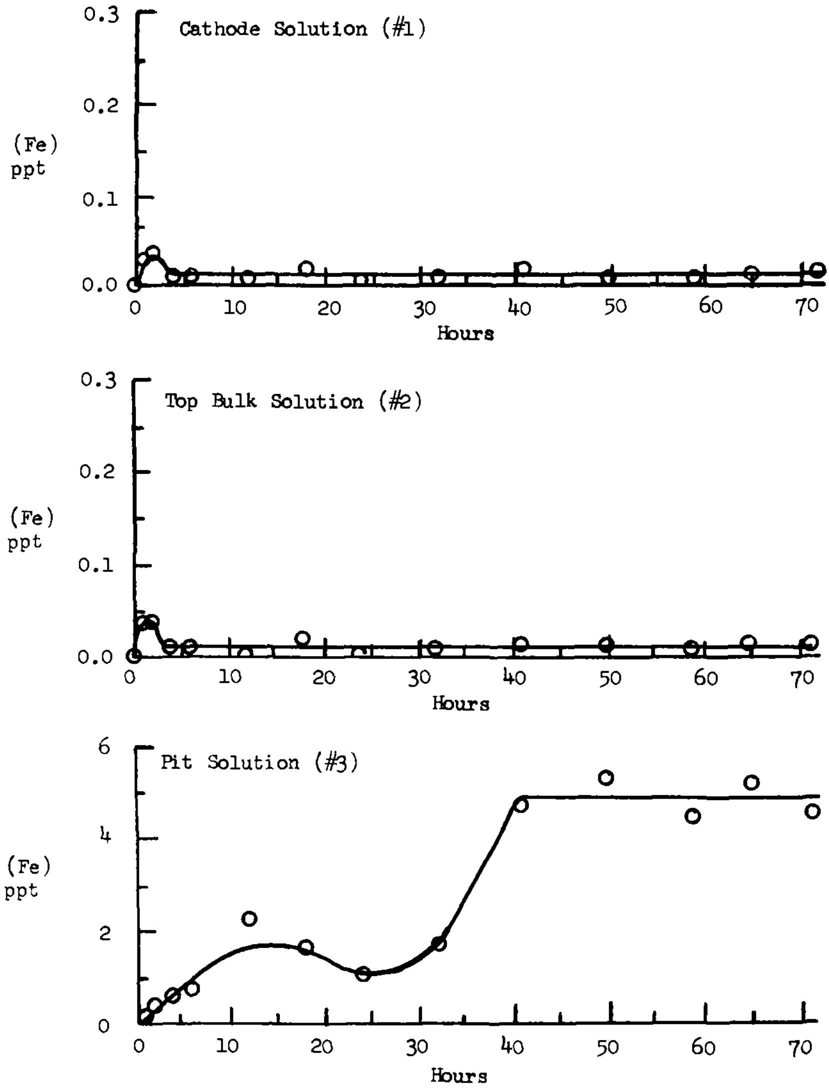

FIG. 9—*Iron concentration as a function of time.*

carbonate was exceeded and plays an integral part in the reduction of calcium concentration in the cell. The calculations also show that at 32 h when the pH was 10.9 all of the available bicarbonate would have been completely depleted and the complexing of calcium would cease. This accounts for the large change in calcium slope.

Calcium in the pit was less affected by the depletions in the upper region and, except for the slight anomaly between 24 and 41 h, it underwent a

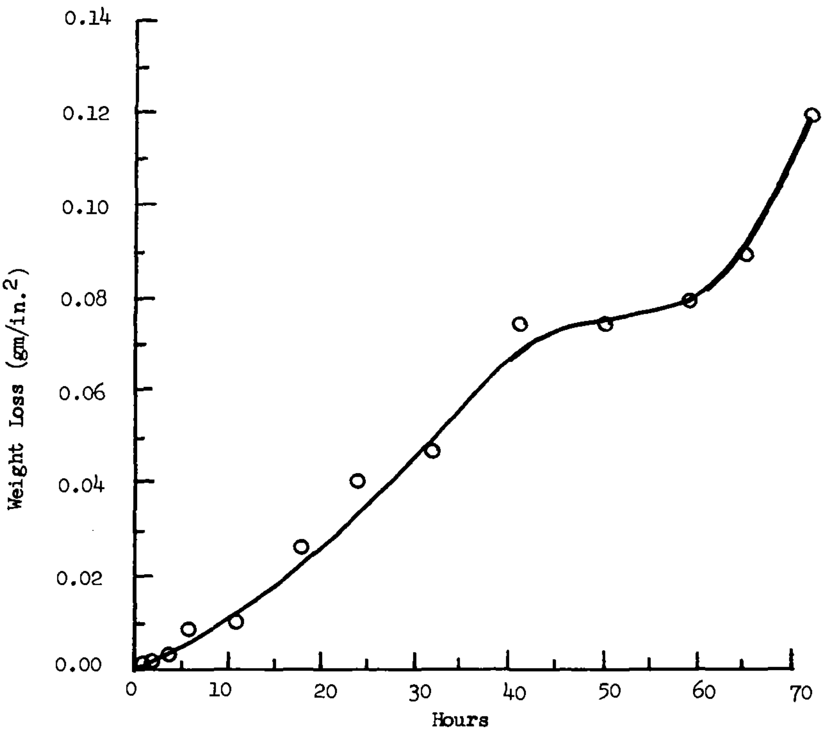

FIG. 10—*Weight loss as a function of time.*

gradual depletion. The fact that this calcium did not reappear in the upper solution indicates that, like magnesium, it was incorporated into the products of the iron precipitates. The results of the X-ray and emission spectrometry analyses show that calcium was present in the bridge and cathode products but not in the pit products. The incorporation of calcium from the pit, therefore, must have taken place at the interface between the pit and upper solution.

Sodium was a very difficult ion for which to obtain consistent measurements, and the values which were averaged were very sporadic. This was due to the large dilution and low sensitivity required for the analysis of the large concentration of sodium in seawater. As a result of the wide range of values, the intervals of confidence are large.

After its initial fluctuations, sodium settled into a simple migration pattern, and the concentrations in Areas 1 and 2 gradually rose while decreasing in the pit. This migration pattern supports a role of balancing changes for sodium.

A mass balance calculation using the sodium concentrations in the top and pit areas indicated that there was a loss of sodium. This depletion

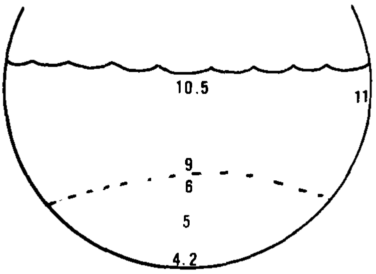

a. After 24 Hours

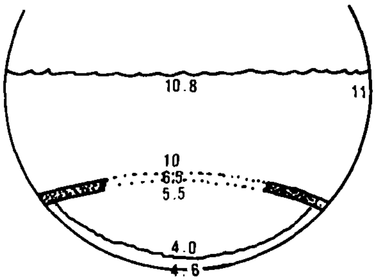

b. After 35 Hours

FIG. 11—*pH profiles.*

appears to be quite negligible, but this is deceiving since the concentration of sodium is so large. Since sodium did not exceed any of its known solubility limits, it must be assumed that the loss was due to incorporation of sodium into the structure of some of the precipitates. The presence of a large quantity of sodium in the bridge was confirmed by the emission spectrometry results.

Iron in Areas 1 and 2 had stabilized at a low value within 4 h and remained there for the duration of the test. Since iron hydroxide is extremely insoluble in the pH range encountered in Areas 1 and 2, the iron in solution was probably in equilibrium with the insoluble material. This governed the final concentration of iron in the upper region. Many of the measured values fell below the sensitivity of the atomic absorption unit so the actual amount of iron in solution was extremely low. Even using the measured value of approximately 10^{-4} M, however, the measured and calculated equilibria values were within one order of magnitude ($\sim 10^{-4}$ to 10^{-5} M).

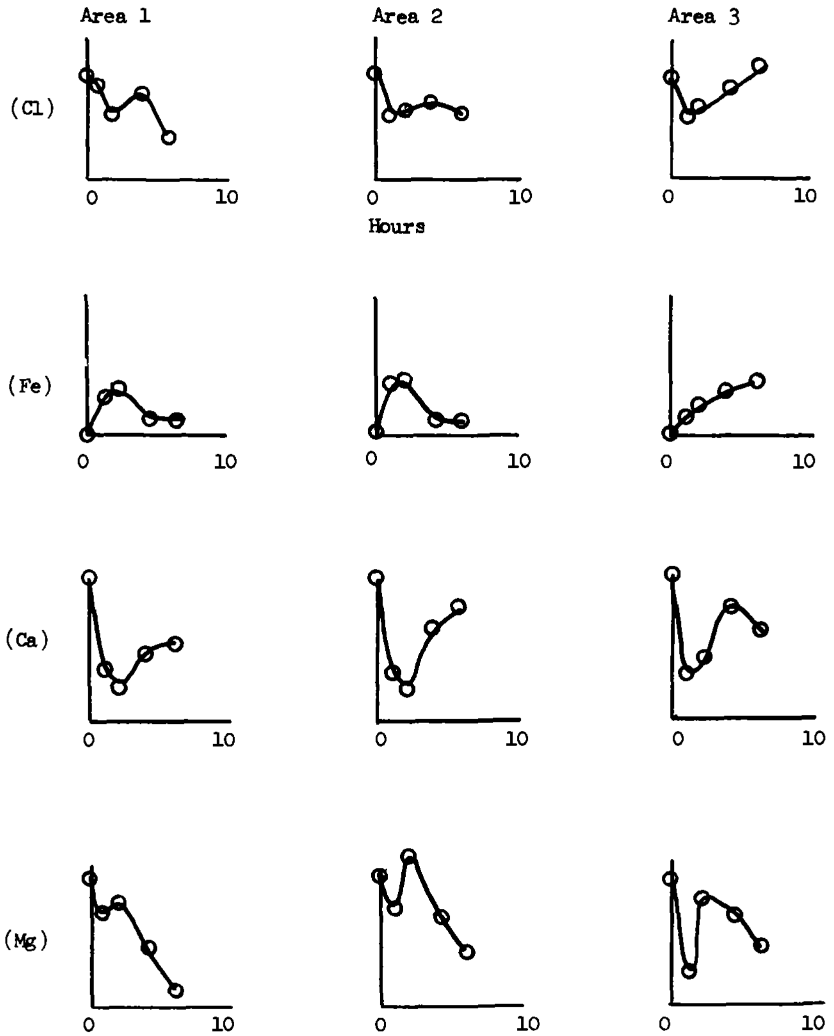

FIG. 12—*Concentration functions during instability period.*

Iron, during this transition period, gradually increased in concentration in the pit due to its generation at the anode. There was a slight anomaly between 18 and 32 h, but this was explained by the sudden release of hydroxyl from the cathode due to magnesium depletion.

Chloride was very similar to sodium, experiencing a drop in concentration in all areas during the first 4 h and then recovering to achieve a gradual migration pattern. The anomaly in the pit between 18 and 32 h was explained earlier.

Sulfate exhibited a behavior that mirrored the pH changes. The concentration leveled off at 6 h to form its first plateau, then dropped between 24 and 32 h. Solubility and stability data indicate that the sulfate would complex all the cations by forming ion pairs, but it does not exceed any of its known solubility limits. Therefore, the decrease in sulfate must be due either to migration or coprecipitation as an impurity. While migration does not seem to be the sulfate's depletion mechanism, there was no readily apparent explanation for the plateaus observed for sulfate in Areas 1 and 2.

Inside the pit the sulfate did appear to be increasing in concentration. Mass balance calculations indicated that there was a slight loss in overall concentration; thus, some of the material from Areas 1 and 2 may have been incorporated into the solid products.

Stabilization (41 to 72 hours)

The period from 41 h until the end of the test was a stabilization period for many ions, apparently caused by the depletions which occurred earlier. In Areas 1 and 2 the solution had essentially been reduced to a sodium solution by the depletion of magnesium and calcium. The sodium concentration was rising to satisfy charge neutrality but had virtually no effect on the hydroxyl ion generated at the cathode. Thus, the hydroxyl was free to migrate towards the pit essentially unimpeded.

The leveling off of the iron concentration in the pit as well as the plateau in the pH curve in the upper solution are important. The leveling off of the pH and iron could be due to the cessation of attack, but the weight loss was still increasing during this period so attack was still occurring. The leveling off could also be due to a steady state equilibrium between the hydroxyl and the iron. The hydroxyl, which was now free to migrate from the cathode to the pit, would react with the iron which had been building up in the acidic pit area and a steady state could be reached. It should be noted that during this time rapid bridge growth occurred, but there was no apparent depletion of ions in solution. Besides iron and hydroxyl, the other ions also stabilized.

Magnesium in the cathode region was unaffected and remained depleted. In the pit region, it had risen slightly from the earlier drop in concentration and stabilized into a slow decline. Again, the magnesium did not reappear in Areas 1 or 2, so it must have become incorporated into the products.

Calcium and sulfate essentially leveled off in all areas during this period, as did the iron and hydroxyl. The chloride and sodium still exhibited a slight migration pattern. These reductions in slope would be expected since the hydroxyl ions were providing most of the needed charge neutrality by complexing iron.

This series of events coincided with the period of rapid bridge building and supports a theory of rapid agglomeration at the interface between the high and low pH regions. It is also important to note that the amorphous patterns obtained when X-raying fresh products confirms that these products were formed from colloids since the only way to obtain an amorphous precipitate is by first forming colloids [7]. The aging of the products into crystalline magnetite (Fe_3O_4) and hematite (Fe_2O_3), which is a known phenomenon among colloids, also provides support for a mechanism involving colloid formation and bridge building.

Conclusions

For many years the study of pitting corrosion has been hampered by a lack of quantitative data about the solution chemistry related to the attack. The data obtained in this study provide information concerning reactions inside the pit as well as those occurring near the cathode. Based on these results, roles and mechanisms were proposed for the major ions. The principal results of the work are as follows.

1. The attack found in seawater was not solely a function of a single anion-cation pair but rather a complex mixture which depended on: (*a*) types of ions present, (*b*) individual ion concentrations, and (*c*) relative ion concentrations (for example, magnesium/sulfate or magnesium/sodium ratio).
2. The anions allowed an increase in hydroxyl concentration near the cathode by forming ion pairs.
3. The initial pH buildup caused precipitation of magnesium hydroxide. This complexing of hydroxyl ions stabilized the pH at a value of 9.5.
4. The complexing of hydroxyl ions at the cathode limited the ions ability to migrate to the pit. Thus, the iron generated at the anode hydrolyzed water and the pH dropped due to free hydrogen ion generation. The reduction in pH in the pit did not first require the formation of solid products over the pit area.
5. Solution potential measurements, stability calculations, and solubility data indicate that the major iron ion present in the pit is the ferrous ion.
6. The formation of amorphous products and visual observations indicate the presence of colloids which appear to be quite important to the cell formation.
7. X-ray and emission analyses have shown that all of the major cations except potassium are incorporated into the bridge structure.

Acknowledgments

The author wishes to thank V. C. Rose, K. H. Mairs, and T. J. Rockett, University of Rhode Island, who have contributed greatly to the general development of the project and helped to stimulate its progress.

APPENDIX

Solution Potential

Electrode potential (E°) is a common term in corrosion studies, whereas solution potential [8] is not as common. A brief explanation of solution potential (Eh) and how it is used in corrosion studies is presented to clarify the term.

If we consider the general half cell reaction

$$\text{oxidation} + ne^- \rightleftharpoons \text{reduction, then } \log K = \log A_{red} - \log A_{ox} + n\text{pE, and pE} = \text{pE}^\circ + n^{-1}\log(A_{ox}/A_{red})$$

where $\text{pE}^\circ = n^{-1} \log K$, and pE is a pure number, which is similar to pH. The value pE corresponds to the oxidizing power of the equilibrium system. The quantity pE is related to the more general redox potential (Eh) by the relationship

$$\text{pE} = -\log(e^-) = \frac{\text{Eh}}{2.3\ \text{RT}/°\text{F}}$$

Thus, elements which have more than one oxidation state (for example, Fe^{3+} and Fe^{2+}) will have the species present in equilibrium with seawater controlled not just by pH but by the solutions redox potential as well. In natural waters the relative concentrations of such pairs is controlled primarily by the concentration of dissolved oxygen. In general, the pH and pE values will not deviate much in a flowing system, but in stagnant areas the oxygen in the water will be stripped and the pE will fall (for example, crevices).

To illustrate how this information is put to use, consider the oxidation state of thallium in seawater (ignoring any possible complexes)

$$Tl^{3+} + 2e^- \rightleftharpoons Tl^+$$

The standard electrode potential (E°) for his reaction is −1.247 V at 25°C. The redox potential (Eh) of seawater is 0.789 V. Then, if one applies the Nernst equation, $E = E^\circ + RT/nF \ln ATl^{3+}/ATl^+$. Thus, $0.729 = -1.247\ (0.0591/2) \log ATl^{3+}/ATl^+$ and $Tl^{3+}/Tl^+ \approx 10^{100}$. This ratio says that any thallium should be present almost entirely as Tl^{3+}. Similar calculations can be carried out for other elements to determine the species expected inside and outside a pit if one knows the solution potential.

References

[1] Fontana, M. and Green, N., *Corrosion*, Vol. 15, Jan. 1959, pp. 25t-31t.

[2] Kolotyrkin, J., *Corrosion*, Vol. 19, Aug. 1963, pp. 261t-268t.

[3] Szklarska-Smialowska, Z., *Corrosion*, Vol. 27, June 1970, pp. 223–233.

[4] Parsons, E., Cudd, H., and Lochte, H., "Synthetic Corrosion Pits and the Analysis of Their Contents," *Journal of Physical Chemistry*, Vol. 45, 1941, p. 1339.

[5] Petersen, C. W., Soltz, G. C. and Mairs, K. H.. *Corrosion*, Vol. 30, No. 10, Oct. 1974.

[6] Petersen, C. W., "Solution Chemistry of Pitting Corrosion in Seawater," Ph. D. thesis, University of Rhode Island, 1974.

[7] Blaedel, W. J. and Meloche, V. M., *Elementary Quantitative Analysis*, Harper and Row, New York, 1963.

[8] Riley, J. P. and Chester, R. in *Introduction to Marine Chemistry*, Academic Press, New York. 1971, pp. 75–79.

P. E. Morris[1]

Use of Rapid-Scan Potentiodynamic Techniques to Evaluate Pitting and Crevice Corrosion Resistance of Iron-Chromium-Nickel Alloys

REFERENCE: Morris, P. E., "**Use of Rapid-Scan Potentiodynamic Techniques to Evaluate Pitting and Crevice Corrosion Resistance of Iron-Chromium-Nickel Alloys,**" *Galvanic and Pitting Corrosion—Field and Laboratory Studies*, *ASTM STP 576*, American Society for Testing and Materials, 1976, pp. 261–275.

ABSTRACT: Rapid-scan potentiodynamic polarization techniques were utilized to determine pitting potentials (E_p) for Types 304 and 316 stainless steel in 25°C, 4 percent sodium chloride. Decreasing the test time by increasing the potential scan rate prevented the development of crevice attack, thereby permitting E_p to be measured accurately and reproducibly. A close examination of the rapid-scan polarization curve for Type 304 stainless steel in the potential region above E_p revealed two distinct linear segments. Static potential test results indicated that the more active linear segment was a response due to pitting attack, and the more noble linear segment was a response due to crevice attack. These observations suggest that if a rapid-scan potentiodynamic technique is employed, then pitting and crevice corrosion resistance might be measured by a single test procedure. In addition to the effect of potential scan rate, it was found that the test electrode surface finish is an important consideration in the determination of pitting resistance or crevice resistance or both.

KEY WORDS: corrosion, pitting, concentration cell corrosion, potentiodynamic polarization, sodium chloride, iron alloys, corrosion tests

The application of electrochemical methods to the study of pitting and crevice corrosion has been discussed in numerous publications [*1–21*].[2] Although several electrochemical techniques have been developed to determine pitting resistance, none of these have been adopted as a standard procedure due to their various limitations. In particular, crevice corrosion of the test electrode during electrochemical pitting evaluations has been a

---

[1] Research scientist, Paul D. Merica Research Laboratory, The International Nickel Company, Incorporated, Suffern, N. Y. 10901.

[2] The italic numbers in brackets refer to the list of references appended to this paper.

recurring problem. Several workers [*2–7*] have reported that crevice attack occurs before the onset of pits, interfering with measurement of the pitting potential. For example, Johnson [*6*] noted that crevice attack caused a negative shift in the measured breakthrough or pitting potential (E_p), whereas a positive shift in E_p with crevice development was observed in the present study using a similar conventional slow-scan potentiodynamic technique.

Crevice corrosion has been easier to study by electrochemical techniques, and various electrochemical crevice corrosion test electrodes have been described in the literature [*5–11*]. These electrodes have been used both to rank metals by crevice corrosion resistance and for mechanistic studies [*12*].

In this investigation, the pitting and crevice corrosion of Types 304 and 316 stainless steel were studied to examine the feasibility of developing an electrochemical test capable of yielding information about both types of corrosion simultaneously. Since crevices are invariably present at electrode-holder junctions, consideration was given to using these crevices to provide information about the electrode's crevice corrosion resistance. The data presented suggest that if a rapid-scan potentiodynamic technique is employed, then the responses due to both pitting and crevice corrosion can be detected, in fact, in a single anodic polarization curve. Furthermore, it is suggested that it may be possible to rank iron-chromium-nickel alloys in terms of their pitting and crevice corrosion resistance by comparing certain portions of their anodic polarization curves. It is also shown that surface preparation is an extremely important parameter in such comparisons.

Experimental

Specimen and Solution Preparation

Chemical compositions of the test electrode alloys, Types 304 and 316 stainless steel, are given in Table 1. Two types of test electrodes were employed in this study, a conventional sheet electrode and a special crevice electrode. The sheet electrodes were rectangular, measuring 8 cm^2 in total area, having been prepared from annealed 0.635-cm-thick sheet. Each electrode was drilled and tapped in one end for mounting by a method described previously [*22*]. The special crevice electrode is shown in Fig. 1. The crevice was formed by forcing the beveled end of a short rubber tube section against one surface of the circular specimen. A bolt through the

TABLE 1—*Nominal chemical composition (percent) of alloys studied.*

	Ni	Cr	Fe	Mo
Type 304 stainless steel	9.5	18.5	72.0	...
Type 316 stainless steel	12.0	17.0	68.0	2.25

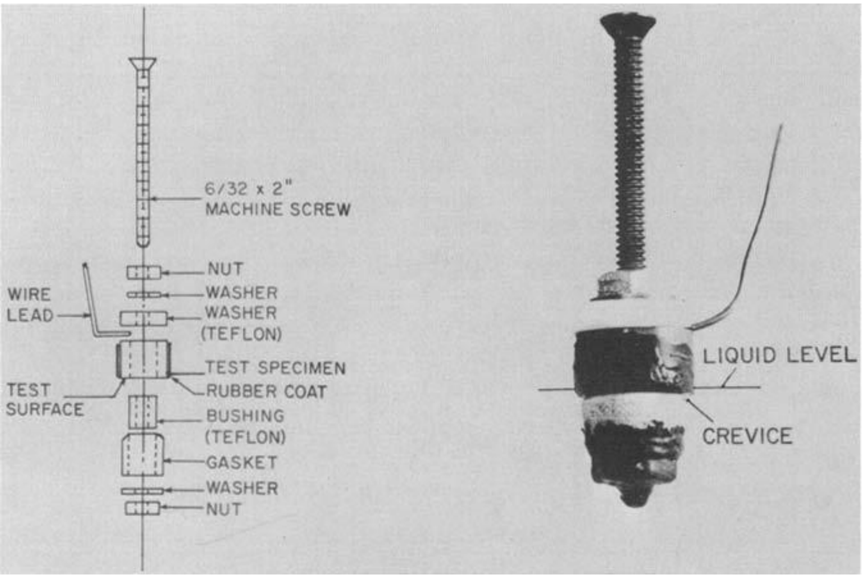

FIG. 1—*Electrochemical crevice test electrode assembly.*

inside of the tube and the center hole of the specimen kept the specimen and tube section in alignment. The specimen edges were masked with a single component epoxy cured at 70°C, so only the specimen within the crevice area was exposed to the environment.

All exposed alloy surfaces were manually abraded either with dry 180 grit or dry 600 grit paper. These abraded surfaces were rinsed with distilled water, dried, and degreased with trichloroethylene before immersion in the test solution. The entire surface preparation was completed 5 min prior to testing.

All tests were performed at 25°C in a 4 percent sodium chloride solution which was prepared by dissolving reagent grade sodium chloride in distilled water.

Apparatus

The polarization test cell was a modified [*23*] one-litre round bottom distillation flask with the calomel reference electrode in direct contact with the test environment.

Potential versus logarithm current density curves were plotted automatically with a commercial potentiostat, motorized potential stepping unit, logarithmic converter, and *x-y* recorder.

Procedure

Cathodic and anodic polarization curves were plotted, as described previously [*23,24*], by scanning potentials at 60.0 V/h from −2.00 V saturated calomel electrode (SCE) to the pitting corrosion region until applied current density reached 5000 $\mu A/cm^2$. After reaching 5000 $\mu A/cm^2$, either the potential scan was discontinued or the scan direction was immediately reversed. Only the anodic portions of the polarization curves determined by these methods are shown and discussed in the present paper.

Two types of supplementary constant potential tests were conducted. One test series consisted of recording the current densities for a 1-min period after turning on the potentiostat. In these tests the electrode was cathodically polarized for 1 min at -2.00 V, just prior to being polarized at the preselected anodic potential. The other test series consisted of holding test electrodes at selected potentials for 16 h to determine the extent and nature of localized attack. Due to the nature of the 180 and 600 grit surfaces, visual examinations for pitting or crevice damage or both were carried out at a low magnification (×5).

Results

Type 304 Stainless Steel

Effect of Scan Rate—The anodic polarization curve in Fig. 2 illustrates a typical slow-scan (1 V/h) potentiodynamic response for Type 304 stainless steel (180 grit surface finish on test electrode) starting at the steady state corrosion potential in a neutral, concentrated chloride environment. A

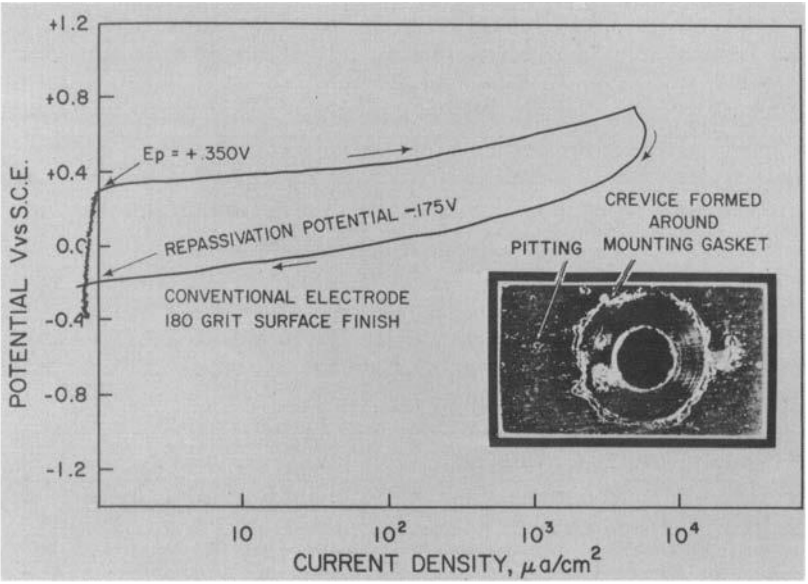

FIG. 2—*Type 304 stainless steel anodic polarization curve and test electrode for a 1.0-V/h potentiodynamic scan in hydrogen purged, 25°C, 4 percent sodium chloride.*

noble E_p value was measured by the active-to-noble potential scan. Reversing the potential scan direction created a hysteresis loop and a repassivation potential more active than E_p. Visual examination of the test electrode subjected to the slow-scan procedure revealed the presence of pits as well as crevice corrosion around the mounting gasket (Fig. 2).

Increasing the potential scan rate from 1 to 60 V/h and initiating this scan at -2.0 V yielded a completely different polarization curve (Fig. 3). The hysteresis loop observed in the rapid-scan test was much smaller. In addition, there was no visual evidence (×5 magnification) of crevice or pitting attack on the test electrode after polarizing, despite the two decade increase in anodic current density through the passive potential region. Note that the same repassivation potential of -0.175 V was observed in the 1 and 60.0 V/h scans.

Pitting—The 60.0-V/h scan rate caused a more active value for E_p (Fig. 3) than was observed at 1.0 V/h (Fig. 2). However, the exact value of E_p was difficult to determine from the rapid-scan curves due to the apparent gradual slope change of the curves. Additional 60.0-V/h polarization curves were then determined in which the potential axis was expanded on the *x-y* recorder so that only the segment of the anodic curve from -0.300 to $+0.400$ V was recorded.

The magnified anodic curve segments shown in Fig. 4 revealed that this area contains two distinct linear regions at more positive locations than E_p,

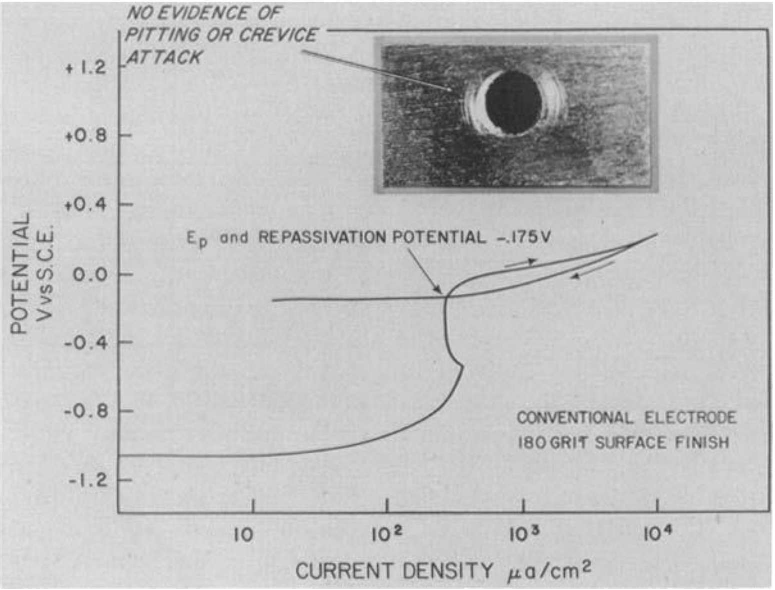

FIG. 3—*Type 304 stainless steel anodic polarization curve and test electrode from a 60.0-V/h potentiodynamic scan in aerated, 25°C, 4 percent sodium chloride.*

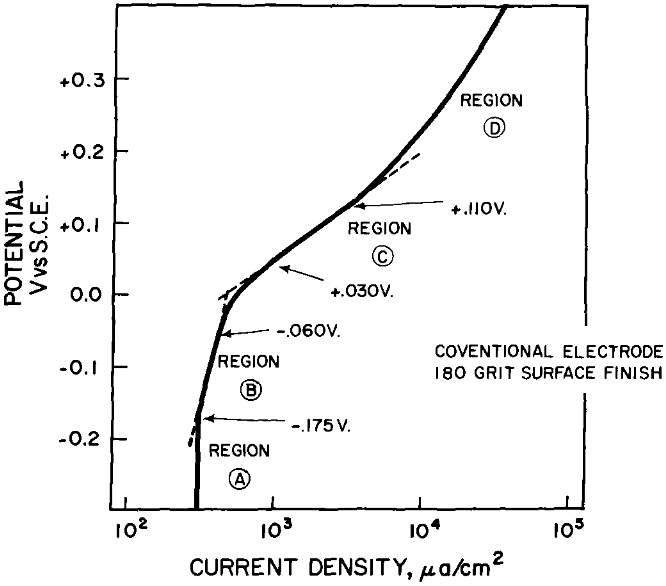

FIG. 4—*Magnified potential axis in the vicinity of* E_p *for 60.0-V/h potentiodynamic scan on Type 304 stainless steel in aerated, 25°C, 4 percent sodium chloride.*

each with a characteristic slope. The more active linear region spans from -0.175 to -0.060 V and the more noble linear region spans from $+0.030$ to $+0.110$ V. For the purposes of the present paper, the passive region, the two linear regions, and the upper-most (nonlinear) region will be referred to as Regions A, B, C, and D, respectively (in order of increasing nobility).

Several constant potential experiments were conducted in an effort to further explore the behavior of the electrode in Regions A and B. The current densities obtained during 60 s at potentials were recorded in each of these regions (Fig. 5). Current density decayed rapidly during the first few seconds at all potentials. At the potential in Region A, the currents continued to decay at a slow rate indicating passive film buildup. At the potential E_p between Regions A and B, the current density reached a plateau after 30 s. At the potential near the active end of Region B, the current density reached a minimum after 30 s and then gradually increased.

In order to investigate the possibility that pitting corrosion occurs in Region B, a test electrode was prepared and held at a potential in Region B for 16 h. For this test electrode the mounting gasket-electrode junction was masked with epoxy paint to reduce possible crevice sites. After 16 h, two large pits developed on one surface as illustrated in Fig. 6, and no evidence of crevice attack could be found at the edge of the epoxy mask.

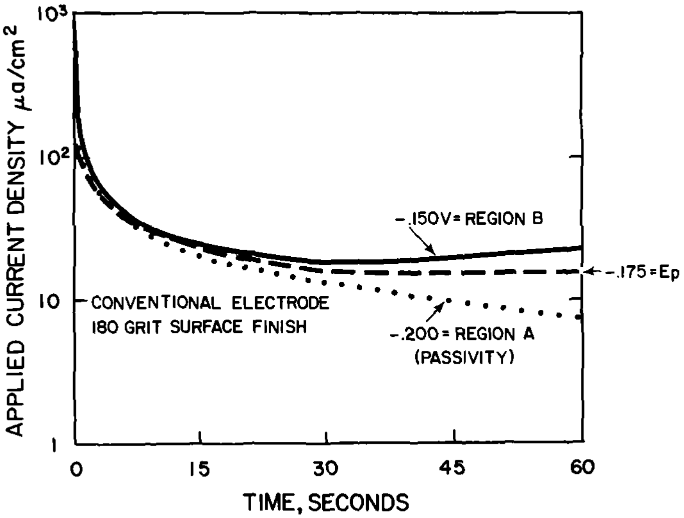

FIG. 5—*Current densities on Type 304 stainless steel for initial 60 s at selected applied constant potentials in aerated, 25°C, 4 percent sodium chloride.*

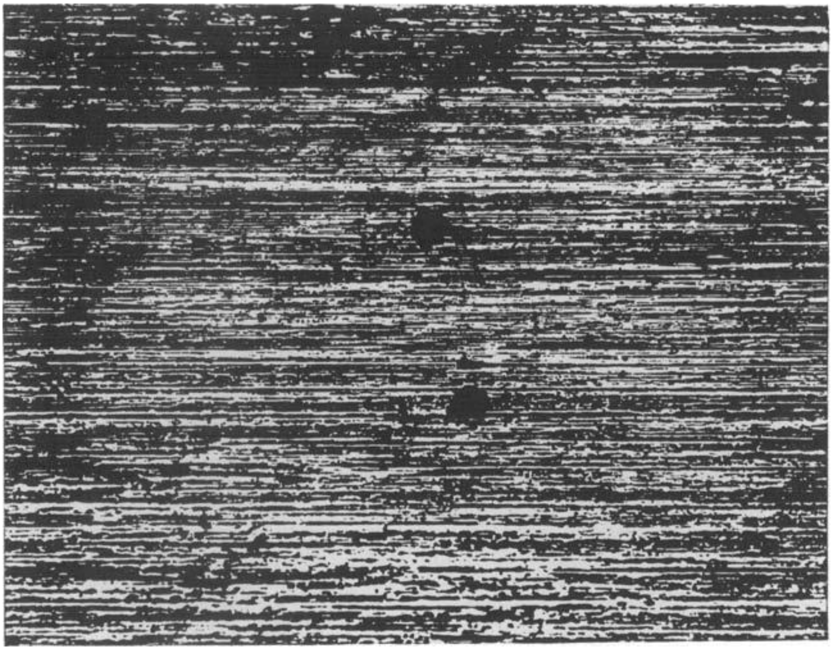

FIG. 6—*Appearance of two pits developed on a Type 304 stainless steel test electrode during 16 h at −0.100 V (SCE) in aerated, 25°C, 4 percent sodium chloride.*

Thus, in Region B pitting occurs and the intersection between Regions A and B could be considered to define E_p.

Crevice Corrosion—In an effort to identify a potential region corresponding to crevice corrosion, 60.0-V/h potentiodynamic polarization curves were determined using the special crevice electrode. Fourteen successive active-to-noble potential scans on this crevice electrode revealed only crevice attack. No evidence of pitting was found. The complete curves were recorded only for the odd numbered scans and are shown in Fig. 7. These curves show that as the crevice propagated with increasing number of scans, the current density at the active-passive transition increased and then remained constant. Similarly, the hysteresis loop grew initially, finally becoming constant. These observations indicate that on continued scanning the crevice environment becomes more aggressive with time until some limiting combination of environmental conditions is achieved.

A close examination of the changes in the magnified anodic polarization curves in the Regions A, B, C, and D (these regions were previously defined in Fig. 4 and that curve is reproduced as the reference curve in Fig. 8) revealed that repeated scanning caused progressive crevice attack and noble shifts in E_p. Note that the magnified curves in Fig. 8 were recorded only on the even numbered scans of the 14-scan experiment. For the first even numbered potential scan, E_p coincided with the intersection between the linear Regions B and C on the reference curve. As the crevice attack

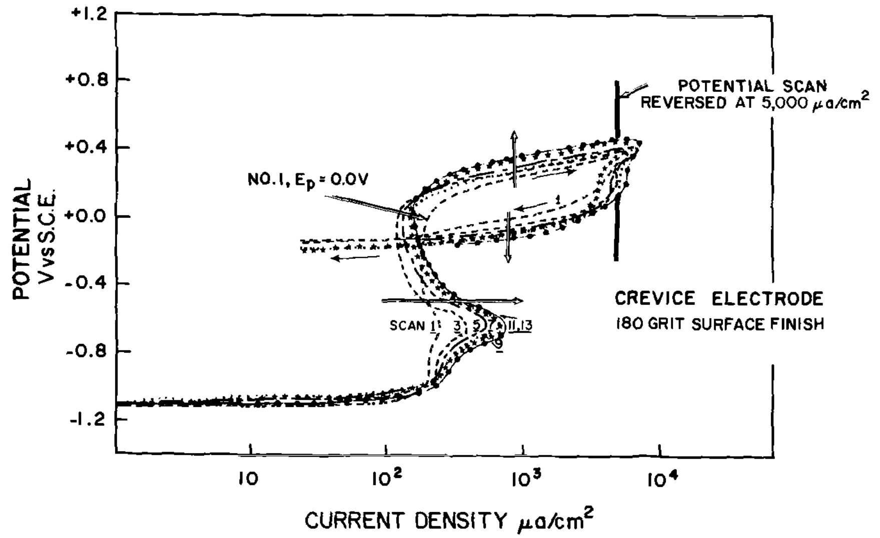

FIG. 7—*Effect of 14 successive 60.0-V/h potentiodynamic scans on the anodic polarization behavior of a Type 304 stainless steel; environment was aerated, 25°C, 4 percent sodium chloride.*

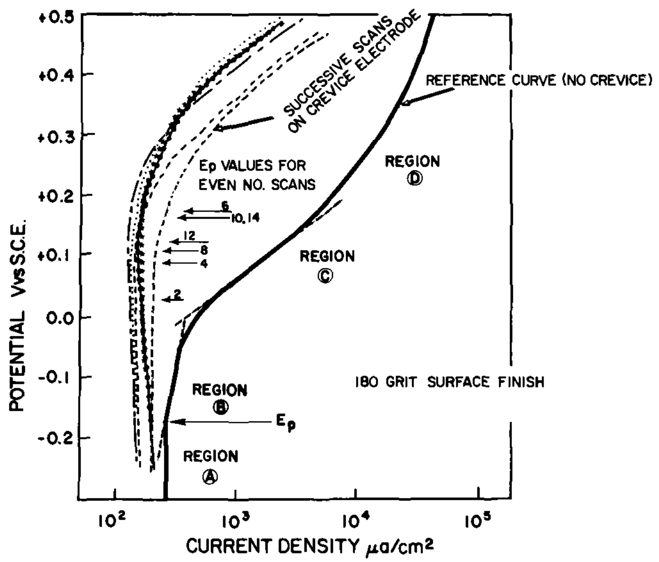

FIG. 8—*Magnified potential axis in the vicinity of* E_p *for successive 60.0-V/h potentiodynamic scans on a Type 304 stainless steel electrode; environment was aerated, 25°C, 4 percent sodium chloride.*

developed during the subsequent potential scans, the E_p values fell within the linear Region C on the reference curve. This observation, together with the observation that only crevice attack occurred on the electrode, suggests that Region C on the reference polarization curve may be related to crevice corrosion. However, further studies are necessary to establish this unambiguously.

Effect of Surface Finish—All of the tests discussed thus far were obtained using Type 304 stainless steel electrodes prepared to a 180 grit surface finish. This surface finish is comparable to the commercial finishes on some stainless steel products. However, in the laboratory it is common practice to test specimens with a finish of 600 grit or finer to enhance visual detection of pit or crevice development. Other workers have noted that surface finish can affect pitting behavior [*19–21*]. In order to confirm that surface finish is an important variable, the previously described experiments were repeated using both creviced and noncreviced electrodes with 600 grit surfaces.

Figure 9 shows that the finer surface finish on the noncreviced electrode raised E_p in the noble direction, from -0.175 to $+ 0.050$ V. The polarization curve obtained using the 600 grit finish was quite similar to the curves obtained using the special crevice test electrode as shown in Fig. 8. Furthermore, visual inspection of this test electrode after polarizing revealed evidence of crevice attack around the mounting gasket. Thus, going from

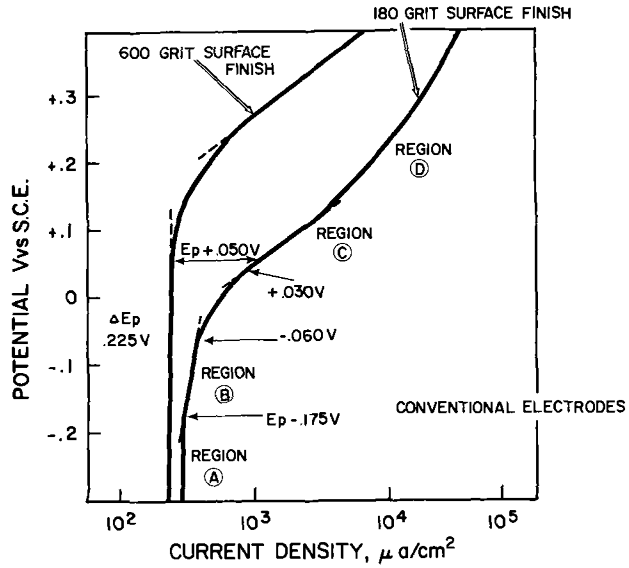

FIG. 9—*Effect of surface finish on the 60.0-V/h potentiodynamic anodic polarization curve for Type 304 stainless steel in the vicinity of* E_p; *environment was aerated, 25°C, 4 percent sodium chloride.*

the rougher 180 grit surface to the finer 600 grit surface appeared to increase pitting resistance but decrease crevice corrosion resistance. It should be noted that evidence of crevice attack was found (×5 magnification) at the mounting gasket crevice site even within the extremely short time of about 15 s required to measure the applied currents above E_p during the 60 V/h potentiodynamic scan.

The 60-s current decay characteristics illustrated in Fig. 10, further describe the effects of mechanical polishing on the pitting resistance of Type 304 stainless steel. The current densities decayed to less than 1 μA/cm^2 during 45 s at potentials of -0.020 and -0.150 V. These potentials corresponded to Regions A and B, respectively, for the rougher 180 grit surfaces. A 16-h constant potential test at -0.150 V failed to produce any evidence of pitting attack. Another 16-h constant potential test just above this E_p produced only crevice attack at the metal-epoxy interface. These observations further confirmed that the 600 grit surface finish led to more resistance to pitting than the 180 grit surface finish.

The effect of fine surface finish on crevice corrosion resistance is demonstrated by the anodic polarization curves shown in Fig. 11. These polarization curves were those obtained on the fourteenth successive 60.0-V/h potential scans on the special crevice electrode. While the E_p values were similar and the repassivation potentials coincided, the current density continued to increase for a longer period of time on the 600 grit finished

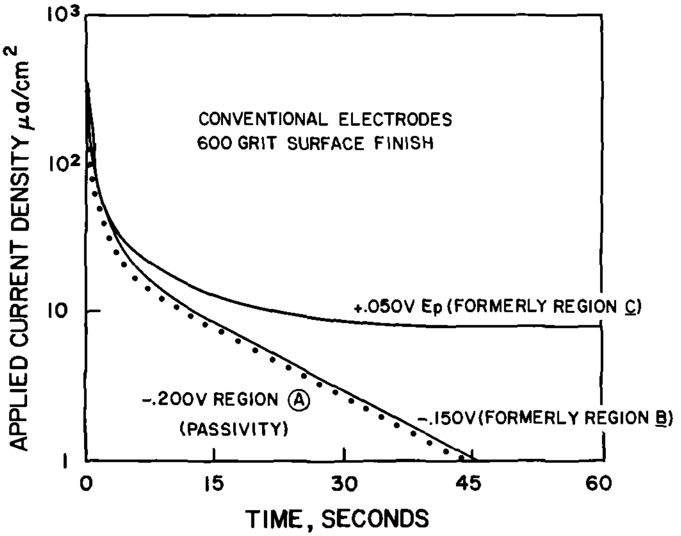

FIG. 10—*Current densities on Type 304 stainless steel for initial 60 s at selected applied static potentials in aerated, 25°C, 4 percent sodium chloride (600 grit surface finish).*

electrode surface after the potential scan was reversed. This suggests that the crevice was more difficult to repassivate on the finer surface finish.

Generally, a comparison of the data for 180 and 600 grit surface finishes suggests that finer mechanical polishing promotes increased resistance to pitting. However, the increase in pitting resistance is accompanied by less crevice corrosion resistance provided that crevice sites exist.

Type 316 Stainless Steel

Having defined the portions of the 60-V/h polarization curve related to pitting of Type 304 stainless steel, it was decided to also examine the behavior of molybdenum-containing Type 316 stainless steel. It has been well established that molybdenum, at levels found in Type 316 stainless steel, is beneficial for pitting resistance. The polarization curve segments illustrated in Fig. 12 confirm electrochemically this beneficial effect of molybdenum. Comparing the measurements on 180 grit surfaces for Type 316 (Fig. 12) and Type 304 (Fig. 9) shows that molybdenum in Type 316 displayed E_p from -0.175 to $+0.070$ V, reduced the slope of the anodic curve above E_p ,and noticeably shortened the potential span of Region B. The noble E_p shift suggests that more oxidizing environments are required to cause pit initiation in Type 316 stainless steel than in Type 304 stainless steel.

Assuming, based on this work, that Region C is an electrochemical response due to crevice corrosion and considering the established fact

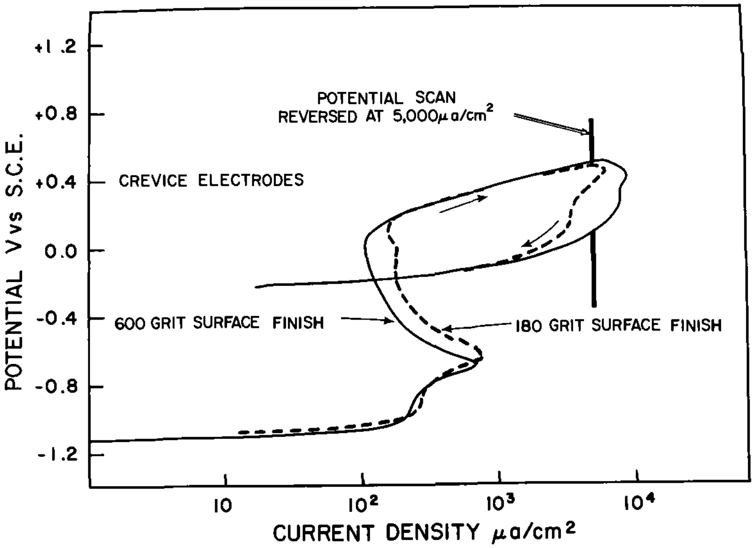

FIG. 11—*Effect of surface finish on Type 304 stainless steel after the fourteenth successive 60.0-V/h potentiodynamic polarization scan, environment was aerated, 25°C, 4 percent sodium chloride.*

that lower current density (a steeper slope in Region C) corresponds to better crevice corrosion resistance, then Type 316 stainless steel (Fig. 12) should be more resistant to crevice corrosion than Type 304 stainless steel (Fig. 9).

The anodic polarization curves for Types 304 and 316 stainless steels obtained using 180 and 600 grit surface finishes are shown in Fig. 13. Two points are evident from this figure. The first one is that Type 316 stainless steel responds to finer surface finishes in a manner similar to Type 304 stainless steel. The second and most generally important point is that any electrochemical comparisons aimed at detecting effects due to compositional differences must be carried out using identical surface finishes.

Discussion

Time is an important variable in the study of pitting and crevice corrosion. This work has shown that increasing the potential scan rate to 60.0-V/h limited pit and crevice development on the electrode by reducing the test time. Consequently, reproducible anodic polarization curves were obtained by eliminating interference from the local environmental changes that are associated with pit or crevice propagation.

Time is also an important factor in constant potential tests. The low current density values at or near E_p require long test periods to produce

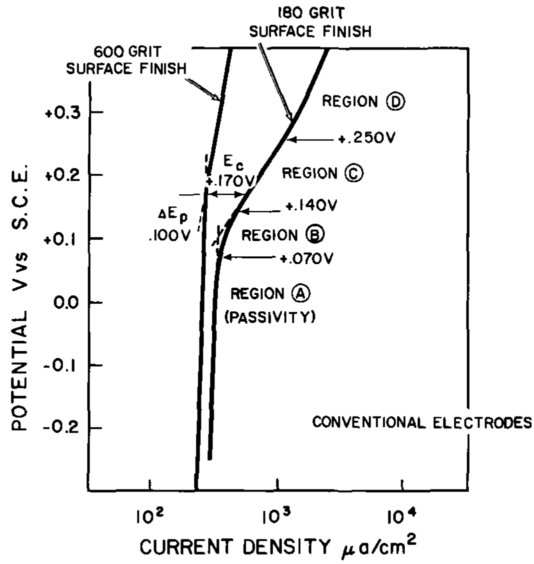

FIG. 12—*Magnified potential axis in the vicinity of* E_p *for 60.0-V/h potentiodynamic scans on Type 316 stainless steel in aerated, 25°C, 4 percent sodium chloride. Also, effect of surface finish is illustrated.*

visual evidence of attack, which then cause the responses from local environment changes to interfere. In this study, measuring the current densities attained at constant potentials during the initial 60 s minimized this interference and helped to define E_p in terms of passivation kinetics.

A close examination of the anodic polarization curve in the potential region near E_p suggests that pits can be developed in constant potential tests only under certain test conditions. If Region B is extremely narrow due to inherent pitting resistance, or a fine surface finish or both, then a potential corresponding to Region B may be difficult to locate. If the potential selected for a static test lies in Region C instead of Region B, then crevice attack would be expected to occur. Thus, if crevice attack is developed in a static potential test, this does not imply that crevice attack occurs at more active potentials than pitting attack. If may simply mean that the electrode was held at a potential in Region C.

Sixteen-hour constant potential tests performed in this investigation produced pits on a 180 grit surface correlating with a well defined Region B on the polarization curve. Attempts to reproduce this attack on a 600 grit surface failed, and for this surface finish Region B was poorly defined. These observations demonstrate how surface finish can cause one to choose a potential outside the pitting region during a static test.

The effects of surface finish on electrochemical response noted in this investigation suggest that laboratory data will be of little value in antici-

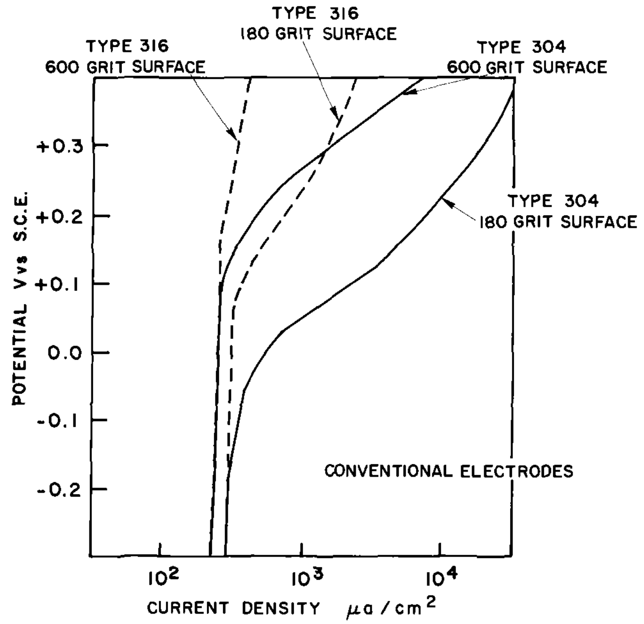

FIG. 13—*Effect of surface finish and alloy composition on the 60.0-V/h potentiodynamic polarization behavior in the vicinity of* E_p *in aerated, 25°C, 4 percent sodium chloride.*

pating in-service corrosion behavior unless surfaces comparable to those used in service are examined. Furthermore, if the surfaces of service equipment are not uniform, some unexpected corrosion behavior may develop. In particular, care should be taken in anticipating the corrosion behavior of ground surfaces adjacent to welded joints, where differences in finish may exist. The crossing of polarization curves for 600 grit finished Type 304 stainless steel and 180 grit finished Type 316 stainless steel in Fig. 13 reveals that under certain conditions surface finish can dominate electrochemical response. If grinding of welded joints is a requirement in service, then electrochemical evaluation of this type of surface finish should be included.

It is also obvious that great care should be taken in selecting a representative environment for laboratory evaluation. Referring again to Fig. 13, it is seen that the anodic polarization curves for a Type 304 stainless steel specimen with a 600 grit finish and a Type 316 stainless steel specimen with a 180 grit finish cross over at a noble potential. Thus, the relative corrosion behavior of these two specimens would be dependent on the oxidizing power of the corrodant used.

A final point that should be noted is the electrochemical responses of pitting corrosion and crevice corrosion appear to be revealed on a single anodic polarization curve. The possibility exists, therefore, that further research will enable a single electrochemical test to be developed capable of defining both these forms of localized corrosion. Further studies are in progress aimed at exploring the relationship between crevice attack and Region C on the anodic polarization curve.

References

[*1*] Pourbaix, M., *Corrosion Science*, Vol. 3, 1963, p. 239.
[*2*] Schwenk, W., *Corrosion Science*, Vol. 5, 1965, p. 245.
[*3*] Leckie, H. P. and Uhlig, H. H., *Journal of the Electrochemical Society*, Vol. 113, 1966, p. 1262.
[*4*] Bond, A. P. and Lizlovs, E. A., *Journal of the Electrochemical Society*, Vol. 115, 1968, p. 1130.
[*5*] Wilde, B. E., *Corrosion*, Vol. 28, No. 8, 1972, p. 283.
[*6*] Johnson, M. J. in *Localized Corrosion—Cause of Metal Failure, ASTM STP 516*, American Society for Testing and Materials, 1972, pp. 262–272.
[*7*] Broli, Aa, Holtan, H., and Midjo, M., *British Corrosion Journal*, Vol. 8, July 1973, p. 175.
[*8*] Rosenfeld, I. L. and Marshakov, I. K., *Corrosion*, Vol. 20, 1964.
[*9*] France, W. D., Jr. and Greene, N. D., Jr., *Corrosion*, Vol. 24, 1968, p. 247.
[*10*] Lizlovs, E. A., *Journal of the Electrochemical Society*, Vol. 117, 1970, p. 1335.
[*11*] Suzuki, T. and Kitamura, *Y.*, *Corrosion*, Vol. 28, No. 1, 1972, p. 1.
[*12*] France, W. D., Jr. in *Localized Corrosion—Cause of Metal Failure, ASTM STP 516*, American Society for Testing and Materials, 1972, pp. 164–200.
[*13*] Pessall, N. and Liu, C., *Electrochimica Acta*, Vol. 16, 1971, pp. 1987–2003.
[*14*] Lizlovs, E. A. and Bond, A. P., *Journal of the Electrochemical Society*, Vol. 116, 1969, p. 574.
[*15*] Herbsheb, G., *Werkstoffe und Korrosion*, Vol. 17, 1966, p. 649.
[*16*] Leckie, H. P., *Journal of the Electrochemical Society*, Vol. 117, 1970, p. 1152.
[*17*] Lizlovs, E. A. and Bond, A. P., "An Evaluation of Some Electrochemical Techniques for the Determination of Pitting Potentials of Stainless Steel," presented at the Annual Meeting, National Association of Corrosion Engineers, Chicago, Ill., 7 March 1974.
[*18*] Jackson, R. P. and Van Rooyen, D. in *Localized Corrosion—Cause of Metal Failure, ASTM STP 516*, American Society for Testing and Materials, 1972, p. 210.
[*19*] Smith, H. A., *Metal Progress*, Vol. 33, 1938, p. 596.
[*20*] Isaacs, H. S. and Kissel, G., *Journal of the Electrochemical Society*, Vol. 119, No. 12, 1972, p. 1628.
[*21*] Hospadaruk, V. and Petrocelli, J. J., *Journal of the Electrochemical Society*, Vol. 113, 1966, p. 878.
[*22*] Greene, N. D. in *Experimental Electrode Kinetics*, Rensselaer Polytechnic Institute, Troy, N. Y., 1965, p. 5.
[*23*] Morris, P. E. and Scarberry, R. C., *Corrosion*, Vol. 26, No. 7, 1970, p. 169.
[*24*] Morris, P. E. and Scarberry, R. C., *Corrosion*, Vol. 28, No. 12, 1972, p. 444.

STP576-EB/Feb. 1976

Compilation of Literature References on Pitting Corrosion[1]

Aluminum

[1] Aziz, P. M. and Godard, H. P., "Pitting Corrosion Characteristics of Aluminum: Influence of Magnesium and Manganese," *Industrial and Engineering Chemistry*, Vol. 44, No. 8, Aug. 1956, pp. 1791–1795.
[2] Porter, F. C. and Hadden, S. E., "Corrosion of Aluminum Alloys in Supply Waters," *Journal of Applied Chemistry*, Vol. 3, Sept. 1953, p. 385.
[3] Aziz, P. M., "Views on the Mechanism of Pitting Corrosion of Aluminum," *Corrosion*, Vol. 9, No. 3, March 1953, pp. 85-90.
[4] Aziz, P. M., "Radioactive Tracers in the Study of Pitting Corrosion on Aluminum," *Journal of the Electrochemical Society*, Vol. 101, No. 3, March 1954, pp. 120–127.
[5] Aziz, P. M. and Godard, H. P., "Pitting Corrosion Characteristics of Aluminum: Influence of Iron and Silicon," *Corrosion*, Vol. 10, No. 9, Sept. 1954, pp. 269–272.
[6] Aziz, P. M. and Godard, H. P., "Influence of Specimen Area on the Pitting Probability of Aluminum," *Journal of the Electrochemical Society*, Vol. 102, No. 10, Oct. 1955, pp. 577–579.
[7] Aziz, P. M., "Application of the Statistical Theory of Extreme Values to the Analysis of Maximum Pit Depth Data for Aluminum," *Corrosion*, Vol. 12, Oct. 1956, p. 495t.
[8] Hagyard, T. and Santhiapillai, J. R., "Pitting Corrosion of Aluminum in Sodium Chloride Solutions," *Journal of Applied Chemistry*, Vol. 9, Part 6, June 1959, pp. 323–330.
[9] Bassett, G. A. and Edeleanu, C., "Pitting of Aluminum at Grain Boundaries After Aging," *Philosophical Magazine*, Vol. 5, No. 60, Dec. 1960, pp. 1217–1220.
[10] Godard, H. P., "The Corrosion Behavior of Aluminum in Natural Waters," *Canadian Journal of Chemical Engineering*, Vol. 38, Oct. 1960, p. 167.
[11] Porter, F. C., "Aluminum and Corrosion: A Review of Progress in 1960," *Corrosion Prevention and Control*, Vol. 8, Jan. 1961, pp. 37–43.
[12] Videm, K., "Pitting Corrosion of Aluminum in Contact with Stainless Steel," *Teknsk Ukeblad*, Vol. 108, No. 33, 1961, pp. 775–784 (Norwegian).
[13] Booth, F. F. and Latimer, K. G., "Aluminum Alloys—Corrosion Behavior in an Industrial Environment," *Corrosion Technology*, Vol. 9, No. 11, Nov. 1962, pp. 315–320.
[14] Ailor, W. H., Jr. and Reinhart, F. M., "Ten-Year Weathering Data on Aluminum Alloys," *Materials Protection*, Vol. 2, No. 6, June 1963, pp. 30–31, 33, 36.
[15] Kaesche, H., "Investigations on the Corrosion of Aluminum," *Werkstoffe und Korrosion*, Vol. 14, No. 7, July 1963, pp. 557–565.
[16] Fujiwari, T. and Shingai, T., "On Micro-Pits Produced by Formation of $FeAl_3$ in Rolled Plate of Extra Super-Duralumin (7075–T6)," *Nippon Kinzoku Gekkai-Si*, Vol. 28, No. 9, 1964, pp. 502–507 (Japanese).

[1] Compiled by L. C. Rowe, Chairman of a Task Group on Pitting Corrosion under ASTM Subcommittee G01.05 on Laboratory Corrosion Tests. Many of the references were contributed by members of the task group; others were obtained from surveys, indexes, and a search of particular journals. No compilation is ever complete, but these references provide a good review of the activity in pitting corrosion during the last 15 years.

[*17*] Koehler, E. L. and Evans, S., "Pitting and Uniform Corrosion of Aluminum by pH 3.5 Citrate Buffer Solution," *Journal of the Electrochemical Society*, Vol. 111, No. 1, Jan. 1964, pp. 17–21.

[*18*] Murray, G. A. W., "Artificial Pits for Quantitative Studies of Corrosion of Aluminum Alloys in Natural Waters," *Corrosion*, Vol. 20, Oct. 1964, pp. 329t–334t.

[*19*] Kaesche, H., "On Uniform Dissolution and Pitting of Aluminum Electrodes," *Korrosion*, Vol. 16, 1964, pp. 17–19.

[*20*] Campbell, H. S., "Corrosion and Protection of Aluminum Alloys Underground," *Journal of the Institute of Metals*, Vol. 93, 1964–65, p. 97.

[*21*] Storchai, E. I. and Turkovskaya, A. V., "Investigation of Susceptibility to Spot and Pitting Corrosion in Some Aluminum Alloys," *Khim Neftyanoe Mashinostr*, No. 3, 1965, pp. 32–34 (Russian).

[*22*] Storchai, E. I. and Turkovskaya, A. V., "Pitting Corrosion of Aluminum Alloys," *Protection of Metals*, Vol. 1, No. 3, May-June 1965, p. 256.

[*23*] Hüber, W. and Wranglén, G., "Studies on the Mechanism of the Pitting Corrosion of Aluminum," *Current Corrosion Research in Scandinavia*, Kemian Keskusliito, r. y., Helsinki, Finland, 1965.

[*24*] Bond, A. P., Bolling, G. F., Domian, H. A., and Biloni, H., "Microsegregation and the Tendency for Pitting Corrosion in High-Purity Aluminum," *Journal of the Electrochemical Society*, Vol. 113, Aug. 1966, p. 773.

[*25*] Freiman, L. I. and Kolotyrkin, Ya. M., "Pitting Corrosion of Aluminum in Solutions of Sodium Perchlorate and Chloric Acid," *Zaschita Metallov*, Vol. 2, No. 4, 1966, pp. 488-490 (Russian).

[*26*] Elze, J., "Causes and Forms of Pitting of Aluminum Anodized by the GX Process," *Mitteilungen der Forschungsgesellschaft Blechverarbeitung*, Vol. 17, 1966 (German).

[*27*] Sugimoto, K., Sawada, Y., and Morioka, S., "Pitting Dissolution Behaviors of Pure Aluminum and SAP (Sintered Aluminum Powders) in Weak Alkaline Aqueous Solutions of NaCl," *Journal of the Japan Institute of Metals*, Vol. 30, No. 10, Oct. 1966, pp. 977–984 (Japanese).

[*28*] Kasen, M. B., Taggart, R., and Polonis, D. H., "The Effects of Environment on Surface Pit Formation in Aluminum," *Philosophical Magazine*, Vol. 13, 1966.

[*29*] Ailor, W. H., "Five-Year Corrosion of Aluminum Alloys at Several Marine Sites," *British Corrosion Journal*, Vol. 1, May 1966, p. 237.

[*30*] Izaki, T. and Arai, K., "Studies on Pitting Corrosion of Aluminum and Its Alloys in Neutral Solutions," *Journal of the Japan Institute of Metals*, Vol. 31, No. 9, Sept. 1967, pp. 1023-1028 (Japanese).

[*31*] Murray, G. A. W., Lamb, H. J., and Godard, H. P., "Role of Iron in Aluminum on the Initiation of Pitting in Water," *British Corrosion Journal*, Vol. 2, No. 6, Nov. 1967, pp. 216–218.

[*32*] Penn, J. H. and Murray, G. A. W., "Effect of Acidic Gelatinous Materials on Pitting Corrosion of Aluminum Hollow-Ware," *British Corrosion Journal*, Vol. 2, No. 5, 1967, pp. 193–194.

[*33*] Johnson, W. K. and Wright, T. E., "The Effect of Small Additions of Copper on the Corrosion Resistance of Aluminum and Aluminum Alloys," *Aluminum*, Vol. 43, No. 8, Aug. 1967, pp. 490–496 (German).

[*34*] Horibe, K., "Studies on Pit Formation on Aluminum Immersed in Artificial Waters," *Journal of the Japan Institute of Light Metals*, Vol. 18, No. 11, Nov. 1968, pp. 579–585 (Japanese).

[*35*] Kassayura, V. P. and Zaretskii, E. M., "Anodic Behavior of Aluminum in Solutions of Sodium Nitrate in the Presence of Chloride Ions," *Protection of Metals*, Vol. 4, No. 4, July-Aug. 1968, p. 343.

[*36*] Tapper, R. W., "Corrosion of Aluminum—Literature Review," *British Corrosion Journal*, Vol. 3, Nov. 1968, pp. 285–287.

[*37*] Tegun, O., "Pitting in Aluminum and its Alloys in Pure Water," *Journal of the Japan Institute of Metals*, Vol. 18, March, pp. 127–138.

[*38*] Sugimoto, K., Sawada, Y., and Morioka, S., "Effects of Matrix Purity and Environment Factors on the Anodic Pitting Dissolution Behaviors of Aluminum," *Nippon Kinzoku Gakkai-Si*, Vol. 32, No. 9, 1968, pp. 842–848 (Japanese).

[*39*] Ailor, W. H., Jr., "Performance of Aluminum Alloys at Other Test Sites," *Metal Corrosion in the Atmosphere, ASTM STP 435*, American Society for Testing and Materials, 1968, p. 285.

[*40*] McGeary, F. L., Summerson, T. J., and Ailor, W. H., Jr., "Atmospheric Exposure of Non-Ferrous Metals and Alloys—Aluminum: Seven-Year Data," *Metal Corrosion in the Atmosphere, ASTM STP 435*, American Society of Testing and Materials, 1968, p. 141.

[*41*] Ailor, W. H., Jr., Evaluation of Aluminum After One-Year Deep Sea Exposure," *Journal of Hydronautics*, Vol. 2, No. 1, Jan. 1968, p. 26.

[*42*] Böhni, H. and Uhlig, H. H., "Environmental Factors Affecting the Critical Pitting Potential of Aluminum," *Journal of the Electrochemical Society*, Vol. 116, 1969, p. 906.

[*43*] Di Russo, E., Prati, A., and Sacchi, F., "Investigation on the Mechanism of Pitting Corrosion of Anodized Alloy Al-Mg-Si for Architectural Purposes," *Allumino*, Vol. 38, No. 1, Jan. 1969, pp. 3–13 (Italian).

[*44*] Ailor, W. H., Jr., "A Review of Aluminum Corrosion in Tap Water," *Journal of Hydronautics*, Vol. 3, No. 3, July 1969, p. 105.

[*45*] Ailor, W. H., Jr., "Aluminum Corrosion at Urban and Industrial Locations," *Journal of the Structural Division*, Vol. 95, No. ST10, Oct. 1969, pp. 2141–2160.

[*46*] Ailor, W. H., Jr., "Aluminum Alloys After Five Years in Seawater," *Materials Performance and the Deep Sea, ASTM STP 445*, American Society for Testing and Materials, 1969, p. 115.

[*47*] Storchai, E. I. and Turkovskaya, A. V., "Use of Charge Curves for Determining the Potential of Pitting Formation on Aluminum Alloys," *Industrial Laboratory*, Vol. 35, No. 6, June 1969, pp. 851–852.

[*48*] Arora, O. P., Isasi, J. A., and Metzger, M., "Protective Films and Structure-Dependent Corrosion in Aluminum," *Corrosion*, Vol. 25, No. 11, Nov. 1969, pp. 445–454.

[*49*] Horibe, K., "Studies on Pit Formation on Aluminum Immersed in Artificial Waters," *Journal of the Japan Institute of Light Metals*, Vol. 19, No. 3, March 1968, pp. 105–111, 184–188 (Japanese).

[*50*] Ishida, S., "Some Studies on Pit Formation on Aluminum Immersed in Waters," *Proceedings of the Third International Congress on Metallic Corrosion*, National Association of Corrosion Engineers, Vol. 1, Houston, Tex., 1969, pp. 179–185.

[*51*] Richardson, J. A. and Wood, G. C., "A Study of the Pitting Corrosion of Al by Scanning Electron Microscopy," *Corrosion Science*, Vol. 10, 1970, p. 313.

[*52*] Lorking, K. F. and Mayne, J. E. O., "The Corrosion of Aluminum," *Journal of Applied Chemistry*, Vol. 11, May 1961, p. 170.

[*53*] Goto, K., Ito, G., and Shimizu, Y., "Effect of Some Oxidizing Agents on Pitting Corrosion of Aluminum in Neutral Water," *Journal of Japan Institute of Light Metals*, Vol. 20, Feb. 1970, pp. 88–94 (Japanese).

[*54*] Paydya, B. A., Sampat, S. S., Vora, J. C., and Trivedi, A. M., "Corrosion of Aluminum in Salt Mixtures and the Influence of Copper Ions on Corrosion," *Werkstoffe und Korrosion*, Vol. 21, No. 10, 1970, pp. 801–803 (German).

[*55*] Pourbaix, M., "Some Aluminum Corrosion Problems and Their Practical Repercussions," *Revue de l'Aluminum*, Vol. 386, June 1970, pp. 639–647 (French).

[*56*] Storchai, E. I. and Turkovskaya, A. V., "Pitting of Aluminum Alloys in Solutions of of NaCl Without Oxidizing Agent," *Zaschita Metallov*, Vol. 6, No. 6, 1970 (Russian).

[*57*] Johnson, W. K., "Recent Developments in Pitting Corrosion of Aluminum," *British Corrosion Journal*, Vol. 6, 1971, p. 200.

[*58*] deDeMichele, S. M. and Galvele, J. R., "Morphology of Pitting Corrosion of Aluminum in Different Electrolytes," *Metalurgia A.B.M.*, Vol. 27 (165), Aug. 1971, pp. 589–596 (Portuguese).

[*59*] Inoue, T., Kato, M., Goto, K., Ito, G., and Shimizu, Y., "Effects of pH and Dissolved Oxidizing Agents on Pitting Corrosion of Aluminum," *Journal of the Japan Institute of Light Metals*, Vol. 21, No. 1, Jan. 1971, pp. 27–35 (Japanese).

[*60*] Ronzhin, M. N., Pedanova, V. G., and Rozenfeld, I. L., "Method of Studying the Electrochemical Heterogeneity of Welds in Aluminum Alloys," *Zavodskaia Laboratoriia*, Vol. 37, No. 7, 1971, pp. 792–795 (Russian).

[*61*] Bogar, F. D. and Foley, R. T., "The Influence of Chloride Ion on the Pitting of

Aluminum," *Journal of the Electrochemical Society*, Vol. 119, No. 4, April 1972, pp. 462–464.

[*62*] Dunn, C. G. and Witter, D. R., "h-Pits Produced by Hydrating and Annealing Aluminum Foil," *Journal of the Electrochemical Society*, Vol. 119, No. 9, 1972.

[*63*] Rosenfeld, I. L., Ronzhin, M. N., and Pedanova, V. G., "Effect of Temperature on the Pitting Formation Potential of Aluminum and Its Alloys," *Zaschita Metallov*, Vol. 8, No. 5, 1972.

[*64*] Flasks, V. Ya., "Statistical Model of Size Distribution of Pitting During Atmospheric Corrosion of Aluminum Alloys," *Zaschita Metallov*, Vol. 9, No. 4, 1973.

[*65*] Inoue, T. and Kato, M., "Studies on Pitting Corrosion of Aluminum Using Macro and Micro-Autoradiography," *Journal of the Japan Institute of Light Metals*, Vol. 23, No. 2, Feb. 1973, pp. 78–86 (Japanese).

[*66*] de Wexler, S. B. and Galvele, J. R., "Anodic Behavior of Aluminum Straining and a Mechanism for Pitting," *Journal of the Electrochemical Society*, Vol. 121, No. 10, 1974.

[*67*] Bonewitz, R. A., "An Electrochemical Evaluation of 3003, 3004, and 5050 Aluminum Alloys for Desalination," *Corrosion*, Vol. 30, No. 2, 1974, pp. 53–59.

[*68*] Ishida, S. and Nakamura, H., "Study on Pitting Aluminum Corroded by the Natural Waters," *Proceedings of the Fifth International Congress on Metallic Corrosion*, National Association of Corrosion Engineers, Houston, Tex., 1974, pp. 257–259.

[*69*] Kato, M. and Inoue, T., "Effects of Dissolved Oxidizing Agents and Inhibitors and Pitting Corrosion of Aluminum in Water," *Proceedings of the Fifth International Congress on Metallic Corrosion*, National Association of Corrosion Engineers, Houston, Tex., 1974, pp. 260–263.

[*70*] Foroulis, Z. A., "On the Significance of the Critical Potential of Pitting of Aluminum in Chloride Solutions," *Proceedings of the Fifth International Congress of Metallic Corrosions*, National Association of Corrosion Engineers, Houston, Tex., 1974, pp. 326–331.

[*71*] Videm, K., "Chloride Absorption and Pitting Corrosion of Aluminum: Influence of Electrical Field in the Oxide Film," *Proceedings of the Fifth International Congress on Metallic Corrosion*, National Association of Corrosion Engineers, Houston, Tex., 1974, pp. 264–269.

[*72*] Franz, F. and Novak, P., "Effect of Rotation on the Pitting Corrosion of Aluminum Electrodes," *Localized Corrosion*, R. W. Staehle, B. F. Brown, J. Kruger, and A. Agrawal, Eds., National Association of Corrosion Engineers, Houston, Tex., 1974, pp. 576–579.

[*73*] Craig, H. L., Jr., "Kinetic Studies of Aluminum Pitting Reactions, "*Localized Corrosion*, R. W. Staehle, B. F. Brown, J. Kruger, and A. Agrawal, Eds., National Association of Corrosion Engineers, Houston, Tex., 1974, pp. 600–607.

[*74*] Kaesche, H., "Pitting Corrosion of Aluminum and Intergranular Corrosion of Aluminum Alloys," *Localized Corrosion*, R. Staehle, B. F. Brown, J. Kruger, and A. Agrawal, Eds., National Association of Corrosion Engineers, Houston, Tex., 1974, pp. 516–525.

[*75*] Zahavi, J. and Metzger, M., "Breakdown of Films and Initiation of Pits on Aluminum," *Localized Corrosion*, R. W. Staehle, B. F. Brown, J. Kruger, and A. Agrawal, Eds., National Association of Corrosion Engineers, Houston, Tex., 1974, pp. 547–555.

[*76*] Pryor, M. J., "The Influence of the Defect Structure of Aluminum Oxide Films on the Pitting of Aluminum in Chloride Solutions," *Localized Corrosion*, R. W. Staehle, B. F. Brown, J. Kruger, and A. Agrawal, Eds., National Association of Corrosion Engineers, Houston, Tex., 1974, pp. 2–11.

[*77*] Galvele, J. R., de Micheli, S. M., Muller, I. L., de Wexler, S. B., and Alanis, I. L., "Critical Potentials for Localized Corrosion of Aluminum Alloys," *Localized Corrosion*, R. W. Staehle, B. F. Brown, J. Kruger, and A. Agrawal, Eds., National Association of Corrosion Engineers, Houston, Tex., 1974, pp. 580–599.

[*78*] Wood, G. C., Sutton, W. H., Richardson. J. A., Riley, T. N. K., and Malherbe, A. G., "The Mechanism of Pitting of Aluminum and Its Alloys," *Localized Corrosion*, R. W. Staehle, B. F. Brown, J. Kruger, and A. Agrawal, Eds., National Association of Corrosion Engineers, Houston, Tex., 1974. pp. 526–546.

Copper

[*79*] Tracy, A. W., "Copper and Its Alloys, Classes and Types, Corrosion Characteristics and Applications," *Proceedings*, Short Course on Process Industry Corrosion, National Association of Corrosion Engineers, 1960, pp. 83–97.

[*80*] Hatch, G. B., "Unusual Cases of Copper Corrosion," *Journal of American Water Works Association*, Vol. 53, No. 11, 1961, pp. 1417–1428.

[*81*] Young, F. W., Jr., "Etch Pits at Dislocations in Copper," *Journal of Applied Physics*, Vol. 32, Feb. 1961, pp. 192–201.

[*82*] Tracy, A. W., "Corrosion of Copper Alloys," *Chemical Engineering*, Vol. 69, No. 1, 8 Jan. 1962, pp. 130, 132–133.

[*83*] Subramanyan, N., Venugopalan, K., and Dandapani, B., "A Note on the Corrosion of Heat Exchanger Tubes of Transformer Rectifier Coolers," *Current Engineering Practice*, Vol. 5, No. 7, Jan. 1963, pp. 8–10.

[*84*] Bertocci, V., Hulett, L. D., and Jenkins, L. H., "On the Formation of Electrochemical Etch Pits on the (III) Face of Copper," *Journal of the Electrochemical Society*, Vol. 110, No. 12, Dec. 1963.

[*85*] Tracy, A. W., "Where and When to Use Copper Alloys," *Chemical Engineering Progress*, Vol. 59, No. 9, Sept. 1963, pp. 78–83.

[*86*] Van Muylder, J., Pourbaix, M., Van Laer, P., de Zoubov, N., and Pourbaix, A., "Relationship Between Electrode Voltage and Mechanism of Copper Corrosion in Presence of Brussels Water," Report No. 126, Centre Belge d'Etude de la Corrosion, Brussels, Belgium, May 1965 (French).

[*87*] Van Muylder, J., Pourbaix, M., and Van Laer, P., "Electrochemical Characteristics of Corrosion Pitting of Copper in Presence of Water and Aqueous Chloride Solutions," Report No. 127, Centre Belge D'Etude de la Corrosion, Brussels, Belgium, May 1965 (French).

[*88*] Campbell, H. S., "Pitting Corrosion of Copper Water Pipes," *Proceedings of Second International Congress on Metallic Corrosion*, National Association of Corrosion Engineers, Houston, Tex., 1966, pp. 237–242.

[*89*] von Franque, O., "Pitting Corrosion on Copper Pipes," *Wersktoffe und Korrosion*, Vol. 19, 1968, pp. 377–384.

[*90*] Lucey, V.F., "Developments Leading to the Present Understanding of the Mechanisms of Pitting Corrosion of Copper," *British Corrosion Journal*, Vol. 7, 1972, pp. 36–41.

[*91*] Campbell, H. S., "A Review: Pitting Corrosion of Copper and Its Alloys," *Localized Corrosion*, R. W. Staehle, B. F. Brown, J. Kruger, and A. Agrawal, Eds., National Association of Corrosion Engineers, Houston, Tex., 1974, pp. 625–638.

Electroplated Coatings

[*92*] Flint, D. N., "Pitting Corrosion Causes Electroplate Breakdown," *Industrial Finishing*, Vol. 12, No. 143, 1960, pp. 48–51.

[*93*] Hospadaruk, V. and Petrocelli, J. V., "The Relative Reactivity of Various Nickel Electrodeposits," *Plating*, Vol. 48, No. 5, May 1961, pp. 479–487.

[*94*] Flint, G. N. and Melbourne, S. H., "The Corrosion of Decorative Ni + Cr Coatings: A Metallographic and Potential Study," *Transactions*, Institute of Metal Finishing, Vol. 38, Part 2, pp. 35–44, Part 3, pp. 89–94, May 1961; or *Journal of Metal Finishing*, Vol. 7, June 1961, pp. 218–221, 233.

[*95*] Wesley, W. A., "Pitting of Decorative Nickel-Chromium Coatings," *Technical Proceedings of American Electroplaters Society*, Vol. 50, 1963, pp. 9–16.

[*96*] Maloof, S. R., "The Electrochemical Behavior of Decorative Nickel-Chromium Coatings in 3% NaCl under Potentiostatic Conditions," *Journal of the Electrochemical Society*, Vol. 116, Sept. 1969, p. 1293.

Environmental Effects

[*97*] Haarmann, R. and Rädeker, W., "Pitting Corrosion Caused by Molten Metals," *Metalloberfläche*, Vol. 14, No. 2, 1960, pp. 36–40.

[*98*] Gilbert, P. T., "Corrosion Problems Arising in Tubular Heat-Exchange Equipment," *Society Chemical Industry Monograph No. 10* (Corrosion Problems of the Petroleum Industry), 1960, pp. 111–120.

[*99*] Chen, N. G., "Pitting Corrosion Inhibitor," *Journal of Applied Chemistry*, Vol. 33, Oct. 1960, pp. 2300–2305 (Russian).

[*100*] Rowe, L. C. and Walker, M. S., "Effect of Mineral Impurities in Water on the Corrosion of Aluminum and Steel," *Corrosion*, Vol. 17, No. 7, July 1961, pp. 353t–356t.

[*101*] Kolotyrkin, Ya. M., "Effects of Anions on the Dissolution Kinetics of Metals," *Journal of the Electrochemical Society*, Vol. 108, No. 3, March 1961, pp. 209–216.

[*102*] Otsu, T. and Okawa, M., "Corrosion Testing on Condenser Tubes by Model Condenser at Shin-Tokyo Power Plant," *Sumitomo Light Metal Tech Reports*, Vol. 2, No. 1, Jan. 1961, pp. 11–38 (Japanese).

[*103*] Raifsnider, P. J. and Wachter, A., "Pitting Corrosion by Water Flood Brines," *Corrosion*, Vol. 17, No. 7, July 1961, pp. 326t-328t.

[*104*] Sakiyama, K. and Fujimoto, M., "Effects of Free Chlorine on the Pitting Corrosion of Gas Cooler Tubes," *Corrosion Engineering*, Vol. 11, No. 7, July 1962, pp. 299–303 (Japanese).

[*105*] Kiwaki, J. and Inai, T., "On Corrosion by Gland Packing," *Review of Kobe University Mercantile Marine*, Part 2, No. 11, March 1964, pp. 21–29 (Japanese).

[*106*] Varga, J. and Sebestyen, G., "Observations on Pitting Velocity Exponent in Flow System," *Periodica Polytechnica*, Mechanical Engineering, Vol. 8, No. 3, 1964, pp. 343–352.

[*107*] Ervin, G., Jr. and MacKay, T. L., "Catastrophic Oxidation of Beryllium Metal," *Journal of Nuclear Materials*, Vol. 12, May 1964, pp. 30–39.

[*108*] Voogel, P., "Pit Corrosion in Internally Painted Cargo and Cargo/Ballast Tanks of Ocean-Going Crude Oil Tankers," *Journal of Oil Color Chemicals Association*, Vol. 48, No. 7, July 1965, pp. 597–602.

[*109*] Dega, R. L., "Corrosion at the Seal," *Mechanical Engineering*, Vol. 88, No. 11, 1966, pp. 48–52.

[*110*] Kolotyrkin, Ya. M., "Effect of the Nature of the Anions on the Kinetics and Mechanism of the Dissolution (Corrosion) of Metals in Electrolyte Solutions," *Protection of Metals*, Vol. 3, No. 2, March-April 1967, p. 101.

[*111*] Rossum, J. R., "Prediction of Pitting Rates in Ferrous Metals from Soil Parameters," *Journal of the American Water Works Association*, Vol. 61, No. 6, 1969.

[*112*] France, W. D., Jr. and Greene, N. D., "Comparison of Chemically and Electrolytically Induced Pitting Corrosion," *Corrosion*, Vol. 26, No. 1, Jan. 1970, pp. 1–4.

[*113*] Brigham, R. J., "Discussion: Chemically and Electrolytically Induced Pitting," *Corrosion*, Vol. 26, No. 5, 1970, p. 200.

[*114*] Azim, A. A. A., "Pitting Corrosion of Pb in $H_2SO_4 + HClO_4$," *Corrosion Science*, Vol. 10, No. 6, June 1970, pp. 421–433.

[*115*] Trabanelli, G. and Zucchi, F., "Measuring the Corrosion Resistance of Four Alloys in Cl Solutions," *Materials Protection and Performance*, Vol. 9, July 1970, p. 16.

[*116*] Beck, T. R., Mahaffey, D. W., and Olsen, J. H., "Pitting and Deposits with an Organic Fluid by Electrolysis and by Fluid Flow," *Journal of the Electrochemical Society*, Vol. 119, No. 2, 1972, pp. 155–160.

[*117*] Barkow, A. G., "Don't Bet on a Pit," *Materials Protection and Performance*, Vol. 11, No. 10, 1972.

[*118*] Mansfeld, F., "Passivity and Pitting of Al, Ni, Ti, and Stainless Steel in $CH_4OH + H_2SO_4$," *Journal of the Electrochemical Society*, Vol. 120, No. 2, 1973.

[*119*] Brigham, R. J. and Tozer, E. W., "Temperature as a Pitting Criterion," *Corrosion*, Vol. 29, No. 1, 1973, pp. 33–36.

[*120*] Postelthwaite, R., Brierley, A., and Walmsley, M. J., "Pitting and Elevated Temperatures," *Localized Corrosion*, R. W. Staehle, B. F. Brown, J. Kruger, and A. Agrawal, Eds., National Association of Corrosion Engineers, Houston, Tex., 1974, pp. 415–426.

Graphite

[*121*] Henning, G. R., "Influence of Lattice Defects and Catalysts on the Surface Reactions of Graphite Single Crystals," *Zeitschrift fur Elektrochemie*, Vol. 66, 1962, pp. 629–635 (German).

[*122*] Blackman, L. C. F., "Oxidation Pitting of Pyrolytic Graphite and Vitreous Carbon," *Carbon*, British Coal Utilisation Research Association, Vol. 5, April 1967, pp. 96–97.

[*123*] McCarroll, B. and McKee, D. W., "Interaction of Atomic Hydrogen and Nitrogen with Graphite Surface," *Nature*, Vol. 225, Feb. 1970, pp. 722–723.

Iron and Steel

[*124*] Freiman, L. I. and Kolotyrkin, Ya. M., "Pitting Corrosion of Iron by Perchlorate Ions," *Doklady Akademii Nauk S.S.S.R., Seriia Fizicheskvi Khimii*, Vol. 153, No. 4, 1963, pp. 886–888, and *Corrosion Science*, Vol. 5, No. 3, 1965, pp. 199-202.

[*125*] Becker, K. E., "Investigation of Pitting Failure of Surfaces Under Normal Stressing," *Proceedings*, Institute of Mechanical Engineers, Vol. 178, No. 3N, 1964, pp. 56–70.

[*126*] Herbsleb, G. and Engell, H. J., "Investigation into Pitting Corrosion of Passive Iron in Sulphuric Acid Containing Chloride Ions," *Werkstoffe und Korrosion*, Vol. 17, 1966, pp. 365–376.

[*127*] Herbsleb, G., "Pitting Corrosion on Metals with Electron-Conductive Passive Layers," *Werkstoffe und Korrosion*, Vol. 17, 1966.

[*128*] Razim, C., "The Influence of Case Structure of Case-Hardened Gears on Susceptibility to Pitting," *Härterei Technische Mittalungen*, Vol. 22, No. 4, 1967, pp. 317–325.

[*129*] Andreeva, Y. A., Shiganova, L. N., and Krasil'shchikov, A. I., "Pitting Corrosion of Iron," *Protection of Metals*, Vol. 4, No. 3, 1968, p. 231, translated from *Zaschita Metallov*, Vol. 4, No. 3, May 1968, pp. 255–259 (Russian).

[*130*] Ashworth, V., Boden, P. J., Leach, J. S., and Nehru, A. Y., "On the Cl^- Breakdown of Passive Films on Mild Steel," *Corrosion Science*, Vol. 10, 1970, p. 481.

[*131*] Vetter, Von K. J. and Strehblow, H. H., "Lochfrabpotentiale und Lochfrabinhibitionspotentiale an Reinem Eisen," *Berichte BunsenGesellschaft*, Vol. 74, 1970, p. 449.

[*132*] Jones, R. L., Strattan, L. W., and Osgood, E. D., "The Potentiostatic Passivation of Mild Steel in 300°C NaOH Solutions," *Corrosion*, Vol. 26, No. 10, Oct. 1970, pp. 399–406.

[*133*] Mueller, W. A., "Electrochemical Study of Crevice Corrosion of Steels in Solutions of Sodium Chloride and Chlorine Dioxide," *Proceedings*, National Association of Corrosive Engineers, 26th Conference, 1970, pp. 468-476.

[*134*] Janik-Czachor, M., Szummer, A., and Szklarska-Smialowska, Z., "Effect of Sulphur and Manganese on Nucleation of Corrosion Pits in Iron," *British Corrosion Journal*, Vol. 7, March 1972, pp. 90–93.

[*135*] Pourbaix, A., "Characteristics of Localized Corrosion of Steel in Chloride Solutions," *Corrosions*, Vol. 27, No. 11, Nov. 1971, pp. 449–454.

[*136*] Schwerdtfeger, W. J., "Polarization Measurements as Related to Corrosion of Underground Steel Piling," *Journal of Research*, National Bureau of Standards, Vol. 75, No. 2, April-June 1971, pp. 107–121.

[*137*] Janik-Czachor, M., "Electrochemical and Microscopic Study of Pitting Corrosion of Ultra-Pure Iron," *British Corrosion Journal*, Vol. 6, No. 2, March 1971, pp. 57–60.

[*138*] Janik-Czachor, M., Wagner, G. H., and Desestret, A., "Evaluation Tests on the Pitting Resistance of Iron-Chromium Alloys," *Corrosion, Traitements, Protection, Finition*, Vol. 19, No. 5, Aug.-Sept. 1971, pp. 249–255 (French).

[*139*] Bardal, E., "pH and Potential Measurements on Mild Steel and Cast Iron During Periodic Cathodic Polarization at 20 and 90°C," *Corrosion Science*, Vol. 11, No. 6, June 1971, pp. 371–382.

[*140*] Spink, G. M. and Ives, M. B., "The Influence of an Air-Formed Film on the Nucleation and Morphology of Etch Pits in Pure Iron," *Journal of the Electrochemical Society*, Vol. 118, No. 6, 1971.

[*141*] Prause, W. and Engell, H. J., "Electrochemical Behavior and Scaling of High-Alloy Manganese Steel," *Werstoffe und Korrosion*, Vol. 22, No. 5, May 1971, pp. 409–420 (German).

[*142*] Butler, G., Stretton, P., and Beynon, J. G., "Initiation and Growth of Pits on High-Purity Iron and Its Alloys and Chromium and Copper in Neutral Chloride Solutions," *British Corrosion Journal*, Vol. 7, July 1972, pp. 168–173.

[*143*] Tousek, J., "Die Kinetik der Lochfrasskorrosion von Metallen," *Corrosion Science*, Vol. 12, 1972, pp. 1–13.

[*144*] Szklarska-Smialowska, Z., "Influence of Sulfide Inclusions on the Pitting Corrosion of Steels," *Corrosion*, Vol. 28, No. 10, 1972, pp. 388–396.

[*145*] Freiman, L. I., Lap, Le Min, and Raskin, G. S., "Role of Local Changes in the Composition of the Solution on the Development of Pitting in Iron," *Zashchita Metallov*, Vol. 9, No. 6, 1973.

[*146*] Peterson, C. W, Soltz, G. C., and Mairs, K., "A Study of an Iron Macro-Pit Induced by Seawater," *Corrosion*, Vol. 30, No. 10, 1974, pp. 366–370.

[*147*] Vetter, K. J. and Strehblow, H. H., "Pitting Corrosion in an Early Stage and Its Theoretical Implications," *Localized Corrosion*, R. W. Staehle, B. F. Brown, J. Kruger, and A. Agrawal, Eds., National Association of Corrosion Engineers, Houston, Tex., 1974, pp. 240–251.

[*148*] McBee, C. L. and Kruger, J., "Events Leading to the Initiation of the Pitting of Iron," *Localized Corrosion*, R. Staehle, B. F. Brown, J. Kruger, and A. Agrawal, Eds., National Association of Corrosion Engineers, Houston, Tex., 1974, pp. 252–260.

[*149*] Davolio, G. and Soragni, E., "Pitting and Crevice Corrosion of Carbon Steel in Inhibited Acid Solutions," *Localized Corrosion*, R. W. Staehle, B. F. Brown, J. Kruger, and A. Agrawal, Eds., National Association of Corrosion Engineers, Houston, Tex., 1974, pp. 270–277.

Iron-Chromium-Nickel Alloys

[*150*] Firestone, J. T., "Rapid Pitting Corrosion on Gas Scrubber: Salt Accumulations Cause Attack Noticeable in Only Three Weeks," *Corrosion*, Vol. 16, No. 12, Dec., 1960, pp. 9–10.

[*151*] Menascé, S. and Montuelle, J., "Electrochemical Study of Pit Corrosion of Stainless Steel in Acid Media," *Comptes Rendus*, Vol. 251, 11 July 1960, pp. 235–236 (French).

[*152*] Graver, D. L., "Pitting Corrosion of Stainless Steel," *Steel Horizons*, Vol. 23, 1961.

[*153*] Schmeling, E. and Röschenbleck, B., "Pit Corrosion and Surface Film Formation on Lead," *Werkstoffe und Korrosion*, Vol. 12, April 1961, pp. 215–223 (German).

[*154*] Brauns, E. and Schwenk, W., "The Kinetics of Pit Corrosion on Passive Chrome-Nickel Steels," *Werkstoffe und Korrosion*, Vol. 12, No. 2, Feb. 1961, pp. 73–80 (German).

[*155*] Brauns, E. and Schwenk, W., "Investigation of Pitting on Chemically Resistant Austenitic Steels," *Archive Fur Das Eisenhuttenwesen*, Vol. 32, June 1961, pp. 387–396 (German).

[*156*] Tagaya, M. and Inaba, T., "Local Corrosion of Stainless Steels in the Atmosphere," *Technology Reports*, Vol. 11, March 1971, pp. 129–135.

[*157*] Prazak, M. and Cibal, V., "The Potentiostatic Investigation of the Effects of Some Alloying Elements on the Electrochemical and Corrosion Properties of Stainless Steels," *Corrosion Science*, Vol. 2, Jan.-March 1962, pp. 71–84.

[*158*] Pourbaix, M., Klimzack-Mathieiu, L., Mertens, Ch., Meunier, J., Vanleugen-Haghe, Cl., de Munck, L., Laureys, J., Neelemans, L., and Warzee, M., "Potentiokinetic and Corrosimetric Investigations of the Corrosion Behavior of Alloy Steels," *Corrosion Science*, Vol. 3, 1963, p. 239.

[*159*] Defranoux, J. M., "Methodes Electrochimiques D'Etude du Comportement des Aciers Inoxydables en Milieu Chlorure," *Corrosion Science*, Vol. 3, 1963, pp. 75–78.

[*160*] Uhlig, H. H. and Gilman, J. R., "Pitting of 18-8 Stainless Steel in Ferric Chloride Inhibited by Nitrates," *Corrosion*, Vol. 20, Sept. 1964, p. 289t.

[*161*] Tomashov, N. D., Chernova, G. P., and Marcova, O. N., "Effect of Supplementary

Alloying Elements on Pitting Corrosion Susceptibility of 18 Cr-14 Ni Stainless Steel," *Corrosion*, Vol. 20, May, 1964, p. 166t.

[*162*] Adachi, Y., "Study of Pitting Corrosion in Stainless Steel: Part I. Effect of Surface Condition of Steel on Pitting Corrosion," *Tetsu-to-Hagane*, Vol. 50, No. 4, 1964, pp. 565–567.

[*163*] Rosenfeld, I. L. and Danilow, I. S., "Pitting of Passive Stainless Steels," *Zeitschrift Fur Physikalische Chemie*, Vol. 220, No. 3/4, 1964, pp. 257–282 (German).

[*164*] Herbsleb, G., "The Inhibition of Chloride Corrosion (Pitting Corrosion) of Stainless Steels by Nitrate, Sulphate, and Chromate Ions, and Methods of Determining the Pitting-Corrosion Potential," *Werkstoffe und Korrosion*, Vol. 16, Nov. 1965, pp. 929–939 (German).

[*165*] Adachi, H. Y., "Effect of Heat Treatment on Stainless Steel: Study on Pitting Corrosion for Stainless Steel," *Journal of the Iron and Steel Institute of Japan*, Vol. 5, No. 2, 1965.

[*166*] Steigerwald, R. F., "Effect of Cr Content on Pitting Behavior of Fe-Cr Alloys," *Corrosion*, Vol. 22, No. 4, April 1966, pp. 107–112.

[*167*] Hospadoruk, V. and Petrocelli, J. V., "The Pitting Potential of Stainless Steels in Chloride Media," *Journal of the Electrochemical Society*, Vol. 113, Sept. 1966, p. 878.

[*168*] Leckie, H. P. and Uhlig, H. H., "Environmental Factors Affecting the Critical Potential for Pitting in 18:8 Stainless Steel," *Journal of the Electrochemical Society*, Vol. 113, No. 12, 1966, pp. 1262–1267.

[*169*] Lebet, R. and Piotrowski, A., "Resistance to Pitting of Types 202 and 321 Steels to Sulfuric Acid and Sodium Chloride Solutions," *Corrosion*, Vol. 22, Sept. 1966, p. 257.

[*170*] Novakovski, V. M. and Sorokina, A. N., "Model Study of Chloride Pitting in 18:8 Stainless Steel," *Corrosion Science*, Vol. 6, 1966, pp. 227–233.

[*171*] Riskin, I. V., Ionakh, B., and Turkovskaya, A. V., "Electrochemical Study of Pitting Corrosion in Chromium-Nickel Steel Kh18N10T Under Heat-Transfer Conditions," *Zashchita Metallov*, Vol. 2, No. 6, 1966, pp. 657–663 (Russian).

[*172*] Schwenk, W., "Theory of Stainless Steel Pitting," *Proceedings of the Second International Congress on Metallic Corrosion*, National Association of Corrosion Engineers, Houston, Tex., 1966, pp. 256–265.

[*173*] Szklarska-Smialowska, Z. and Janik-Czachor, M., "Pitting Corrosion of 13 Cr-Fe Alloy in Na_2SO_4 Solutions Containing Chloride Ions," *Corrosion Science*, Vol. 7, No. 2, Feb. 1967, pp. 65–72.

[*174*] Strunkin, V. A., Korobkina, V. P., and Tseitlin, Kh. L., "Comparative Sensitivity to Pitting Corrosion of Austenitic and Austenitic-Ferritic Stainless Steels," *Protection of Metals*, Vol. 3, July 1967, p. 335.

[*175*] Banks, W. P. and Hutchison, M., "Preventing Pitting and General Corrosion of Stainless Steel in Phosphoric Acid," *Materials Protection*, Vol. 7, No. 9, Sept. 1968, p. 37.

[*176*] Horvath, J. and Uhlig, H. H., "Critical Potentials for Pitting Corrosion of Ni, Cr-Ni, Cr-Fe, and Related Steels," *Journal of the Electrochemical Society*, Vol. 115, No. 8 1968, p. 791.

[*177*] Ijzermans, A. B. and Vander Krogt, A. J., "Pitting Corrosion of an Austenitic Cr-Ni Stainless Steel in H_2SO_4 Containing H_2S," *Corrosion Science*, Vol. 8, 1968, p. 679.

[*178*] Janik-Czachor, M. and Szklarska-Smialowska, Z., "Pitting Corrosion of Single Crystals of the Fe-16 Cr Alloy in Solutions Containing Cl^- Ions," *Corrosion Science*, Vol. 8, 1968, pp. 215–220.

[*179*] Mears, D. C. and Rothwell, G. P., "Effects of Probe Position on Potentiostatic Control During the Breakdown of Passivity," *Journal of the Electrochemical Society*, Vol. 115, Jan. 1968, pp. 36–38.

[*180*] Novokshchenova, S. M., Babakov, A. A., and Knyazheva, V. M., "Effect of Silicon on the Tendency of Steel Type Kh20N20 Toward Pitting Corrosion," *Protection of Metals*, Vol. 4, No. 6, Nov.-Dec.. 1968, p. 585.

[*181*] Steensland, O., "Pitting Corrosion of Stainless Steels," *Corrosion Prevention and Control*, Vol. 15, No. 3, May-June, 1968, p. 25.

[*182*] Defranoux, J. M., "Sur le Comportement des Aciers Inoxydables en Presence D'Eau de Mer Froide et Chaude," *Corrosion Science*, Vol. 8, 1968, pp. 245–258.

[*183*] Bond, A. P. and Lizlovs, E. A., "Anodic Polarization of Austenitic Stainless Steels in Chloride Media," *Journal of the Electrochemical Society*, Vol. 115, No. 11, 1968.

[*184*] Suzuki, T. and Kitamura, Y., "A Study on the Pitting Growth of Stainless Steels by an Artificial Pit Method," *Corrosion Engineering*, Vol. 17, No. 12, 1968.

[*185*] Suzuki, T. and Kitamura, Y., "A Study on Prevention of Pitting Corrosion of Stainless Steel by Cathodic Current," *Corrosion Engineering*, Vol. 17, No. 4, 1968.

[*186*] Wiegand, H., Speckhardt, H., and Spahn, H., "Corrosion by Pitting and Fatigue Cracking of Austenitic Chromium-Nickel Steel," *Stahl und Eisen Heft*, Vol. 14, July 1968.

[*187*] Steensland, O., "Contribution to the Discussion on Pitting Corrosion of Stainless Steels," *Anti-Corrosion Methods Material*, Vol. 15, May 1968, pp. 8–11, 19.

[*188*] Pouillard, E. and Chiota, J. P., "Influence of Sulfite Ions in Pitting Corrosion of Stainless Steels in Sodium Chloride Solution," *Revue de Metallurgie*, Vol. 65, No. 9, 1968, pp. 599–607 (French).

[*189*] Szklarska-Smialowska, Z. and Janik-Czachor, M., "Electrochemical Investigation of the Nucleation and Propagation of Pits in Iron-Chromium Alloys," *British Corrosion Journal*, Vol. 1, May 1969, p. 138.

[*190*] Wilde, B. E. and Williams, E., "On the Breakdown of Passivity on Stainless Steels in Halide Media," *Journal of the Electrochemical Society*, Vol. 116, Nov. 1969, p. 1539.

[*191*] Lizlovs, E. A. and Bond, A. P., "Anodic Polarization of Some Ferritic Stainless Steels," *Journal of the Electrochemical Society*, Vol. 116, 1969, p. 574.

[*192*] McCollough, I. S. and Scully, J. C., "Pitting Attack on an Austenitic Stainless Steel in H_2SO_4," *Corrosion Science*, Vol. 9, 1969, pp. 707–709.

[*193*] Böhni, H. and Uhlig, H. H., "Effect of Alloyed Re on the Critical Pitting Potentials, of 18% Cr/10% Ni Stainless Steels," *Corrosion Science*, Vol. 9, 1969, p. 353.

[*194*] Stolica, N., "Pitting Corrosion on Fe-Cr and Fe-Cr-Ni Alloys," *Corrosion Science*, Vol. 9, 1969, pp. 205–216, 455.

[*195*] Smialowski, M., Szklarska-Smialowska, Z., Rychcik, M., and Szummer, A., "Effect of Sulphide Inclusions in a Commercial Stainless Steel on the Nucleation of Corrosion Pits," *Corrosion Science*, Vol. 9, 1969, p. 123.

[*196*] Forchhammer, P. and Engell, H. J., "Investigation into the Pitting Corrosion of Passive Austenitic Cr-Ni Steels in Neutral Chloride Solutions," *Werkstoffe und Korrosion*, Vol. 20, No. 1, 1969, p. 214.

[*197*] Suzuki, T. and Kitamura, Y., "Pit Growth of Austenitic Stainless Steel and Its Prevention," *Corrosion Engineering*, Vol. 18, No. 3, 1969.

[*198*] Ohtani, N., Aihara, K., and Takamoto, S., "Observation on Etch Pits on a 18:8 Stainless Steel by Motion Pictures," *Journal of the Japan Institute of Metals*, Vol. 33, No. 4, April 1969, pp. 432-436 (Japanese).

[*199*] Novokovsky, V. M. and Sorokina, A. N., "Electrochemistry of Pitting and Corrosion Cracking of Stainless Steel," *Proceedings of the Third International Congress on Metallic Corrosion*, National Association of Corrosion Engineers, Vol. 1, Houston, Tex., 1969, pp. 159–166.

[*200*] Tomashov, N. D., Markova, O. N., and Chernova, G. P., "The Effect of Grain Size in Austenitic Steel 1Kh18N9T on Its Susceptibility to Pitting Corrosion," *Protection of Melts*, Vol. 6, 1970, p. 16.

[*201*] Ijzermans, A. B., "Pitting Corrosion and Intergranular Attack of Austenitic Cr-Ni Stainless Steels in NaSCN," *Corrosion Science*, Vol. 10, 1970, p. 607.

[*202*] Szklarska-Smialowska, Z., Szummer, A., and Janik-Czachor, M., "Electron Microprobe Study of the Effect of Sulphide Inclusions on the Nucleation of Corrosion Pits in Stainless Steels," *British Corrosion Journal*, Vol. 5, 1970, p. 159.

[*203*] Bianchi, G., Cerquetti, A., Mazza, F., and Torchio, S., "Chemical Etching and Pitting of Stainless Steel," *Corrosion Science*, Vol. 10, 1970, p. 19.

[*204*] Hisamatsu, Y. and Yoshii, T., "Effect of Passivation Pretreatments on the Pitting Corrosion of Austenitic Stainless Steels," *Journal of the Japan Institute of Metals*, Vol. 34, No. 12, Dec. 1970, pp. 1207–1213 (Japanese).

[*205*] Fujii, M. and Kumada, M., "Pitting Dissolution Behavior in the Cold Worked 18 Cr-8 Ni Stainless Steel," *Journal of the Japan Institute of Metals*, Vol. 34, No. 10, Oct. 1970, pp. 1001–1004 (Japanese).

[*206*] Fujii, M. and Kumada, M., "Effects of the Oxide Film on the Pitting Corrosion in 18 Cr-8 Ni Stainless Steel," *Journal of the Japan Institute of Metals*, Vol. 34, No. 10, Oct. 1970, pp. 1005–1011 (Japanese).

[*207*] Fujii, M. and Kumada, M., "Studies on a Few Environmental Factors Affecting Pitting in Stainless Steels," *Journal of the Japan Institute of Metals*, Vol. 34, No. 6, June 1970, pp. 666–671 (Japanese).

[*208*] Monnier, A., Coriou, H., Pinard-Legry, G., and Plante, G., "Selective Growth of Pits on a Stainless Steel in a Chlorinated Oxidizing Medium," *Comptes Rendus*, Series C., Vol. 271, Oct. 1970, pp. 981–984 (French).

[*209*] Rice, La Vern, "Behavior of Metals in Desalination Environments: Third Progress Report," *Proceedings*, National Association of Corrosion Engineers, 26th Conference, Houston, Tex., 1970, pp. 589–596.

[*210*] Defranoux, J. M., "The Resistance of Stainless Steels to Localized Corrosion in Sea Water," *Corrosion Traitements, Protection, Finition*, Vol. 18, No. 6, Oct. 1970, pp. 359–367 (French).

[*211*] Vrahely, E., "A Simple Method for Measuring the Pitting Tendency of Stainless Steels," *Banyaszati es Kohaszati Lopok Kohaszat*, Vol. 103, No. 1, Jan. 1970, pp. 25–27 (Hungarian).

[*212*] Hisamatsu, Y. and Yoshii, T., "Effect of Passivation Pre-Corrosion Treatments on the Pitting Corrosion of Austenitic Stainless Steels," *Journal of the Japan Institute of Metals*, Vol. 34, No. 12, Dec. 1970, pp. 1207–1213 (Japanese).

[*213*] Forchhammer, P. and Engell, H. J., "Investigations of the Corrosion of Stainless Steel by Potentiokinetic Measurements," *Corrosion Science*, Vol. 11, 1971, p. 49.

[*214*] Jackson, R. P. and Van Rooyen, D., "Electrochemical Evaluation of Resistance of Stainless Alloys to Chloride Media," *Corrosion*, Vol. 27, No. 5, 1971, pp. 203–210.

[*215*] Dockal, C. and Weber, J., "Contributions to the Methodology of Pitting Corrosion Potential Measurement on Austenitic Chromium Nickel Steels," *Werkstoffe und Korrosion*, Vol. 22, 1971, pp. 686–690.

[*216*] Lizlovs, E. A. and Bond, A. P., "Anodic Polarization Behavior of 25% Chromium Ferritic Stainless Steels," *Journal of the Electrochemical Society*, Vol. 118, No. 1, 1971.

[*217*] Tomashov, N. D., Chernova, G. P., and Markova, O. N., "The Mechanism of Pit Formation in Steels," *Protection of Metals*, Vol. 7, March-April 1971, p. 85.

[*218*] Wilde, B. E. and Williams, E., "The Relevance of Accelerated Electrochemical Pitting Tests to the Long-Term Pitting and Crevice Corrosion Behavior of Stainless Steels in Marine Environments," *Journal of Electrochemical Society*, Vol. 118, July 1971, p. 1057.

[*219*] Pessall, N. and Liu, C., "Determination of Critical Pitting Potentials of Stainless Steels in Aqueous Chloride Environments," *Electrochimica Acta*, Vol. 16, No. 11, Nov. 1971, pp. 1987–2003.

[*220*] Wilde, B. E. and Williams, E., "The Use of Current/Voltage Curves for the Study of Localized Corrosion and Passivity Breakdown on Stainless Steels in Chloride Media," *Electrochimica Acta*, Vol. 16, No. 1, Nov. 1971, pp. 1971–1985.

[*221*] Sato, N., Kudo, K., Sato, T., and Okamoto, G., "Initiation of Chloride-Pitting Corrosion of Austenitic Stainless Steel in Sulfate Solution," *Corrosion Engineering*, Vol. 20, No. 1, 1971.

[*222*] Suzuki, T. and Kitamura, Y., "Influence of Oxidizing Agents on the Pitting Dissolution of Austenitic Stainless Steel," *Corrosion Engineering*, Vol. 20, No. 4, April 1971, pp. 165–169.

[*223*] Yoshii, T. and Hisamatsu, Y., "Pit Growth in Pitting Corrosion of Austenitic Stainless Steels," *Journal of the Japan Institute of Metals*, Vol. 35, No. 2, Feb. 1971, pp. 151–155 (Japanese).

[*224*] Yashii, T., Hisamatsu, Y., and Matsumura, Y., "On the Shape of Pits Developed Potentiostatically in the Surface of Austenitic Stainless Steel," *Journal of the Japan Institute of Metals*, Vol. 35, No. 6, June 1971, pp. 633–637 (Japanese).

[*225*] Matsumura, Y., Hisamatsu, Y., and Yoshii, T., "Application of the Microelectrode System to a Study of Pitting Corrosion of Austenitic Stainless Steel," *Journal of the Japan Institute of Metals*, Vol. 35, No. 8, Aug. 1971, pp. 820–825 (Japanese).

[*226*] Fujii, M. and Kumada, M., "Surface Film on 18 Cr-8 Ni Stainless Steel and Pitting Corrosion," *Journal of the Japan Institute of Metals*, Vol. 35, No. 7, July 1971, pp. 653–657 (Japanese).

[*227*] Monnier, A., Coriou, H., Pinard-Legry, G., and Plante, G., "Electrochemical Study of the Evolution of Pits on a Stainless Steel in an Oxidizing Chloride-Containing Medium," *Cebelcor Technical Report No. RT. 190*, Centre Belge D'Etude de la Corrosion, Brussels, Belgium, Jan. 1971 (French).

[*228*] Desestret, A., "Stress-Corrosion and Pitting of Stainless Steels in Chloride Solutions," *Formage Traitements Metaux*, Vol. 22, Feb. 1971, pp. 45–51 (French).

[*229*] Tomashov, N. D., Chernova, G. P., and Markova, O. N., "Mechanism of the Development of Pitting in Chromium 18%-Nickel 14% and Chromium 18%-Nickel 14% Molybdenum 2.5% Steels," *Zashchita Metallov*, Vol. 7, No. 2, March-April 1971, pp. 104–111 (Russian).

[*230*] Konstantinova, E. V. and Kurasanova, B. I., "Breakdown Potential of Stainless Steels in Sea Water of Various Compositions," *Zashchita Metallov*, Vol. 7, No. 4, July-Aug. 1971, pp. 446–448 (Russian).

[*231*] Johnson, M. J., "Relative Critical Potentials for Pitting Corrosion of Some Stainless Steels," *Localized Corrosion, ASTM STP 516*, American Society for Testing and Materials, 1972, pp. 262–272.

[*232*] Bianchi, G., Cerquetti, A., Mazza, F., and Torchio, S., "Susceptibility to Pitting of Stainless Steel Oxidized in Dry Air," *Proceedings of the 4th International Congress on Metallic Corrosion*, National Association of Corrosion Engineers, Houston, Tex., 1972, pp. 614–619.

[*233*] Rarey, C. R. and Aronson, A. H., "Pitting Corrosion of Sensitized Stainless Steel," *Corrosion*, Vol. 28, No. 7, 1972, pp. 255–258.

[*234*] Brigham, R. J., "Pitting of Molybdenum Bearing Austenitic Stainless Steel," *Corrosion*, Vol. 28, No. 5, 1972, pp. 177–179.

[*235*] Suzuki, T. and Kitamura, Y., "Critical Potential for Growth of Localized Corrosion of Stainless Steel in Chloride Media," *Corrosion*, Vol. 28, No. 1, 1972, pp. 1–6.

[*236*] Yoshii, T. and Hisamatsu, Y., "On Chemical Pitting of Austenitic Stainless Steel," *Journal of the Japan Institute of Metals*, Vol. 36, No. 8, 1972 (Japanese).

[*237*] Sato, N., Nakagawa, T., Judo K., and Sakashita, M., "Generation and Propagation of Chloride Pits on Rotating Stainless Steel Electrode in Acid Solutions," *Transactions*, Japan Institute of Metals, Vol. 13, No. 2, 1972 (Japanese).

[*238*] Chigal, V., Koshova, I., and Kubelka, Yu., "Revealing the Role of Sulfides in the Initiation of Pitting Corrosion of Kh18N9T Type Steels," *Zashchita Metallov*, Vol. 8, No. 1, 1972 (Russian).

[*239*] Freiman, L. I. and Kharitonova, L. Ya, "Potentiodynamic Determination of Pitting and Repassivation Potentials in Stainless Steel," *Zashchita Metallov*, Vol. 8, No. 6, 1972 (Russian).

[*240*] Bond, A. P., "Effects of Molybdenum on the Pitting Potentials of Ferritic Stainless Steels at Various Temperatures," *Journal of the Electrochemical Society*, Vol. 120, No. 5, 1973.

[*241*] Shvabe, K. and Le Dang, Ankh, "Inhibition of Pitting in Chrome-Nickel Steels," *Zashchita Metallov*, Vol. 9, No. 5, 1973 (Russian).

[*242*] Shams El Din, A. M., Badran, M. M., and Khalil, S. E., "Corrosion Behavior of Manganese Containing Stainless Steels: III. Their Susceptibility Towards Pitting Corrosion," *Werkstoffe und Korrosion*, Vol. 24, 1973, pp. 290–295.

[*243*] Brigham, R. J. and Tozer, E. W., "Effect of Alloying Additions on the Pitting Resistance of 18% Cr Austenitic Stainless Steel," *Corrosion*, Vol. 30, No. 5, 1974, pp. 161–166.

[*244*] Eklund, G. S., "Initiation of Pitting at Sulfide Inclusions in Stainless Steels," *Journal of the Electrochemical Society*, Vol. 121, No. 4, 1974.

[*245*] Seys, A. A., Brabers, M. J., and Van Haute, A. A., "Analysis of the Influence of Hydrogen Pitting Corrosion and Stress Corrosion of Austenitic Stainless Steel in Chloride Environment," *Corrosion*, Vol. 30, No. 2, 1974, pp. 47–52.

[*246*] Fujii, M. and Kumada, M., "Effect of Oxide Film on the Pitting Corrosion in Austenitic Stainless Steels," *Proceedings of the Fifth International Congress of Metallic*

Corrosion, National Association of Corrosion Engineers, Houston, Tex., 1974, pp. 307–312.

[*247*] Isaacs, H. S., "Surface Potential Scanning of Stainless Steel During Pitting Corrosion," *Localized Corrosion*, R. W. Staehle, B. F. Brown, J. Kruger, and A. Agrawal, Eds., National Association of Corrosion Engineers, Houston, Tex., 1974, pp. 158–167.

[*248*] Wilde, B. E., "On Pitting and Protection Potentials: Their Uses and Possible Misuse for Predicting Localized Corrosion Resistance of Stainless Alloys in Halide Media," *Localized Corrosion*, R. W. Staehle, B. F. Brown, J. Kruger, and A. Agrawal, Eds., National Association of Corrosion Engineers, Houston Tex., 1974, pp. 342–352.

[*249*] Pickering H. W. and Frankenthal, R. P., "Mechanism of Pit and Crevice Propagation on Iron and Stainless Steels," *Localized Corrosion*, R. W. Staehle, B. F. Brown, J. Kruger, and A. Agrawal, Eds., National Association of Corrosion Engineers, Houston, Tex., 1974, pp. 261–269.

[*250*] Tomashov, N. D., Chernova, G. P., and Marcova, O. N., "Investigation of Pitting Repassivation in 18 Cr-14 Ni Steels Additionally Alloyed with V, Si, Mo, or Re," *Localized Corrosion*, R. W. Staehle, B. F. Brown, J. Kruger, and A. Agrawal, Eds., National Association of Corrosion Engineers, Houston, Tex., 1974, pp. 363–367.

[*251*] Coriou, H., Monnier, A., Legry, G. P., and Plante, G., "Electrochemical Study of Pit Growth on Stainless Steel in an Oxidizing Chloride Media," *Localized Corrosion*, R. W. Staehle, B. F. Brown, J. Kruger, and A. Agrawal, Eds., National Association of Corrosion Engineers, Houstin, Tex., 1974, pp. 368–372.

[*252*] Bianchi, G., Cerquetti, A., Mazza, F., and Torchio, S., "Pitting Corrosion of Austenitic Stainless Steel and Properties of Surface Oxide Films," *Localized Corrosion*, R. W. Staehle, B. F. Brown, J. Kruger, and A. Agrawal, Eds., National Association of Corrosion Engineers, Houston, Tex., 1974, pp. 399–409.

[*253*] Szklarska-Smialowska, S., "The Pitting of Iron-Chromium-Nickel Alloys," *Localized Corrosion*, R. W. Staehle, B. F. Brown, J. Kruger, and A. Agrawal, Eds., National Association of Corrosion Engineers, Houston, Tex., 1974, pp. 312–341.

[*254*] Smialowska, S. and Czachor, M., "The Analysis of Electrochemical Methods for the Determination of Characteristic Potentials of Pitting Corrosion," *Localized Corrosion*, R. W. Staehle, B. F. Brown, J. Kruger, and A. Agrawal, Eds., National Association of Corrosion Engineers, Houston, Tex., 1974, pp. 353–362.

Nickel

[*255*] Tousek, J., "Pitting Corrosion of Nickel in the Presence of Inorganic Inhibitors," *Collection of Czechoslovak Chemical Communications*, Vol. 33 (9), 1968, pp. 2792–2798 (German).

[*256*] Garz, I., Worch, H., and Schatt, W., "Untersuchungen Uber Die Anodische Auflosung und Die Lochfrasskorrosion Von Nickel-Einkristall-Elektronden," *Corrosion Science*, Vol. 9, 1969, p. 71.

[*257*] Schatt, W. and Worch, H., "Die Anodische Auflosung Von Nickeleinkristallen-Lochfrabkorrosion und Versetzungsatzung," *Corrosion Science*, Vol. 9, 1969, p. 869.

[*258*] Hodge, F. G. and Wilde, B. E., "Effect of Chloride Ion in the Anodic Dissolution Kinetics of Chromium-Nickel Binary Alloys in Dilute Sulfuric Acid," *Corrosion*, Vol. 26, 1970, p. 146.

[*259*] Garz, I. and Worch, H., "Pitting Corrosion in Nickel Single-Crystal Electrodes of Differing Purity," *Wissenschaftliche Zeitschrift der Technischen Hochschule Otto Von Guerische*, Vol. 14, No. 1, 1970, pp. 77–79 (German).

[*260*] Tousek, J., "The Pitting of Nickel," NLL trans.-647-714 (9022.401); NLL-LTI-734-5581 (9022.401) (N71-35607), 1971, available from the National Lending Library, Boston, Mass. (Spanish and English).

[*261*] Tokuda, T. and Ives, M. B., "Pitting Corrosion of Ni," *Corrosion Science*, Vol. 11, 1971, p. 297.

[*262*] Tokuda, T. and Ives, M. B., "Aggressive Ion Accessibility and the Morphology of Corrosion Pits," *Journal of the Electrochemical Society*, Vol. 118, No. 9, 1971.

[*263*] Schatt, W. and Worch, H., "Nähere Charakterisierung der bei Nickeleinkristallen zum Lochfrab Führenden Versetzungen," *Corrosion Science*, Vol. 11, 1971, p. 623.

[*264*] Zamin, M. and Ives, M. B., "Effect of Chloride Ion Concentration on the Anodic Dissolution Behavior of Nickel," *Corrosion*, Vol. 29, No. 8, 1973, pp. 319–324.

[*265*] Zamin, M. and Ives, M. B., "The Anodic Polarization Behavior of Nickel in Acidic Chloride Solution," *Journal of the Electrochemical Society*, Vol. 121, No. 9, 1974.

Test Methods

[*266*] Greene, N. D. and Fontana, M. G., "An Electrochemical Study of Pitting Corrosion in Stainless Steels: Part 1. Pit Growth; Part 2. Polarization Measurements," *Corrosion*, Vol. 15, Jan. 1959, pp. 48–60.

[*267*] Franck, V. F., "Electrochemical Studies of Pitting Corrosion of Passive Metals," *First International Congress on Metallic Corrosion*, Butterworth, London, 1962, pp. 120–126.

[*268*] Vjiive, N. and Matsumoto, K., "Study of the Pitting Mechanism by Means of Radioactive Isotopes," *Genshiryoku Kogyo*, Vol. 9, No. 7, July 1963, pp. 17–21 (Japanese).

[*269*] Herman, R. S., "Radiographic-Photographic Method for Measuring Depth and Distribution of Pitting," *Corrosion*, Vol. 20, No. 11, Nov. 1964, pp. 361t-366t.

[*270*] de Sterke, A., "Determination of Size of Cavities in Pitting Corrosion by Radiographic Contrast Measurement," *Materialprufung*, Vol. 6, No. 10, Oct. 1964, pp. 343-346.

[*271*] Peters, B. F., "Radiography for Corrosion Evaluation," *Materials Evaluation*, Vol. 23, No. 3, March 1965, pp. 129–135.

[*272*] de Waard, C., Nicholson, J. W., and Posch, W., "Simple Method for the Potentiostatic Determination of Pitting Potential in One Single Experiment," *Werkstoffe und Korrosion*, Vol. 19, 1968, pp. 782–785.

[*273*] Jones, D. A. and Greene, N. D., "Electrochemical Detection of Localized Corrosion," *Corrosion*, Vol. 25, No. 9, 1959.

[*274*] Wilde, B. and Williams, E., "On the Correspondence Between Electrochemical and Chemical Accelerated Pitting Corrosion Tests," *Journal of the Electrochemical Society*, Vol. 117, No. 6, 1970, p. 775.

[*275*] Bohni, H., "Pitting Corrosion of Metals and Methods for Its Investigation," *Schweizer Archive*, Vol. 36, No. 2, Feb. 1970, pp. 41–45 (German).

[*276*] Board, P. W., Holland, R. V., and Steele, R. J., "Prediction of Pitting Corrosion in Tinplate from Capacitance Measurements," *British Corrosion Journal*, Vol. 7, March 1972, pp. 87–89.

[*277*] Szklarska- Smialowska, Z. and Janik-Czachor, M., "The Analysis of Electrochemical Methods for the Determination of Characteristic Potentials of Pitting Corrosion," *Corrosion Science*, Vol. 11, 1971, p. 901.

[*278*] Verink, E. D., Jr. and Pourbaix, M., "Use of Electrochemical Hysteresis Technique in Developing Alloys for Saline Exposures," *Corrosion*, Vol. 27, Dec. 1971, p. 495.

[*279*] Verink, E. D., Jr. and Pourbaix, M., "Use of Potentiokinetic Methods at Successively Increasing and Decreasing Electrode-Potentials in Developing Alloys for Saline Exposures," Cebelcor Technical Report No. RT. 191, Centre Belge d'Etude de la Corrosion, Bruxelles, Belgium, June 1971.

[*280*] Freiman, L. I., Kharitonova, L. Ya, and Kolotyrkin, Ya. M., "Stimulation of Pitting Corrosion by Ultra-Violet Light," *Zashchita Metallov*, Vol. 7, No. 5, Sept.-Oct. 1971, pp. 594–597 (Russian).

[*281*] Bond, A. P., "Pitting Corrosion: A Review of Recent Advances in Testing Methods and Interpretation," *Localized Corrosion—Cause of Metal Failure, ASTM STP 516*, American Society for Testing and Materials, 1972, pp. 250–261.

[*282*] Seys, A. A. and Van Haute, A. A., "Pitting Potential Measurements by Means of the Static Potential Band Method," *Proceedings of Fifth International Congress on Metallic Corrosion*, National Association of Corrosion Engineers, Houston, Tex., 1975.

[*283*] Suzuki, T. and Kitamura, Y., "Testing Method for Localized Corrosion of Stainless Steel Considering the Corrosion Potential in Its Environment," *Proceedings of Fifth International Congress on Metallic Corrosion*, National Association of Corrosion Engineers, Houston, Tex., 1975.

[*284*] Seys, A. A. and Van Haute, A. A., "Pitting Potential Measurements by Means of the Static Potential Band Method," *Corrosion*, Vol. 29, No. 8, 1973, pp. 329–334.

[*285*] Smialowska, S. and Czanchor, M., "The Analysis of Electrochemical Methods for the Determination of Characteristic Potentials of Pitting Corrosion," *Localized Corrosion*, R. W. Staehle, B. F. Brown, J. Kruger, and A. Agrawal, Eds., National Association of Corrosion Engineers, Houston, Tex., 1974, pp. 353–363.

[*286*] Franz, F. and Novak, P., "Effect of Rotation on the Pitting Corrosion of Aluminum Electrodes," *Localized Corrosion*, R. W. Staehle, B. F. Brown, J. Kruger, and A. Agrawal, Eds., National Association of Corrosion Engineers, Houston, Tex., 1974, pp. 576–579.

Theoretical

[*287*] Stern, M., "The Relation Between Pitting Corrosion and the Ferrous-Ferric Oxidation-Reduction Kinetics on Passive Surfaces," *Journal of the Electrochemical Society*, Vol. 104, Oct. 1957, p. 600.

[*288*] Eldredge, G. G., "Analysis of Corrosion Pitting by Extreme-Value Statistics and Its Application to Oil Well Tubing Caliper Surveys," *Corrosion*, Vol. 13, No. 1, Jan. 1957, pp. 51t-60t.

[*289*] Greene, N. D. and Fotana, M. G., "A Critical Analysis of Pitting Corrosion," *Corrosion*, Vol. 15, 1959, p. 41.

[*290*] Edeleanu, C., "The Propagation of Corrosion Pits in Metals," *Journal of the Institute of Metals*, Vol. 89, No. 3, Nov. 1960, pp. 90–94.

[*291*] Robinson, F. P. A., "Pitting Corrosion: Cause, Effect, Detection, and Prevention," *Corrosion Technology*, Vol. 7, No. 8, Aug. 1960, pp. 237-239, 266.

[*292*] Schafer, G. J., Gabriel, J. R., and Foster, P. K., "On the Role of the Oxygen Concentration Cell in Crevice Corrosion and Pitting," *Journal of the Electrochemical Society*, Vol. 107, No. 12, Dec. 1960, pp. 1002–1004.

[*293*] Tarasova, L. N., Romanov, V. V., and Kudinova, N. I., "Study of the Pitting Corrosion of Metals by Means of Models," *Journal of Applied Chemistry*, Vol. 33, Oct. 1960, pp. 2285–2290.

[*294*] Kohle, H., "The Fundamentals of Corrosion," *Technische Uberwachung*, Vol. 4, No. 5, May 1963, pp. 161–165 (German).

[*295*] La Que, F. L., "What We Do and Don't Know About Corrosion," *Materials in Design Engineering*, Vol. 57, No. 1, Jan. 1963, p. 99.

[*296*] Schenk, W., "Discussion of the Cause and Stability of Pitting Corrosion in Relation to the 'All or Nothing' Principle of Passivity and a Kinetic Model," *Corrosion Science*, Vol. 3, No. 2, June 1963, pp. 107–121.

[*297*] Kolotyrkin, Ya. M., "Pitting Corrosion of Metals," *Proceedings of the Second International Congress on Metallic Corrosion*, National Association of Corrosion Engineers, Houston, Tex., 1966, pp. 23–32, and *Corrosion*, Vol. 19, No. 8, Aug. 1963, pp. 261t-268t.

[*298*] Schwenk, W., "Theory of Stainless Steel Pitting," *Corrosion*, Vol. 12, No. 4, April 1964, pp. 129t–137t.

[*299*] Hoar, T. P., Mears, D. C., and Rothwell, G. P., "The Relationship Between Anodic Passivity, Brightening, and Pitting," *Corrosion Science*, Vol. 5, 1965, pp. 279–289.

[*300*] Greene, N. D. and Judd, G., "Relation Between Anodic Dissolution and Resistance to Pitting Corrosion," *Corrosion*, Vol. 21, 1965, p. 15.

[*301*] Vetter, K. J., "A Thermodynamic Theory of Pitting Corrosion," *Berichte der Bunsengesellschaft fur Physikalische Chemie*, Vol. 8, 1965, pp. 683–688.

[*302*] France, W. D., Jr., "Controlled Potential Investigations of Localized Corrosion Phenomena," Ph.D. thesis, University Microfilms, No. 67-4167.

[*303*] Hubner, W., "Pitting Corrosion of Passivated Metals," *Svensk Kemisk Tidskrift*, Vol. 78, No. 6/7, 1966, pp. 321-355 (Swedish).

[*304*] Finley, H. F., "An Extreme-Value Statistical Analysis of Maximum Pit Depths and Time to First Perforation," *Corrosion*, Vol. 23, No. 4, 1967.

[*305*] Kaesche, H., "Mechanism of Pitting Corrosion," *Corrosion Traitements Protection Finition*, Vol. 17, No. 8, 1969.

[*306*] Prazhak, M., Toushek, Ya., and Spanilyi, V., "Role of Anion Absorption in Pitting Corrosion and Stress Corrosion Cracking of Metals," *Protection of Metals*, Vol. 5, 1969, p. 329.

[*307*] Rosenfeld, I. L. and Danilov, I. S., "Electrochemical Aspects of Pitting Corrosion," *Proceedings of the Third International Congress on Metallic Corrosion*, Vol. 1, National Association of Corrosion Engineers, Houston, Tex., 1966, pp. 139–151.

[*308*] Swann, P. R., "Mechanism of Corrosion Tunneling with Special Reference to Cu_3Au," *Corrosion*, Vol. 25, No. 4, 1969, pp. 147–150.

[*309*] Brown, B. F., "Concept of the Occluded Corrosion Cell," *Corrosion*, Vol. 26, 1970, p. 249.

[*310*] Leckie, H. P., "A Contribution to the Applicability of Critical Pitting Potentials," *Journal of the Electrochemical Society*, Vol. 117, 1970, pp. 1152.

[*311*] Pourbaix, M., "Significance of Protection Potential in Pitting and Intergranular Corrosion," *Corrosion*, Vol. 26, No. 10, Oct. 1970, p. 431–438.

[*312*] Pourbaix, M., "Metallic Corrosion," Technical Report No. RT-175, Belge D'Etude de la Corrosion, Brussels, Belgium, June 1970.

[*313*] Vermilyea, J., "Concerning the Critical Pitting Potential," *Journal of the Electrochemical Society*, Vol. 118, No. 4, 1971, p. 529.

[*314*] Szklarska-Smialowska, Z., "Review of Literature on Pitting Corrosion Published Since 1960," *Corrosion*, Vol. 27, No. 6, 1971, pp. 223–233.

[*315*] Bosch, R. M. and Defrancq, J., "The Problem of Initiation and Growth in Pitting Corrosion," Cebelcor Technical Report No. RT-196, Centre Belge D'Etude de la Corrosion, Brussels, Belgium, June 1971.

[*316*] Tousek, J., "The Question of the Pitting Corrosion Mechanism," *Werkstoffe und Korrosion*, Vol. 23, 1972, pp. 109–112.

[*317*] Pourbaix, M., "Significance of Protection Potential in Pitting, Intergranular Corrosion, and Stress-Corrosion Cracking," *Journal of Less-Common Metals*, Vol. 28, 1972, p. 51.

[*318*] Frankenthal, R. P. and Pickering, H. W., "On the Mechanism of Localized Corrosion of Iron and Stainless Steel: Part I. Electrochemical Studies; Part II. Morphological Studies," *Journal of the Electrochemical Society*, Vol. 119, No. 10, Oct. 1972, p. 1297 and 1304.

[*319*] Ciolac, S., "Corrosion Pitting in Metals: Part I. Interdependence Pitting-Passivity, Theory and Development Stages of the Pitting Process; Part II. Methods of Investigation and Protection," *Studii Si Cercetari De Chimie*, Vol. 21, 1973, No. 5, pp. 597–610, No. 6, pp. 669–684.

[*320*] Uhlig, H. H., "Distinguishing Characteristics of Pitting and Crevice Corrosion," *Materials Protection and Performance*, Vol. 12, Feb. 1973, pp. 42–44.

[*321*] Hisamatsu, Y. and Ichikawa, K., "Etch-Pitting as a Faceting Dissolution Process," *Corrosion Engineering*, Vol. 23, No. 3, 1974, and *Proceedings of the Fifth International Congress on Metallic Corrosion*, National Association of Corrosion Engineers, Houston, Tex., 1974, pp. 275–280.

[*322*] Rosenfeld, I. L., "Local Corrosion Process," *Proceedings of the Fifth International Congress on Metallic Corrosion*, National Association of Corrosion Engineers, Houston, Tex., 1974, pp. 53–73.

[*323*] Ives, M. B., "Etch Pitting—Theory and Observation," *Localized Corrosion*, R. W. Staehle, B. F. Brown, J. Kruger, and A. Agrawal, Eds., National Association of Corrosion Engineers, Houston, Tex., 1974, pp. 78–103.

[*324*] Vetter, K. J. and Strehblow, H. H., "Pitting Corrosion in an Early Stage and Its Theoretical Implications," *Localized Corrosion*, R. W. Staehle, B. F. Brown, J. Kruger, and A. Agrawal, Eds., National Association of Corrosion Engineers, Houston, Tex., 1974, pp. 240–251.

[*325*] Hoar, T. P.,"Bright Pitting," *Localized Corrosion*, R. W. Staehle, B. F. Brown, J. Kruger, and A. Agrawal, Eds., National Association of Corrosion Engineers, Houston, Tex., 1974, pp. 112–116.

Titanium

[*326*] Pigott, R. A. and Schreir, L. L., "Micropitting of Titanium During Anodic Oxidation in Formic Acid," *Nature*, Vol. 189, 21 Jan. 1961, pp. 216–217.

[*327*] Fischer, W. R., "Study of Pitting Corrosion, Especially on Titanium: Part I. Corrosion Investigations; Part II. Electrochemical Studies," *Technische Mittetilangen Krupp, Ausgabe A. Forschungsberichte*, Vol. 22, No. 3 and 4, 1964, pp. 65-82, 125–142.

[*328*] Dugdale, I. and Cotton, J. B., "The Anodic Polarization of Titanium in Halide Solutions," *Corrosion Science*, Vol. 4, 1964, p. 397.

[*329*] Posey, F. A. and Bohlmann, E. G., "Pitting of Titanium Alloys in Saline Waters," *Desalination*, Vol. 3, 1967, p. 269.

[*330*] Kolotyrkin, Ya. N. and Strunkin, V. A., "Pitting of Titanium on Application of an Alternating Current," *Zashchita Metallov*, Vol. 6, No. 5, 1970.

[*331*] Mansfeld, F., "The Effect of Water on Passivity and Pitting of Titanium in Solutions of Methanol and Hydrogen Chloride," *Journal of the Electrochemical Society*, Vol. 118, Sept. 1971, p. 1412.

[*332*] Cotton, J. B., "Pitting Corrosion of Titanium," *British Corrosion Journal*, Vol. 7, March 1972, pp. 59–69.

[*333*] Beck, T. R., "Pitting of Titanium: Part I. Titanium-Foil Experiments; Part II. One-Dimensional Pit Experiments," *Journal of the Electrochemical Society*, Vol. 120, No. 10, 1973.

[*334*] Beck, T. R., "A Review: Pitting Attack of Titanium Alloys," *Localized Corrosion*, R. W. Staehle, B. F. Brown, J. Kruger, and A. Agrawal, Eds., National Association of Corrosion Engineers, Houston, Tex., 1974, pp. 644–650.

Tungsten

[*335*] Maloof, S. R., "Dislocation Etch Pitting Studies on Tungsten Single Crystals Under Potentiostatic Conditions," *Corrosion*, Vol. 24, No. 9, Sept. 1968, pp. 283–290.

[*336*] Stolica, N. D., "Pitting of Tungsten in LiCl-Methanol-H_2O Solutions," *Proceedings of the Fifth International Congress on Metallic Corrosion*, National Association of Corrosion Engineers, Houston, Tex., 1975.

Zinc

[*337*] Kaesche, H., "Investigation of Pitting of Galvanized Steel Tubes and the Effect of Element Formation on Copper Precipitation," *VDI-Berichte*, No. 72, 1963, pp. 64-71 (German).

[*338*] Kamel, R., "Natural Pitting on Cleaved Surfaces of Zinc Crystals," *Acta Metallurgica*, Vol. 11, No. 6, June 1963, pp. 629–630.

[*339*] Davies, D. E. and Lotlikar, M. M., "Passivation and Pitting Characteristics of Zinc," *British Corrosion Journal*, Vol. 1, Jan. 1966, p. 149.

[*340*] Lotlikar, M. M. and Davies, D. E., "The Potentiostatic Investigation of the Passivity and Pitting Characteristics of High-Purity Zinc," *Proceedings of the Third International Congress on Metallic Corrosion*, Vol. 1, National Association of Corrosion Engineers, Houston, Tex., 1969, pp. 167–177.

[*341*] Krug, H. and Borchers, H., "Pitting Corrosion Under Hydrogen Bubbles Adherent to the Surface of Zinc," *Werkstoffe und Korrosion*, Vol. 22, No. 4, 1971, pp. 309–311 (German).

Zirconium

[*342*] Tomiki, T. and Ogawa, S., "Electro-Microscopic Observation on Chemically Etched Surfaces of Polycrystalline Zirconium," *Journal of Japan Institute of Metals*, Vol. 24, 1960, pp. 522–526.

[*343*] Kolotyrkin, Ya. M. and Gil'man, V. A., "Effect of Chloride Ions on the Electrochemical and Corrosion Behavior of Zirconium," *Doklady Akadamie Nauk S.S.S.R.*, Vol. 137, 21 March 1961, pp. 642–645 (Russian).

[*344*] Gil'man, V. A. and Kolotyrkin, Ya. M., "The Mechanism of the Corrosion Pitting of Zirconium in Halide Solutions," *Doklady Akademie Nauk S.S.S.R.*, Vol. 143, 21 March 1962, pp. 640–642 (Russian).

[*345*] Stoops, D. J., Carver, M. D., and Kato, H., "Corrosion of Zirconium in Cupric and Ferric Chlorides," Non-Atomic Energy Commission Publication 5945, 1962, available from U.S. Department of the Interior, Bureau of Mines, Washington, D.C.

Summary

The Galvanic and Pitting Corrosion symposia have presented recent laboratory and field corrosion study results in a broad spectrum of corrosive environments that include controlled clean and polluted air, distilled water, 3.5 percent sodium chloride solutions, tap water, seawater, hot brine solutions, organic solutions, and dry high resistivity to wet low resistivity soils.

Pitting is a form of localized corrosion attack which can lead to early failure. Galvanic corrosion has also been the reason for many premature failures. Unfortunately, there are numerous engineering alloys that are highly susceptible to pitting corrosion, for example, the stainless steels and the 2000 and 7000 series aluminum alloys. The aluminum alloys are additionally susceptible to galvanic attack since they are anodic to all other engineering metals (and their alloys) except magnesium and zinc.

The paper by Baboian on electrochemical techniques for predicting galvanic corrosion covers potential, current, and polarization measurements. Although each of these can be useful in determining galvanic effects, he has pointed out that measurements should be made in the actual environment to which materials are exposed. Where potential and current measurements have limitations with regard to localized galvanic corrosion, polarization techniques can be quite useful in predicting the susceptibility to this type of corrosion.

The examination of the galvanic attack of aluminum alloys by ferrous and nonferrous cathodic materials in aqueous media by Mansfeld and Kenkel presents, in effect, a galvanic series for these galvanic couples in specific media. Although some may quarrel with the relatively short test duration, it is obvious that their data can provide a basis for preliminary design.

Compton found that the distribution of cathodic protection current between members of copper steel and stainless steel aluminum in galvanic couples varied by a ratio 940 to 0.05 as the relative areas were varied from 100:1 to 1:100. Polarization and current distribution measurements have shown that at about a 1:1 ratio of cathode to anode, cathodic protection does not appear to be practical.

The method for performing corrosion tests of weldments by Compton and Turley is a straight-forward approach to determining the susceptibility of weld and heat affected zones to accelerated galvanic corrosion attack. Of the nine ferrous and nonferrous weldment systems tested, there was only one wherein the base metal would provide cathodic protection to the smaller surface areas of the weld and heat affected zones.

The galvanic corrosion tests of Shick and Mitchell on underground cable materials using the galvanostatic polarization technique to determine potential and current density established that semiconducting polyethylene jacketing of power cables becomes the cathode of a galvanic cell (polyethylene coupled to concentric neutral copper wires) because the polyethylene contains carbon particles. Another significant result is that aerated soil increased the corrosion rates by orders of magnitude as compared to deaerated soil.

Escalante and Gerhold in their galvanic coupling of stressed stainless steels to the anodic materials iron, zinc, and magnesium at six different underground sites found that the higher strength work-hardened stainless steel alloy Type 301 was inferior to alloy Type 304 and 26 Cr-1Mo in its resistance to cracking. Alloy Type 301 consistently cracked at stresses that were only 22 to 36 percent of the alloy's yield stress as compared to alloys Type 304 and 26 Cr-1Mo that never failed even though the stress levels were from 34 to 93 percent of yield stress. Since there was no failure of noncoupled Type 301 specimens, it is concluded (rightly so) by Escalante and Gerhold that cracking is the result of hydrogen embrittlement that occurs due to the cathodic reaction at alloy Type 301 cathode.

An extensive galvanic corrosion investigation in the Panama Canal Zone including atmosphere, soil, and seawater environments has been described by Pelensky et al. They describe test techniques and initial results of this work.

Specimens of galvanized steel sheet were exposed to polluted and clean air by Spence and Haynie. They show that corrosion of zinc film is essentially a linear function of time. Although weight losses were approximately the same in both environments, uniform corrosion of the zinc occurred in the polluted exposure, whereas pitting was observed in the clean air environment.

Covington describes the pitting problems encountered in titanium tubes in heat exchangers handling hot saturated brine. Two types of pits appear: symmetrical pits about 0.6 cm in diameter which are associated with scratches containing iron, and irregular pits believed to be associated with salt plugs.

The studies by Cornwell et al of pitting of copper tubing by domestic water conclude that in certain types of domestic waters the presence of of carbon residue from the tube manufacturing operations will result in pitting failure in a period of only three months. The authors' solution to this problem is to reduce the carbon contamination through abrasive cleaning.

This position is questioned by Cohen who maintains that it has never been conclusively demonstrated that carbon films on the inside diameter of copper water tubing are the cause of pitting corrosion. Cohen's position is that the cause of pitting in copper water tubes is the chemical make up of a given water system and that the proper solution to this problem is to treat the corrosive water through the addition of lime or caustic soda.

Cornwell et al, in response to Cohen, agree that pitting of copper water tubing is related to specific waters, but their test results show that carbon free tubes did not pit in the same waters that caused rapid failure of carbon containing copper tubes. It is apparent from the data presented by both parties that the pitting corrosion of copper water tubes can be related to both water chemistry and residue carbon films. The service experience related by both parties support their particular position (carbon removal versus water chemistry control), and there is little doubt that both are correct for the case histories given.

Mansfeld covers the pitting behavior of titanium, nickel, 6061 aluminum and Type 304 stainless steel in methanol in the presence of sulfates or chlorides. The behavior of metals in these environments contrast sharply the behavior in aqueous systems. For example, titanium corrodes rapidly in anhydrous methanol because passivation cannot occur. However, additions of water at a concentration as low as 0.6 percent leads to passivation of the titanium.

The review on "Measurement and Evaluation of Pitting Corrosion" by Rowe elaborates on the visual nondestructive and destructive techniques that are used to determine density of pits (number/cm^2) and maximum depth of pitting attack. This review came about through the development of a Recommended Practice for Measurement and Evaluation of Pitting Corrosion by ASTM Subcommittee G01.05 on Laboratory Corrosion Tests.

The basic approach presented by Rowe is to visually examine metals at low magnification to determine the general magnitude of pitting attack. It is correctly emphasized that metal weight loss alone is not a satisfactory procedure for the determination of the extent of pitting. The destructive cross sectioning of pits to provide microscopic measurement or the progressive machining to the bottom of a pit can provide accurate measurements but these techniques are costly, time consuming, and impractical where numerous specimens are involved. The nondestructive measurement techniques of a micrometer or a dial indicator with a sharp tungsten tip or a microscope with a graduated focusing knob are more rapid but do have the limitation of not being able to measure those pits that are not completely open to their bottom.

Rowe makes a most valid point that measurement of maximum pit depth or the average of a number of deepest pits is often the most meaningful method of demonstrating the magnitude of pitting corrosion. An equally important test of the effect of pitting is the change in mechanical properties of the corroded material. These can include ultimate and tensile yield strength, elongation, and reduction in area. The measure of the effect of pitting on the fatigue strength of a material is most important when the material is to be exposed to cyclical stress in a corrosive environment.

Crews proposes a statistical treatment of pitting corrosion data which calculates the prediction intervals of pit depth which can be used to obtain quantitative estimates of service life or corrosion rate in normally encountered environments. The statistical treatment in this paper utilizes a prepared computer program which provides calculated values of both the regression and the distribution, expressed as prediction intervals of pit depth for times both within the exposure period of the test and extrapolated exposure times.

The crevice corrosion test cell presented by Anderson offers a new method of determining susceptibility of a material to localized corrosion. The advantages of the new test configuration are that it provides 40 small crevices per specimen, is inexpensive to produce, and can be used to statistically predict corrosion initiation and propagation.

Anderson's tests on stainless steel, copper, and nickel alloys were performed in seawater. However, the test fixture uses the plastic material Delrin which is highly resistant to many corrosive environments such as acid and alkali solutions, and it could, therefore, be used in these environments.

Petersen uses a unique apparatus to duplicate the environment of a pit. Although this is a difficult if not an impossible task, the results of his work show some interesting correlations between corrosion of carbon steel and solution changes within a cavity. He finds a correlation between pH change and reaction of magnesium and calcium in the electrolyte.

The problem associated with measurements of the critical potentials of stainless steels is covered by Morris. Using the rapid-scan potentiodynamic polarization technique, crevice corrosion can be prevented, thereby permitting accurate and reproducible measurement of the pitting potential.

The compilation of literature references on pitting corrosion includes sections on aluminum, copper, electroplated coatings, environmental effects, graphite, iron and steel, iron-chromium-nickel alloys, nickel, test methods, theoretical, titanium, tungsten, zinc, and zirconium.

Thus, the authors of the papers have presented a wide range of test techniques and results in various environments with a range of materials. This information represents the cumulative efforts of many years of work and is presented herein as a guide to present and future investigations.

Index